The Dissertation Committee for Sara Navidi
certifies that this is the approved version of the following dissertation:

Development of Site Amplification Model for Use in Ground Motion Prediction Equations

Committee:

_____
Ellen M. Rathje, Supervisor

_____
Robert B. Gilbert

_____
Chadi El Mohtar

_____
Lance Manuel

_____
Thomas W. Sager

Development of Site Amplification Model for Use in Ground Motion Prediction Equations

by

Sara Navidi, B.S.; M.S.

Dissertation

Presented to the Faculty of the Graduate School of

The University of Texas at Austin

in Partial Fulfillment

of the Requirements

for the Degree of

Doctor of Philosophy

The University of Texas at Austin

May 2012

To my parents

Development of Site Amplification Model for Use in Ground Motion Prediction Equations

Sara Navidi, Ph.D.

The University of Texas at Austin, 2012

Supervisor: Ellen M. Rathje

The characteristics of earthquake shaking are affected by the local site conditions. The effects of the local soil conditions are often quantified via an amplification factor (AF), which is defined as the ratio of the ground motion at the soil surface to the ground motion at a rock site at the same location. Amplification factors can be defined for any ground motion parameter, but most commonly are assessed for acceleration response spectral values at different oscillator periods. Site amplification can be evaluated for a site by conducting seismic site response analysis, which models the wave propagation from the base rock through the site-specific soil layers to the ground surface. An alternative to site-specific seismic response analysis is site amplification models. Site amplification models are empirical equations that predict the site amplification based on general characteristics of the site. Most of the site amplification models that already used in

ground motion prediction equations characterize a site with two parameters: the average shear wave velocity in the top 30 m (V_{S30}) and the depth to bedrock. However, additional site parameters influence site amplification and should be included in site amplification models.

To identify the site parameters that help explain the variation in site amplification, ninety nine manually generated velocity profiles are analyzed using seismic site response analysis. The generated profiles have the same V_{S30} and depth to bedrock but a different velocity structure in the top 30 m. Different site parameters are investigated to explain the variability in the computed amplification. The parameter Vratio, which is the ratio of the average shear wave velocity between 20 m and 30 m to the average shear wave velocity in the top 10 m, is identified as the site parameter that most affects the computed amplification for sites with the same V_{S30} and depth to bedrock.

To generalize the findings from the analyses in which only the top 30 m of the velocity profile are varied, a suite of fully randomized velocity profiles are generated and site response analysis is used to compute the amplification for each site for a range of input motion intensities. The results of the site response analyses conducted on these four hundred fully randomized velocity profiles confirm the influence of Vratio on site amplification. The computed amplification factors are used to develop an empirical site amplification model that incorporates the effect of Vratio, as well as V_{S30} and the depth to bedrock. The empirical site amplification

model includes the effects of soil nonlinearity, such that the predicted amplification is a function of the intensity of shaking. The developed model can be incorporated into the development of future ground motion prediction equations.

Contents

Chapter 1

Introduction

1.1 Research Significance

When an earthquake occurs, seismic waves are released at the source (fault), they travel through the earth, and they generate ground shaking at the ground surface. The characteristics of shaking at a site depend on the source characteristics and change as they travel through their path to get to the site (Figure 1.1). The wave amplitudes generally attenuate with distance as they travel through the bedrock in the crust (i.e. path effect) and they are modified by the local soil conditions at the site (i.e. site effect). The important property of the local soil conditions that influence ground shaking is the shear wave velocity. Although seismic waves may travel a longer distance through the bedrock than through the local soils, the influence of the local soil conditions can be significant.

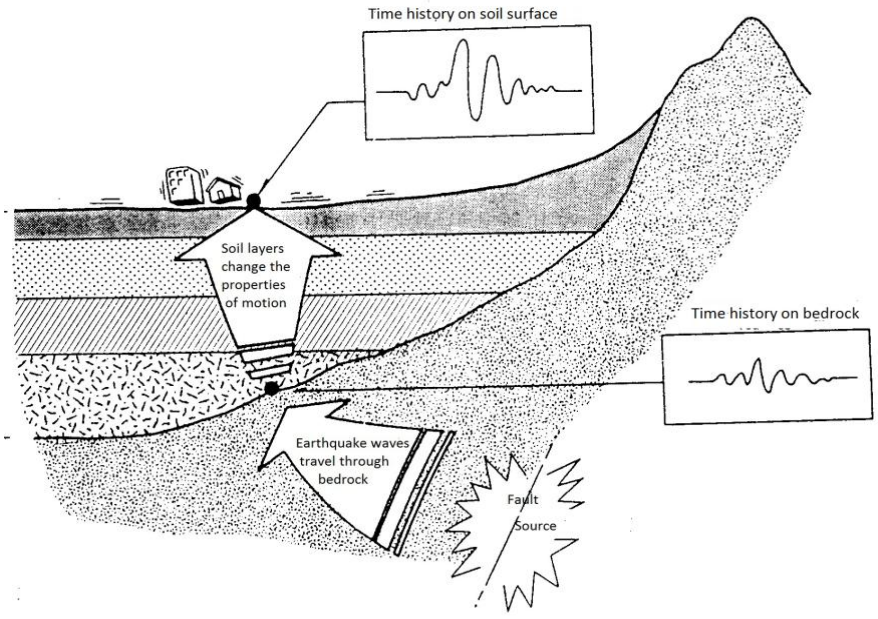

Figure 1.1 Propagation of seismic waves from source to surface.PSL, http://seismo.geology.upatras.gr/MICROZON-THEORY1.htm

The effects of the local soil conditions are often quantified via an amplification factor (AF), which is defined as the ratio of the ground motion at the soil surface to the ground motion at a rock site at the same location. Amplification factors can be defined for any ground motion parameter, but most commonly are assessed for acceleration response spectral values at different periods.

Two main alternatives are available to evaluate the amplification of acceleration response spectra due to local soil conditions:

- Site-specific Site Response Analysis
- Empirical Ground Motion Prediction Equations

Site response analysis propagates waves from the underlying bedrock through the soil layers to the ground surface. Most often site response analysis is performed using a one-dimensional assumption in which the soil and bedrock surfaces extend infinitely in the horizontal direction and all boundaries are assumed horizontal. The nonlinear response of the soil can be modeled via the equivalent linear approximation or through fully nonlinear approaches. Site response analysis provides a detailed assessment of site amplification but requires significant information about the site, including the shear wave velocity profile from the surface down to bedrock and characterization of nonlinear soil properties, as well as selection of appropriate input rock motions.

An alternative to site-specific site response analysis is an empirical estimate of site amplification that uses an empirical equation to predict the site amplification based on the input motion and the general characteristics of the site. This approach is incorporated in empirical ground motion prediction equations (GMPEs). GMPEs are statistical models that predict an acceleration response spectrum at a site as a function of earthquake magnitude (M), site to source distance (R), local site conditions, and other parameters. GMPEs are developed predominantly from recorded ground motions from previous earthquakes. To account for local site conditions, the site is characterized simply by one or two parameters (e.g. the average shear wave velocity over the top 30 m) and the amplification at each period is related to these parameters. The amplification relationship included in a ground

motion prediction equation is often called a site response or site amplification model. While these models are relatively simple, and ignore important details about the shear wave velocity profile and nonlinear properties at a site, they are important tools that can be used to estimate site amplification for a range of applications. Yet enhancements in these models can be made to improve their ability to predict site amplification.

1.2 Research Objectives

The main objective of this research is to improve the site amplification models included in ground motion prediction equations. Important site details that control site amplification will be identified and statistical models will be developed that include these parameters. These models then can be implemented in ground motion prediction equations. To meet these objectives, first the important site parameters that influence site amplification are identified. To identify these site parameters, hypothetical shear wave velocity profiles are generated and their seismic response computed using the equivalent linear approach. Various site parameters are computed from the hypothetical velocity profiles and the relationship between each of these parameters and the computed site amplification. After identifying appropriate site parameters for use in the empirical site amplification model, appropriate functional forms for the statistical model are developed. The developed functional forms are fit to the computed amplification data.

1.3 Outline of Dissertation

The following dissertation consists of nine chapters. After the Introduction in Chapter 1, Chapter 2 introduces modeling site amplification in ground motion prediction equations and reviews the current state-of-the-art in site amplification models. Identification of site parameters that affect site amplification is discussed in Chapter 3. In this chapter sites with manually generated shear wave velocity profiles are used to identify the parameters that most strongly influence the computed site amplification. Chapter 4 presents the statistical generation of fully randomized shear wave velocity profiles that are used to compute amplification factors for use in developing the site amplification model. The nonlinear soil properties and the input motions that are applied to these sites are also discussed in this chapter. In Chapter 5 through 7, the process of developing the functional form of the site amplification model that includes the identified site parameters is presented. Chapter 5 discusses the component of the proposed model for linear-elastic conditions and the nonlinear component is discussed in Chapter 6. In Chapter 7, the linear and nonlinear components of the developed functional form are combined and the final model is presented. Chapter 8 demonstrates how the proposed model works to predict the surface response spectrum of an actual site, and also compares the developed amplification model with models developed by other researchers. Chapter 9 provides a summary, conclusions, and recommendations for future studies.

Chapter 2

Modeling Site Amplification in Ground Motion Prediction Equations

2.1 Introduction

Site amplification has been included in ground motion prediction equations (GMPE) for several decades. The initial site amplification models simply distinguished between rock and soil sites and incorporated the site amplification by a scaling parameter or by defining different statistical models for soil and rock sites (e.g. Boore et al 1993; Campbell 1993; and Sadigh et al 1997). The ground motion prediction equation of Abrahamson and Silva (1997) was the first to include nonlinear effects in the site amplification model. Nonlinear effects represent the influence of soil nonlinearity, where the stiffness of the soil decreases and the damping increases as larger shear strains are induced in the soil. As a result of soil nonlinearity, amplification is a nonlinear function of the input rock motion. While the incorporation of nonlinear effect in the Abrahamson and Silva (1997) GMPE was

an improvement, the model only distinguishes between soil and rock, and did not directly use shear wave velocity information in the amplification prediction. Boore et al (1997) was the first to directly use the average shear wave velocity in the top 30 m (V_{S30}) to predict site amplification, but their model did not include soil nonlinearity.

The evolution of site amplification models used in GMPEs is described in the next sections.

2.2 Site Amplification Models

The general form of a ground motion prediction equation is:

$$\ln(Sa) = f_m + f_R + f_{site} \quad (2.1)$$

where Sa is the spectral acceleration at a given period and f_m , $f_{R,}$ and f_{site} are functions that represent the ground motion scaling that accounts for magnitude (f_m), site-to-source distance (f_R), and site effects (f_{site}). The function f_{site} is considered the "Site Amplification Model" or "Site Response Model" in the ground motion prediction equation and it includes parameters that describe the site and the rock input motion intensity.

An alternative form of equation (2.1) can be written in terms of the spectral acceleration on soil (Sa_{soil}), the spectral acceleration on rock (Sa_{rock}), and an amplification factor (AF) using:

$$Sa_{soil} = Sa_{rock} \cdot AF \quad (2.2)$$

$$\ln(Sa_{soil}) = \ln(Sa_{rock} \cdot AF) = \ln(Sa_{rock}) + \ln(AF) \quad (2.3)$$

Comparing equations (2.1) and (2.3), it is clear that $f_{m \text{ and }} f_R$ work together to predict ln (Sa_{rock}) and f_{site} represents ln(AF).

Researchers have modeled ln(AF) using different parameters and functional forms, but most models incorporate the effects of V_{S30} (i.e., V_{S30} scaling). Some models incorporate the effects of the soil depth (i.e., soil depth scaling).

2.2.1 V_{S30} Scaling

V_{S30} is computed from the travel time for a shear wave travelling through the top 30 m of a site. It is computed by:

$$V_{S30} = \frac{30 \text{ m}}{\sum_{i=1}^{n} \frac{h_i}{V_{S,i}}} \quad (2.4)$$

where $V_{S,i}$ is the shear wave velocity of layer i, and h_i is the thickness of layer i. Only layers within the top 30 m are used in this calculation.

The scaling of ground motions with respect to V_{S30} generally consists of two terms: a linear-elastic term that is a function of V_{S30} alone, and a nonlinear term that accounts for nonlinear soil effects. The nonlinear term is a function of both V_{S30} and

the input rock intensity. The linear term represents site amplification at small input intensities where the soil response is essentially linear elastic. The nonlinear term incorporates the effect of soil nonlinearity at larger input intensities. The resulting functional form for the site amplification model (ln(AF)) is:

$$\ln(AF) = f_{site} = \ln(AF)_{LN} + \ln(AF)_{NL} \qquad (2.5)$$

Boore et al (1997) were the first to use V_{S30} in their site amplification model. Their model did not include nonlinearity effect and is written as:

$$\ln(AF) = a \times \ln\left(\frac{V_{S30}}{V_{ref}}\right) \qquad (2.6)$$

where a and V_{ref} are coefficients estimated by regression. In their model amplification varies log-linearly with V_{S30}.

Choi and Stewart (2005) expanded the Boore et al. (1997) site amplification model to include both linear and nonlinear site amplification effects. The general form of the model is given as:

$$\ln(AF) = a \times \ln\left(\frac{V_{S30}}{V_{ref}}\right) + b \times \ln\left(\frac{PGA_{rock}}{0.1}\right) \qquad (2.7)$$

where PGA_{rock} is the peak ground acceleration on rock in g unit, 0.1 is the reference PGA_{rock} level for nonlinear behavior, and b is a function of V_{S30}. This model does not explicitly separate the linear and nonlinear components, because the $\ln\left(\frac{PGA_{rock}}{0.1}\right)$ term contributes to the AF prediction at small values of PGA_{rock}.

The Choi and Stewart (2005) model was developed by considering recorded ground motions at sites with known V_{S30} and computing the difference between the observed ln(Sa) and the ln(Sa) predicted by an empirical ground motion prediction equation for rock conditions. This difference represents ln(AF) because the observed motion is ln(Sa,soil) and the predicted motion on rock is ln(Sa,rock). Using the observed ln(AF), Choi and Stewart (2005) found that b is negative and generally decreases towards zero as V_{S30} increases (Figure 2.1). This decrease in b with increasing V_{S30} indicates that nonlinearity becomes less significant as sites become stiffer.

Figure 2.2 shows predictions of amplification versus PGA_{rock} for three sites with V_{S30}= 250 m/s, 350 m/s, and 550 m/s using the Choi and Stewart (2005) model. Amplification is shown for PGA and a spectral period of 0.2 s. For all three shown sites, amplification decreases as input intensity increases. The softest site (i.e., V_{S30}=250 m/s) has the greatest reduction in amplification. Again, note that the nonlinear component of the Choi and Stewart (2005) model extends to small PGA_{rock}, as the AF continues to change as PGA decreases to small values.

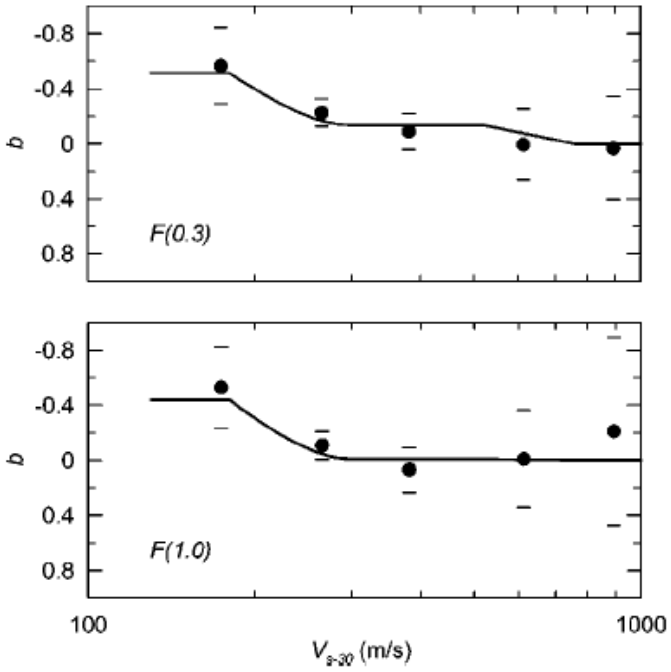

Figure 2.1 Derived values of b as a function of V_{S30} by Choi and Stewart (2005) for periods of 0.3 and 1.0 s.

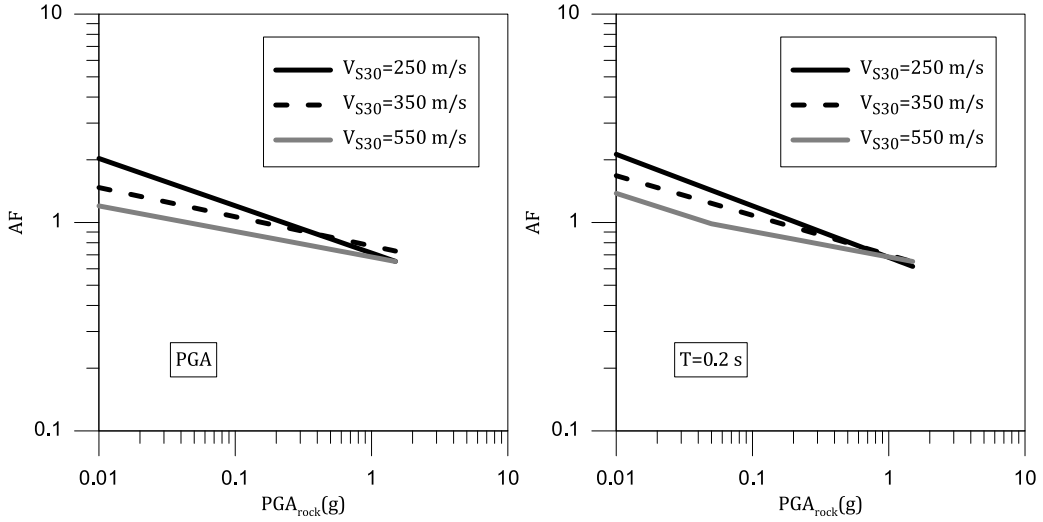

Figure 2.2 Amplification for PGA and T=0.2 s as a function of input intensity (PGA_{rock}) as predicted by Choi and Stewart (2005) for a range of V_{S30}.

Walling et al (2008) proposed a more complex site response model including the nonlinear effect:

$$\ln(AF) = \begin{cases} a \times \ln\left(\frac{V_{S30}}{V_{lin}}\right) + b \times \ln\left(PGA_{rock} + c \times \left(\frac{V_{S30}}{V_{lin}}\right)^n\right) & \text{for } V_{S30} < V_{lin} \\ a \times \ln\left(\frac{V_{S30}}{V_{lin}}\right) & \text{for } V_{S30} \geq V_{lin} \end{cases} \quad (2.8)$$

where the linear component of the model is similar those previously discussed (with V_{lin} similar to $V_{ref)}$, but the nonlinear component is different. The main difference between the Walling et al. (2008) model and the approach of Choi and Stewart (2005) is the treatment of the coefficient b. Walling et al. (2008) models b as independent of V_{S30} and adds a parameter to the input intensity that is V_{S30}-dependent (i.e., $c \times \left(\frac{V_{S30}}{V_{lin}}\right)^n$). With derived values of c and n positive, the functional form in equation (2.8) results in the term $c \times \left(\frac{V_{S30}}{V_{lin}}\right)^n$ decreasing with decreasing V_{S30}. This results in soil nonlinearity affecting smaller V_{S30} more than larger V_{S30}.

Walling et al. (2008) developed the regression parameters for equation (2.8) using simulated amplification factors computed using the equivalent-linear method. Figure 2.3 shows the predicted amplification versus input intensity for two sites with V_{S30}= 270 and 560m/s at spectral period of 0.2s as presented in Walling et al. (2008). Amplification decreases when the input intensity increases and the reduction in amplification with input intensity is larger for the softer site (i.e., V_{S30}=270 m/s). The Walling et al (2008) model was developed using simulations of sites with V_{S30} between 270 m/s and 900 m/s.

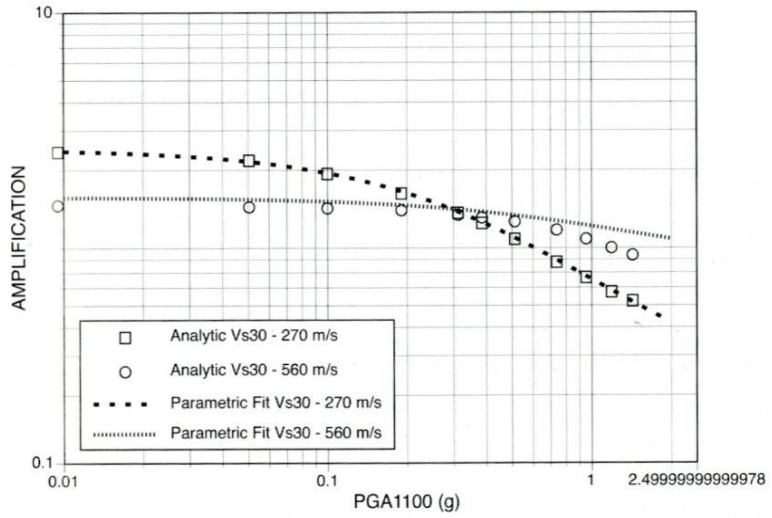

Figure 2.3 Example of the parametric fit for V_{S30}=270 and 560 m/s using equation (2.8) at T=0.2 s (Walling et al 2008).

The current state–of-the-art in GMPEs is represented by models developed in the "Next Generation of Ground-Motion Attenuation Models" (NGA) project (peer.berkeley.edu/ngawest). This effort took place over five years to develop improved GMPEs for shallow crustal earthquake in the western U.S. and similar active tectonic zones. This effort was organized by the Pacific Earthquake Engineering Research center (PEER). Different GMPE were developed by five teams: Abrahamson and Silva (2008), Boore and Atkinson (2008), Campbell and Bozorgnia (2008), Chiou and Youngs (2008), and Idriss (2008). Although each team developed their own GMPE, the teams interacted with one another extensively. They all used the same database of recorded ground motions, but they were free to use the entire database or select subsets of it. The site amplification models included in the NGA

relationships are discussed below. The Idriss (2008) model is not discussed because it does not explicitly use V_{S30}.

Abrahamson and Silva (2008) adopted the form of the nonlinear site amplification model developed by Walling et al (2008). The regression coefficients for the nonlinear component of the site amplification model were constrained by the values obtained by Walling et al. (2008). Only the coefficient for the linear-elastic component of the model (i.e., a) term was estimated in the regression analysis from the recorded motions. Figure 2.4 shows the variation of amplification with V_{S30} under four different shaking levels using the Abrahamson and Silva (2008) site amplification model for T=0.2 s. The amplification model shows that the amplification decreases with increasing PGA_{rock} for V_{S30} smaller than V_{lin}. The reduction in AF with increasing PGA_{rock} is strongest at the smallest V_{S30}.

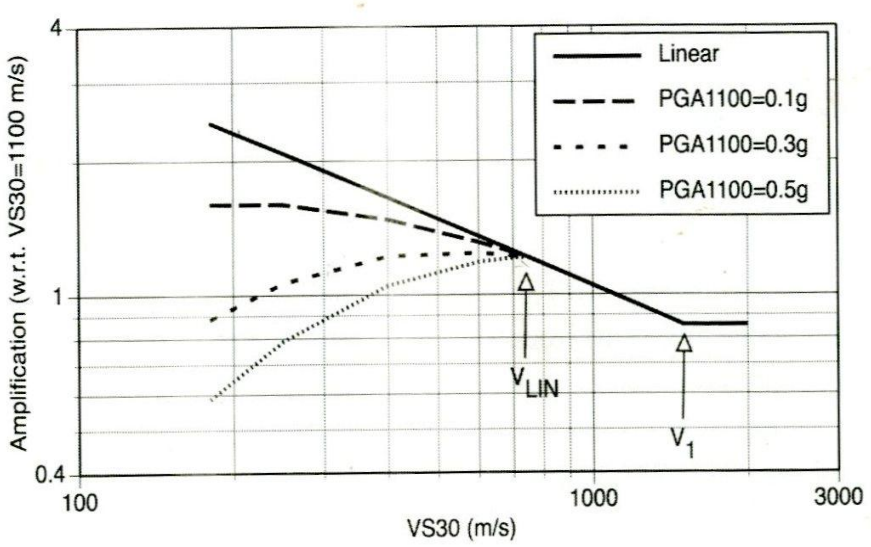

Figure 2.4 Amplification vs. V_{S30} for different input intensities at T=0.2 s (Abrahamson and Silva 2008).

Boore and Atkinson (2008) used a modified version of the Choi and Stewart (2005) model. Boore and Atkinson (2008) explicitly separated the linear and nonlinear components and simplified the V_{S30}-dependence of the parameter b. In Figure 2.5, the amplification predicted by Boore and Atkinson (2008) at spectral periods of 0.2 and 3.0 s is plotted versus PGA_{rock} (PGA4nl in Figure 2. 5) for five values of V_{S30}. For stiffer sites (V_{S30} ≥760 m/s), the amplification does not vary with input intensity. As V_{S30} decreases, the influence of input intensity becomes important with less amplification occurring at larger values of PGA_{rock}. The change in amplification with input intensity is most significant for softer sites (smaller V_{S30}) such that deamplification (i.e. amplification less than 1.0) is possible at large input

intensities and small V_{S30}. At longer periods, the amplification tends to be larger than at short periods.

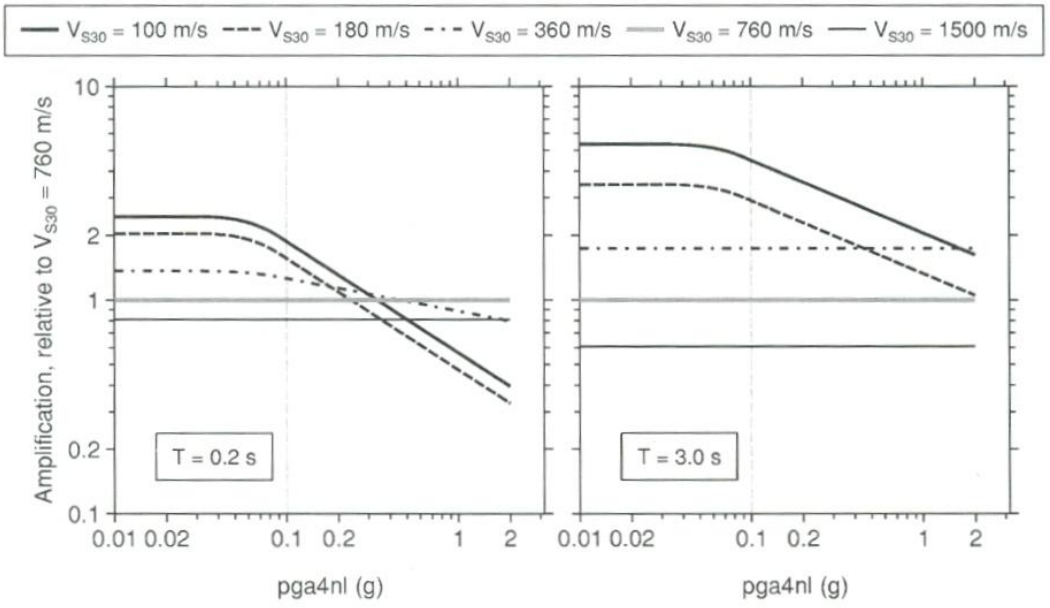

Figure 2.5 Amplification for T=0.2 s and T=3.0 s as a function of input intensity (pga4nl), for a suite of V_{S30} (Boore and Atkinson 2008).

Campbell and Bozorgnia (2008) adopted the functional form proposed by Boore et al. (1997) for the linear component of their site amplification model. To constrain the nonlinear effect, they adopted the form proposed by Walling et al (2008). Figure 2.6 shows the amplification of PGA predicted by the Campbell and Bozorgnia (2008) as a function of PGA_{rock} for sites with different values of V_{S30}. Similar to the other models, the reduction of amplification with increasing in input intensity is more significant for softer sites.

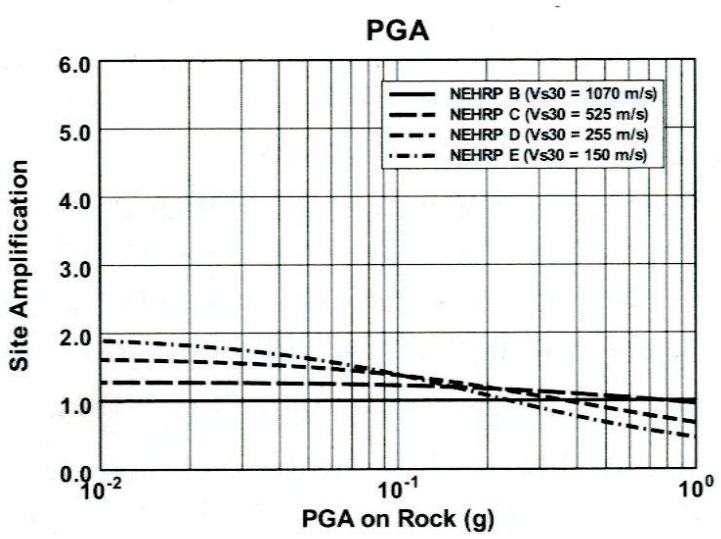

Figure 2.6 Amplification for PGA as a function of input intensity (PGA on rock), for a suite of V_{S30} (Campbell and Bozorgnia 2008).

Chiou and Youngs (2008) used a modified version of Choi and Stewart (2005) site amplification model. While Choi and Stewart (2005) normalized PGA_{rock} by 0.1 g, Chiou and Youngs (2008) use the following form:

$$\ln(AF) = a \times \ln\left(\frac{V_{S30}}{V_{ref}}\right) + b \times \ln\left(\frac{Sa_{rock}+c}{c}\right) \qquad (2.9)$$

This functional form separates the linear and nonlinear components because for small Sa_{rock}, the $\ln\left(\frac{Sa_{rock}+c}{c}\right)$ term will tend to zero. Chiou and Youngs (2008) model b as V_{S30}-dependent.

Figure 2.7 plots amplification versus V_{S30} for different input intensities as predicted by the Chiou and Youngs (2008) NGA model. Amplification is shown for spectral periods of 0.01, 0.1, 0.3, and 1.0 sec. At small input intensities (i.e. 0.01g) where the linear term dominates, amplification increases log-linearly as V_{S30} decreases. This effect is larger at longer periods. At larger input intensities, the amplification at each V_{S30} is reduced due to soil nonlinearity (i.e. soil stiffness reduction and increased damping). This effect is largest at small V_{S30} and shorter periods.

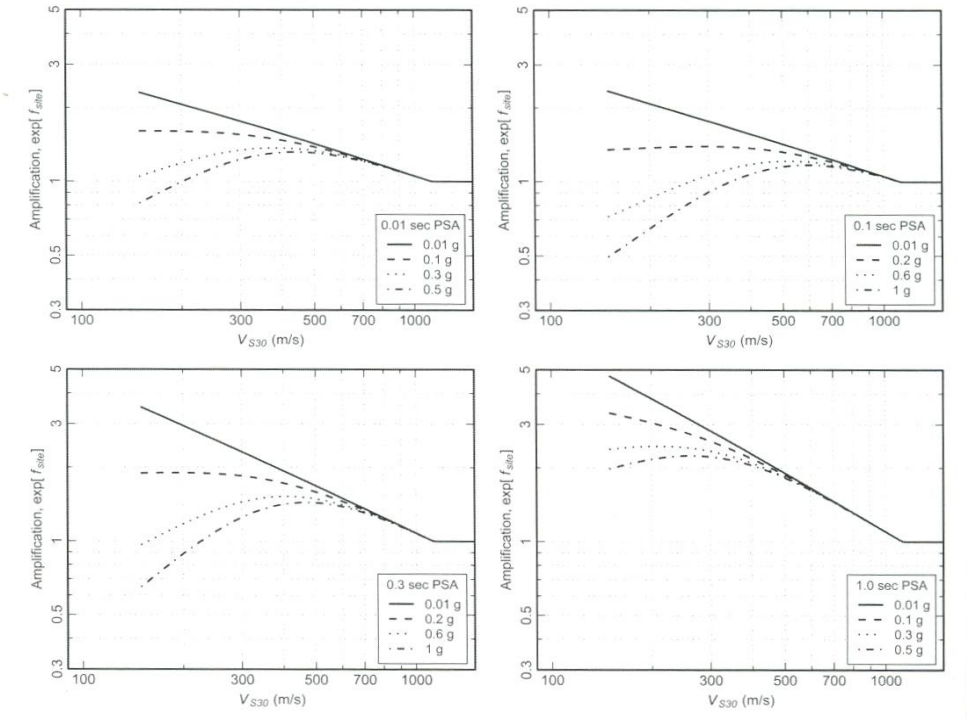

Figure 2.7 Site amplification as a function of spectral period, V_{S30} and level of input intensity (Chiou and Youngs 2008).

2.2.2 Soil Depth Scaling

The Abrahamson and Silva (2008), Campbell and Bozorgnia (2008), and Chiou and Youngs (2008) NGA models include a soil depth term in addition to V_{S30} when predicting site amplification at long periods. Because the natural period of a soil site is proportional to the soil depth (i.e., deeper sites have longer natural periods), deeper soil sites will experience more amplification at long periods than shallow soil sites. The scaling of site amplification with soil depth is commonly considered independent of input intensity (i.e., not influenced by soil nonlinearity). Each NGA model defines soil depth as the depth to a specific shear wave velocity horizon. Abrahamson and Silva (2008) and Chiou and Youngs (2008) use the depth to V_S equal to or greater than 1.0 km/s (called $Z_{1.0}$), while Campbell and Bozorgnia (2008) use the depth to a V_S equal to or greater than 2.5 km/s (called $Z_{2.5}$). Essentially, $Z_{1.0}$ represents the depth to "engineering" rock while $Z_{2.5}$ represents the depth to hard rock.

Because softer soils tend to be underlain by deeper alluvial basins, $Z_{1.0}$ and $Z_{2.5}$ are highly correlated to V_{S30}. Using the measured $Z_{1.0}$ and V_{S30} values from the recording stations in the NGA database, Abrahamson and Silva (2008) developed a relationship between $Z_{1.0}$ and V_{S30} (Figure 2.8). This relationship predicts $Z_{1.0}$ close to 200 m (0.2 km) for V_{S30} =500 m/s and $Z_{1.0}$ close to 700 m (0.7 km) for V_{S30} =200 m/s. Because the NGA data are dominated by sites in southern California and most of these sites are located in the deep alluvial valleys common in southern California,

the depths are not necessarily representative of areas in other parts of the western United States.

As noted previously, soil depth predominantly affects long period amplification because soil depth affects the natural period of a site and the associated periods of amplification. Figure 2.9 shows the predicted acceleration response spectra for a soil site with V_{S30} = 270 m/s and different values of $Z_{1.0}$ as predicted by the Abrahamson and Silva (2008) NGA model for a M=7.0 earthquake at a distance of 30 km. At short periods (less than 0.4 s) $Z_{1.0}$ does not influence the response spectrum, while at longer periods the response spectra are significantly affected by $Z_{1.0.}$ For example, at a spectral period of 1.0 s, the spectral acceleration for $Z_{1.0}$=0.1 km is 0.08 while the spectral acceleration for $Z_{1.0}$=1.1 km is close to 0.25. This represents an amplification of greater than 3.0. At longer periods the effect of $Z_{1.0}$ is even more pronounced. At a spectral period of 5.0 s, the response spectra in Figure 2.9 indicate an amplification of greater than 4.0 between $Z_{1.0}$=0.1 km and 1.1 km.

As mentioned previously, the Campbell and Bozorgnia (2008) model considers the depth to the 2.5 km/s velocity horizon as the soil depth ($Z_{2.5}$). Figure 2.10 shows the site amplification as a function of $Z_{2.5}$ as predicted by the Campbell and Bozorgnia (2008) NGA model. The $Z_{2.5}$ effect is only significant at deep sites ($Z_{2.5}$> 3 km) with amplification as large as 2.0 to 3.0 for deep sites and long periods. There is also a slight reduction in amplification for shallow profiles ($Z_{2.5}$< 1.0 km).

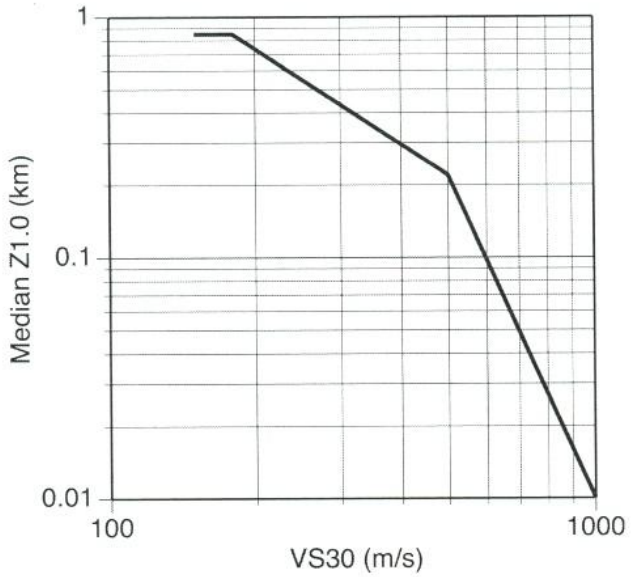

Figure 2.8 Relation between median $Z_{1.0}$ and V_{S30} for NGA database (Abrahamson and Silva 2008).

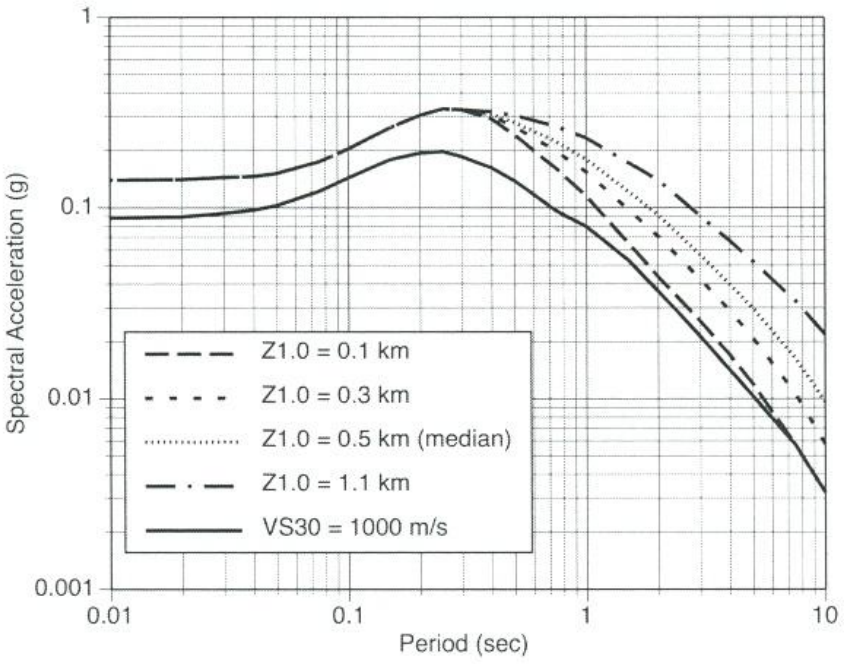

Figure 2.9 Example scaling with soil depth (Abrahamson and Silva 2008).

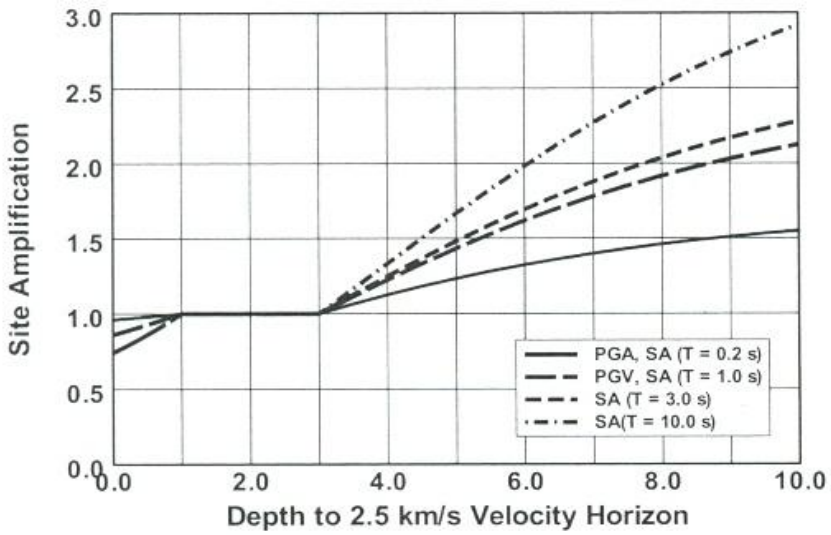

Figure 2.10 Effect of basin depth on site amplification (Campbell and Bozorgnia 2008).

Kottke (2011) proposed a functional form to model the $Z_{1.0}$ effect that couples with V_{S30} scaling of the linear-elastic component of the amplification model. Using site amplification simulations, Kottke (2011) showed that the slope of the linear relationship between amplification and $\ln(V_{S30}/V_{ref})$ is $Z_{1.0}$ dependent. The modified linear component can be written as:

$$\ln(\mathrm{AF}) = \mathrm{a} \times\propto\times \ln\left(\frac{V_{S30}}{V_{ref}}\right) \qquad (2.10)$$

Where $\propto$ is defined as:

$$\propto = \left(\frac{\min(Z_{min}, Z_{1.0})+1}{Z_{min}+1}\right)^{b} \qquad (2.11)$$

Where the Z_{min} parameter is frequency dependent (Figure 2.11) and represents the depth above which soil depth effect is negligible. As shown in Figure 2.11, Z_{min} decreases as frequency increases (i.e., period decreases). Figure 2.12 shows parameter $\propto$ versus frequency for three different $Z_{1.0}$ values. As the depth of the soil profile increases, a smaller range of frequency is affected by the soil depth effect.

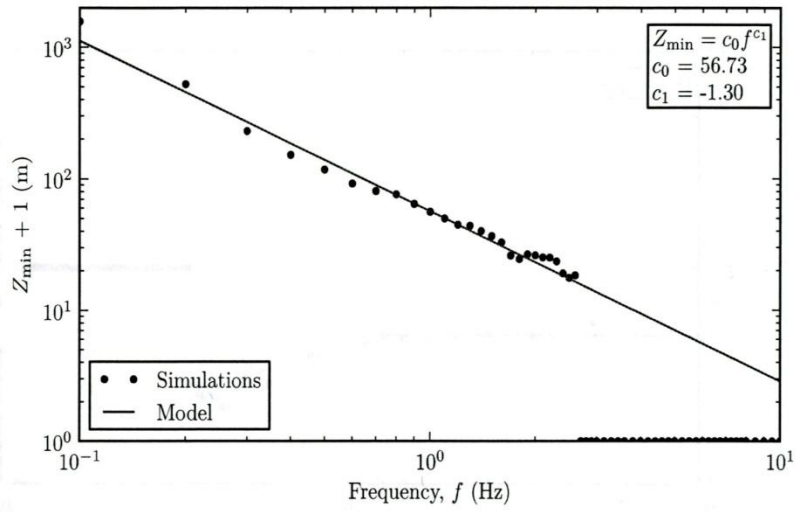

Figure 2.11 The variation of Z_{min} with frequency (Kottke 2011).

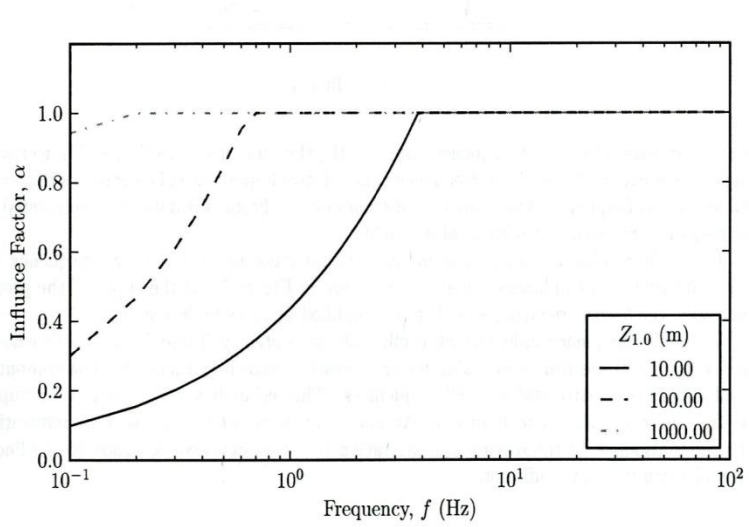

Figure 2.12 The influence factor model (∝) for three different $Z_{1.0}$ values (Kottke 2011).

2.3 Unresolved Issues

It is known that the details of the shear wave velocity profile at a site affect site amplification. Currently, only site response analysis can take this detailed information into account when predicting site amplification. As discussed above, the existing ground motion prediction equations consider just the average shear wave velocity in the top 30 m and the depth to rock as site parameters. While this site characterization is an improvement over qualitative descriptions of "rock" and "soil", additional site parameters can be included in the models that will improve the empirical prediction of site amplification. First, the parameters that influence site amplification should be identified. To identify these parameters, a site response

study is performed as discussed in the next chapter. Then, the findings from these analyses need to be expanded to any possible site. Numerous site profiles with a wide range of site parameters should be analyzed. To be able to analyze a reasonable number of soil profiles, 400 soil profiles are statistically generated and analyzed. The response of the fully randomized profiles under different level of input intensities are considered to develop a model that incorporates the effect of the identified site parameters in site amplification.

Chapter 3

Identification of Site Parameters that Influence Site Amplification

3.1 Introduction

As discussed in previous chapter, the average shear wave velocity in top 30 m (V_{S30}) and depth to rock ($Z_{1.0}$ or $Z_{2.5}$) are considered important site parameters that are incorporated in site amplification models of GMPEs. This research aims to identify further effective site parameters to improve site amplification predictions in empirical ground motion prediction equations. The approach to identify these site parameters is to perform wave propagation analysis (i.e., site response analysis) for sites with different velocity profiles and relate the computed amplification factors to characteristics of the site profiles. This study focuses on parameters that can be determined from the shear wave velocity profile within the top 30 m because the shear wave velocity information below 30 m is not always available.

In this exploratory part of the research, ninety-nine V_s profiles are generated manually and analyzed by the program Strata (Kottke and Rathje 2008), which performs 1D equivalent-linear site response analysis. The manually generated profiles allow for different velocity structures within the top 30 m while at the same time maintaining a constant V_{S30}. Amplification factors (AF) are calculated for all the generated profiles at multiple input intensities and spectral periods. These data are used to identify parameters that strongly influence the site amplification.

3.2 Site Profiles

Profiles with the same average shear wave velocity (V_{S30}) but different shear wave velocity structures within the top 30 meters are generated. The profiles also have the same depth to engineering rock ($Z_{1.0}$=150 m). The same V_{S30} and $Z_{1.0}$ in the profiles facilitates investigation of other site parameters that influence the site response. Profiles of 150 m depth are developed for five different V_{S30} values (V_{S30} = 225, 280, 350, 450, and 550 m/s) using the baseline profiles shown in Figure 3.1. For each V_{S30} value, the profiles are manually varied in the top 30 meters (keeping V_{S30} constant) with the profiles below 30 m kept at the baseline values. The half space below 150 m for all baseline profiles has a V_S equal to 1100 m/s. Eighteen to twenty four profiles are generated for each V_{S30} value and ninety-nine total profiles are analyzed.

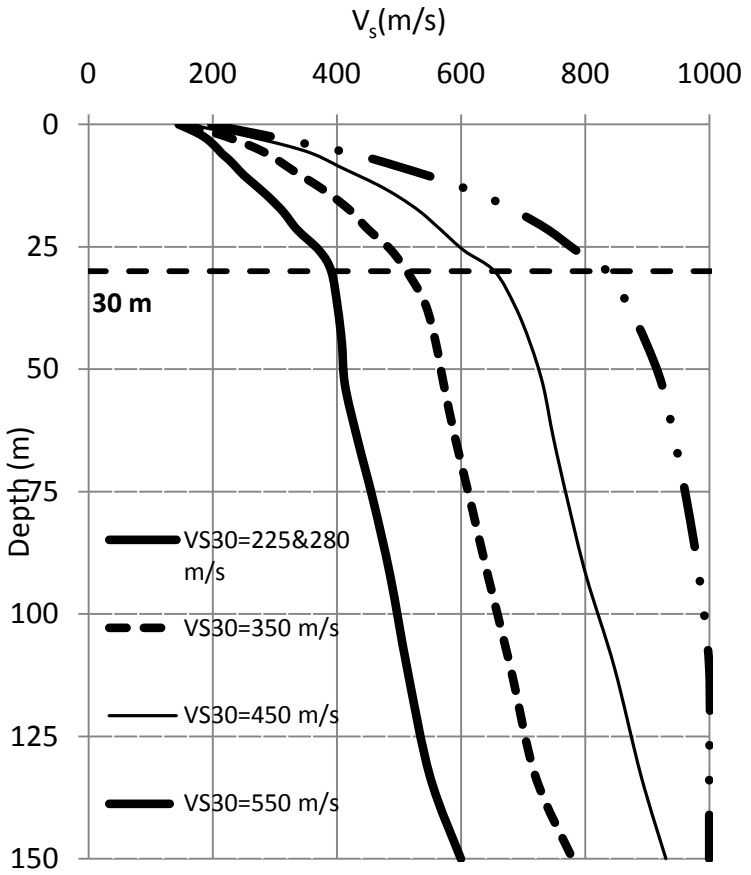

Figure 3.1 Baseline shear wave velocity profiles used for each V_{S30} value.

The top 50 m of all of the generated profiles, along with the baseline profile, for each V_{S30} value are shown in Figure 3.2. In all the generated profiles, the velocity increases with depth with no inversion in the shear wave velocity (i.e. an inversion is when a smaller V_S is found below a larger V_S). The minimum shear wave velocity is limited to 100 m/s in the generated profiles and for each V_{S30} the profiles all have the same maximum V_S as controlled by the baseline velocity profile at 30m.

In addition to the shear wave velocity profile, the unit weight and the shear modulus reduction and damping curves of the soil layers are required for site response analysis. The shear modulus reduction and damping curves describe the variation of the shear modulus and damping ratio with shear strain, and represent the nonlinear properties of the soil. For each of the profiles, the same unit weights, as well as shear modulus reduction and damping curves are used. The Darendeli (2001) model is used to develop the modulus reduction and damping curves as a function of mean effective stress (σ'_0), Plasticity Index (PI), and over-consolidation ratio (OCR). In this study PI and OCR are taken to be 10 and 1.0, respectively, for all layers. To model the stress dependence, the 150 m of soil is split into 5 layers (Figure 3.3) and the nonlinear property curves computed for the mean effective stress at the middle of each layer. The resulting shear modulus reduction and damping curves for each layer are shown in Figure 3.4. Generally, the shear modulus reduction curve shifts up as mean effective stress increases, while the damping curve shifts down.

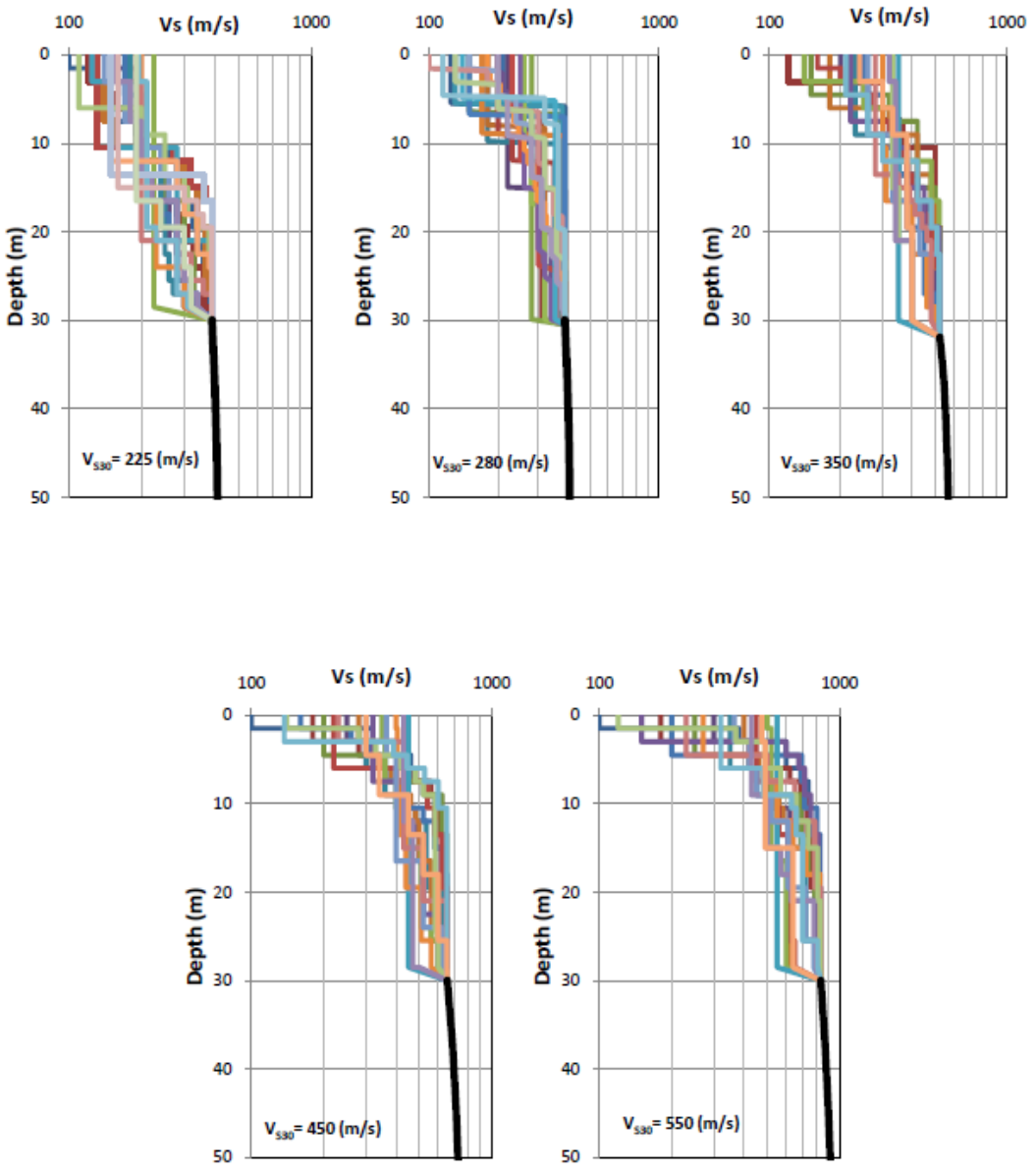

Figure 3.2 Generated profiles for each V_{S30} value.

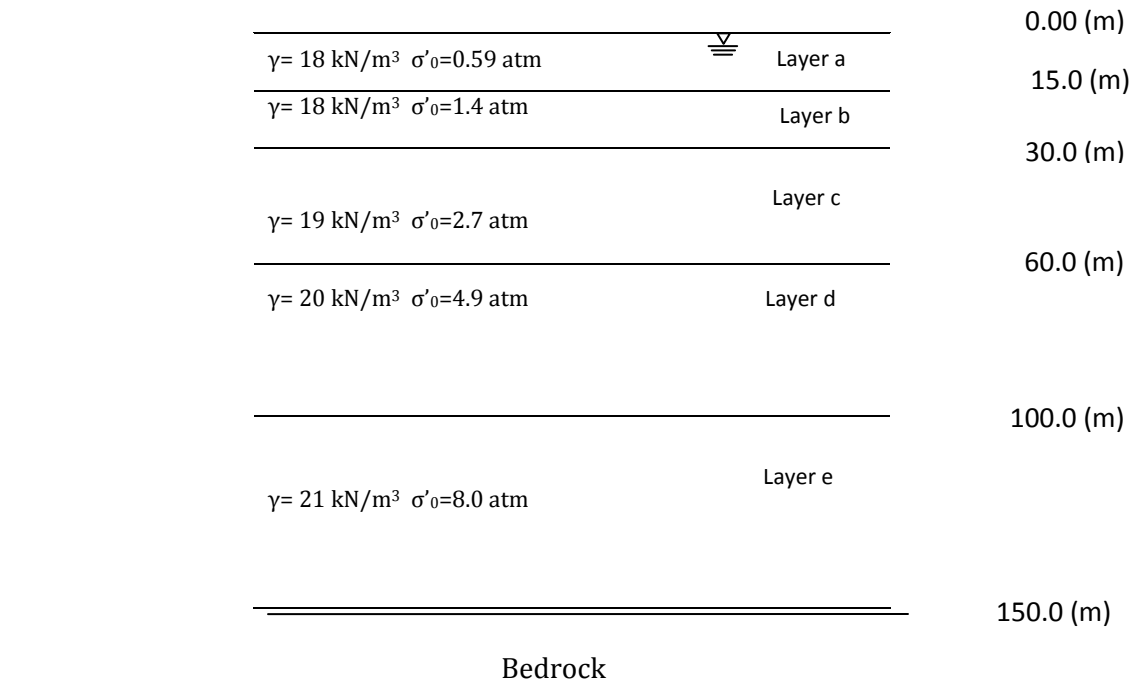

Figure 3.3 Soil layers used to determine the nonlinear soil property curves used in the analyses.

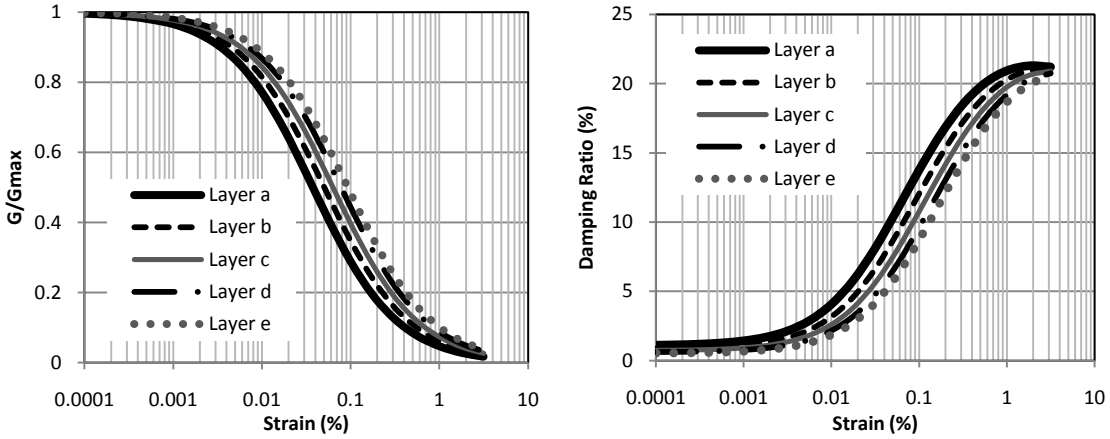

Figure 3.4 Shear modulus and damping curves used in the analyses (PI=10, OCR=1.0).

3.3 Input Motions

The Random Vibration Theory (RVT) approach to equivalent-linear site response analysis is used. The RVT method allows equivalent linear site response to be calculated without the need to specify an input time series. Rather, the RVT method specifies the Fourier Amplitude Spectrum (FAS) of the input motion and propagates the FAS through the soil column using frequency domain transfer functions. The program Strata can generate input FAS from a specified input response spectrum or through seismological theory. For this study, the input motion is specified by seismological theory using the single-corner frequency, ω^2 point source model (Brune 1970). This model and its use in RVT predictions of ground shaking is discussed further in Boore (2003). To specify the input motion, the earthquake magnitude, site-to-source distance, and source depth is provided by user. The other seismological parameters in the model (Table 3.1) are taken from Campbell (2003) and represent typical values for the Western US region.

To consider the nonlinear behavior, the analyses are performed at multiple input intensities. Earthquake magnitude and site-source distance are varied to obtain different input intensities from the seismological method. The magnitude, distance, and depth corresponding used to generate the different input intensities are given in Table 3.2 along with the resulting PGA_{rock}. The range of magnitudes is between 6.5 and 7.8 while the range of Epicentral distances is 6 to 180 km. The resulting

PGA_{rock} values are from 0.01g to 1.5g and the resulting rock response spectra are shown in Figure 3.5.

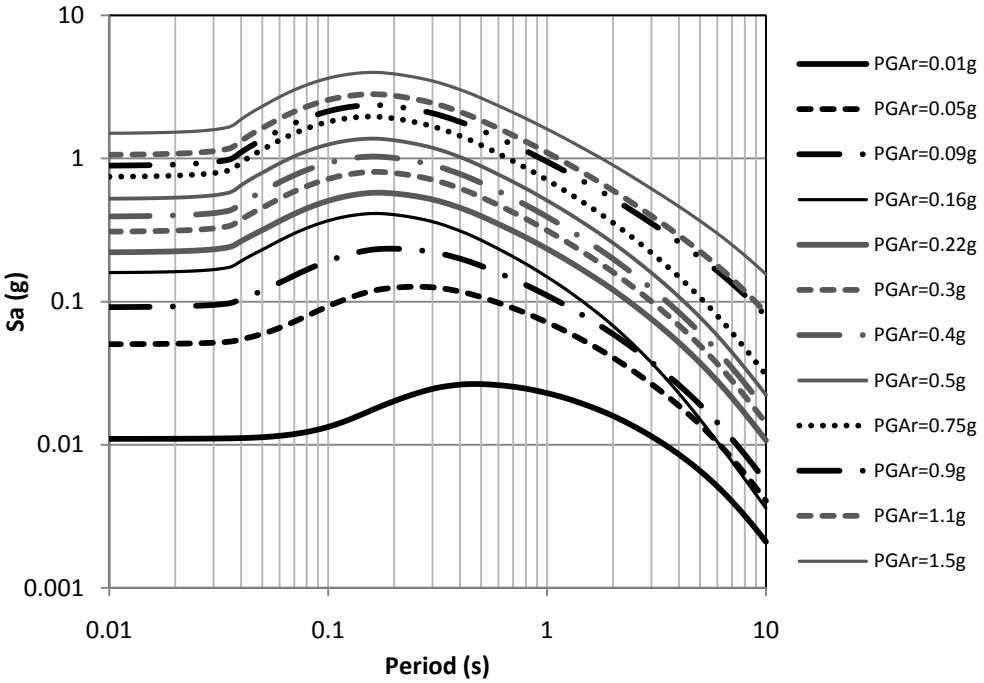

Figure 3.5 Response spectra of RVT input motions.

Table 3.1 Seismological parameters used in single-corner frequency, ω^2 point source model.

Parameter	Value
Stress drop, $\Delta\sigma$ (bar)	100
Path attenuation, $Q(f)=af^b$	
Coefficient a	180
Power b	0.45
Site attenuation, κ_0 (sec)	0.04
Density, ρ (g/cm^3)	2.8
Shear-wave velocity of crust (km/sec)	3.5

Table 3.2 Corresponding magnitude, distance, and depth to input intensities.

Magnitude	Distance (km)	Depth (km)	PGA_{rock}
7.0	180	3	0.01 g
7.0	68	3	0.05 g
7.0	40	3	0.09 g
6.5	20	3	0.16 g
7.0	21	3	0.22 g
7.0	16	3	0.3 g
7.0	21	3	0.4 g
7.0	10	3	0.5 g
7.0	7	3	0.75 g
7.6	9	3	0.9 g
7.5	7	3	1.1 g
7.8	6	3	1.5 g

3.4 Site Characteristics

It is important to understand which spectral periods are influenced by the seismic response of a site. One simple parameter that can be used to consider the period range most affected by a site's response is the site period, T_S. T_S is the period corresponding to first mode and represents the entire V_S profile from the rock to the surface. The site period is estimated as:

$$T_S = 4H/\overline{V}_S \qquad (3.1)$$

where H is the soil thickness and $\overline{V}_S$ is the average shear wave velocity of the soil. $\overline{V}_S$ is computed from the travel time for a shear wave travelling through the entire soil

profile. The V_S profiles developed for a given V_{S30} category, each having same V_{S30} and same V_S profile below 30 m, all have the same T_S. The values of T_S for the five V_{S30} values considered in this study are listed in Table 3.3. T_S ranges from approximately 0.75 to 1.5 s for the five V_{S30} profiles considered.

The detailed velocity structure in the top 30 meters affects site amplification as well. To estimate the period range affected by the top 30 m, another site period corresponding to the top 30 m is defined and called T_{30}. T_{30} is computed as:

$$T_{30} = 4(30\text{ m})/V_{S30}\text{ (m/s)} \qquad (3.2)$$

where V_{S30} is the average shear wave velocity in the top 30 meters of the site. Table 3.3 presents T_{30} values for the five V_{S30} categories. T_{30} ranges from approximately 0.2 to 0.55 s for the five V_{S30} profiles considered.

T_S and T_{30} decrease as V_{S30} increases because the period is inversely proportional to V_S. Therefore, stiffer sites have shorter site periods and shorter periods are affected most by the site' amplification. The T_S for each category of V_{S30} is greater than its corresponding T_{30} because T_S is associated with the entire depth of the profile and T_{30} with only the top 30m.

Table 3.3 T_S and T_{30} values for each V_{S30}.

V_{S30} (m/s)	T_S (sec)	T_{30} (sec)
225	1.54	0.53
280	1.45	0.43
350	1.10	0.34
450	0.87	0.27
550	0.72	0.22

To further investigate the period range in which the detailed velocity structure in the top 30 m V_S profile affects the response, 1D frequency domain transfer functions are computed for different profiles. A transfer function describes the ratio of the Fourier Amplitude Spectrum (FAS) of acceleration at any two points in the soil column. Figure 3.6 plots the acceleration transfer functions between the surface and the bedrock outcrop for three selected velocity profiles in the V_{S30}=225 and 450 m/s categories. The soil properties are assumed linear elastic for calculating these transfer functions. The transfer functions are plotted versus period in Figure 3.6 and the corresponding periods for T_{30} and T_S are indicated. For periods near T_S, the transfer functions of different profiles in the same V_{S30} category are very similar because the transfer function in this period range is controlled by the full V_S profile. Starting at periods around T_{30} and at periods shorter than $T_{30,}$ the transfer functions vary significantly between the different profiles even though they have the same V_{S30}. This variability in the transfer function illustrates the influence of the details of

the top 30 m V_S profile in this period range. It can be concluded that the details of the top 30 m of a site are important at periods shorter than T_{30}. As a result, the period range influenced by the top 30 m depends on V_{S30} (since T_{30} is V_{S30} dependent). Because the transfer functions in Figure 3.6 are for linear-elastic conditions, an additional consideration will be the influence of input intensity and soil nonlinearity. As the input intensity increases the soil becomes more nonlinear, both T_S and T_{30} will shift to long periods. As a result, the period range affected by the top 30 m will increase to longer periods as input intensity increases.

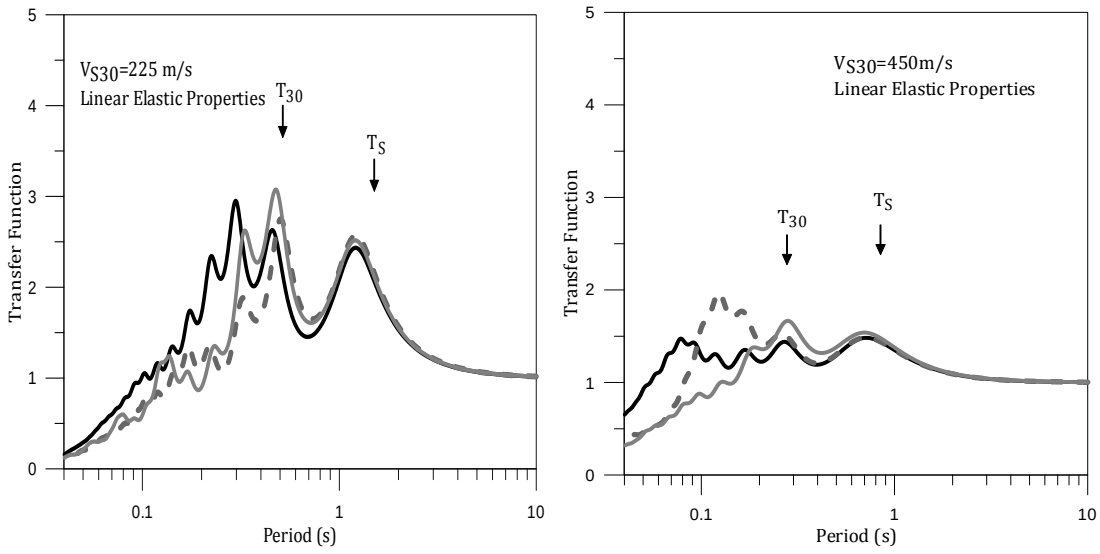

Figure 3.6 Linear-elastic transfer function for 3 selected sites in V_{S30}=225 and 450 m/s.

All the generated profiles in each category of V_{S30} have the same value of V_{S30} but a different V_S structure in the top 30 meters. Several parameters are identified from the velocity profiles as candidates that affect the computed site amplification. These parameters are V_{min}, thV_{min}, $depthV_{min}$, MAXIR and Vratio. These parameters are defined as:

- V_{min} is the minimum shear wave velocity in the V_S profile
- thV_{min} is the thickness of the layer with the minimum shear wave velocity
- $depthV_{min}$ is the depth to the top of the layer with V_{min}
- MAXIR is the maximum impedance ratio within the V_S profile as defined by the ratio of the V_S of two adjacent layers ($V_{s,upper}$ / $V_{s,lower}$)
- Vratio is the ratio of the average shear wave velocity ($\overline{Vs}$) between 20 m and 30 m to the average shear wave velocity in top 10 m. Vratio is defined as:

$$\text{Vratio} = \frac{V_{S(20-30)}}{V_{S(10)}} \tag{3.3}$$

Where

$$V_{S(20-30)} = \frac{10\text{ m}}{\sum \frac{h_{iS}}{V_{S,i}}} \quad \text{for depths 20 to 30 m} \tag{3.4}$$

and

$$V_{S10} = \frac{10\text{ m}}{\sum \frac{h_{iS}}{V_{S,i}}} \quad \text{for depths 0 to 10 m} \tag{3.5}$$

The concept of Vratio is similar to the impedance ratio for MAXIR, except that it represents a more global impedance ratio in the top 30 m. It also has the advantage of using information from a significant portion of the top 30 m of a profile, and it also indicates how much the shear wave velocity increases in top 30 m. Vratio can also indicate if a large scale velocity inversion occurs in the top 30 m when it takes on values less than 1.0

To minimize the effect of soil nonlinearity both in studying the variability in AF and the parameters that affect the variability, low levels of shaking are considered first. To generalize the results of the study, larger level of shaking are then considered.

3.5 Amplification at Low Input Intensities

3.5.1 Variability in Amplification Factors

Based on the existing empirical models of site amplification, all sites with the same V_{S30} and $Z_{1.0}$ should have the same AF. Figure 3.7 plots amplification factor versus period for all of the generated sites for each of the V_{S30} categories subjected to the lowest input intensity (0.01g). The amplification factors for a given V_{S30} are not constant and show significant scatter. The amount of scatter (i.e. variability) varies with V_{S30} and period. At smaller V_{S30}, the variability in the amplification factors is more significant. The period range in which the variability in AF is most significant

also depends on V_{S30}. As V_{S30} increases, this period range decreases. At periods greater than T_{30}, less variability is observed. The period at which the maximum variability in the AF occurs is also V_{S30} dependent. For V_{S30}=225 m/s, the maximum variability is observed at a spectral period of 0.3 sec. Stiffer sites (V_{S30}=280 m/s and 350 m/s) display the maximum variability at a spectral period of 0.2 sec and the stiffest sites (V_{S30}=450 m/s and 550 m/s) display the maximum variability at a spectral period of 0.1s.

To quantify the variability in AF, the standard deviation of ln(AF) at each period for each category of V_{S30} is calculated. The standard deviation (σ_{lnAF}) is calculated for the ln(AF) because ground motions are commonly assumed to be log-normally distributed and to be consistent with its use in ground motion prediction equations (see Section 2.2). Figure 3.8 shows the σ_{lnAF} values computed from the data in Figure 3.7. σ_{lnAF} smaller than about 0.05 is considered small enough such that the variability is minimal. The data in Figure 3.8 show that σ_{lnAF} is greater than 0.05 at periods less than about T_{30} for each V_{S30}, which is consistent with the observations from the transfer functions. Additionally, the values of σ_{lnAF} are V_{S30} dependent, with sites with smaller V_{S30} producing larger values of σ_{lnAF}.

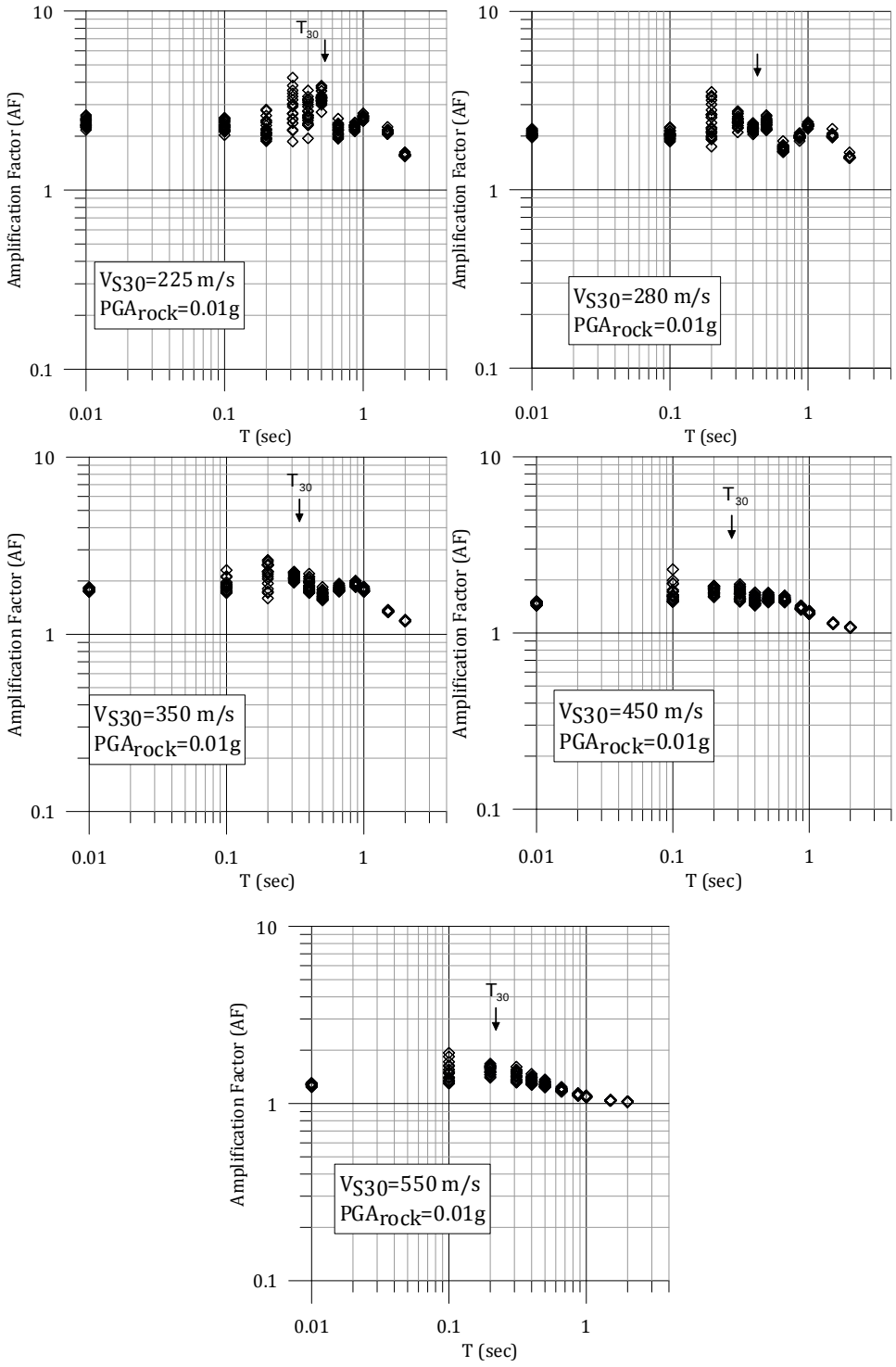

Figure 3.7 Amplification factor vs. period for all the generated profiles, PGA_{rock}=0.01g.

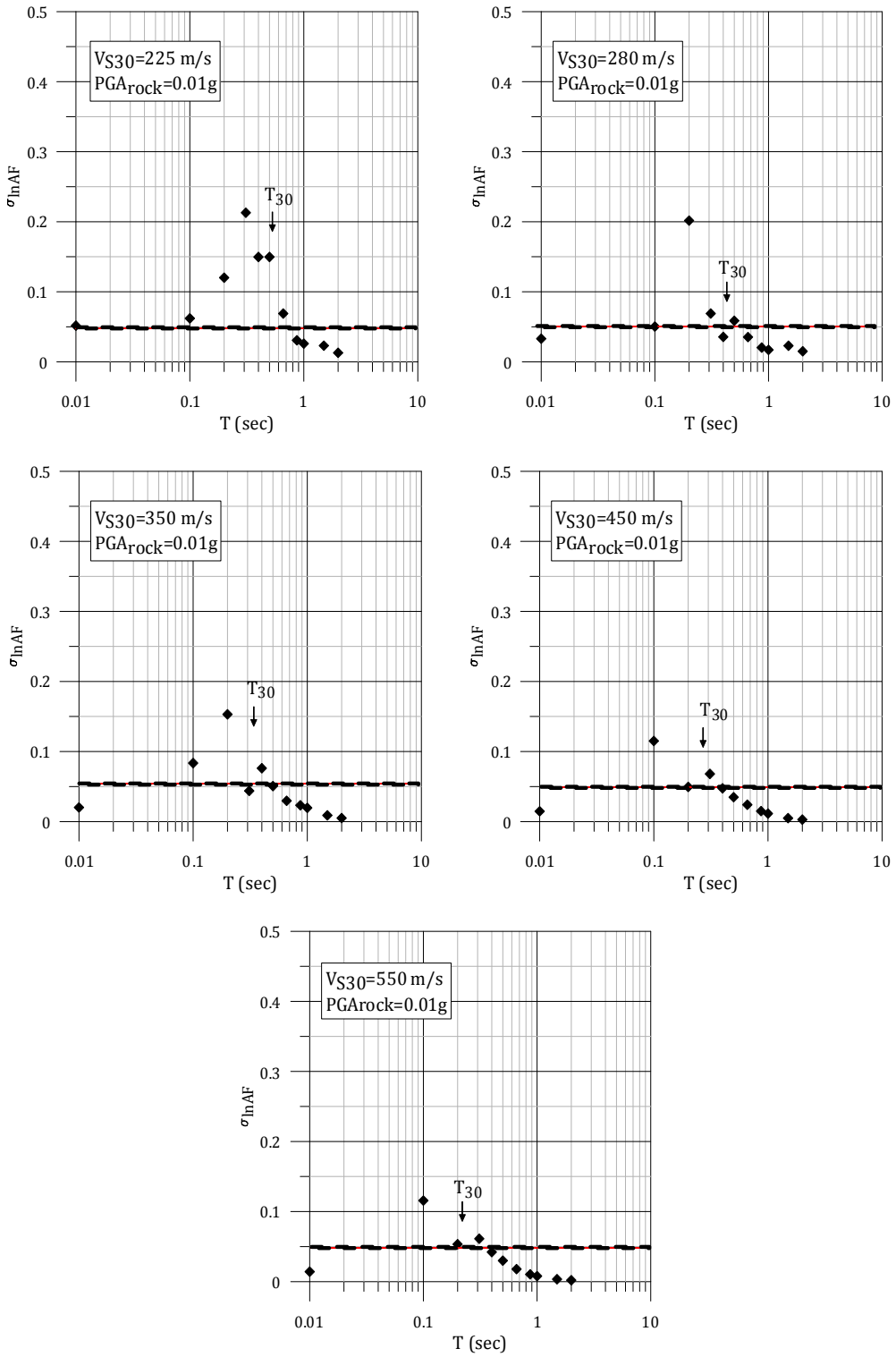

Figure 3.8 σ_{lnAF} versus period for all the generated profiles, PGA_{rock}=0.01g.

3.5.2 Identification of site parameters that explain variation in AF

The identification of the site parameters that explain the variability in AF is initiated by relating the data in Figure 3.7 to various site parameters. Considering the periods that have large σ_{lnAF} values, only periods of 0.1 s, 0.2 s, and 0.3 s will be considered here.

To investigate the site parameters that explain the variability in AF, the difference between each ln(AF) and the average ln(AF) for a given period, input intensity, and V_{S30} is considered. This difference represents the residual and is defined as:

$$\text{Residual} = \ln(AF) - \mu_{lnAF} \tag{3.6}$$

where ln(AF) represents the AF for a single V_S profile with a given V_{S30} and μ_{lnAF} is the average ln(AF) for all sites with the same V_{S30} (Figure 3.9).

The residual measures the difference between a specific value of AF and the average value of AF for all sites with the same V_{S30} for a given period and input intensity. If a trend is observed between the calculated residuals and a site parameter, then that parameter influences site amplification and potentially should be included in predictive models for AF to reduce its variability. As mentioned previously, the minimum velocity in the profile (V_{min}), the thickness of the layer with the minimum velocity (thV_{min}), the depth to the layer with the minimum velocity

(depthV_{min}), the maximum impedance ratio (MAXIR), and Vratio are the site characteristics that are considered.

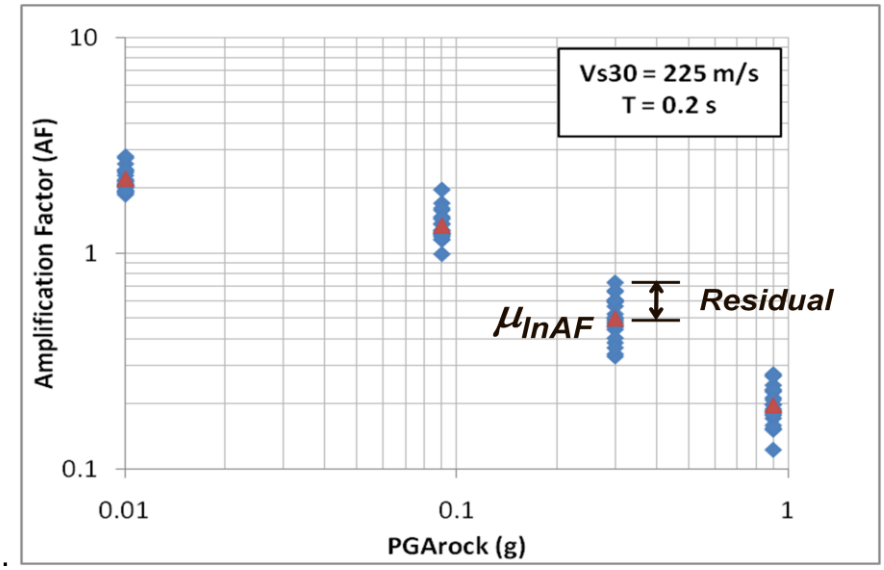

Figure 3.9 Definition of calculated residual.

The first candidate parameter is V_{min}. While the absolute value of V_{min} is important, its value relative to V_{S30} provides information about the range of velocities within the top 30 meters. To consider the relative effect of V_{min}, residuals are plotted versus V_{S30}/V_{min} instead of V_{min}. The minimum value of V_{S30}/V_{min} is 1.0, which represents a site with constant velocity equal to V_{S30} in the top 30 meters. Larger values of V_{S30}/V_{min} indicate smaller values of V_{min}. Figure 3.10 shows the residuals versus V_{S30}/V_{min} for all V_{S30} categories at a spectral period of 0.2 s and PGA_{rock}=0.01g. For V_{S30}≤350m/s the residuals generally increase with increasing V_{S30}/V_{min}, while there is little influence of V_{S30}/V_{min} on the residuals for V_{S30}=450

and 550 m/s. However, as shown in Figure 3.8, there is little variability in AF for sites with V_{S30} = 450 and 550 m/s at this period ($\sigma_{lnAF} \sim 0.05$).

Other parameters that may influence AF are thV_{min}, MAXIR, $depthV_{min}$ and Vratio. In all the generated profiles in this study, the minimum velocity occurs at the ground surface, such that all profiles have $depthV_{min}$ equal to zero. Thus, this parameter cannot be considered with the present dataset. The residuals versus thV_{min}, MAXIR, and Vratio for a spectral period of 0.2 s and PGA_{rock}=0.01g are plotted in Figure 3.11, 3.12, and 3.13, respectively. The relationship between the residuals and thVmin is quite weak (Figure 3.11). The relationship between the residuals and MAXIR (Figure 3.12) is stronger, particularly for V_{S30} = 280 m/s and 350 m/s, but the relationship is weak for V_{S30}=225 m/s. The relationship between the residuals and Vratio (Figure 3.13) is very strong for V_{S30} = 280 m/s and 350 m/s, and moderately strong for V_{S30}=225 m/s.

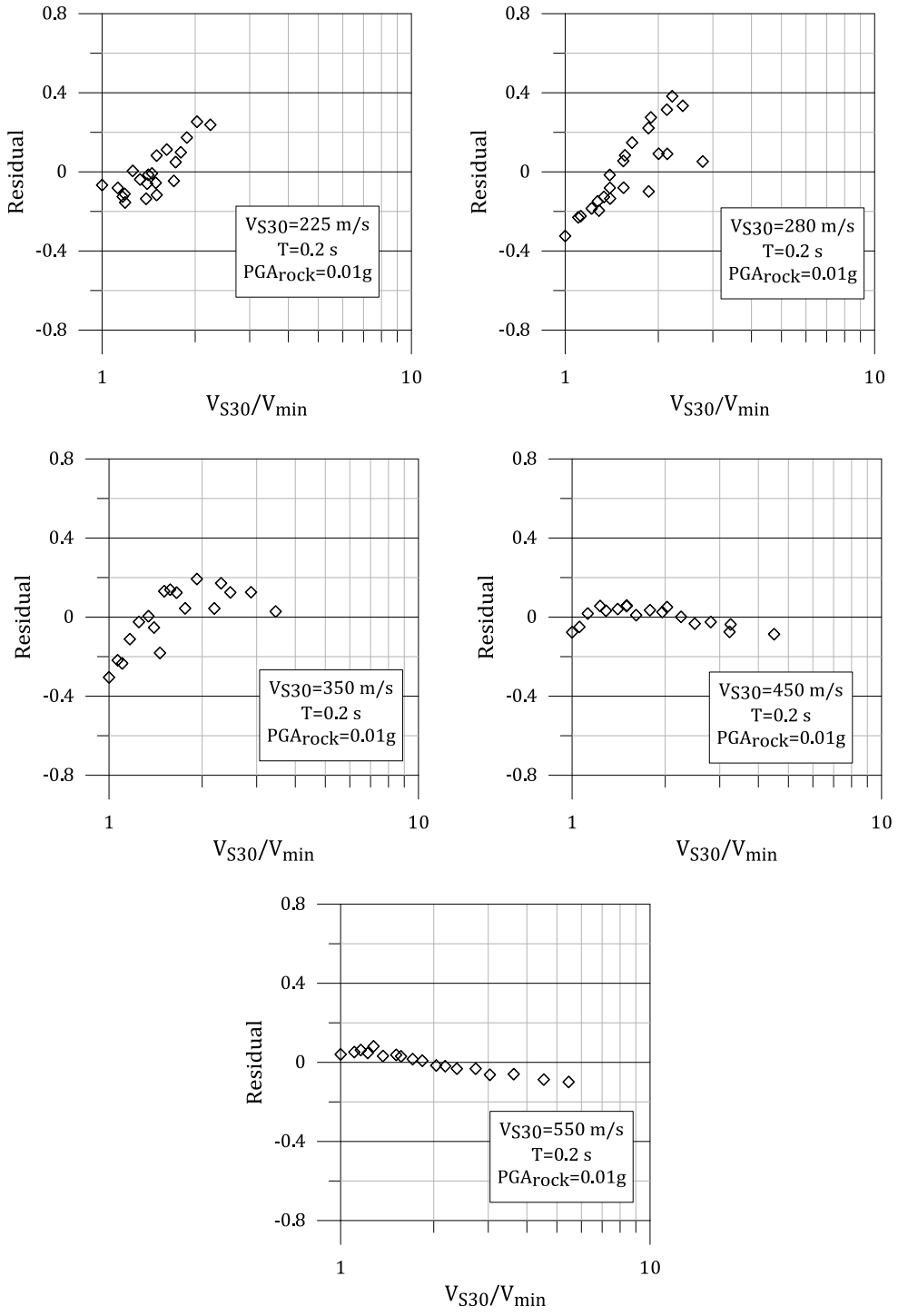

Figure 3.10 Residual versus V_{S30}/V_{min} for all the profiles at spectral period of 0.2 s and PGA_{rock}=0.01g.

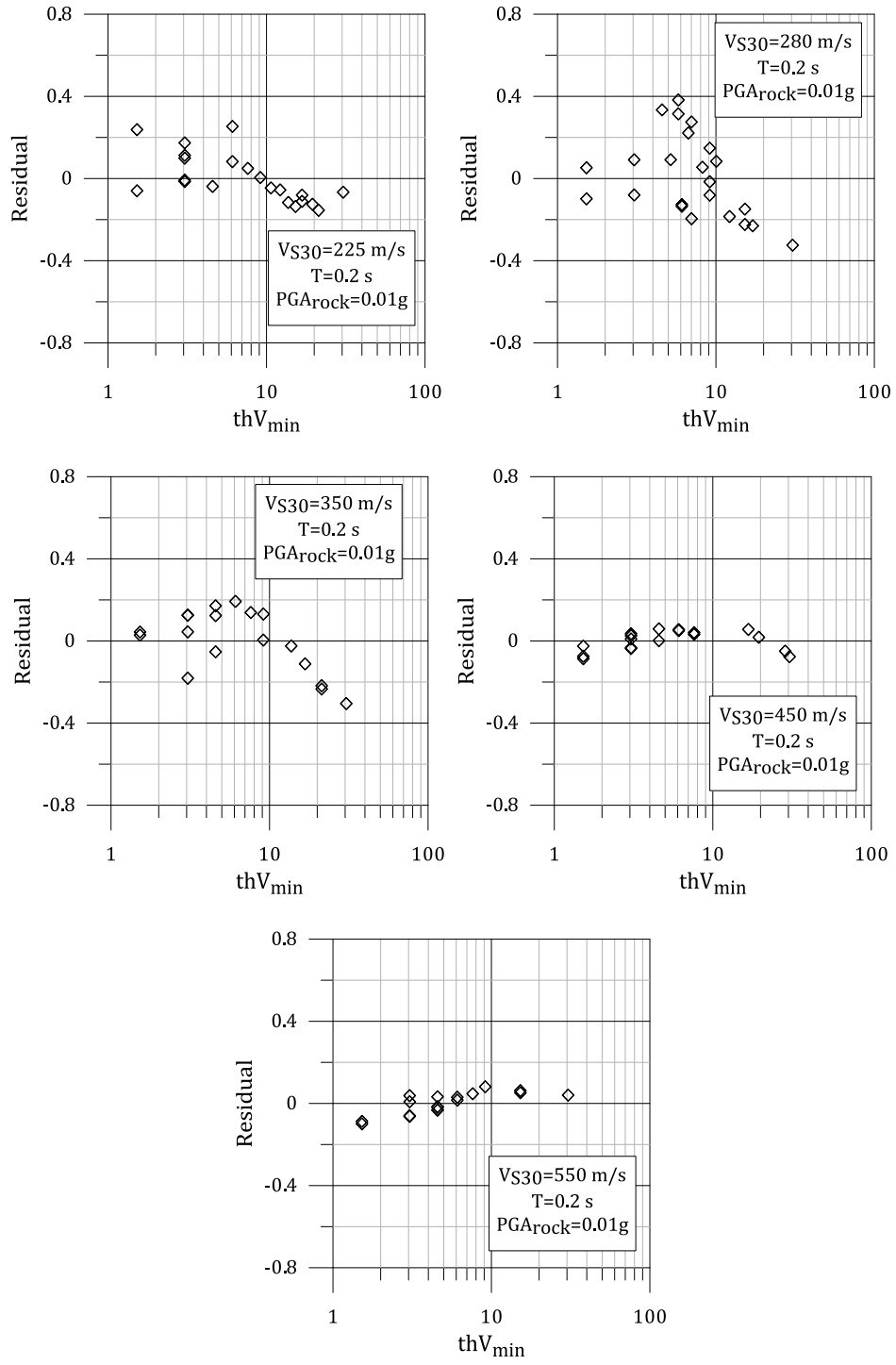

Figure 3.11 Residual versus thV_{min} for all the profiles at spectral period of 0.2 s and PGA_{rock}=0.01g.

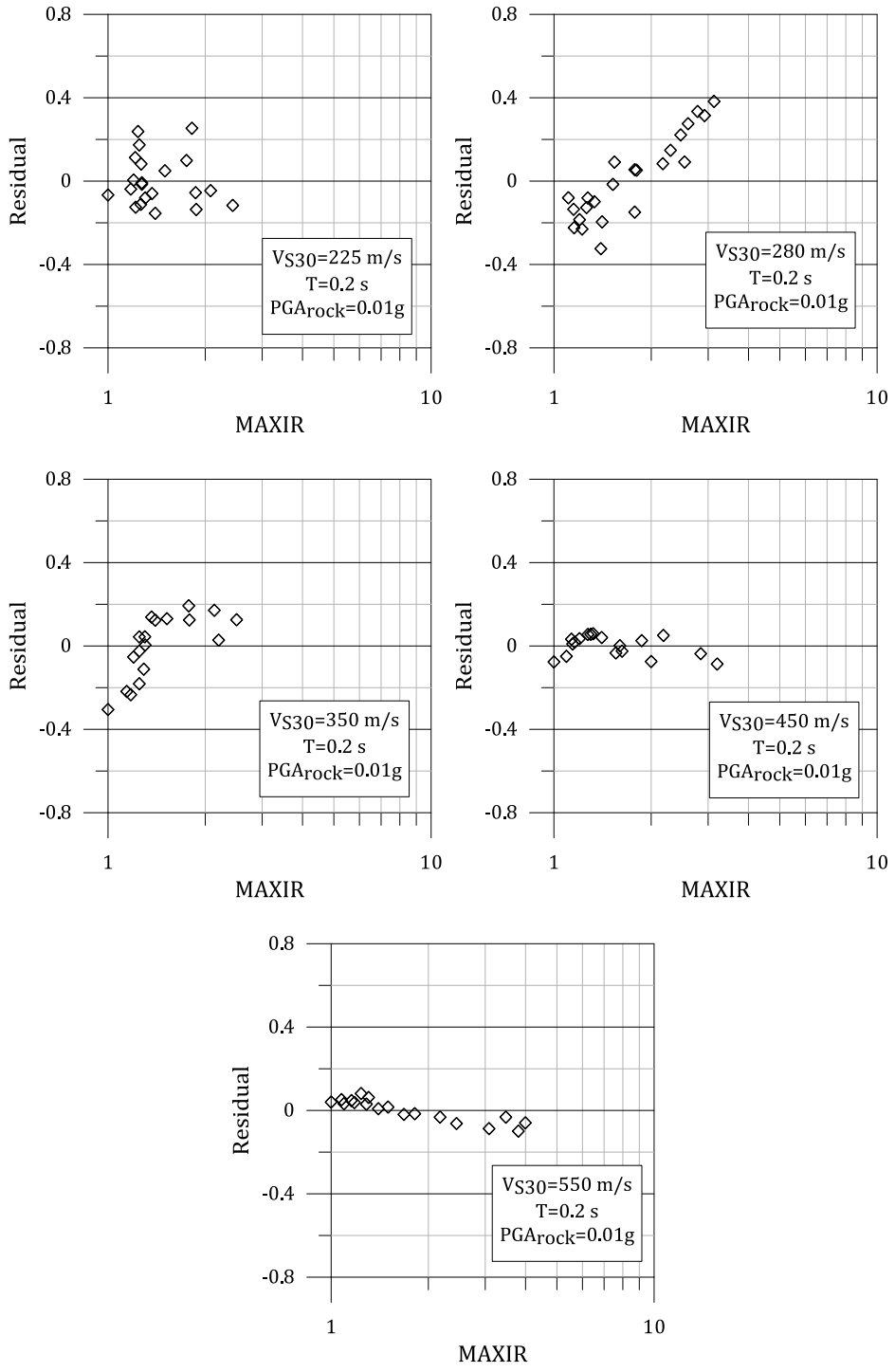

Figure 3.12 Residual versus MAXIR for all the profiles at spectral period of 0.2 s and PGA_{rock} =0.01g.

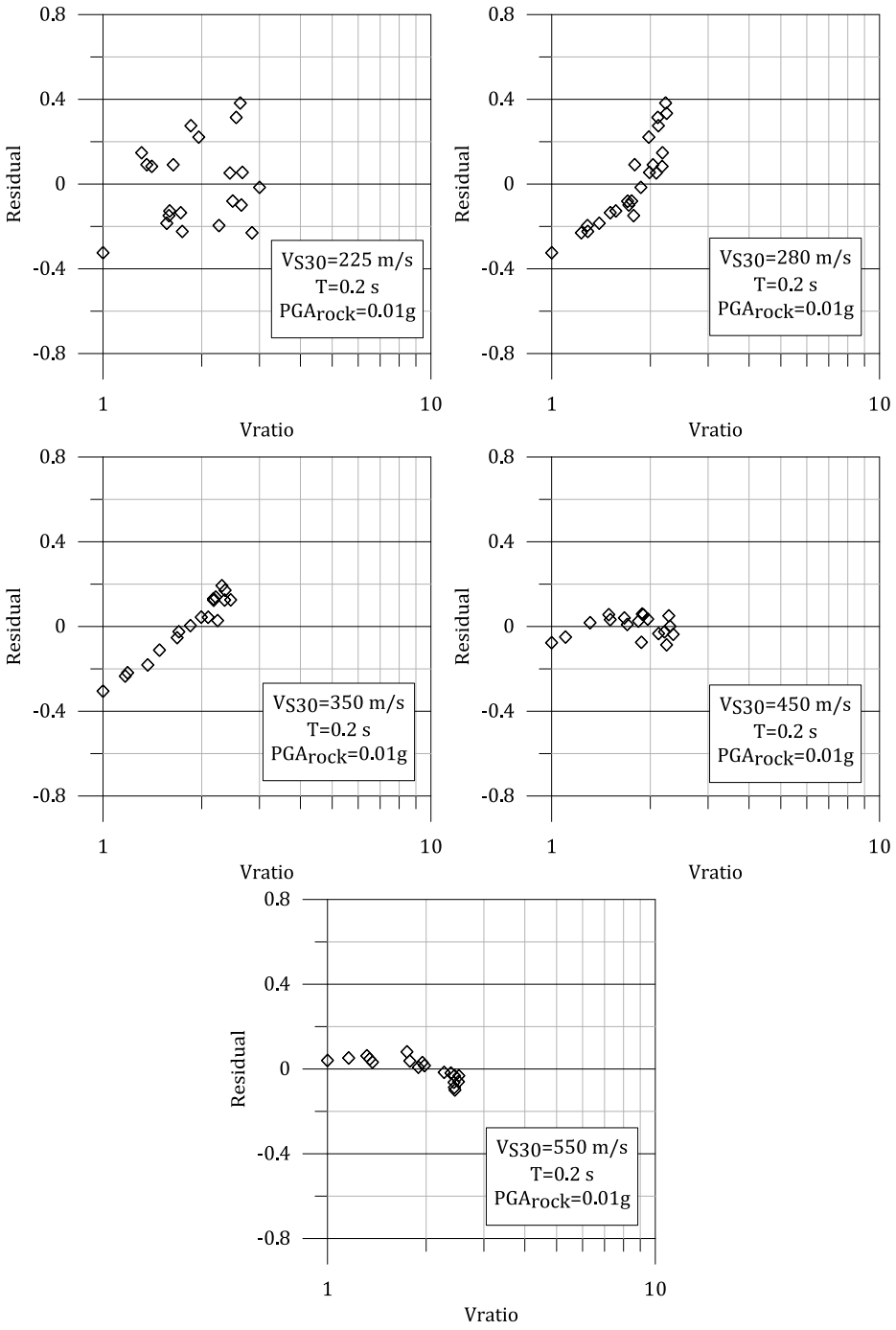

Figure 3.13 Residual versus Vratio for all the profiles at spectral period of 0.2 s and PGA_{rock} =0.01g.

Evaluating the relationship between the residuals and the four parameters, Vratio is considered to best explain the variability in AF at this spectral period because the relationship between that residuals and Vratio is stronger than the three other parameters. Generally a linear relationship between the residual and ln(Vratio) is observed. Considering σ_{lnAF} in Figure 3.8, the variability in AF is significant for periods of 0.1s, 0.2s, and 0.3s for most of the V_{S30} values. Figures 3.14 and 3.15 show the residuals versus Vratio for PGA_{rock}=0.01g at spectral period of 0.1 s and 0.3 s respectively. A strong linear relationship is still observed between the residuals and ln (Vratio). However, the intercept and slope of the linear fit is V_{S30} and period dependent.

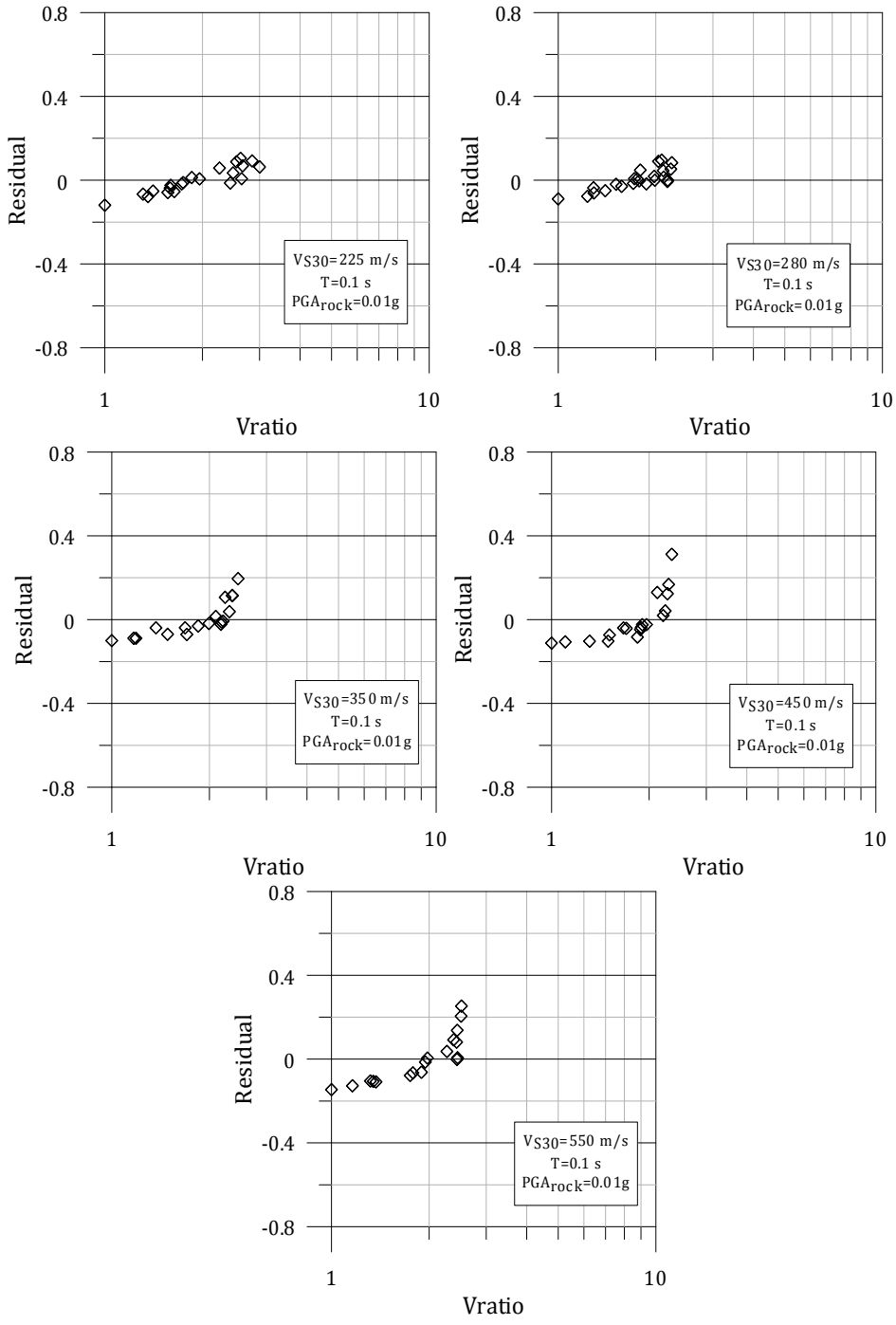

Figure 3.14 Residual versus Vratio for all the profiles at spectral period of 0.1 s and PGA_{rock}=0.01g.

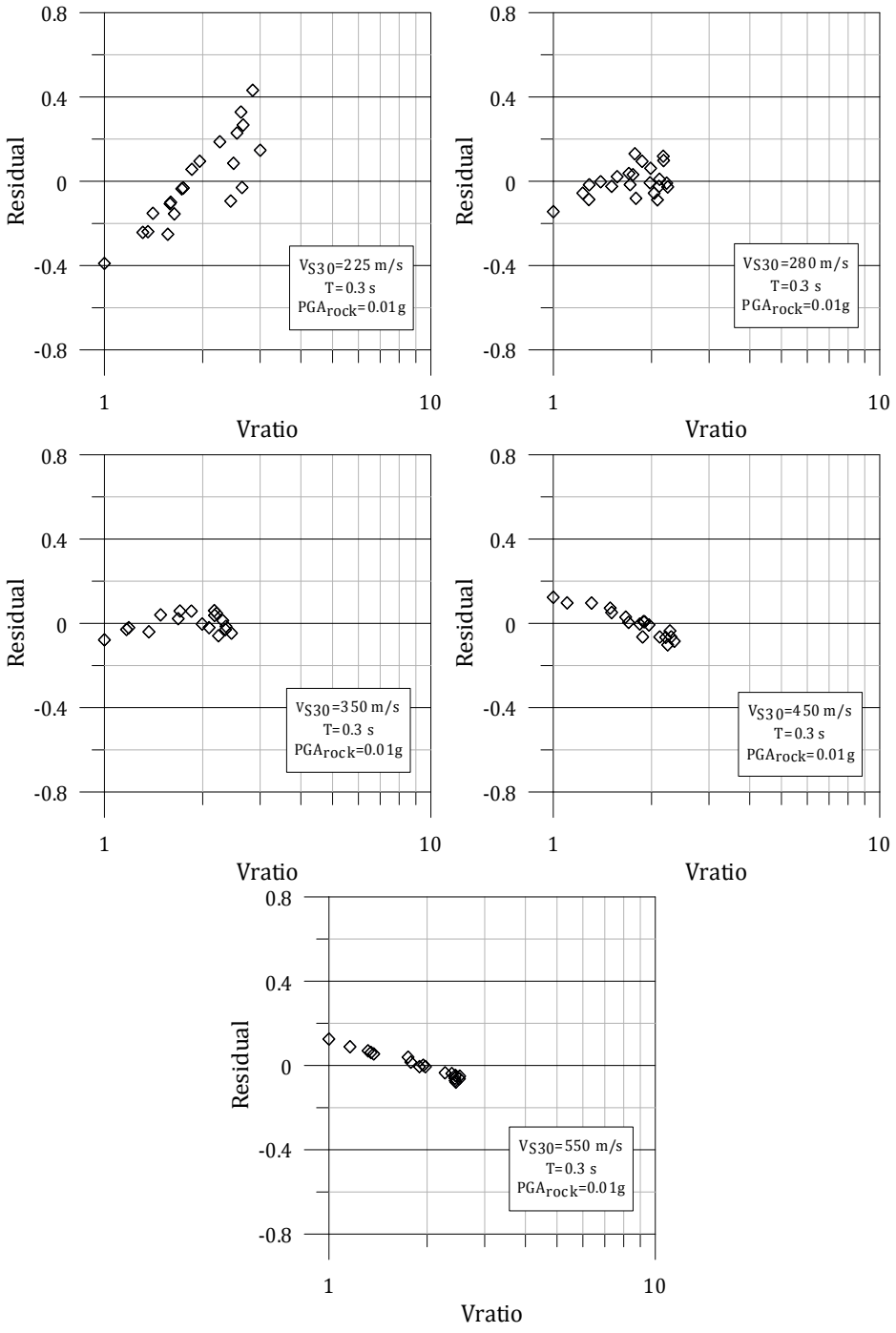

Figure 3.15 Residual versus Vratio for all the profiles at spectral period of 0.3 s and PGA_{rock}=0.01g.

3.6 Amplification at Moderate Input Intensities

3.6.1 Variability in Amplification Factors

Soil layers show nonlinear behavior at larger input intensities because large strains are induced which soften the soil and increase the material damping. Therefore, amplification becomes a nonlinear function of input intensity at higher shaking levels. To investigate the variability in AF at moderate intensities, the results for PGA_{rock}=0.3g are presented.

In Figure 3.16, AF versus period is shown for all the generated sites at PGA_{rock}=0.3g. Comparing the AFs at each spectral period in Figure 3.16 with those in Figure 3.7 for PGA_{rock}=0.01g, it is clear that there is an increase in amplification variability. Figure 3.17 shows σ_{lnAF} versus period for each V_{S30} category for the AF results shown in Figure 3.16. The largest values of σ_{lnAF} are observed at V_{S30}=225 m/s. All the periods in this category of V_{S30} have significant variation in AF (i.e. σ_{lnAF} >0.05). σ_{lnAF} is as large as 0.4 at T=0.66 s for this value of V_{S30}. For all sites with V_{S30} ≤ 350 m/s, σ_{lnAF} is significant at almost all periods considered (≤ 2.0 s). The maximum value of σ_{lnAF} occurs at longer periods as V_{S30} decreases. Comparing each V_{S30} category subjected to PGA_{rock}=0.3g to their corresponding profiles subjected to PGA_{rock}=0.01g, the period range with σ_{lnAF} greater than 0.05 increases. The maximum σ_{lnAF} occurs generally at longer periods for PGA_{rock}=0.3g than for

PGA_{rock}=0.01g. These observations indicate that the period range which is affected by the details in the top 30 m V_S profile increases as the shaking level increases.

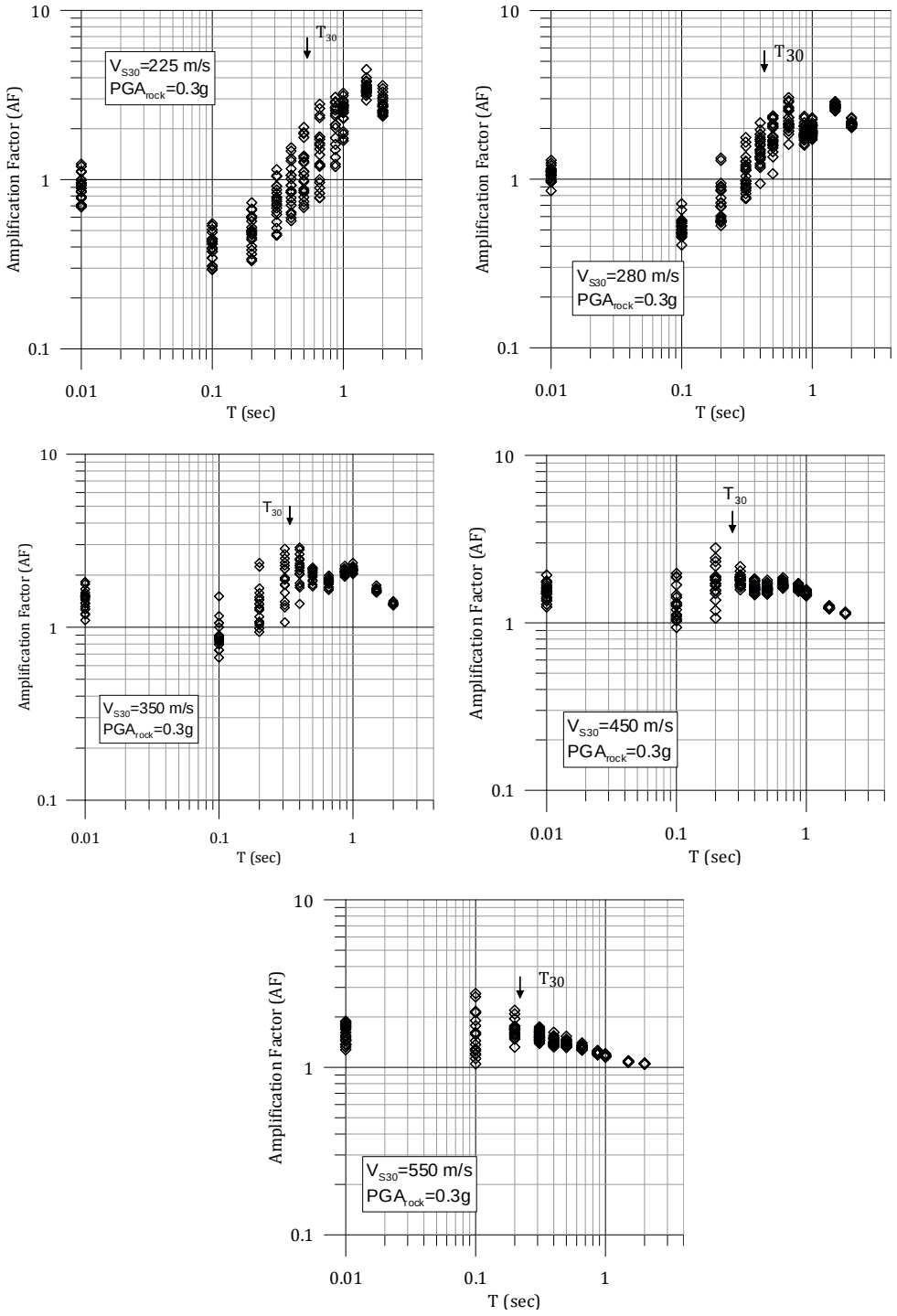

Figure 3.16 Amplification factor versus period for all the generated profiles, PGA_{rock}= 0.3g.

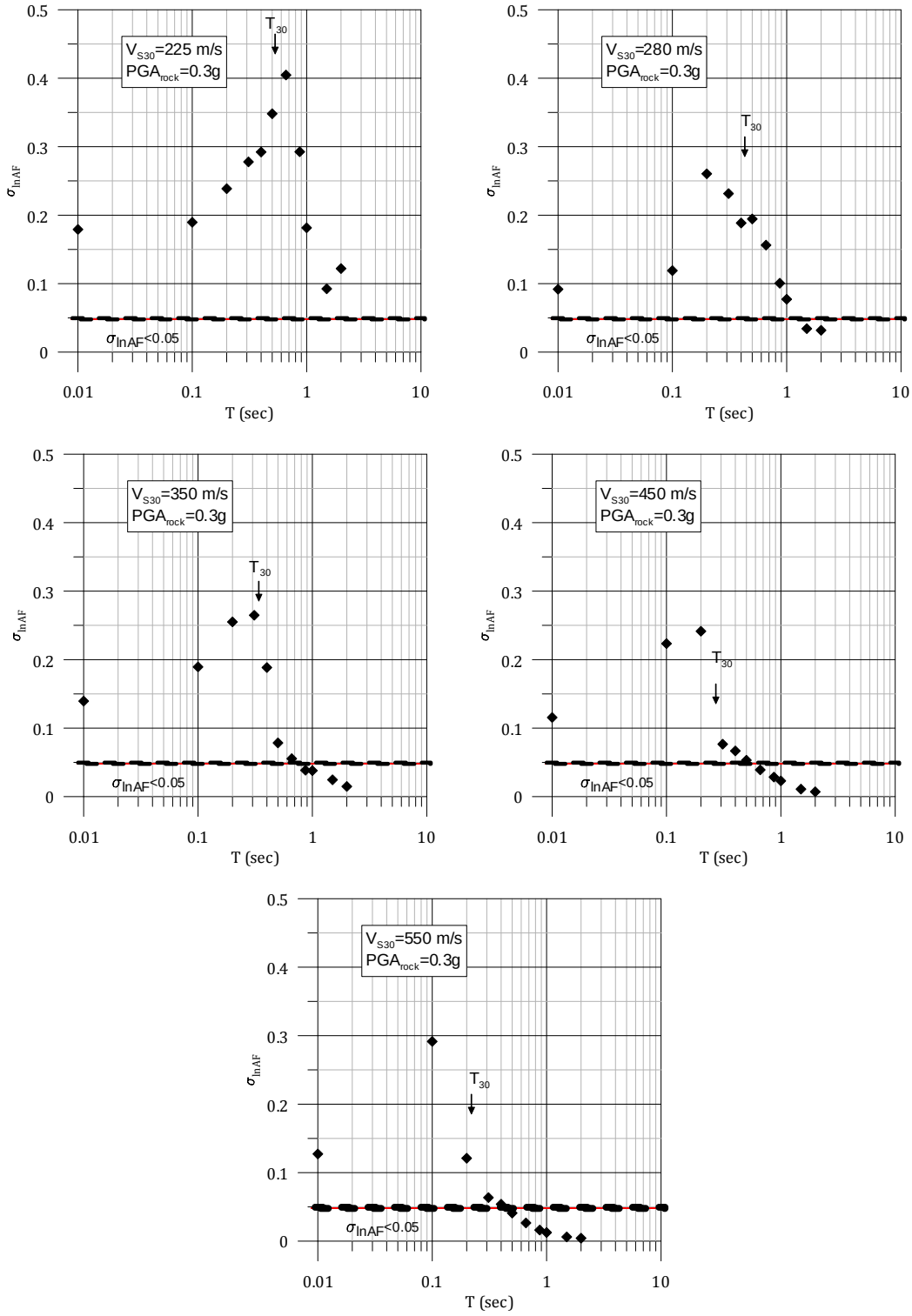

Figure 3.17 σ_{lnAF} versus period for all the generated profiles, PGA_{rock}=0.3 g.

3.6.2 Influence of site parameters on site amplification

Considering the periods of maximum σ_{lnAF} in Figure 3.17, the residuals are investigated at periods of 0.2 s (period of maximum σ_{lnAF} for V_{S30}=280 and 450 m/s), 0.66 s (period of maximum σ_{lnAF} for V_{S30}=225 m/s) and T=1.0 s (period of large σ_{lnAF} for V_{S30}=225 m/s).

The residuals for the AF results for PGA_{rock}=0.3g at a spectral period of 0.2 s are plotted versus Vratio in Figure 3.18. Generally, a linear trend between the residuals and ln(Vratio) is observed, similar to the results for PGA_{rock}=0.01g. However, the relationship appears to break down at small V_{S30} (i.e., 225 and 280 m/s) and larger Vratio (i.e., 2 to 3). Figure 3.19 plots the velocity profiles over the top 30 m for four V_{S30} = 225 m/s sites with Vratio around 2.5 but very high residuals (+0.4) and very low residuals (-0.4) in Figure 3.18. The profiles with very low residuals have a thick, soft layer (i.e., layer with $V_S \leq 160$ m/s and thickness > 10 m) with a large impedance ratio (i.e., MAXIR) immediately below. The MAXIR is well above 2.0 for these profiles, while the profiles with large residuals have MAXIR of between 1.5 and 1.7. The induced shear strains for the four profiles are also shown in Figure 3.19. The large MAXIR leads to significant shear strains, in excess of 2%, in the layers above the depth of MAXIR. The rapid increase in strain across the impedance contrast induces a rapid change in stiffness and damping which reduces the amplification at high frequencies. While the sites with large residuals also experience large strains (~ 1 to 1.5%), the increase in strain with depth is not as

rapid and that allow for more wave motion to travel through the soil. The data in Figures 3.18 and 3.19 indicate that sites with very large MAXIR may experience very large strains at moderate input motion intensities, which leads to smaller amplification.

The maximum value of σ_{lnAF} for V_{S30}=225 m/s occurs at T=0.66 s, while the value of σ_{lnAF} is also significant at a spectral period of 0.66 s for V_{S30}=280 m/s (Figure 3.17). Figure 3.20 shows the residuals versus Vratio for all the generated sites subjected to PGA_{rock}=0.3g at spectral period of 0.66 s. For $V_{S30} \geq 350$ m/s, the residuals are almost zero at this spectral period because σ_{lnAF} is less than 0.05 (Figure 3.17). However a linear trend is generally observed between the residuals and ln(Vratio) for the softer profiles (V_{S30}=225 and 280 m/s). However, the data is scattered for V_{S30}=225 m/s and Vratio greater than about 2.3. These are the same sites discussed in Figure 3.19, and the scatter is due to the large MAXIR and thick soft layers in the profiles. Figure 3.21 shows the residual versus Vratio for T=1.0. For V_{S30}=225 m/s, a linear trend is observed between the residuals and ln(Vratio) except for sites with Vratio greater than 2.3, as discussed previously. Generally at all periods where the variability in amplification is significant (i.e., σ_{lnAF} >0.05), the calculated residuals for these AF have a linear trend with ln(Vratio). However, there are some profiles that break down this trend. These profiles tend to have a thick, very soft layer near the surface that may be unrealistic.

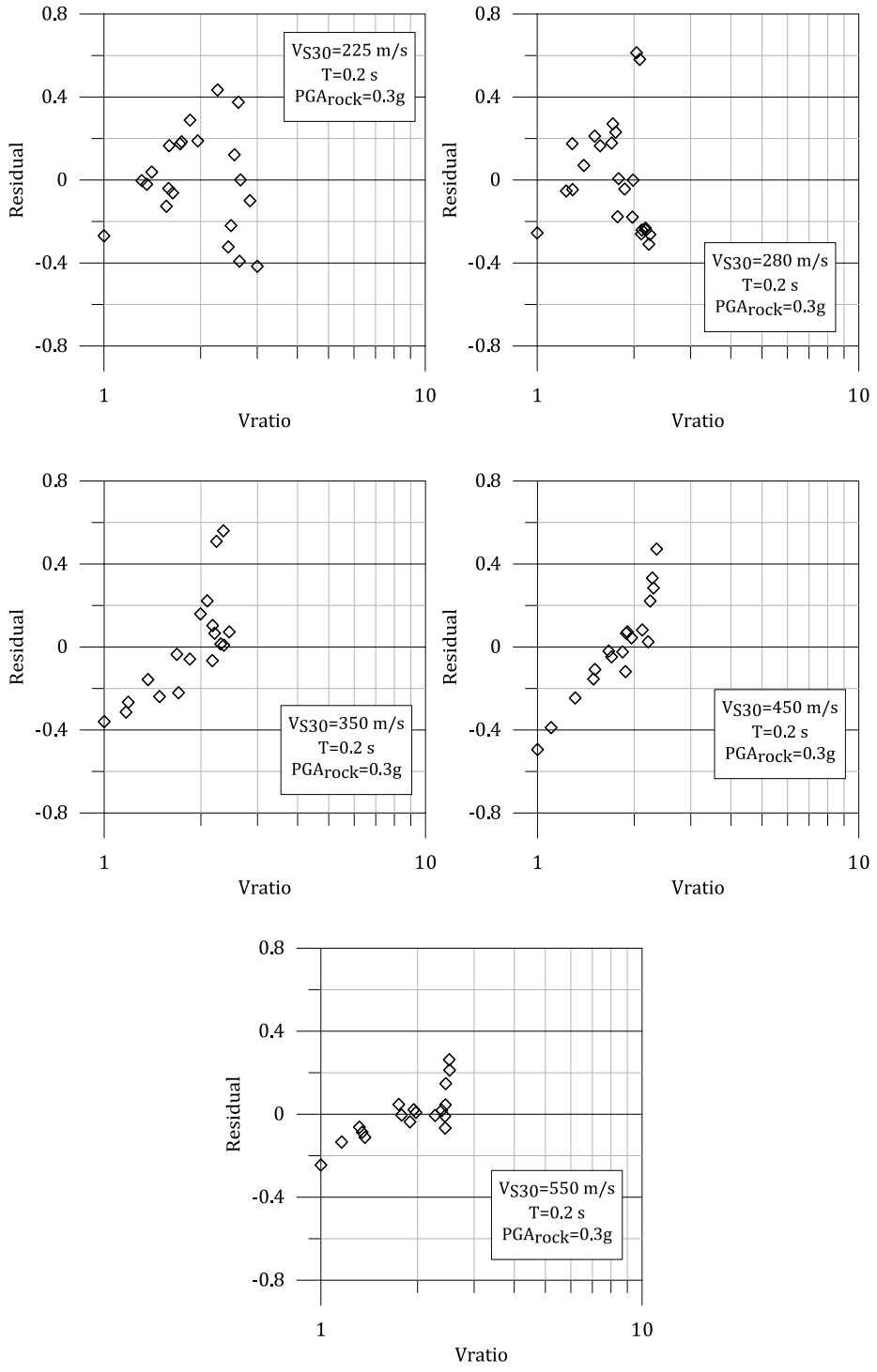

Figure 3.18 Residual versus Vratio for all the profiles at spectral period of 0.2 s and PGA_{rock}=0.3g.

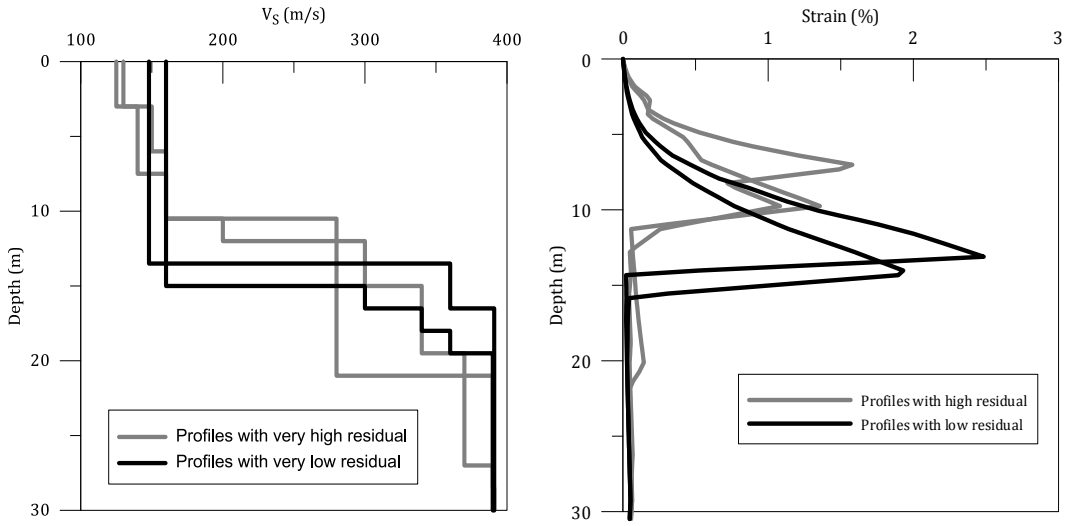

Figure 3.19 V_S profile for sites with Vratio ~ 2.5 but very low and very high residuals and the induced shear strains.

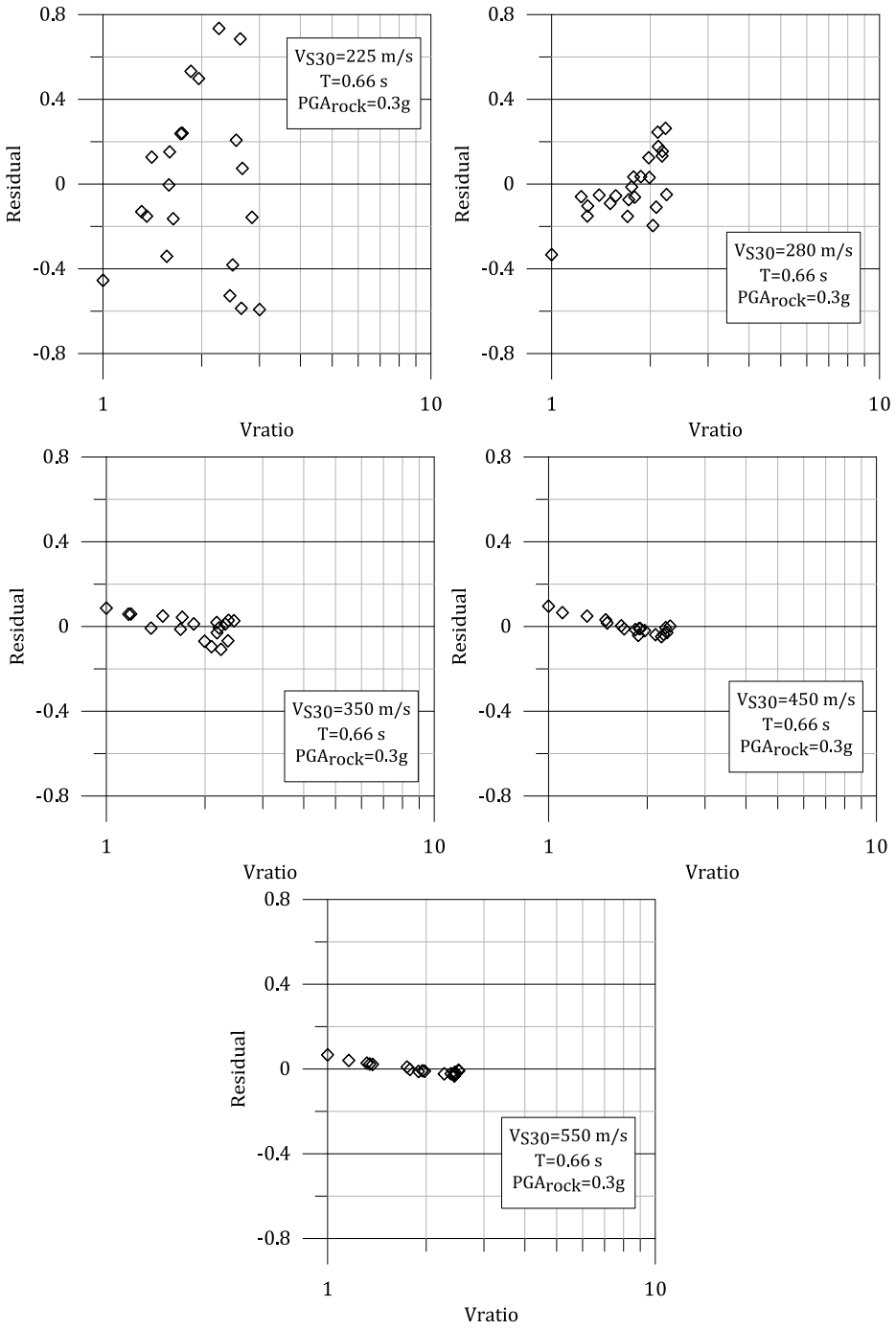

Figure 3.20 Residual versus Vratio for all the profiles at spectral period of 0.66 s and PGA_{rock}=0.3.

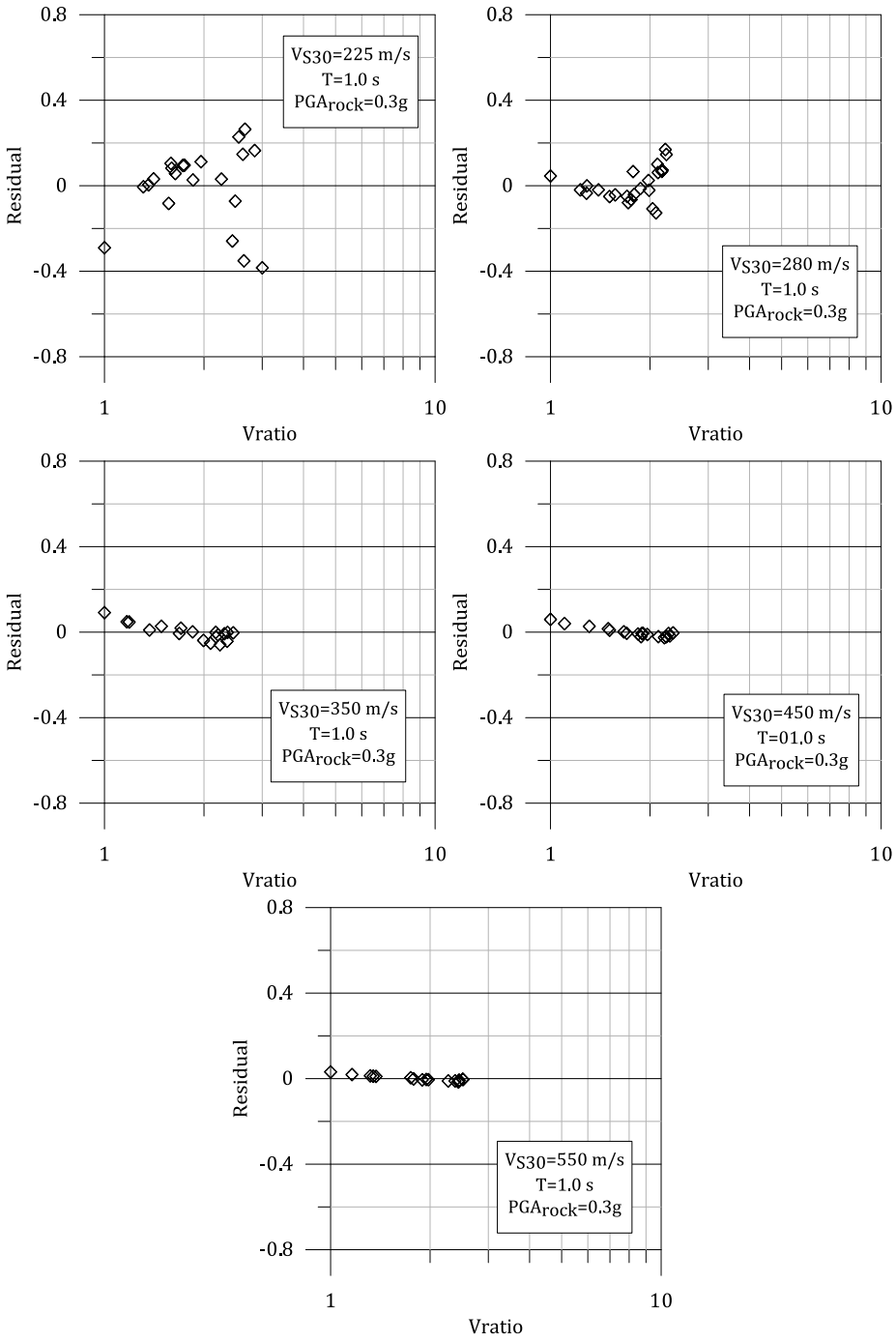

Figure 3.21 Residual versus Vratio for all the profiles at spectral period of 1.0 s and PGA_{rock}=0.3g.

3.7 Amplification at High Input Intensities

3.7.1 Variability in Amplification Factors

To study the effect of higher input intensity on site response, amplification factors for the generated profiles at PGA_{rock}=0.9g are plotted versus period at Figure 3.22. The variability in AF is significant (i.e σ_{lnAF}>0.05) at all periods for V_{S30}=225, 280, and 350 m/s and significant at periods less than or equal to 1.0 s for the stiffer sites (V_{S30}=450 and 550 m/s).

The calculated σ_{lnAF} of the AF values in Figure 3.22 are shown versus period in Figure 3.23. Again, input intensity level affects the location of the maximum σ_{lnAF}. The location of the maximum σ_{lnAF} moves to longer periods as the input intensity increases. For example, for V_{S30}=280 m/s the maximum σ_{lnAF} occurs at T=0.2 s for PGA_{rock}=0.3g while the location of maximum σ_{lnAF} shifts to T=1.0 s for PGA_{rock}=0.9g. While the location of the maximum σ_{lnAF} shifts to longer periods and the period range of $\sigma_{lnAF} \geq 0.05$ expands with increasing input intensity, the maximum σ_{lnAF} remains around 0.3 to 0.4 for both the moderate and high intensity input motions.

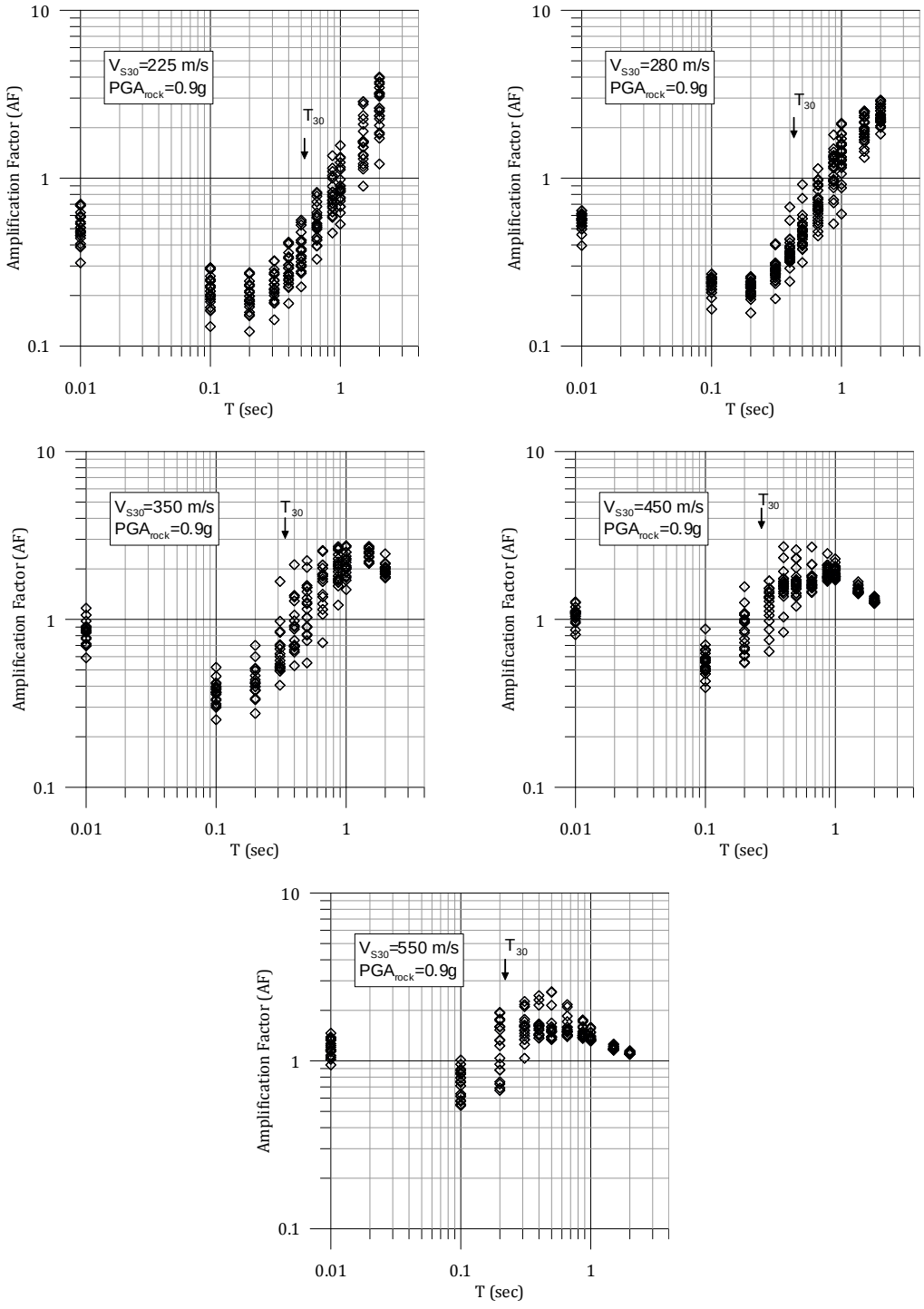

Figure 3.22 Amplification factor versus period for all the generated profiles, PGA_{rock}= 0.9g.

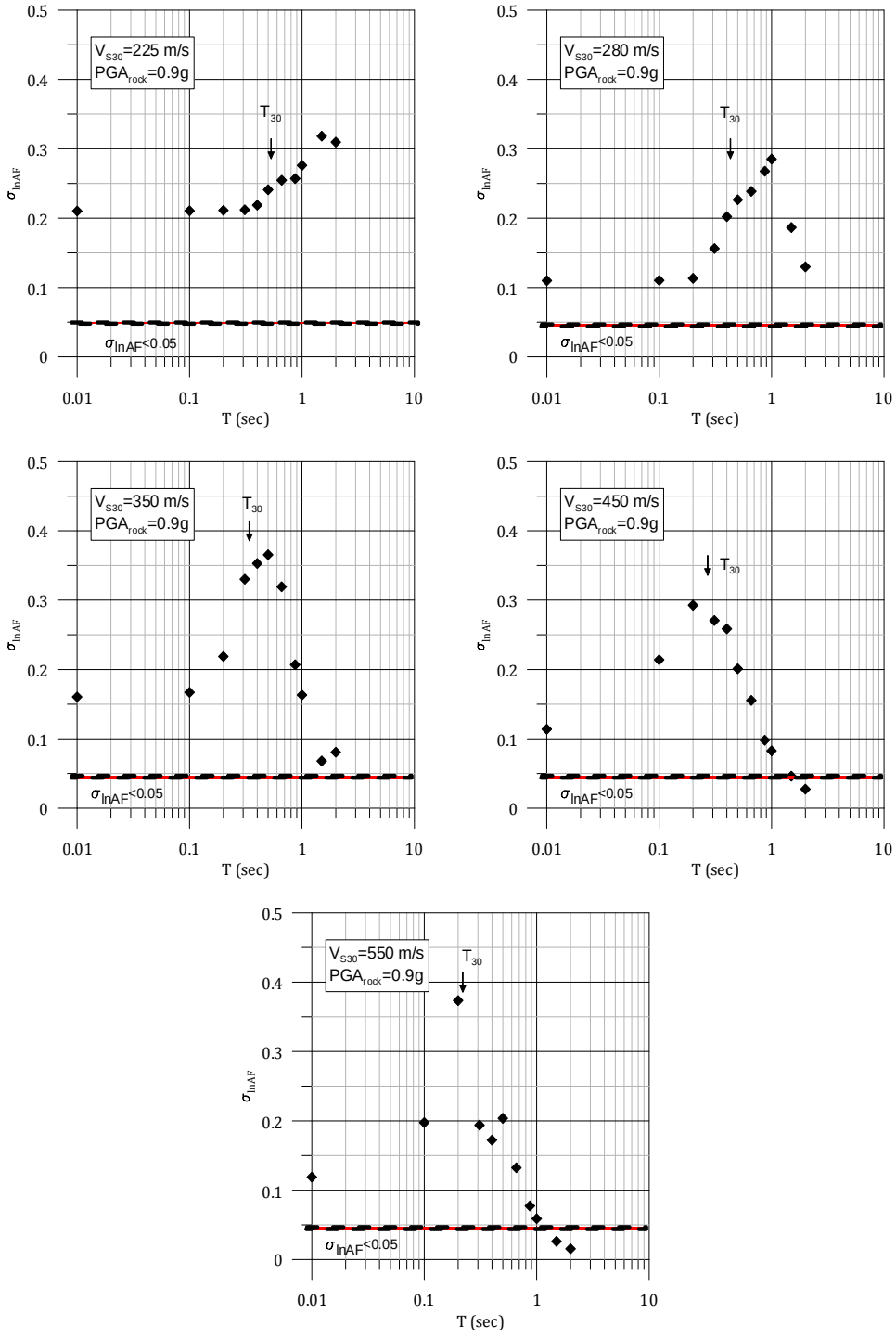

Figure 3.23 σ_{lnAF} versus period for all the generated profiles, PGA_{rock}=0.9g.

3.7.2 Influence of site parameters on site amplification

As investigated in previous sections, the Vratio of the V_S profile affects amplification at low and moderate shaking levels. In this section, the effect of this site parameter under high level of shaking (0.9g) is examined. Considering the periods of the maximum σ_{lnAF} in Figure 3.23, the residuals are investigated at periods of 0.2 s (period of maximum σ_{lnAF} for V_{S30}=450 and 550 m/s), 0.5 s (period of maximum σ_{lnAF} for V_{S30}=350 m/s), and 1.0 s (period of maximum σ_{lnAF} for V_{S30}= 280 m/s).

Figure 3.24 shows the calculated residuals versus Vratio for all the generated sites at spectral period of 0.2 s. A linear relationship between residuals and ln(Vratio) is again observed. This relationship is now strong even for the larger V_{S30} sites (i.e., 550 m/s) because of soil nonlinearity. The residuals versus Vratio are plotted at a spectral period of 0.5 s in Figure 3.25. The maximum σ_{lnAF} occurs at T= 0.5 s for V_{S30}=350 m/s and σ_{lnAF} is significant for all the other V_{S30} values at this period. The linear trend between the residuals and ln(Vratio) is strong for $V_{S30}\leq$ 350 m/s. At longer spectral periods (1.0 s) as shown in Figure 3.26, the same trend as that of for spectral period of 0.5 s is observed between residuals and ln(Vratio).

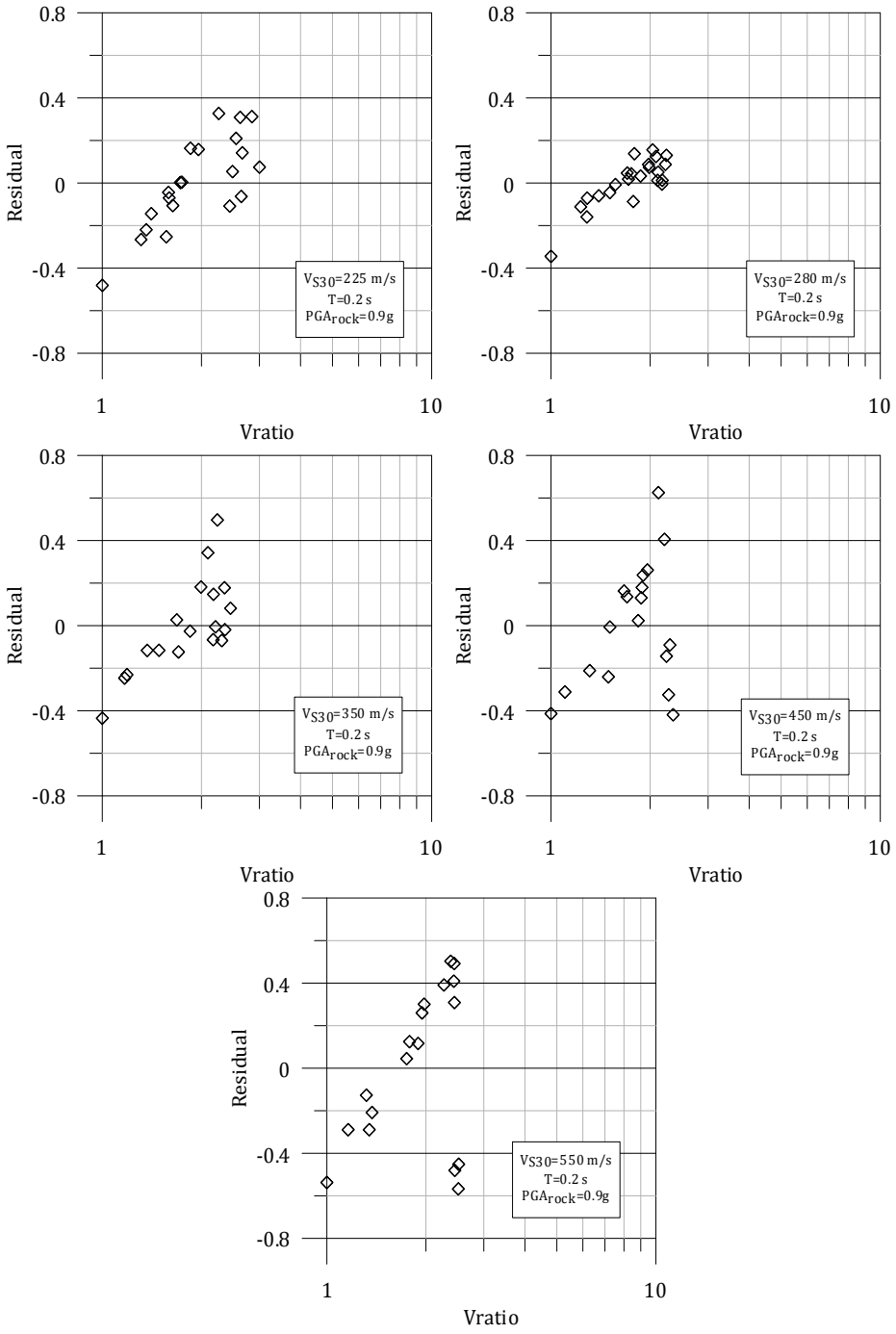

Figure 3.24 Residual versus Vratio for all the profiles at spectral period of 0.2 s and PGA_{rock}=0.9g.

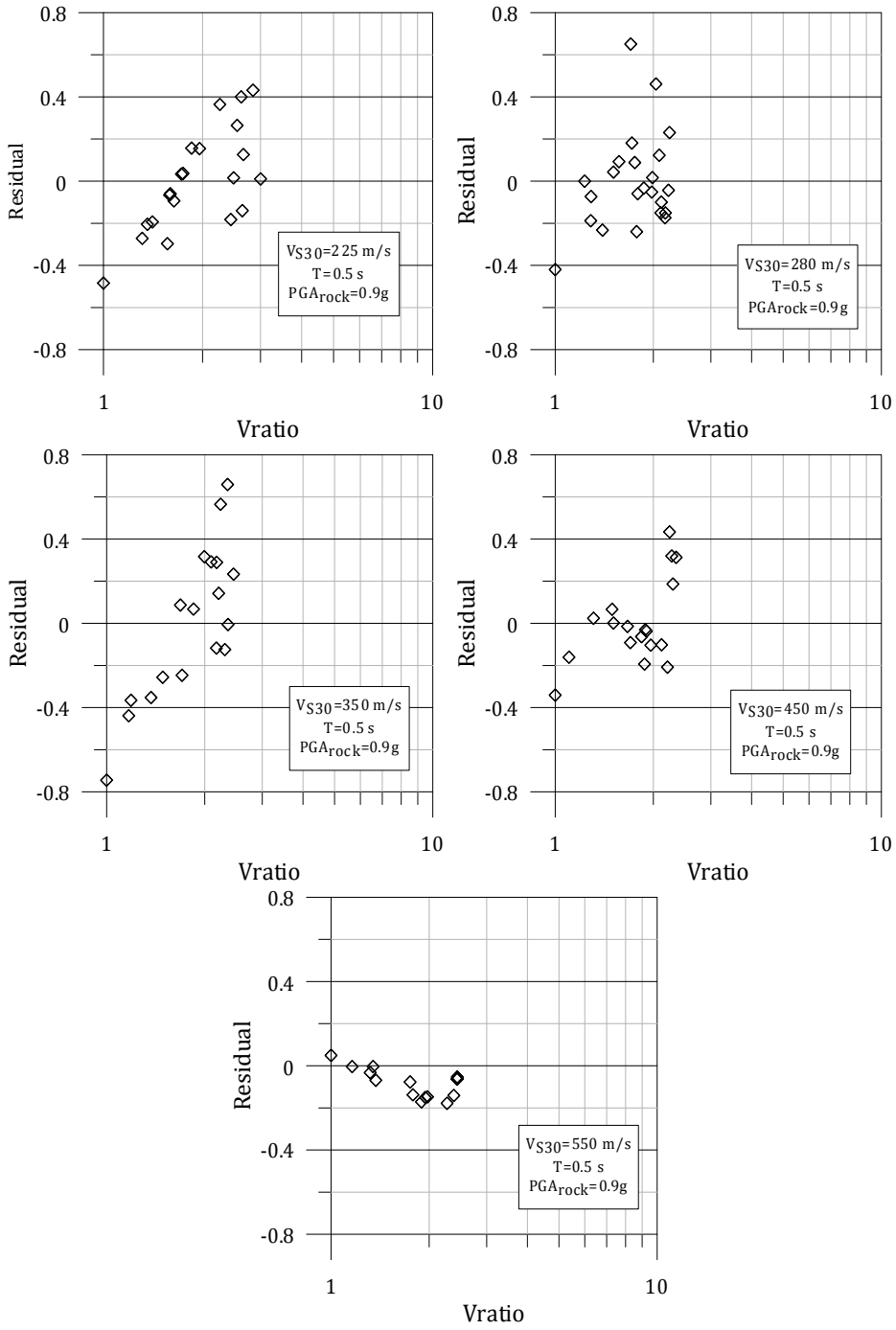

Figure 3.25 Residual versus Vratio for all the profiles at spectral period of 0.5 s and PGA_{rock}=0.9g.

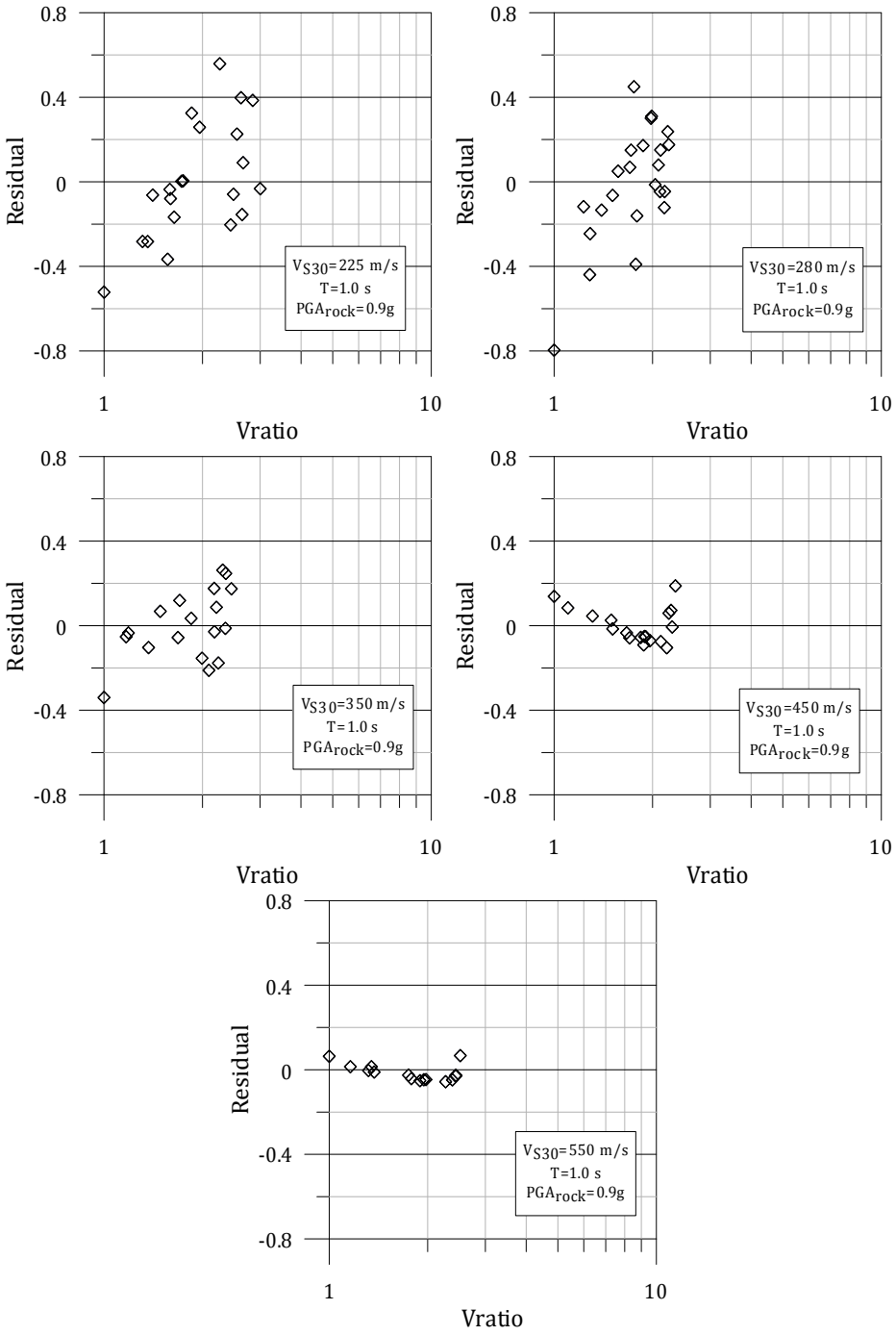

Figure 3.26 Residual versus Vratio for all the profiles at spectral period of 1.0 s and PGA_{rock}=0.9g.

3.8 Summary

Ninety-nine profiles are manually generated using five baseline profiles. The generated profiles from each baseline profile have the same average shear wave velocity in top 30 m, the same velocity structure at depths greater than 30m, and the same depth to bedrock. Site response analyses are performed using the equivalent linear approach using the site response program Strata (Kottke and Rathje 2008). The site amplification factors computed for the generated profiles are studied and the variability in computed amplification investigated.

At low input intensity, sites with the same average shear wave velocity and depth to rock but a different structure in the V_S profile in the top 30 meters have different amplification factors at some periods. These periods are correlated to T_{30}. The variability in the amplification factors at these periods indicates that the detailed velocity structure in the top 30 meters of a V_S profile influences the computed AF. As input intensity increases, the period range affected by the top 30 meters increases.

The parameters V_{min}, thV_{min}, $depthV_{min}$, MAXIR and Vratio are considered to explain the variability in amplification factors. The parameter Vratio is identified as the parameter that most strongly influences the computed amplification. A linear relationship is observed between residuals and ln(Vratio). Residuals versus ln(Vratio) plots for different V_{S30} and at different periods show that the effect of

Vratio on amplification is V_{S30} and period dependent. To generalize the findings of this chapter, a suite of fully randomized velocity profiles will be analyzed.

Chapter 4

Statistical Generation of Velocity Profiles

4.1 Introduction

As discussed in the previous chapter Vratio can help explain the variability in the computed amplification factors for sites with the same average shear wave velocity in top 30 meter (V_{S30}) and depth to engineering rock ($Z_{1.0}$). To generalize the effect of Vratio to a wider range of sites, the seismic response of sites with a wide range of velocity profiles is assessed and used to develop predictive models for site amplification that include Vratio. The site response program Strata (Kottke and Rathje, 2008) can generate hypothetical velocity profiles using Monte Carlo simulations, and can also statistically vary layer thickness, nonlinear soil properties, and depth to the bedrock. In this study four hundred hypothetical velocity profiles are generated using Strata and their seismic responses are used to develop the site

amplification model. This chapter describes the generation of the velocity profiles, while the next chapters describe the development of the site amplification model.

4.2 Development of Randomized Velocity Profiles for Site Response Analysis

4.2.1 Modeling Variations in Site Properties

A soil profile consists of discrete layers that describe the variation of soil properties with depth. In seismic site response analysis, each soil layer is characterized by a thickness, mass density, shear wave velocity, and nonlinear properties (i.e., G/Gmax vs. shear strain, and D vs. shear strain).

The site response program Strata (Kottke and Rathje 2008) uses Monte Carlo simulations to develop different potential realizations of the site properties. The goal of a Monte Carlo simulation is to estimate the statistical properties of the response of a complex system. To achieve this goal, each of the properties of the system is selected from defined statistical distribution and the response of the system is computed. The response is computed for many realizations of site properties and the calculated response from each realization is then used to estimate the statistical properties of the system's response. Monte Carlo

simulations require that each of the components in the system has a complete statistical description.

The Monte Carlo randomization feature in Strata can randomize layer thickness, the shear wave velocity of a layer, the nonlinear soil properties of a layer, and the depth to bedrock. In this study, layer thicknesses, shear wave velocity, and depth to bedrock are randomized; nonlinear properties are not. Strata uses the statistical models developed by Toro (1995) to randomize the layer thicknesses and associated shear wave velocities. In this approach, layer thicknesses are first generated and then shear wave velocities are assigned to each layer.

Layering is modeled as a Poisson process, which is a stochastic process with the event occurring at a given rate (λ). For a homogeneous Poisson process this rate is constant, while for a non-homogeneous Poisson process the rate of occurrence varies. For the layering problem, the event is a layer interface and its rate is defined in terms of the number of layer interfaces per meter. The rate of interface occurrence is depth dependent (i.e., thinner layers tend to occur near the surface, thicker layers tend to occur at depth), thus a non-homogeneous Poisson process is used. Toro (1995) developed a depth-dependent layering rate model using the layer thicknesses measured at 557 sites, mostly from California. The resulting model of depth-dependent layering rate is shown in Figure 4.1. Note that the rate varies from 0.22 (per meter) at the ground surface (i.e., average layer thickness = $1/\lambda = 4.5$ m)

to 0.05 (per meter) at a depth 50 m (i.e., average layer thickness = 20 m) to 0.02 (per meter) at a depth of 200 m (i.e., average layer thickness = 50 m).

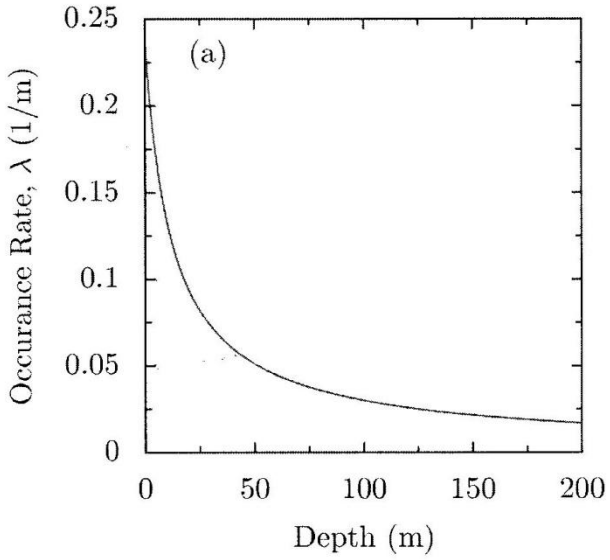

Figure 4.1 Variation of layer interface occurrence rate with depth (Toro 1995).

After developing the layering profile (i.e., layer thicknesses) using the non-homogeneous Poisson process, a shear wave velocity is assigned to each layer. In the Toro (1995) model, the shear wave velocity at mid-depth of the layer is described by the log-normal distribution. The log-normal distribution is used based on statistical investigation of shear wave velocity data from the same 557 sites used in developing the layering model. The log-normal distribution is described by the median shear wave velocity (i.e., the average of ln(Vs)) at mid-depth of the layer and the standard deviation of the natural logarithm of the shear wave velocity (σ_{lnVs}).

The median shear wave velocity for the layer is taken from a user-specified baseline velocity profile for the site, at the depth of the layer. The σ_{lnVs} is assigned by the user to model a specific amount of variability. Given the baseline shear wave velocity for layer *i* ($V_{s,o}(i)$, assumed to represent the mean in logarithmic space), the standard deviation of the natural logarithm of V_s (σ_{lnVs}), and a random standard normal variable for layer *i* (Z_i), the shear wave velocity of layer *i* ($V_s(i)$) can be computed as (Toro 1995):

$$V_s(i) = exp\left(\ln\left[V_{s,o}(i)\right] + Z_i \cdot \sigma_{lnVs}\right) \quad (4.1)$$

The key issue is then the selection of the values of Z_i for each layer. Some researchers have assumed that Z_i values are perfectly correlated between layers (McGuire et al. 1989, Toro et al. 1992), while others have assumed zero correlation (Costantino et al. 1991). Neither of these assumptions is consistent with velocity data and they represent extreme conditions (i.e., perfect correlation vs. statistical independence). Toro (1995) developed a model for the interlayer correlation of Z_i based on analysis of the same 557 shear wave velocity profiles previously discussed. In this model, the standard normal variable for the surface layer (Z_1, i = 1) is independent of all other layers and defined as:

$$Z_1 = \varepsilon_1 \quad (4.2)$$

where ε_1 is a random normal variable with zero mean and unit standard deviation. Z_i is correlated with the layer above it using (Toro 1995):

$$Z_i = \rho_{IL} \cdot Z_{i-1} + \varepsilon_i \cdot \sqrt{1 - \rho_{IL}^2} \quad (4.3)$$

where Z_{i-1} is the standard normal variable of the previous layer, ε_i is a new normal random variable with zero mean and unit standard deviation, and ρ_{IL} is the interlayer correlation coefficient. Toro (1995) modeled the interlayer correlation as depth (d) and layer thickness (t) dependent:

$$\rho_{IL}(d,t) = [1 - \rho_d(d)] \cdot \rho_t(t) + \rho_d(d) \quad (4.4)$$

where $\rho_d(d)$ is the depth-dependent component of the correlation coefficient and $\rho_t(t)$ is the thickness-dependent component of the correlation coefficient. These correlation coefficients are defined as (Toro 1995):

$$\rho_d(d) = \begin{cases} \rho_{200} \cdot \left[\frac{d+d_o}{200+d_o}\right]^b, & d \leq 200m \\ \rho_{200}, & d > 200m \end{cases} \quad (4.5)$$

$$\rho_t(t) = \rho_o \cdot exp\left(\frac{-t}{\Delta}\right) \quad (4.6)$$

where ρ_{200}, d_o, b, ρ_0, and Δ are model parameters.

Toro (1995) developed median shear wave velocity profiles for different site classes (i.e., ranges in V_{S30} that are incorporated in the building code) for use in developing randomized velocity profiles for generic site conditions. Toro (1995) also developed estimates of σ_{lnVs} and inter-layer correlation coefficient model parameters for site classes of V_{S30} > 760 m/s, 360-760 m/s, 180-360 m/s, and < 180 m/s.

The depth to bedrock can be modeled using either a uniform, normal, or log-normal distribution. The statistical properties of the distribution are entered by the user.

4.2.2 Baseline Profiles

The Monte Carlo simulation feature in the program Strata is used to generate generic site profiles for use in site response analysis. As discussed in the previous section, Monte Carlo simulations require a median shear wave velocity profile and σ_{lnVs}. The median shear wave velocity profiles are called baseline profiles in this study. Four baseline profiles with V_{S30} equal to 200, 250, 400, and 550 m/s are used to generate a total of four hundred soil profiles. The developed baseline shear wave velocity profiles are shown in Figure 4.2. These baseline velocity profiles are developed based on the velocity profiles presented by Toro (1995) for different site classes. The developed profiles by Toro (1995) are modified in this study to achieve the desired V_{S30} for each baseline profile. The minimum velocity at the surface varies between about 175 and 400 m/s in the baseline profiles. The baseline profiles with V_{S30} of 200 and 250 m/s reach their maximum shear wave velocities of 750 m/s and 890 m/s, respectively, at a depth of 400 m. The stiffer baseline profiles reach V_S equal to 1,000 m/s at shallower depths (150 m for V_{S30} of 550 m/s and 300 m for V_{S30} of 400 m/s). The site class dependent values of σ_{lnVs} developed by Toro (1995) are used in generating the velocity profiles (Table 4.1).

Generic layering is developed for the site profiles using the non-homogenous layering model of Toro (1995). Depth to bedrock is varied using a uniform distribution. The minimum and maximum depths used for the uniform distribution are specified differently for each baseline velocity profile because each profile encounters rock-like velocities (~ 750 to 1000 m/s) at different depths. The minimum and maximum depths used are listed in Table 4.1 for each baseline profile. The shear wave velocity of the half-space below the velocity profile is specified as 1,000 m/s. Velocities are assigned to each layer using the inter-layer correlation model of Toro (1995). The depth and thickness-dependent model for ρ_{IL} from Toro (1995) is used. The predicted ρ_{IL} from Toro (1995) is plotted versus depth for thicknesses of 5 m, 20 m, and 50 m in Figure 4.3 for site class V_{S30} = 180-360 m/s. This is the site class that is associated with the V_{S30} values of two of the baseline profiles. As shown in Figure 4.3, for a given thickness, the interlayer correlation increases with depth and at the depth of 200 m approaches 1.0 for this site class. It is also observed that thicker layers generally have a smaller interlayer correlation coefficient. In generating the velocity profiles, the shear wave velocity of layers is not allowed to exceed 1000 m/s nor go below 100 m/s.

While the nonlinear properties are not varied in the Monte Carlo simulation, modulus reduction and damping curves are assigned to each layer. The Darendeli (2001) model is used to develop the modulus reduction and damping curves as a function of mean effective stress (σ'_0), Plasticity Index (PI), and over consolidation

ratio (OCR). In this study PI and OCR are taken to be 10 and 1.0, respectively, for all layers. To model the stress dependence, nonlinear property curves are generated for σ'_0 equal to 0.59 atm, 1.4, atm, 2.7 atm, 4.9 atm, 8.0 atm, 15.7 atm, and 33.5 atm. The appropriate curves are assigned to each layer of the baseline profile based on the depth and a computed mean effective stress at the middle of each layer. The thickness, unit weight, and mean effective stress considered for each layer are listed in Table 4.2. The shear modulus reduction and damping curves used for each layer are shown in Figure 4.4.

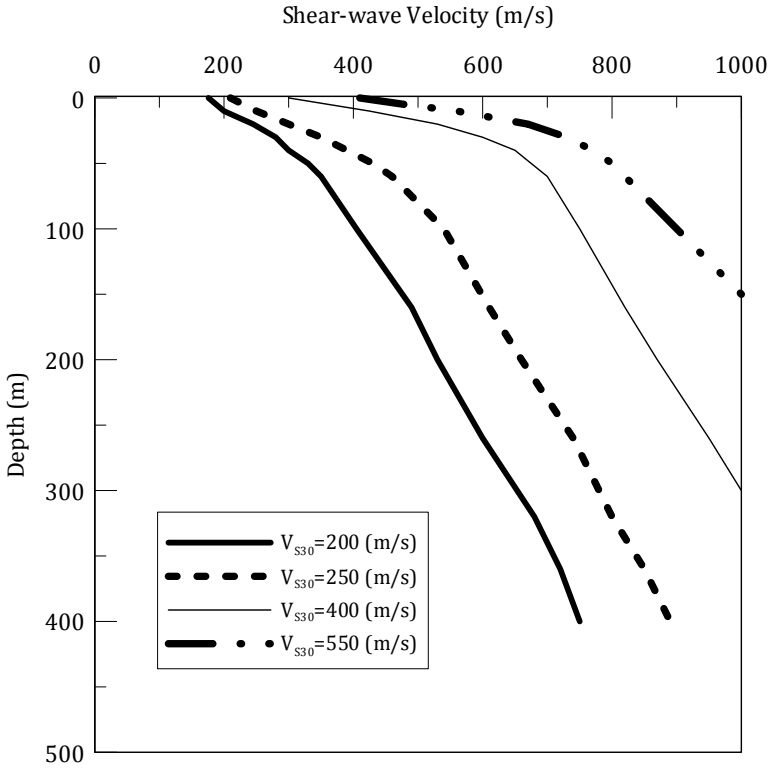

Figure 4.2 Baseline shear wave velocity profiles.

Table 4.1 σ_{lnVs} used in generating profiles from each baseline profile.

V_{S30} (m/s)	σ_{lnVs}	Min Rock Depth (m)	Max Rock Depth (m)
200	0.31	150	650
250	0.31	100	600
400	0.27	30	550
550	0.27	15	300

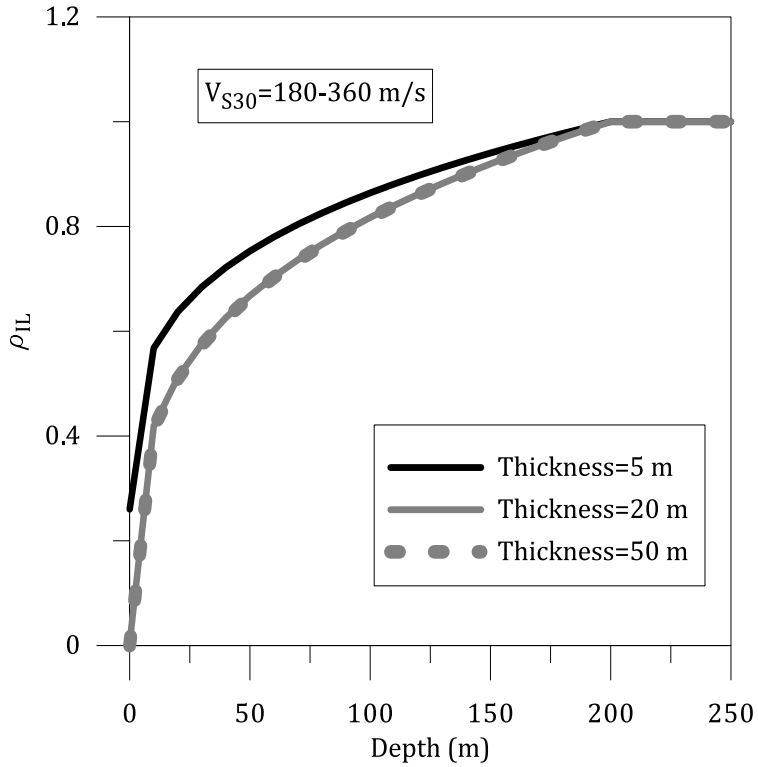

Figure 4.3 The predicted ρ_{IL} from Toro (1995) versus depth for thicknesses of 5 m, 20 m, and 50 m for site classV_{S30} = and 180-360 m/s.

Table 4.2 The thickness, unit weight, and mean effective stress considered for each layer.

Depth (m)	Unit Weight (kN/m^3)	Mean Effective Stress (atm)
0-15	18	0.59
15-30	18	1.4
30-60	19	2.7
60-100	20	4.9
100-150	21	8.0
150-300	22	15.7
300-600	22	33.5

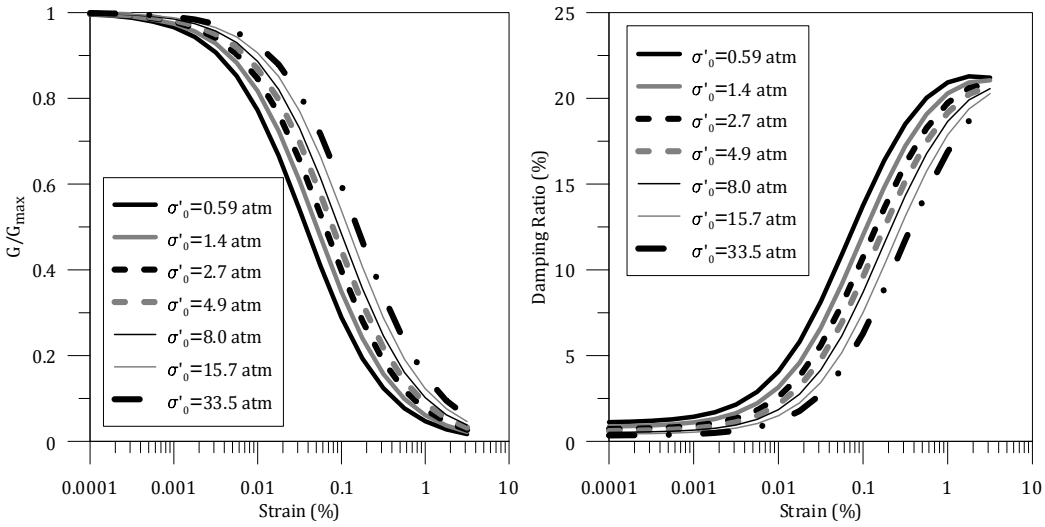

Figure 4.4 Shear modulus and damping curves used in the analyses (PI=10, OCR=1.0).

4.2.3 Generated Shear Wave Velocity Profiles

Four hundred soil profiles are generated by the program Strata using the information previously discussed. Examples of generated profiles from each baseline profile are shown in Figures 4.5 and 4.6. Note that the V_{S30} for each generated profile is different than the V_{S30} for the baseline profile. Each profile generated from a single baseline profile has different layering and a different shear wave velocity profile. While the baseline velocity profiles (Figure 4.2) vary smoothly with depth, the generated profiles vary more irregularly (Figure 4.5, 4.6). In some profiles, an inversion in the shear wave velocity occurs (i.e., the velocity decreases with depth). The irregular pattern is more representative of a real site, while the smooth baseline profiles represent the average over many different sites. However, the average velocity profile for the generated sites for a given baseline profile varies smoothly and matches well the baseline profile.

For each generated velocity profile, site characteristics such as the minimum shear wave velocity, V_{S30}, and the depth to bedrock are different. Various site parameters, including the average shear wave velocity in top 30 m (V_{S30}), the depth to engineering rock ($Z_{1.0}$), and Vratio (i.e., Vratio = $V_{S20\text{-}30}$ / V_{S10}, where $V_{S20\text{-}30}$ is the average shear wave velocity between depths 20 m and 30 m and V_{S10} is the average shear wave velocity in top 10 m) are calculated for each generated profile. Histograms showing the distribution of each of these site parameters are given in Figure 4.7. V_{S30} in the generated profiles varies between 118 m/s and 818 m/s. The

V_{S30} values of the generated profiles are evenly distributed between 150 and 750 m/s, with fewer values less than 150 m/s or greater than 750 m/s. This range indicates that the generated sites include a representative range of soft to stiff soil profiles. The $Z_{1.0}$ values of the generated profiles range from 16 m to 640 m. Because softer sites with small V_{S30} tend to be found in deeper alluvial valleys, there is a relationship between V_{S30} and $Z_{1.0}$. As shown in Figure 4.8 for the generated profiles in this study, the softest sites are associated with the largest values of $Z_{1.0}$. The histograms in Figure 4.7 show that Vratio varies from 0.56 to 2.76 in the generated profiles. Profiles with Vratio less than 1.0 have V_{S10} greater than $V_{S20\text{-}30}$, indicating that the shear wave velocity generally does not increase with depth in the top 30 m. In these cases an inversion in the velocity occurs. In 11% of the generated profiles Vratio is less than one. Large values of Vratio indicate a significant increase in shear wave velocity within the top 30 m.

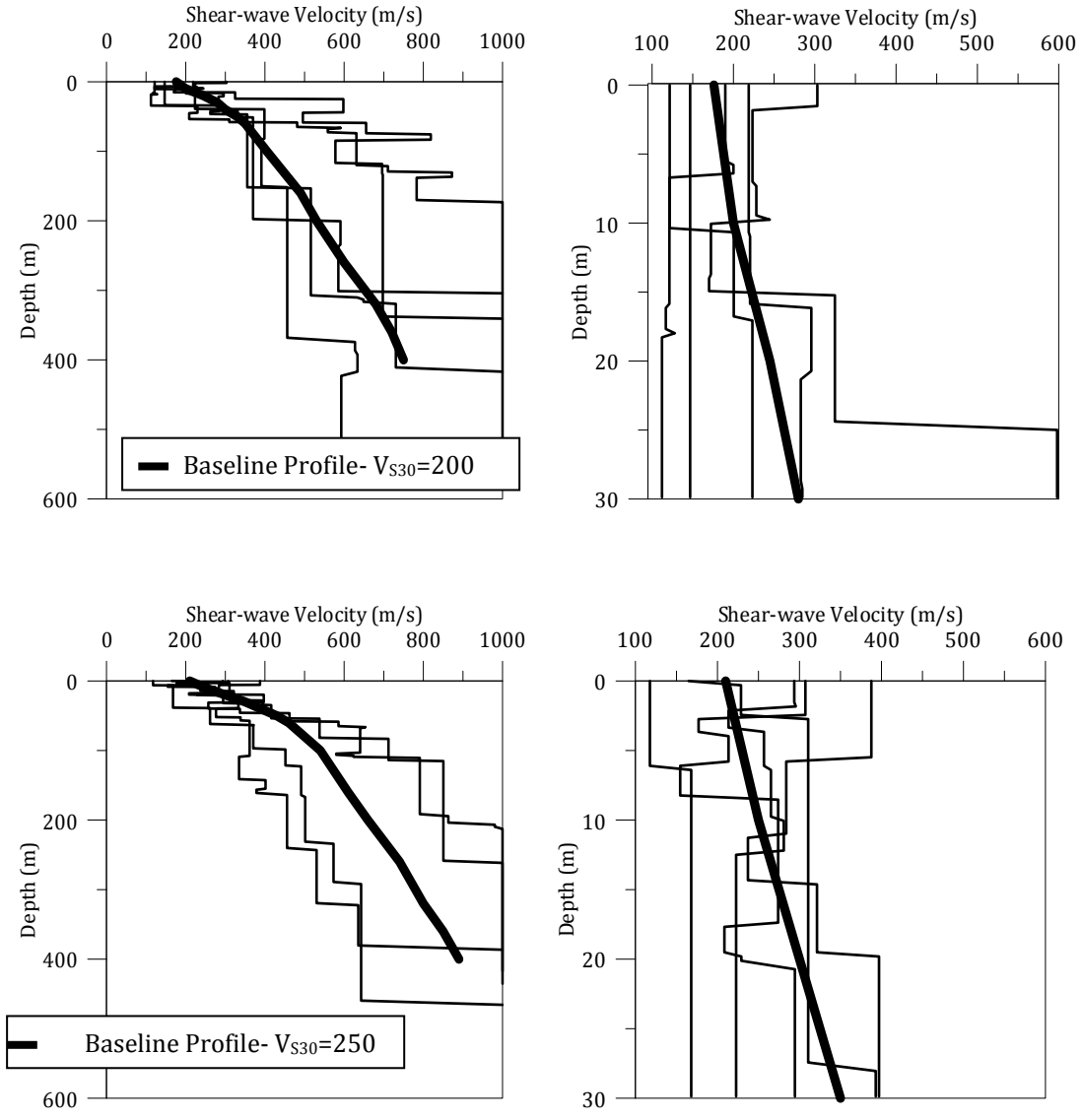

Figure 4.5 Examples of generated velocity profiles from baseline velocity profiles with V_{S30} of 200 and 250 m/s.

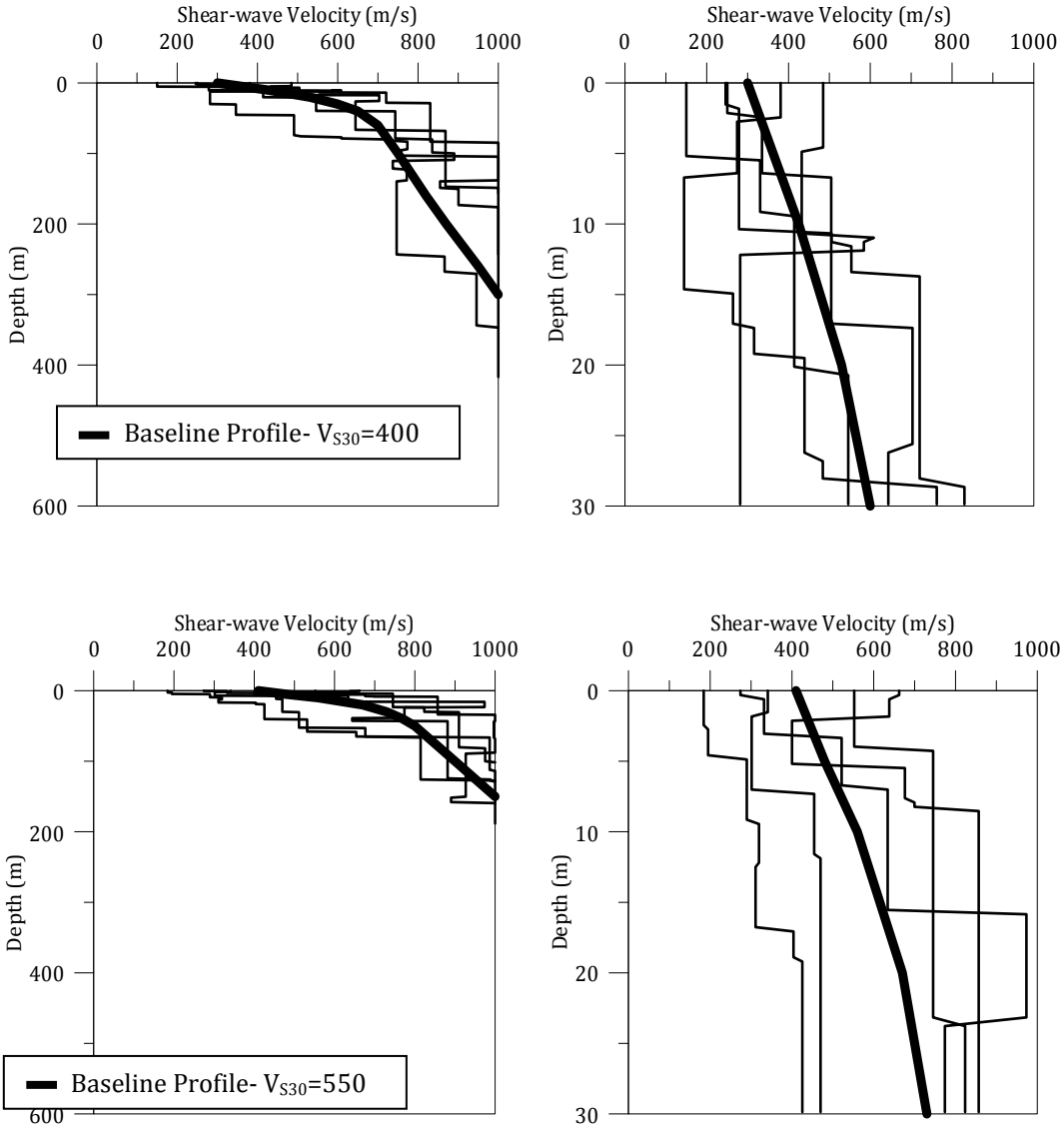

Figure 4.6 Examples of generated velocity profiles from baseline velocity profiles with V_{S30} of 400 and 550 m/s.

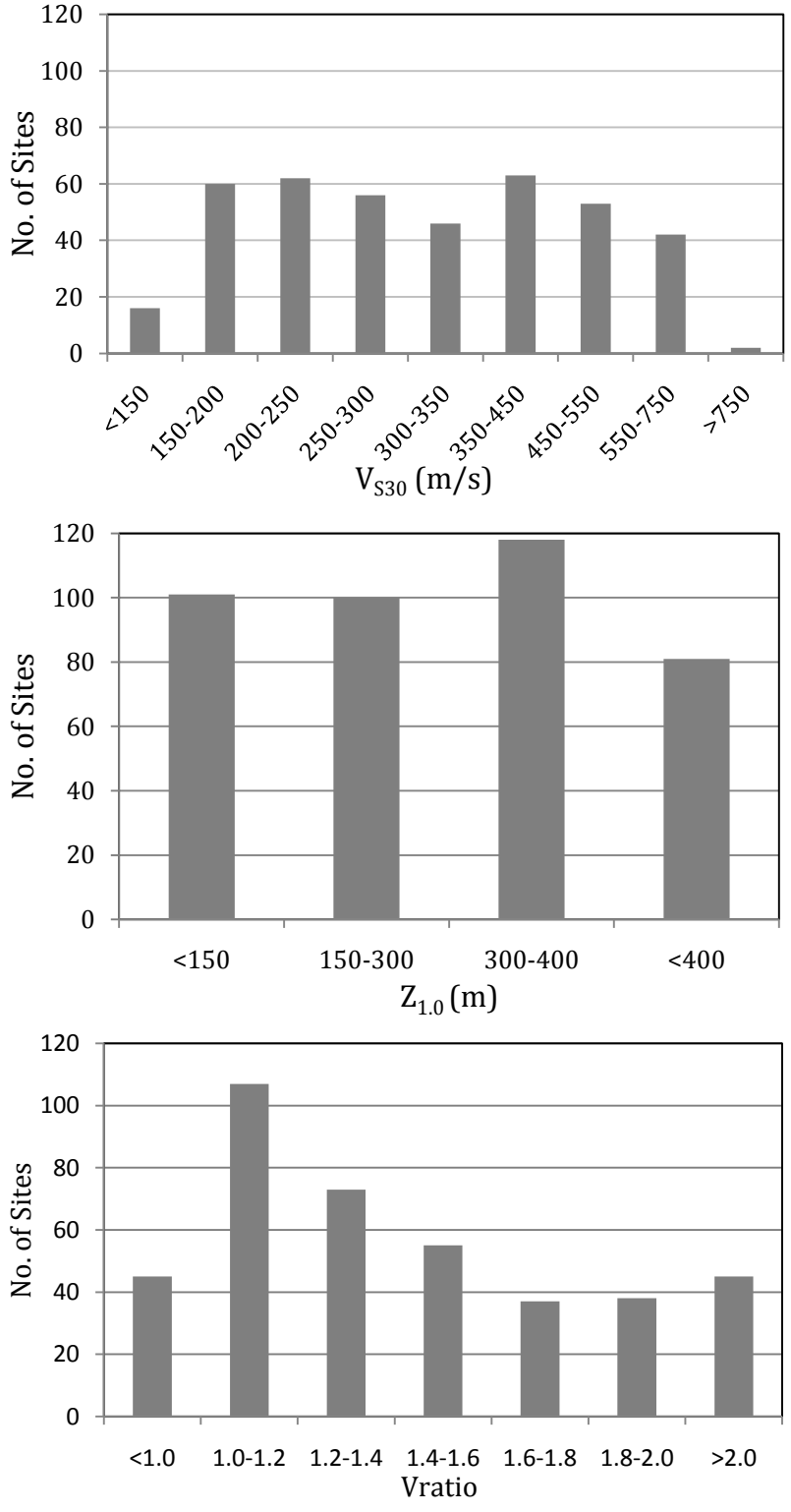

Figure 4.7 Distiribution of V_{S30}, $Z_{1.0}$, and Vratio of the generated soil profiles.

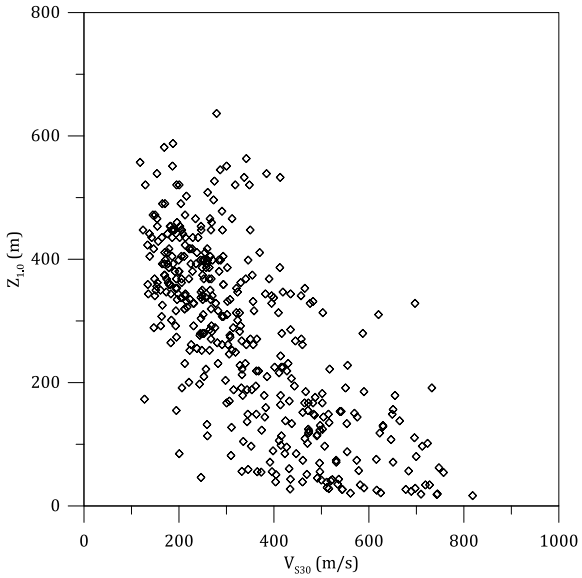

Figure 4.8 Relation between $Z_{1.0}$ and V_{S30}.

4.3 Approach to Development of Amplification Model

The form of empirical site amplification models typically includes two components; a linear elastic component and a nonlinear component. The linear elastic component represents amplification under linear elastic (LE) soil conditions (i.e., low intensity shaking), while the nonlinear component (NL) includes the effects of soil nonlinearity at high intensity shaking. These amplification factors (AF) are generally multiplicative (additive in logarithmic space), which can be written as:

$$\ln (AF)=\ln(AF)_{LE}+ \ln(AF)_{NL} \quad (4.7)$$

The amplification model is developed separately for each period in the response spectrum.

The linear elastic component can be derived from the computed amplification for low intensity input motions. In this study, computed amplification factors from input motions with a rock input PGA of 0.01g are used to develop the linear elastic AF model. Computed amplification factors from larger intensity input motions are used to develop the nonlinear component of the AF model. As discussed earlier, equivalent-linear analysis using the RVT approach is used to compute the seismic response of the generated profiles under a wide range of input intensities. In the RVT approach, the input motion is described by a response spectrum, this response spectrum is converted to a Fourier Amplitude Spectrum (FAS), the FAS is propagated to the ground surface using the site frequency domain transfer function, and the surface FAS is converted to an acceleration response spectrum. The ratio of the surface response spectrum to the input response spectrum at each period defines the AF for each period. The input motions are defined using seismological source theory in which the earthquake magnitude, depth, and source-to-site distance are specified by the user and Strata uses various seismological parameters to define the input FAS and response spectrum. For this study, the magnitude and distance are varied to obtain the desired input intensity levels. Table 4.3 lists the magnitude, depth, and distance used to generate the 10 input intensity levels along

with their corresponding PGA_{rock}. The response spectra of the input motions are shown in Figure 4.9.

Table 4.3 Magnitudes, depths, and distances used to generate input motions.

PGA_{rock}	Magnitude	Depth (km)	Distance (km)
0.01 g	7.0	3.0	180
0.05 g	7.0	3.0	68
0.1 g	7.0	3.0	40
0.22 g	6.5	3.0	20
0.31 g	7.0	3.0	21
0.41 g	7.0	3.0	16
0.52 g	7.0	3.0	10
0.72 g	7.0	3.0	5
0.95 g	7.6	3.0	9
1.60 g	7.8	3.0	6

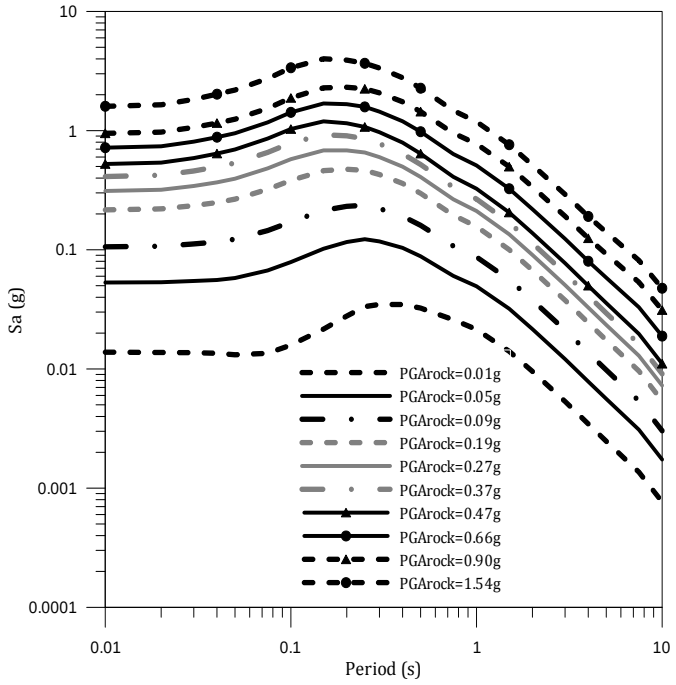

Figure 4.9 Response spectra of RVT input motions.

After computing amplification factors for a range of sites subjected to a range of input intensities, the AF values are used to develop the empirical amplification model. A functional form for the model is developed and the model coefficients are determined through a maximum likelihood regression.

Maximum likelihood estimation, identifies the regression coefficients for a model that make the observed data most likely. The likelihood function (L) is written as:

$$L(\theta|y_1, y_2, \dots, y_n) = f(y_1, y_2, \dots, y_n|\theta) \tag{4.8}$$

where θ represents the parameters of the statistical model, y_i represents the observed values, n is the number of observations, and $f(y_1, y_2, \dots, y_n|\theta)$ represents

the joint probability density function (pdf) of y_i. Assuming that the y_i are independent and indentically distributed, the joint pdf can be written as:

$$f(y_1, y_2, \dots, y_n|\theta) = \prod_{i=1}^{n} f(y_i|\theta) \quad (4.9)$$

It is often more convenient to use the logarithm of the likelihood (log-likelihood) function:

$$\ln L(\theta|y_1, y_2, \dots, y_n) = \sum_{i=1}^{n} \ln f(y_i|\theta) \quad (4.10)$$

The maximum likelihood method identifies the values of the statistical model parameters θ that maximize the likelihood function.

When applying the maximum likelihood approach to regression, y_i represent observed values of the dependent variable and θ are the regression coefficients. In developing the amplification model in this study, the maximum likelihood method is implemented in Excel. The residual of each observation relative to the prediction is computed, each residual is used to compute $\ln f(y_i|\theta)$, and these values summed to represent the log-likelihood. The Solver function in Excel is used to identify the parameters θ that maximize the log-likelihood function

4.4 Summary

This chapter describes the development of randomized velocity profiles for site response analysis. The model used in program Strata (Kottke and Rathje,2008) for variation in site properties such as site depth, layer thickness, and nonlinear properties of soils are discussed. Finally the statistically generated velocity profiles and their correponding site parameters are presented and the approach for developing the site amplification models is discussed.

In Chapteres 5 and 6, the linear and nonlinear components of the model will be presented, respectively. In Chapter 7, the combined model will be presented.

Chapter 5

Models for Linear Site Amplification

5.1 Introduction

This chapter presents the development of the linear elastic component of the predictive amplification model. The functional form is developed separately for shorter periods ($T < 1.0$ s) and longer periods ($T \geq 1.0$ s). At short periods the amplification model includes the effects of V_{S30} and Vratio, while at long periods the amplification model includes the effects of V_{S30} and $Z_{1.0}$.

5.2 Linear Site Amplification (PGA_{rock}=0.01g)

The computed amplification factors (AF) for all the generated sites subjected to the input motion with a PGA_{rock} of 0.01g are used to develop the model for linear elastic amplification (i.e. $\ln(AF)_{LE}$). In Figures 5.1 and 5.2, the computed AFs are plotted versus V_{S30} for spectral periods shorter and longer than 1.0 s, respectively. The data

in Figures 5.1 and 5.2 generally show that a decrease in V_{S30} results in an increase in amplification, which is consistent with previous studies. At shorter periods, amplification (i.e., T≤ 0.5) increases over the full V_{S30} range. At longer periods (T = 5.0 and 10 s in Figure 5.2), the amplification stays close to 1.0 for a range of larger V_{S30} values before beginning to increase at smaller V_{S30}. The V_{S30} below which amplification starts to increase is called V_{ref}. V_{ref} generally decreases as period increases.

Linear elastic AF models developed previously and used in most ground motion prediction equations (e.g., NGA models) incorporate a linear dependence between lnAF and ln(V_{S30}/V_{ref}). This fit takes on the following functional form:

$$\ln(AF)_{LE} = \begin{cases} a_1 \times \ln\left(\frac{V_{S30}}{V_{ref}}\right) & \text{if } V_{S30} < V_{ref} \\ 0 & \text{if } V_{S30} \geq V_{ref} \end{cases} \qquad (5.1)$$

A maximum likelihood regression is used to fit equation (5.1) to the AF data at each spectral period. V_{ref} is fixed based on visual identification from the data (Table 5.1) because regressed values of V_{ref} using the maximum likelihood method were not consistent with the data. Figures 5.3 and 5.4 show the AF data again, along with a linear fit from equation (5.1) in which parameters a_1 and V_{ref} are developed separately for each period. These model parameters (a_1 and V_{ref}) and the resulting standard deviation of the regression (σ_{lnAF}) are shown in Table 5.1. As shown in Table 5.1, V_{ref} is equal to 1000 m/s at short periods and then decreases as spectral period increases beyond 0.5 s. The slope a_1 is almost the same at short periods (~ -

0.45 for $T \leq 0.3$ s), it gets larger in the middle periods (~ -0.5 to -0.7 for T = 0.5 to 2.0 s), and then it becomes smaller at long periods greater than 2.0 s. σ_{lnAF} ranges from 0.11 at PGA, then increases to 0.2 - 0.25 for periods between 0.2 and 1.0s, and then decreases at the longest periods. Comparing the model predictions to the data in Figures 5.3 and 5.4, it appears that a linear fit does not match the data appropriately, particularly at shorter periods and smaller V_{S30}. In these cases, a second-order polynomial may fit the AF data better.

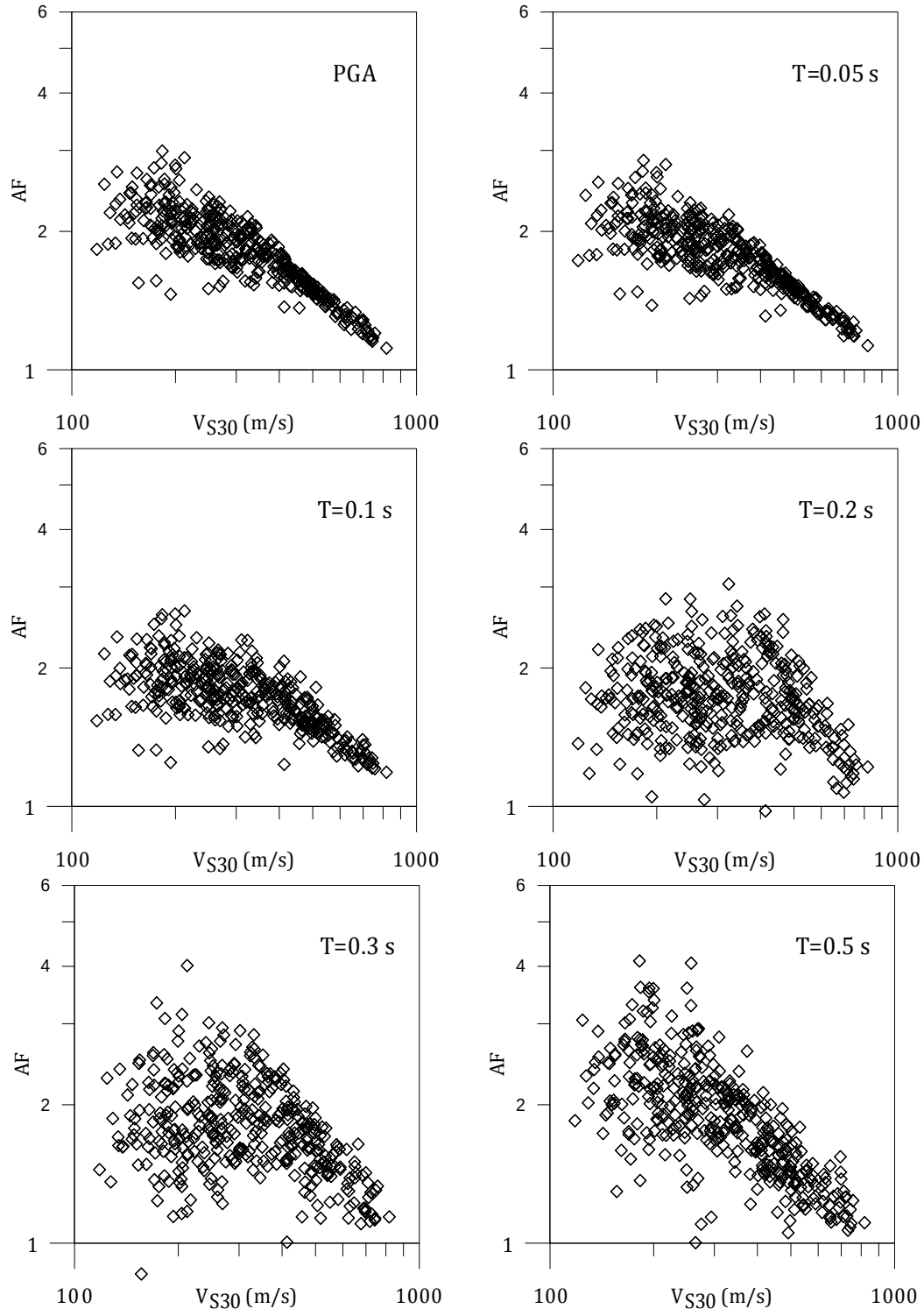

Figure 5.1 Amplification Factor versus V_{S30} for all generated profiles at short periods (T<1.0 s).

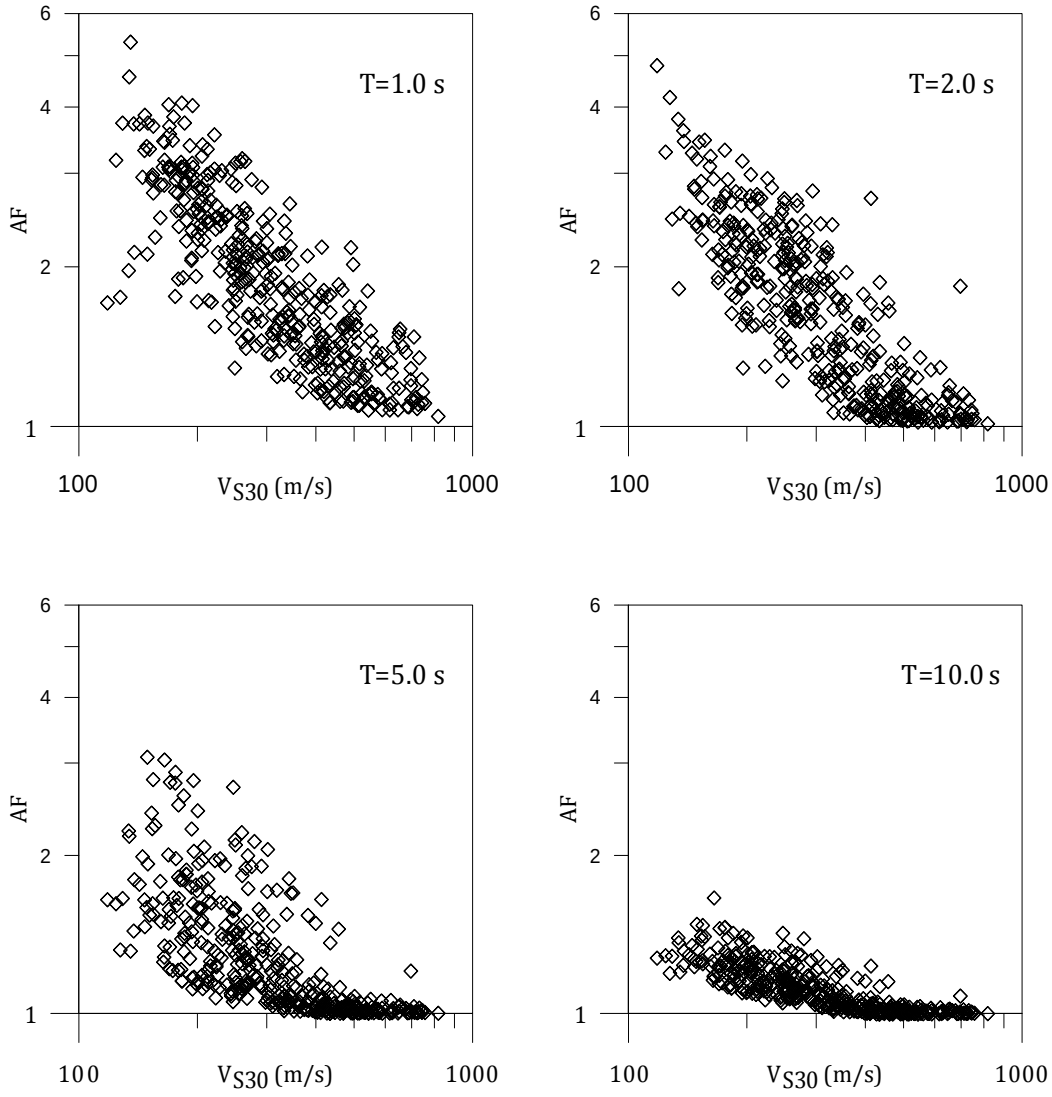

Figure 5.2 Amplification Factor versus V_{S30} for all generated profiles at long periods (T≥1.0 s).

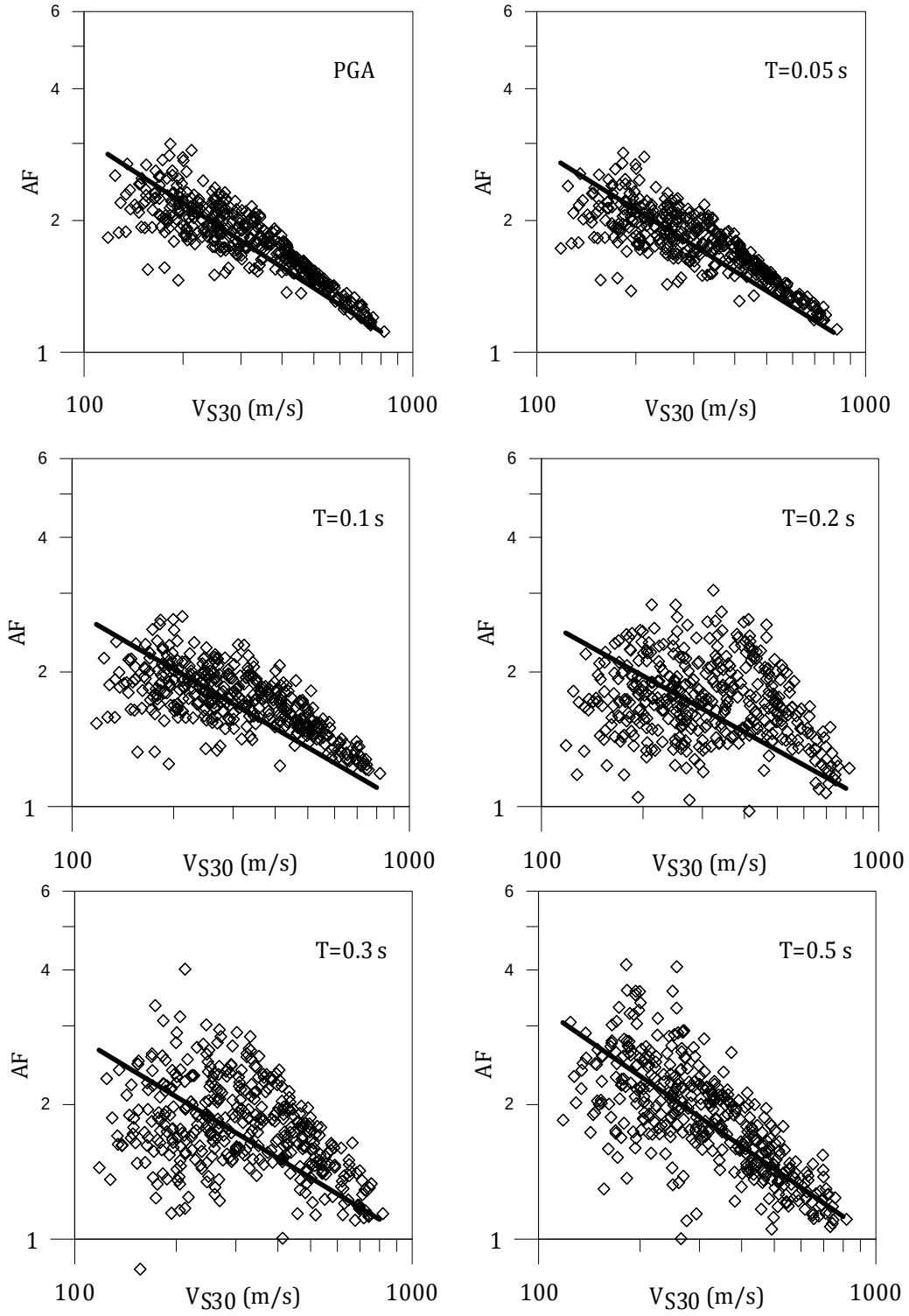

Figure 5.3 Amplification Factor versus V_{S30} and linear fit to data for all generated profiles at short periods (T<1.0 s).

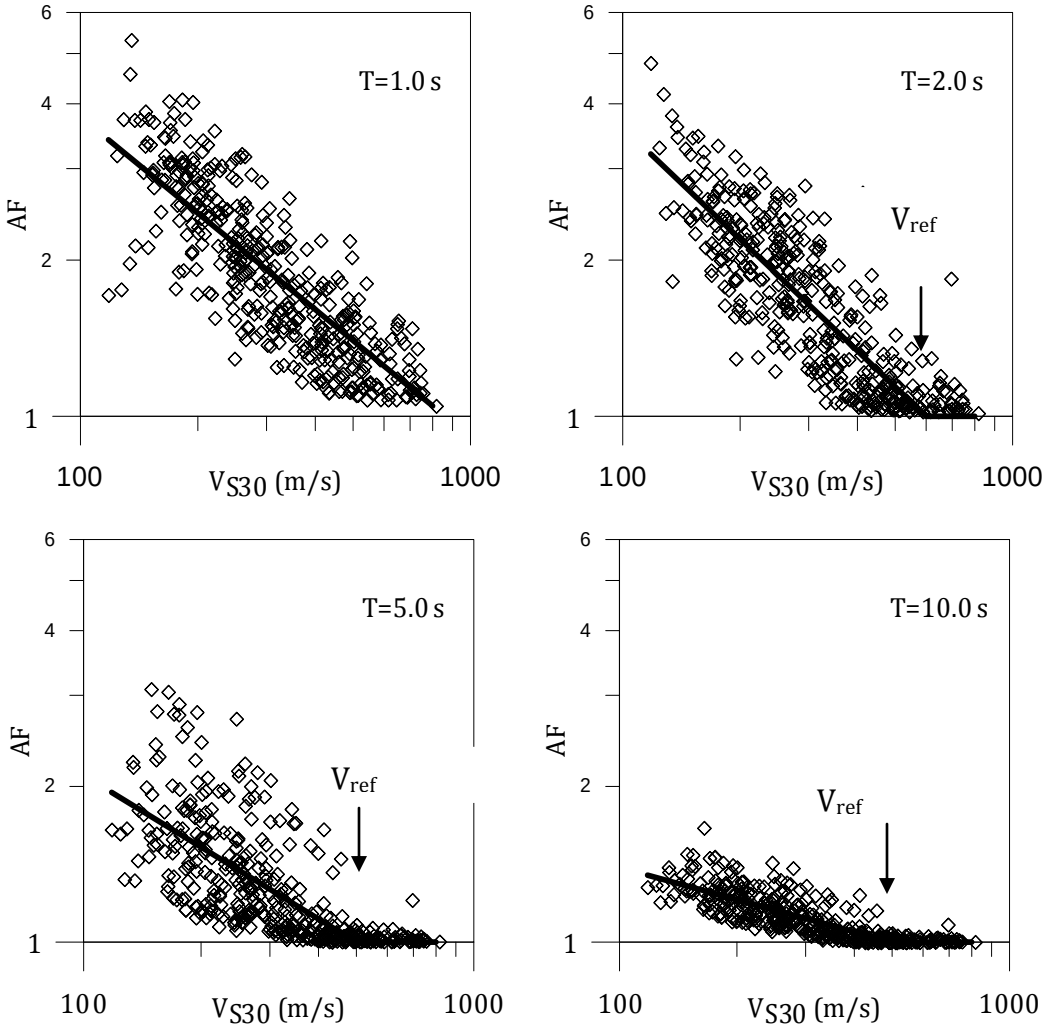

Figure 5.4 Amplification Factor versus V_{S30} and linear fit to data for all generated profiles at long periods (T≥1.0 s).

Table 5.1 Coefficients and σ_{lnAF} of equation (5.1).

T(sec)	a_1	V_{ref} (m/s)	σ_{lnAF}
PGA	-0.49	1000	0.11
0.05	-0.47	1000	0.12
0.1	-0.44	1000	0.15
0.2	-0.42	1000	0.24
0.3	-0.46	1000	0.24
0.5	-0.52	1000	0.20
1.0	-0.62	850	0.20
2.0	-0.72	600	0.19
5.0	-0.46	500	0.18
10.0	-0.21	500	0.06

A second-order polynomial is considered for the relationship between lnAF $\ln(V_{S30}/V_{ref})$. This expression can be described as:

$$\ln(AF)_{LE} = \begin{cases} a_1 \times \ln\left(\frac{V_{S30}}{V_{ref}}\right) + a_2 \times \left[\ln\left(\frac{V_{S30}}{V_{ref}}\right)\right]^2 & \text{if } V_{S30} < V_{ref} \\ 0 & \text{if } V_{S30} \geq V_{ref} \end{cases} \quad (5.2)$$

A maximum likelihood regression is used to fit equation (5.2) to the data at each period. The same V_{ref} values previously identified are used. The values of V_{ref}, a_1, a_2, and σ_{lnAF} for each period are listed in Table 5.2. The resulting second order

polynomials are shown in Figures 5.5 and 5.6, along with the linear fit and the AF data. As compared with the linear fit from equation (5.1), the second order polynomial better fits the data, particularly at smaller V_{S30}. At periods longer than 1.0 s, the parameter a_2 is close to zero indicating that a linear fit best represents the data. Comparing the σ_{lnAF} of polynomial and linear fits, the polynomial fit decreases σ_{lnAF} by 15 to 25% at periods shorter than about 0.5 s but does not significantly decrease it at longer periods. Therefore, the linear fit appears to be appropriate for periods greater than 0.5 s.

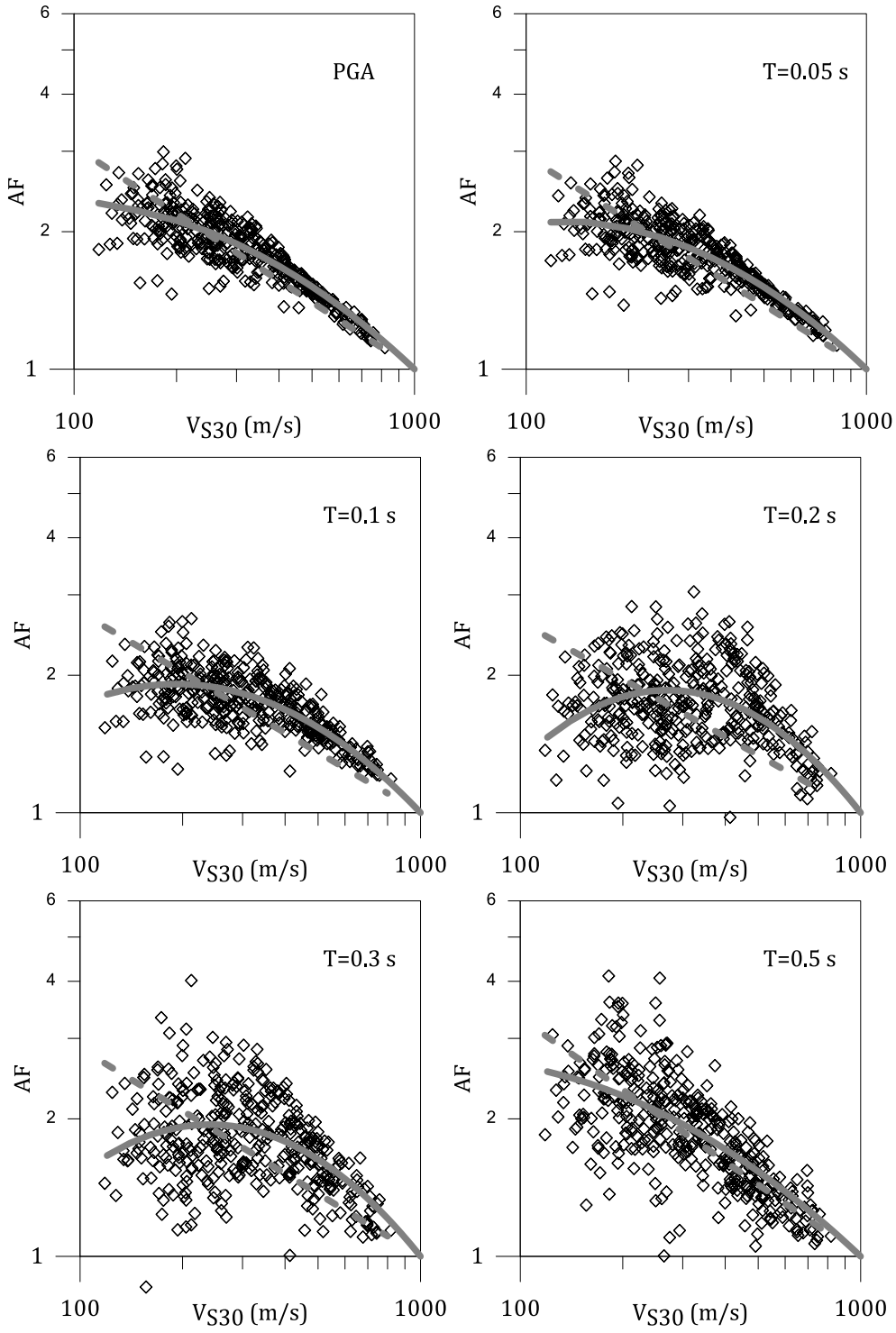

Figure 5.5 Amplification Factor versus V_{S30} along with linear and nonlinear fit to data for all generated profiles at short periods (T<1.0 s).

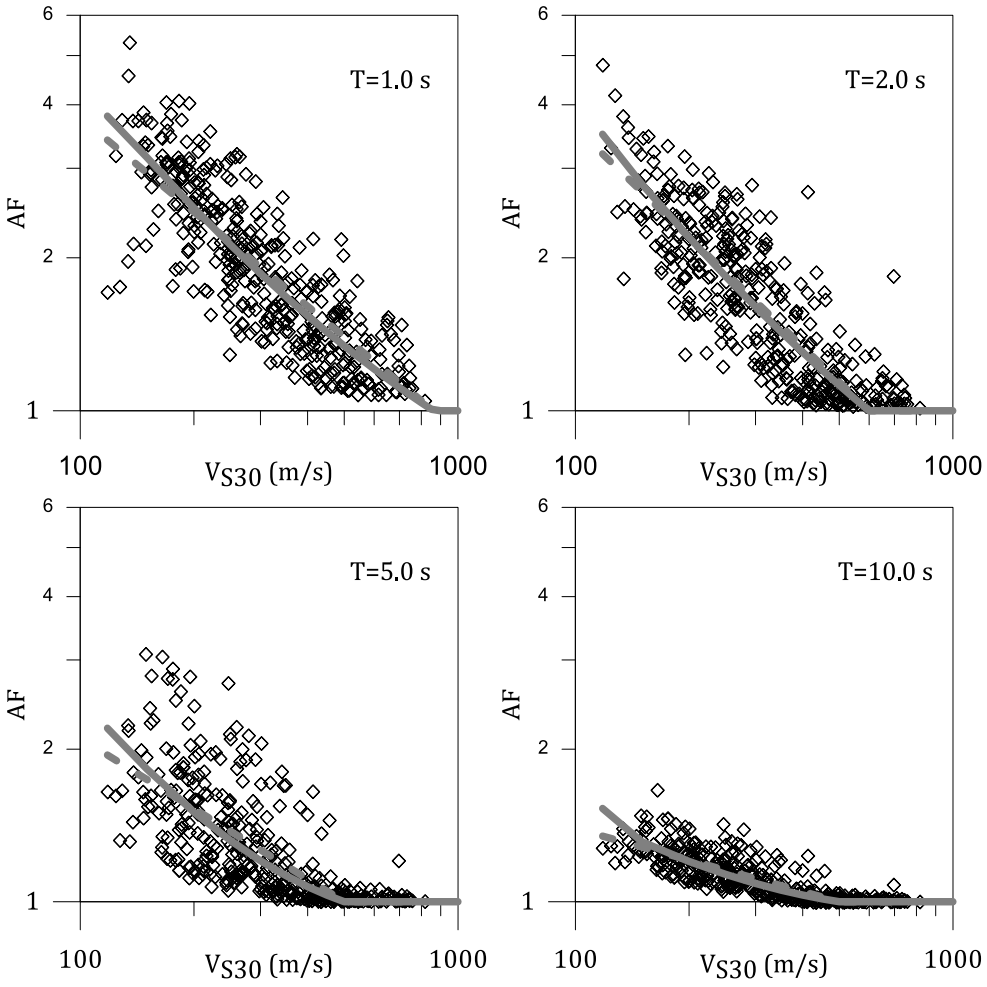

Figure 5.6 Amplification Factor versus V_{S30} along with linear and nonlinear fit to data for all generated profiles at long periods (T≥1).

Table 5.2 Coefficients and σ_{lnAF} of equation (5.2).

T(sec)	a_1	a_2	V_{ref} (m/s)	σ_{lnAF} (Eq 5.2)	σ_{lnAF} (Eq 5.1)	% Reduction
PGA	-0.7	-0.15	1000	0.09	0.11	18
0.05	-0.72	-0.17	1000	0.10	0.12	17
0.1	-0.79	-0.24	1000	0.11	0.15	27
0.2	-0.94	-0.36	1000	0.19	0.24	21
0.3	-0.93	-0.33	1000	0.20	0.24	17
0.5	-0.70	-0.12	1000	0.19	0.20	5
1.0	-0.49	0.09	850	0.19	0.20	5
2.0	-0.62	0.09	600	0.19	0.19	1
5.0	-0.26	0.08	500	0.20	0.18	-11
10.0	-0.12	0.09	500	0.07	0.06	-17

5.3 Influence of Vratio on Amplification

To define the functional form describing the variation in AF with Vratio, the residual of each data point relative to the model developed in equation (5.2) is computed and plotted versus Vratio. The residual is calculated as:

$$\text{Residual} = [\ln (\text{AF})]_{\text{Observed}} - [\ln (\text{AF})]_{\text{Predicted}} \qquad (5.3)$$

where $[\ln(\text{AF})]_{\text{Predicted}}$ is calculated using equation (5.2) for periods shorter than 1.0 s (short periods) and equation (5.1) for $T \geq 1.0$ s (long periods). $[\ln(\text{AF})]_{\text{Observed}}$ is

the computed AF of the soil profile. The calculated residuals are plotted versus Vratio in Figures 5.7 and 5.8 for short and long periods, respectively. There is a strong positive trend between the residuals and Vratio at all 6 short periods. In these cases, sites with larger Vratio experience larger amplification. At long periods, the trend between the residuals and Vratio is not significant indicating that the AF at long periods is not significantly influenced by Vratio.

As previously discussed, AF is V_{S30}-dependent, and thus it is likely that the influence of Vratio on site amplification is also V_{S30} dependent. To identify the functional form that describes the dependence of AF on V_{S30} and Vratio, residuals are plotted versus Vratio for different bins of $V_{S30.}$ Soil profiles are separated into 8 V_{S30} bins as follows: V_{S30}<150 m/s, 150 m/s <V_{S30}<200 m/s, 200 m/s <V_{S30}<250 m/s, 250 m/s <V_{S30}<300 m/s, 300 m/s <V_{S30}<350 m/s, 350 m/s <V_{S30}<450 m/s, 450 m/s <V_{S30}<550 m/s, and 550 m/s <V_{S30}<750 m/s. To normalize the effect of Vratio on AF in a manner similar to Vref, Vratio is normalized by a $Vratio_{ref}$. $Vratio_{ref}$ is set equal to 1.4, which is the average Vratio of all four hundred generated profiles. Residuals are plotted versus ln ($\frac{Vratio}{1.4}$) in Figures 5.9, 5.10, and 5.11 for periods PGA, 0.2 s, and 0.5, respectively. Because the other short periods show similar trend as these periods, only these three periods are shown.

For PGA (Figure 5.9), there is a linear trend between the residual and ln ($\frac{Vratio}{1.4}$) for all V_{S30} bins that can be defined as:

$$\text{Residual} = a_3 \times \ln\left(\frac{\text{Vratio}}{1.4}\right) \quad (5.4)$$

The slope a_3 is different for the different V_{S30} bins, with the largest values occurring at smaller V_{S30}. The slope decreases with increasing V_{S30}, and for V_{S30} greater than about 450m/s the slope is essentially zero.

For periods of 0.2 s (Figure 5.10), a linear trend between the residual and $\ln\left(\frac{\text{Vratio}}{1.4}\right)$ is also observed but the scatter is more significant. Again, the slope of the linear fit (a_3) varies across V_{S30} bins with larger V_{S30} values displaying smaller slopes. For T=0.5 s, a similar trend is observed with the slope decreasing with increasing V_{S30}, and for this period the slope even becomes negative for larger V_{S30} (although significant scatter in the data exists). Figure 5.12 plots the derived values of a_3 versus the median V_{S30} of each bin for periods of PGA, 0.2, and 0.5 s. The data for PGA clearly shows a_3 as a constant at smaller V_{S30} and then a_3 decreases as V_{S30} increases. At V_{S30} of about 500 m/s, a_3 becomes zero. The other periods show similar trends, although not as clearly.

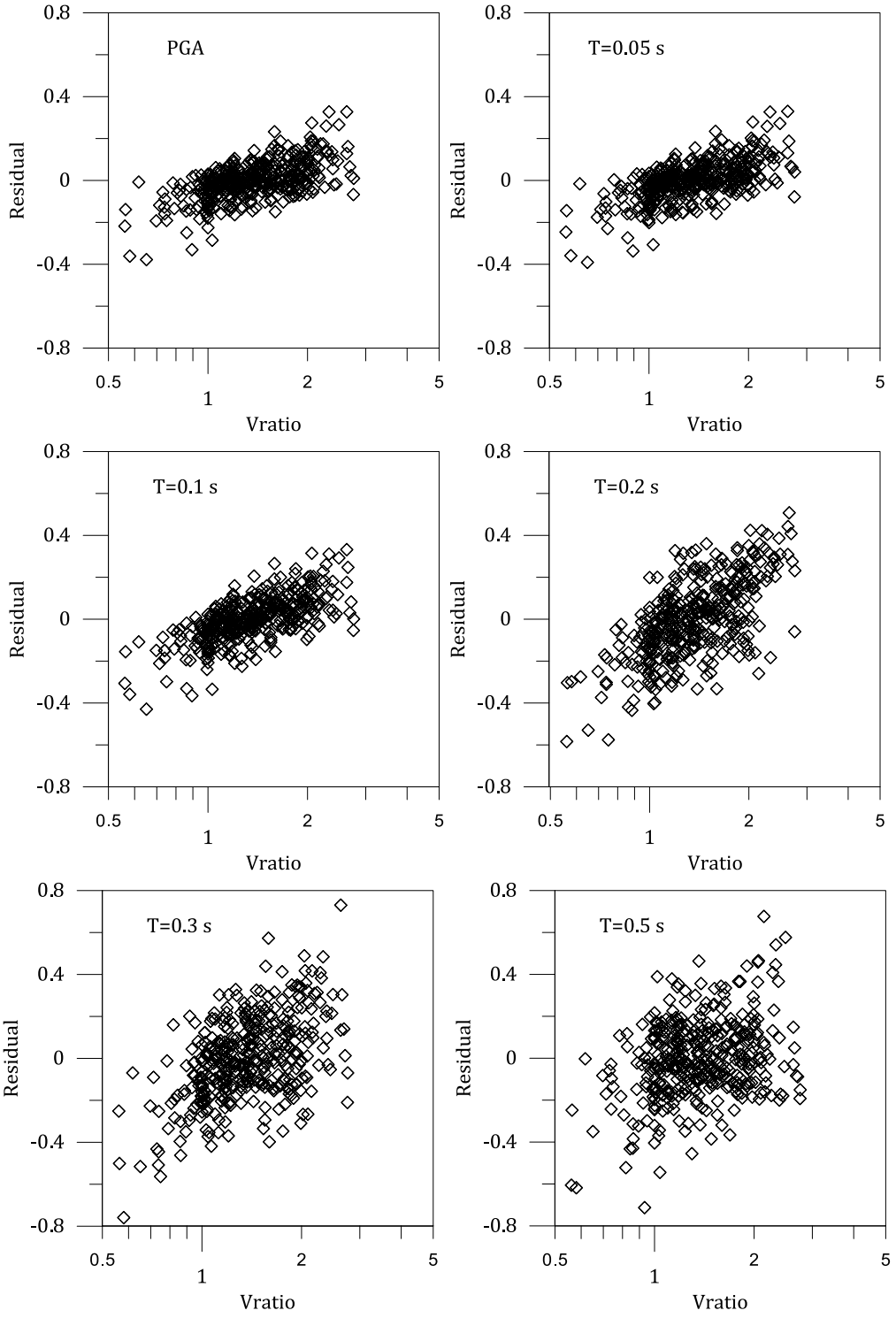

Figure 5.7 Residual versus Vratio at short period.

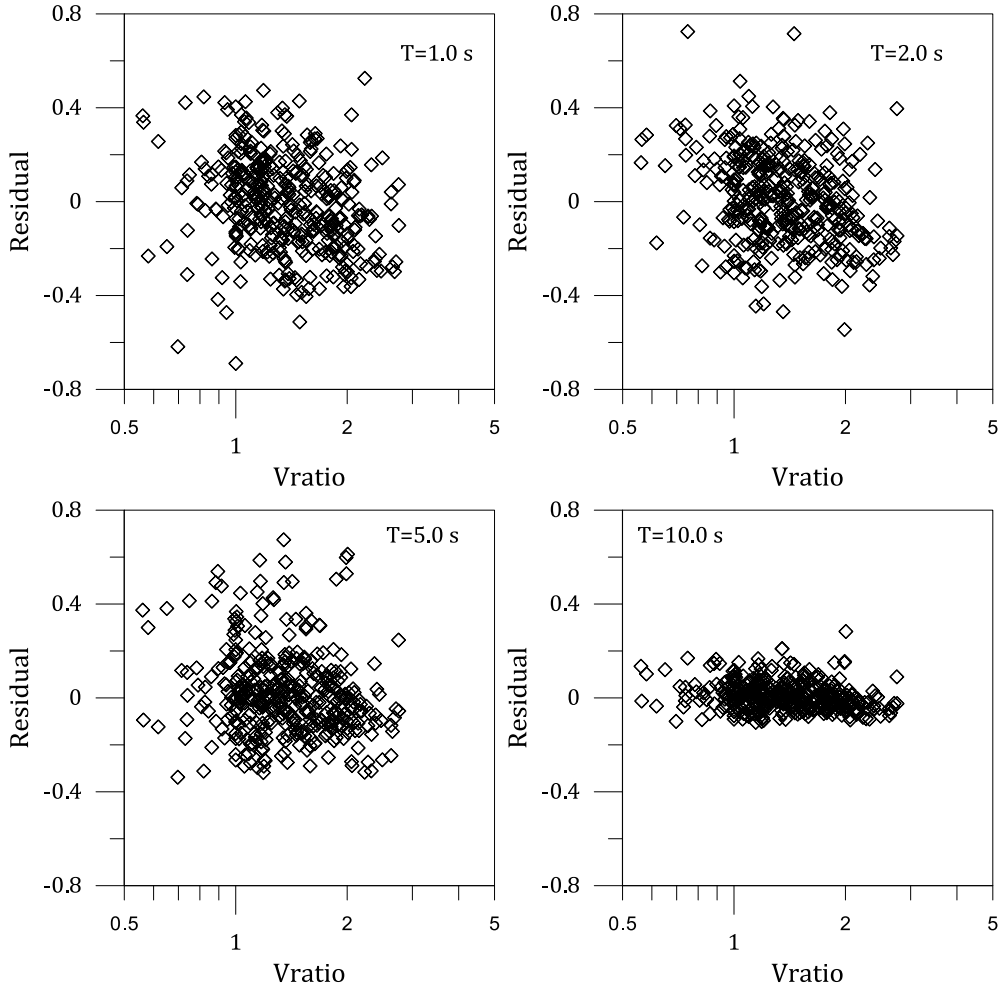

Figure 5.8 Residual versus Vratio at long periods.

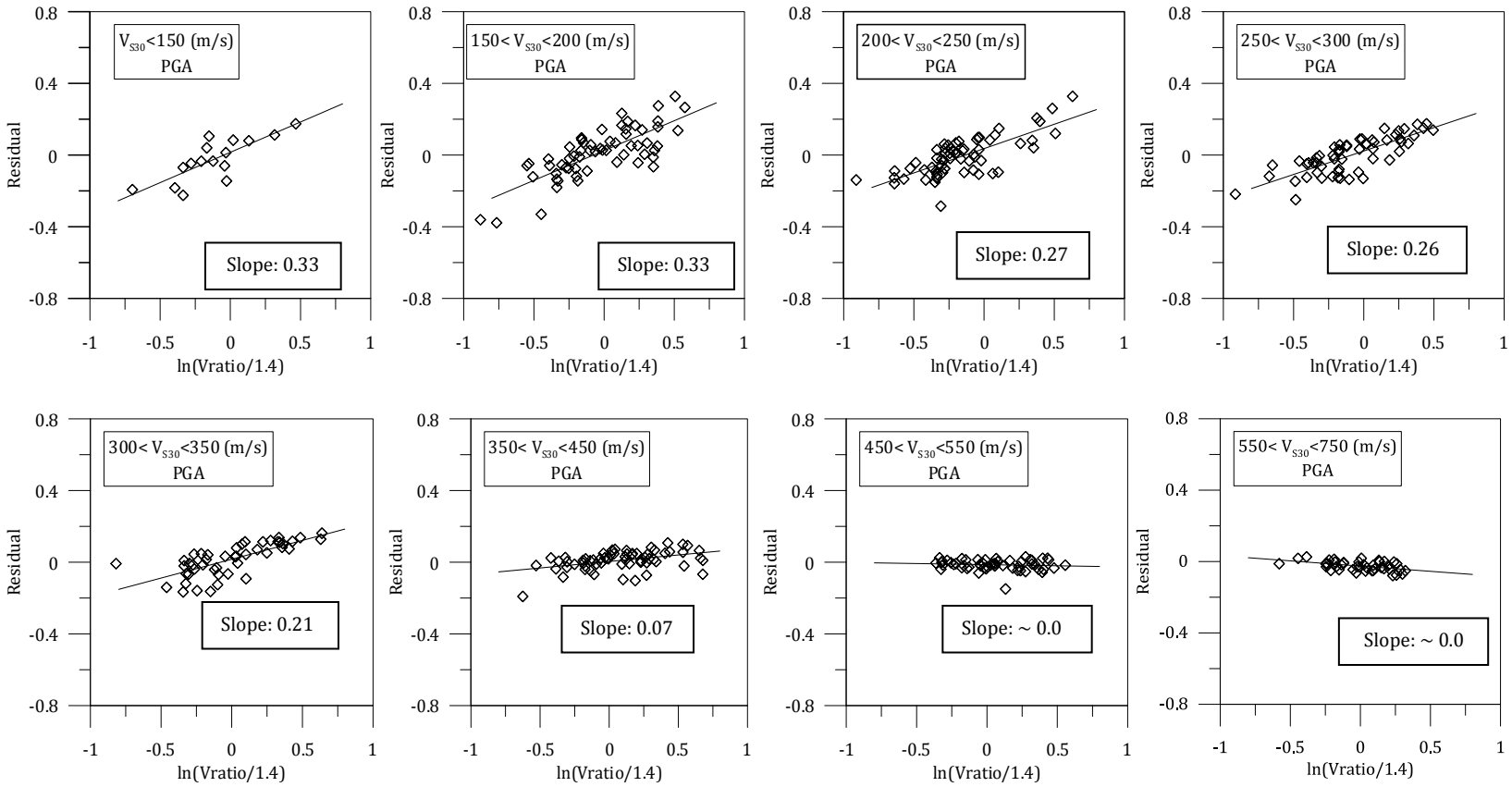

Figure 5.9 Residuals versus ln ($\frac{\text{Vratio}}{1.4}$) for different V_{S30} bins at PGA.

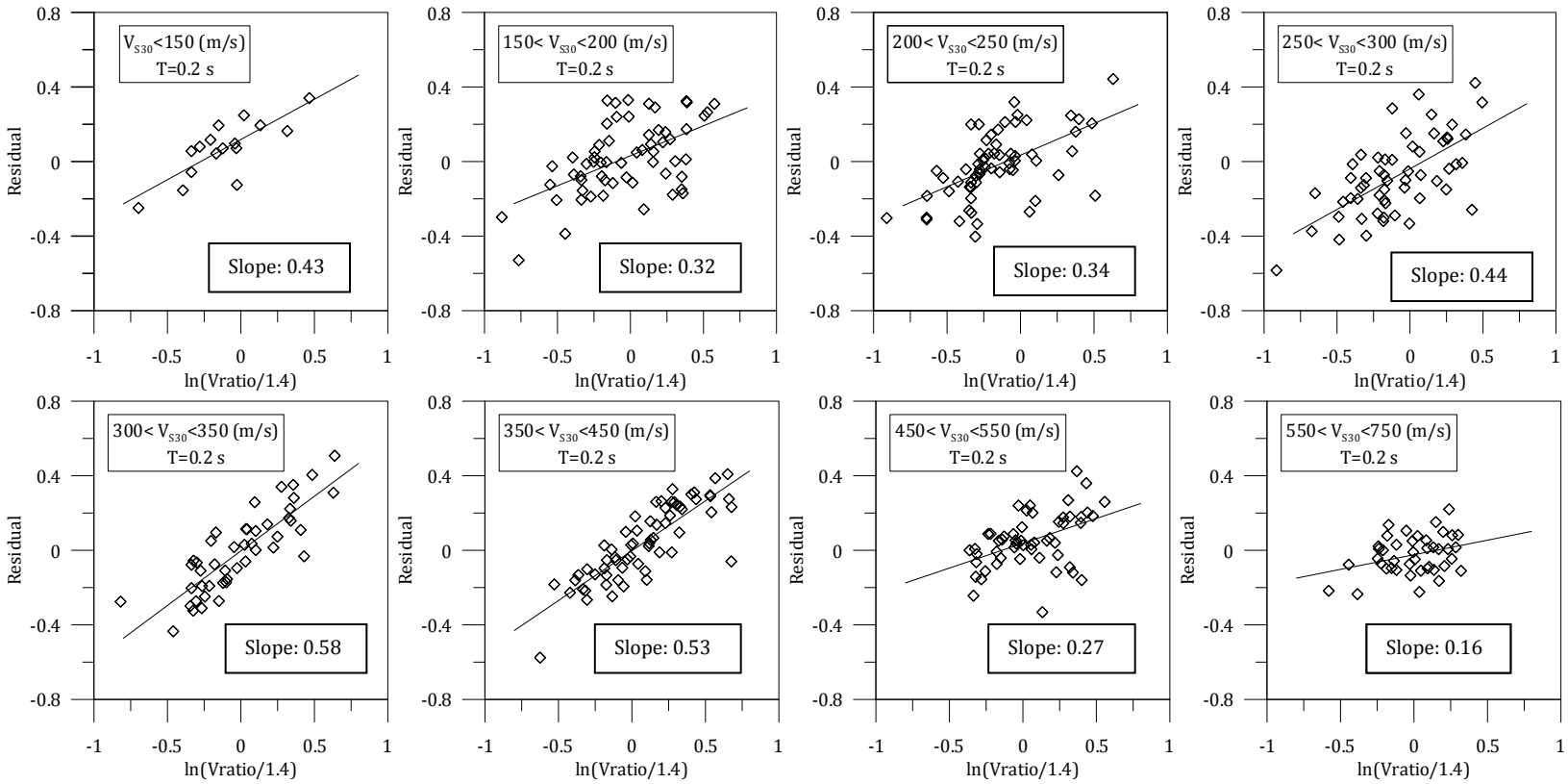

Figure 5.10 Residuals versus ln ($\frac{\text{Vratio}}{1.4}$) for different V_{S30} bins at T=0.2 s.

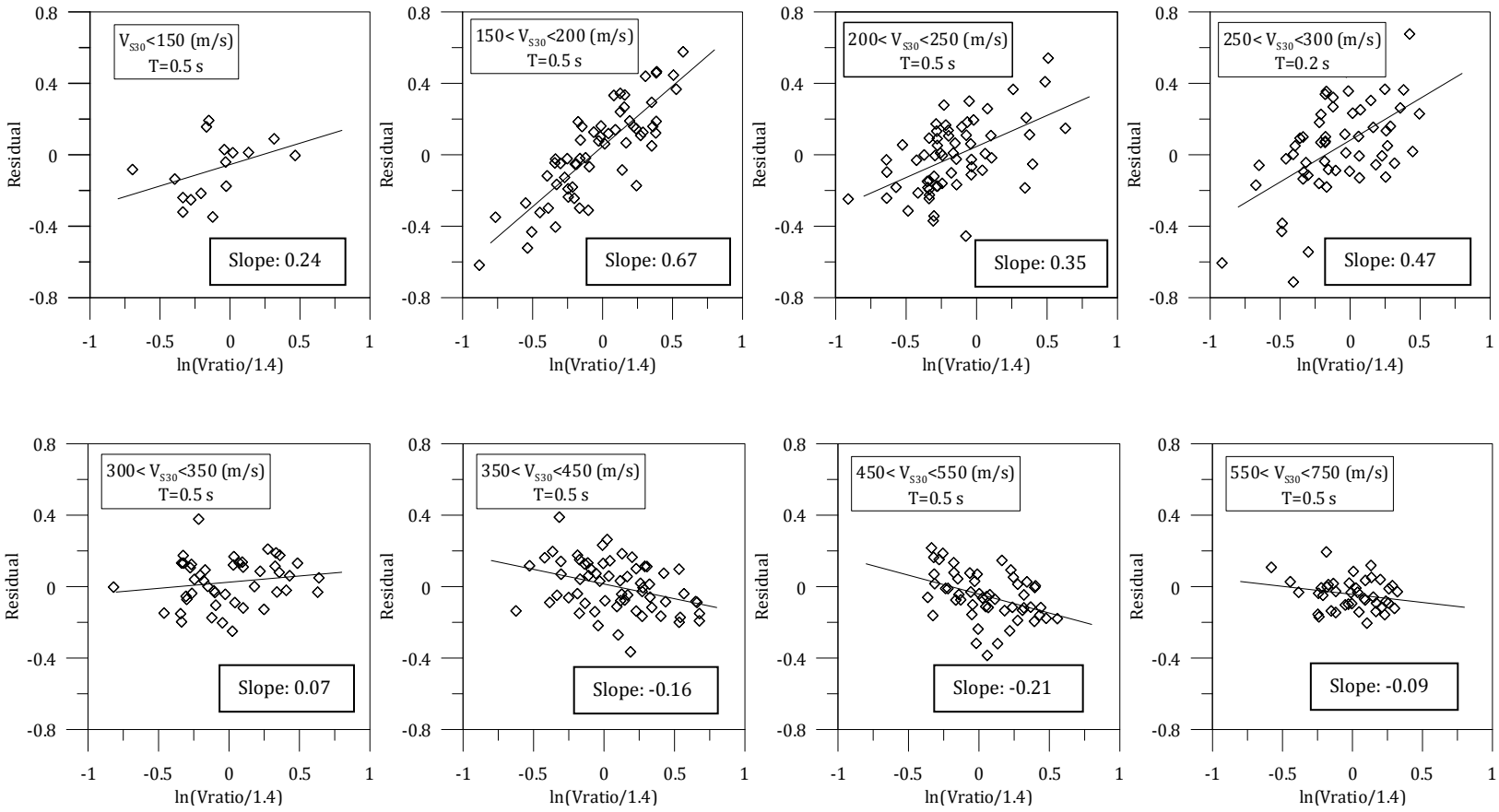

Figure 5.11 Residuals versus ln ($\frac{\text{Vratio}}{1.4}$) for different V_{S30} bins at T=0.5 s.

Using the trends in Figure 5.12, an expression that describes the slope a_3 as a function of V_{S30} is developed. This expression models a_3 as decreasing linearly between V_{S30} values of V_a and V_b, and remaining constant outside of these values. The V_{S30} below which a_3 stays constant is V_a and the V_{S30} value above which a_3 is zero is V_b. a_0 is the value of the slope for V_{S30} less than V_a. The resulting expression is given by:

$$a_3 = \begin{cases} a_0 & \text{if } V_{S30} \leq V_a \\ a_0 - \frac{a_0}{(V_b - V_a)} \times (V_{S30} - V_a) & \text{if } V_a < V_{S30} \leq V_b \\ 0 & \text{if } V_{S30} > V_b \end{cases} \quad (5.5)$$

V_a, V_b, and a_0 are period dependent. This expression will be incorporated into the final form of the linear amplification model, as described next. In Figure 5.12, the estimated values of V_a, and V_b corresponding to PGA, 0.2, and 0.5 s are shown.

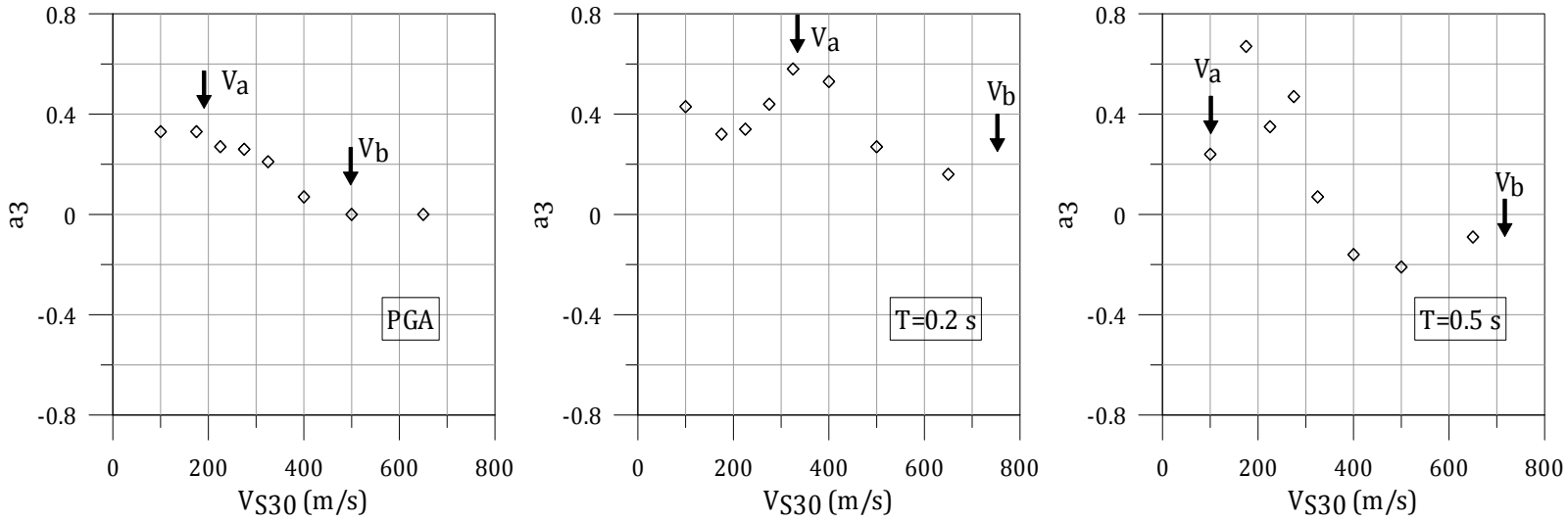

Figure 5.12 a_3 corresponding to each V_{S30} bin versus the median V_{S30} of each bin at PGA, T=0.2 s and 0.5 s.

Considering the influence of Vratio identified above and the functional forms that model this influence, the following model is proposed for the linear amplification factor for spectral accelerations at T≤ 0.5 s:

$$\ln(AF)_{LE} = \begin{cases} a_1 \times \ln\left(\frac{V_{S30}}{V_{ref}}\right) + a_2 \times \left[\ln\left(\frac{V_{S30}}{V_{ref}}\right)\right]^2 + a_3 \times \ln\left(\frac{Vratio}{1.4}\right) & \text{if } V_{S30} < V_{ref} \\ 0 & \text{if } V_{S30} \geq V_{ref} \end{cases}$$

(5.6)

where a_3 is defined by equation (5.5). The parameters a_1, a_2, a_0, V_a, and V_b are estimated by a maximum likelihood regression on the complete AF dataset for an input PGArock of 0.01 g. Table 5.3 lists the model parameters for all 6 short periods.

Table 5.3 Coefficients of the linear amplification model – Equation (5.6).

T (sec)	a_1	a_2	a_0	V_a (m/s)	V_b (m/s)	V_{ref} (m/s)
PGA	-0.69	-0.13	0.34	176	481	1000
0.05	-0.70	-0.15	0.37	147	512	1000
0.1	-0.76	-0.21	0.38	110	737	1000
0.2	-0.90	-0.32	0.44	414	726	1000
0.3	-0.89	-0.28	0.57	100	750	1000
0.5	-0.67	-0.1	0.39	100	750	1000

To evaluate the effect of adding Vratio to the linear amplification model, the standard deviation of the data relative to different models is computed. The standard deviation (σ_{lnAF}) is computed as the standard deviation of the ln residuals (i.e., ln(AFobserved) – ln(AFpredicted)), and it is computed for both the model that does not incorporated Vratio (equation 5.2) and the model that includes Vratio (equation 5.6). The computed values of σ_{lnAF} are listed in Table 5.4 for each period considered. At shorter periods, the inclusion of Vratio decreases the standard deviation by more than 30% while the decrease is about 10% at T=0.5 s.

Table 5.4 Standard deviation of linear amplification models (σ_{lnAF}) with and without considering Vratio.

T (sec)	σ_{lnAF} (without Vratio)	σ_{lnAF} (with Vratio)	% Reduction
PGA	0.09	0.06	33
0.05	0.10	0.06	40
0.1	0.11	0.08	27
0.2	0.19	0.14	26
0.3	0.20	0.16	20
0.5	0.19	0.17	10

The variation of amplification with V_{S30} for different values of Vratio for the developed model (i.e., equation 5.6) is shown in Figure 5.13 for the 6 periods

considered. The curves show how amplification is larger for larger values of Vratio, and this effect is larger at smaller values of V_{S30}.

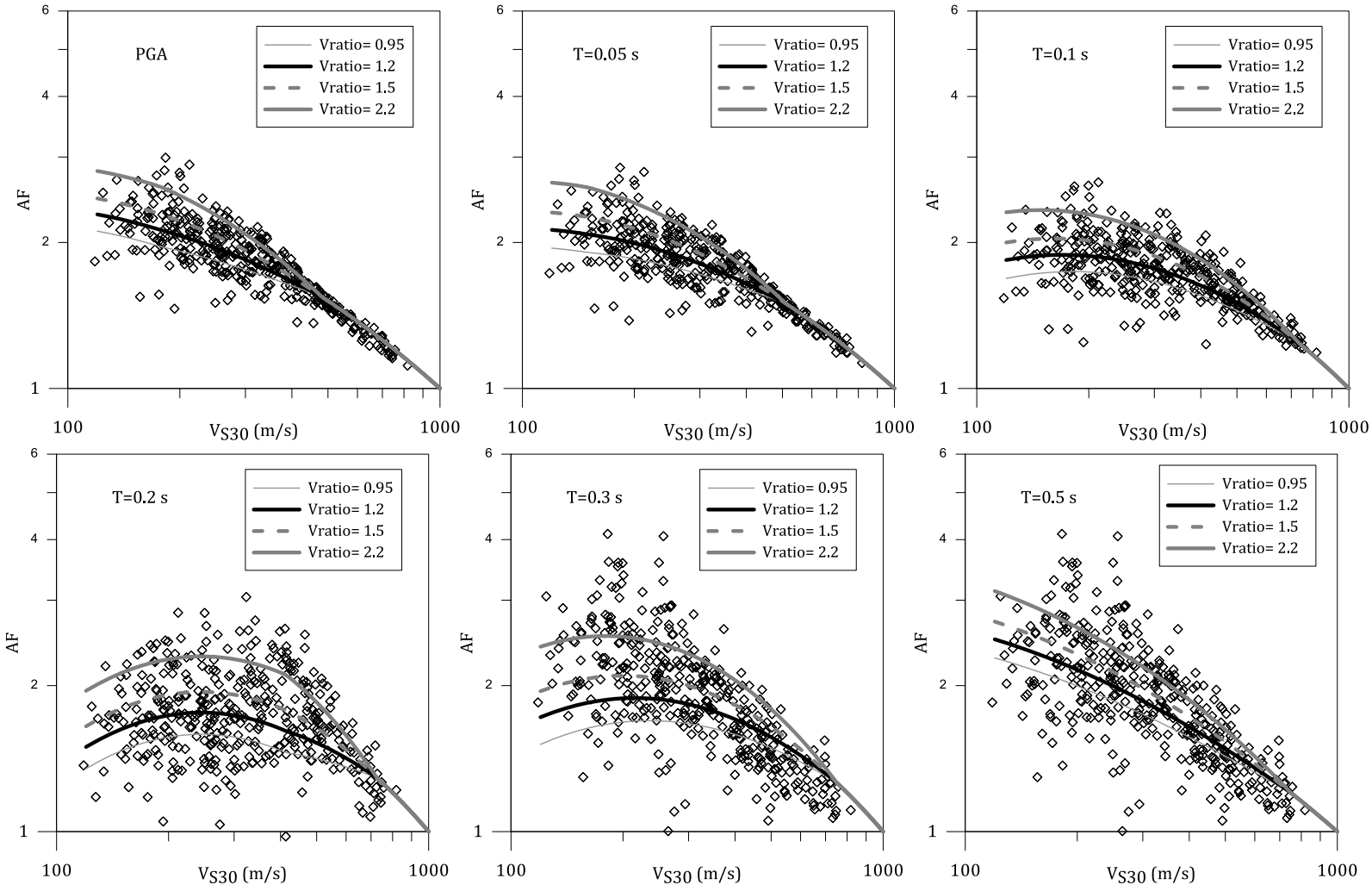

Figure 5.13 Fitted curves to the data for different values of Vratio at all periods considered.

5.4 Influence of $Z_{1.0}$ on Amplification for Long Periods

As discussed in the previous sections, a linear trend between ln(AF) and $\ln(V_{S30}/V_{ref})$ best fits the amplification data for periods greater than or equal to 0.5 s. It is also shown that there is not a strong dependence of AF on Vratio for these periods. Amplification at long periods is controlled predominantly by the depth of soil, such that $Z_{1.0}$ is an important parameter to include in the amplification model. To consider the appropriate functional form for the amplification model that includes $Z_{1.0}$, the amplification data are separated into 4 bins of $Z_{1.0}$ and AF is plotted versus V_{S30}/V_{ref} for each bin. Figure 5.14 plots AF versus V_{S30}/V_{ref} for a spectral period of 1.0 s. The slope of the linear fit of AF versus V_{S30} varies for different bins of $Z_{1.0}$ and generally increases with increasing $Z_{1.0}$. This result indicates that the slope of the linear fit is $Z_{1.0}$ dependent. Figures 5.15, 5.16, and 5.17 show AF versus V_{S30}/V_{ref} for the other long periods, and the same $Z_{1.0}$ trends are observed at the other periods.

A model for this relationship has been proposed by Kottke (2011), as presented in Chapter 2, and is adopted in this study. This model is described as:

$$\ln(AF) = \begin{cases} a_1 \times \alpha \times \ln\left(\frac{V_{S30}}{V_{ref}}\right) & \text{if } V_{S30} < V_{ref} \\ 0 & \text{if } V_{S30} \geq V_{ref} \end{cases} \quad (5.7)$$

where

$$\alpha = \left(\frac{\min(Z^*, Z_{1.0})+1}{Z^*+1}\right)^b \quad (5.8)$$

Z^* is the depth (in meters) above which $Z_{1.0}$ no longer influences the amplification and a_1 is the slope of the ln(AF) versus ln(V_{S30}/Vref) relationship. In the model proposed by Kottke (2011), Z^* is defined as a function of frequency and b is constant at all periods. In this study, Z^* and b are estimated using the maximum likelihood regression method for each period.

The parameters a_1, Z*, and b are computed via a maximum likelihood regression for the four long periods, and the values are listed in Table 5.5 along with the standard deviation of model with and without considering $Z_{1.0}$ effect. Small values of Z* at periods of 1.0 and 2.0 s indicate that a smaller range of depth to bedrock influences amplification at these periods. The reason that larger values of $Z_{1.0}$ do not influence amplification at T = 1.0 s and 2.0 s is because these larger values of $Z_{1.0}$ generate amplification at much longer periods. The larger Z* values for periods of 5.0 and 10 s indicates that all values of $Z_{1.0}$ influence amplification at these periods. Figure 5.18 shows the variation of α with $Z_{1.0}$ for each long period. At T=1.0 s, α approaches 1 for $Z_{1.0}$ greater than 100 m. While for T=10.0 s, α does not reach 1.0 until $Z_{1.0}$ is equal to 1000 m.

The variation of amplification with V_{S30} for different values of $Z_{1.0}$ for the developed model in equations (5.7) and (5.8) is shown in Figure 5.19 for the 4 periods considered. Relationships are shown for four values of $Z_{1.0}$ that represent

the range in the data. The influence of $Z_{1.0}$ at T=1.0 s is not significant different because the derived value of Z* is relatively small. The influence of different values of $Z_{1.0}$ is more readily apparent in the data for periods of 5.0 and 10.0 s. Nonetheless, the reduction in σlnAF when $Z_{1.0}$ is included is relatively modest (Table 5.5).

Table 5.5 Coefficients of the linear amplification model – Equation (5.7).

T(sec)	a_1	Z^* (m)	b	σ_{lnAF} (without $Z_{1.0}$)	σ_{lnAF} (with $Z_{1.0}$)
1.0	-0.63	121	0.70	0.20	0.20
2.0	-0.75	292	0.71	0.19	0.17
5.0	-0.63	490	1.16	0.18	0.16
10.0	-0.44	1000	0.76	0.06	0.05

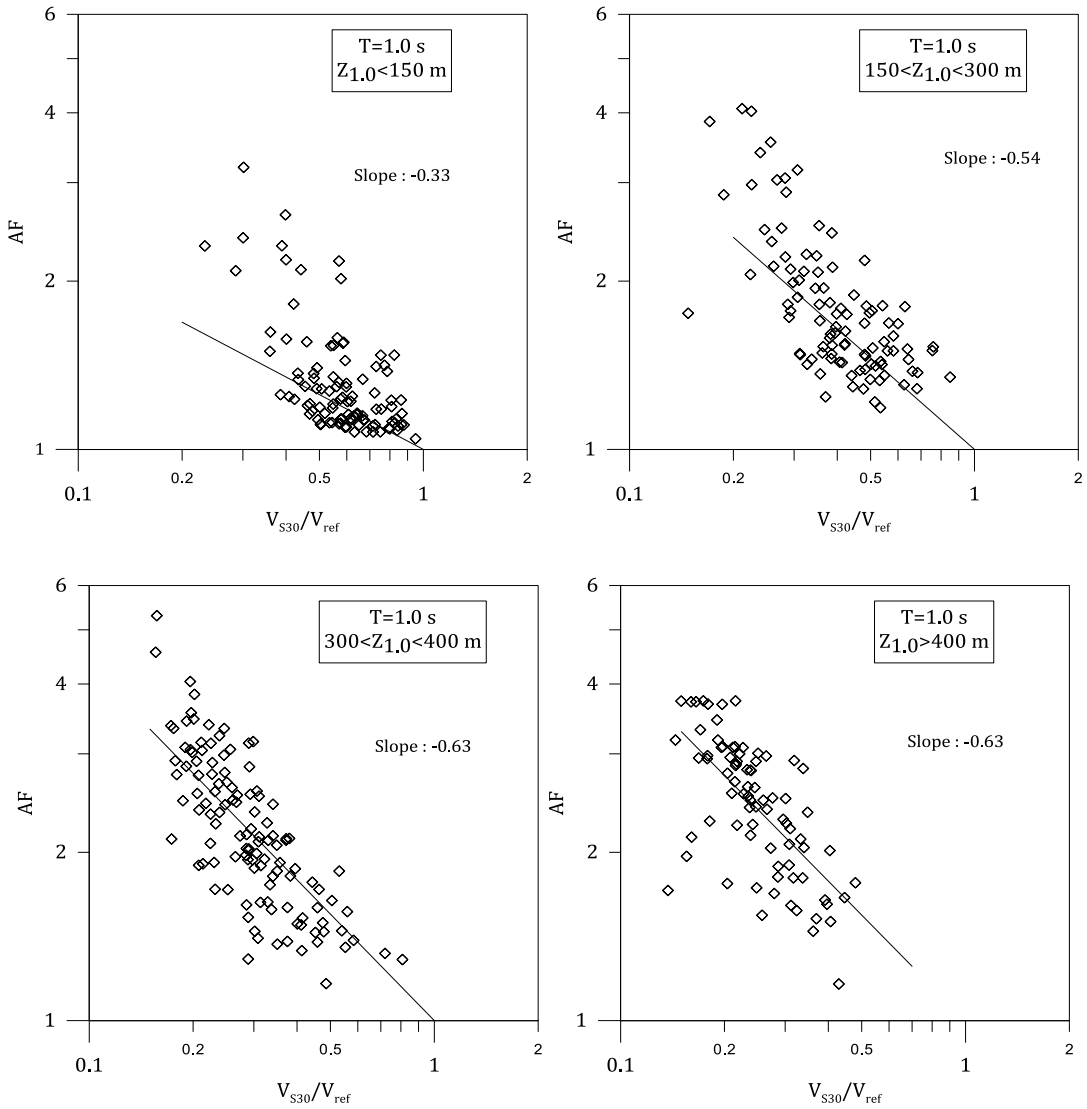

Figure 5.14 AF vesus V_{S30}/V_{ref} for 4 different bins of $Z_{1.0}$ at T=1.0 s.

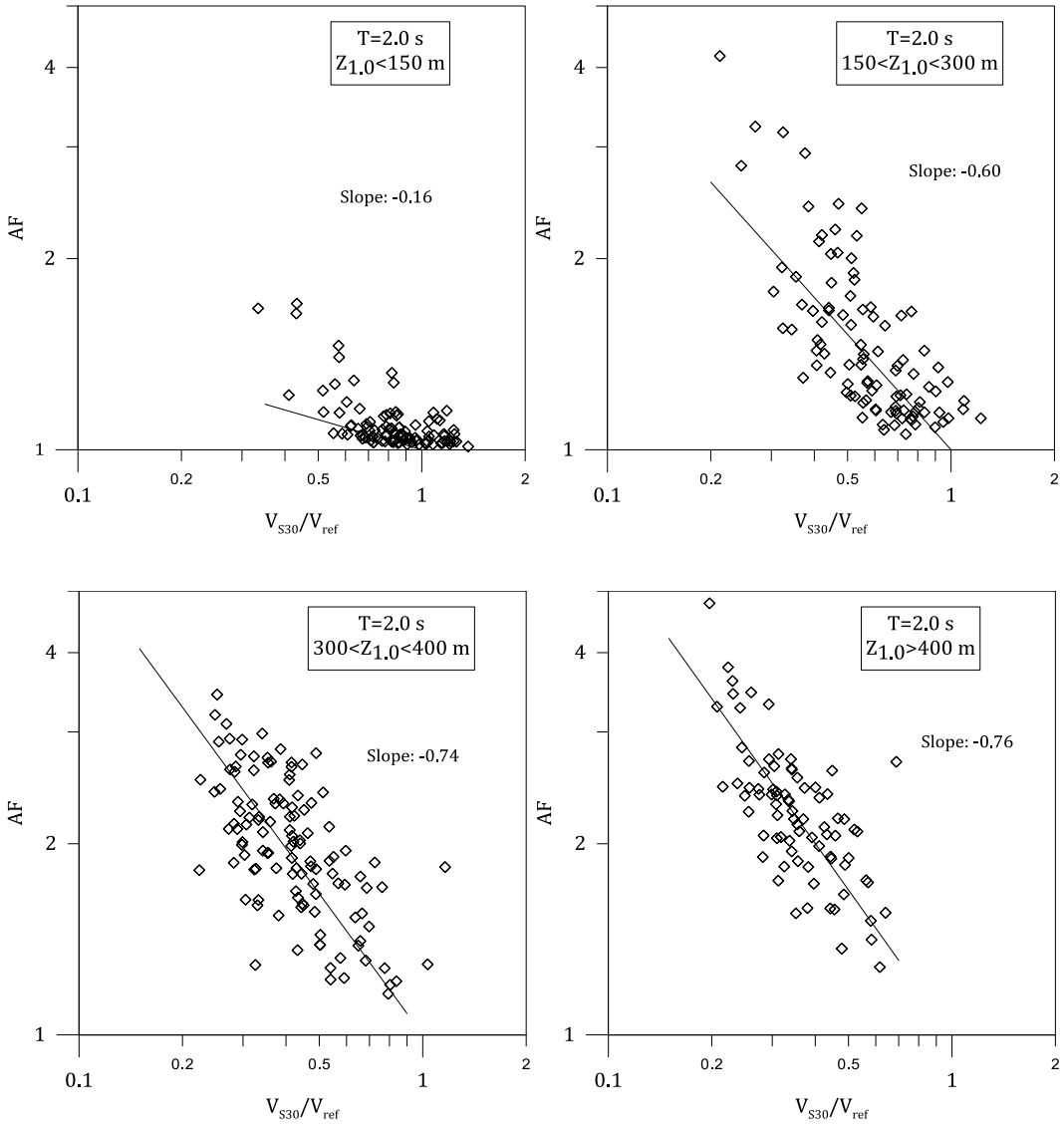

Figure 5.15 AF vesus V_{S30}/V_{ref} for 4 different bins of $Z_{1.0}$ at T=2.0 s.

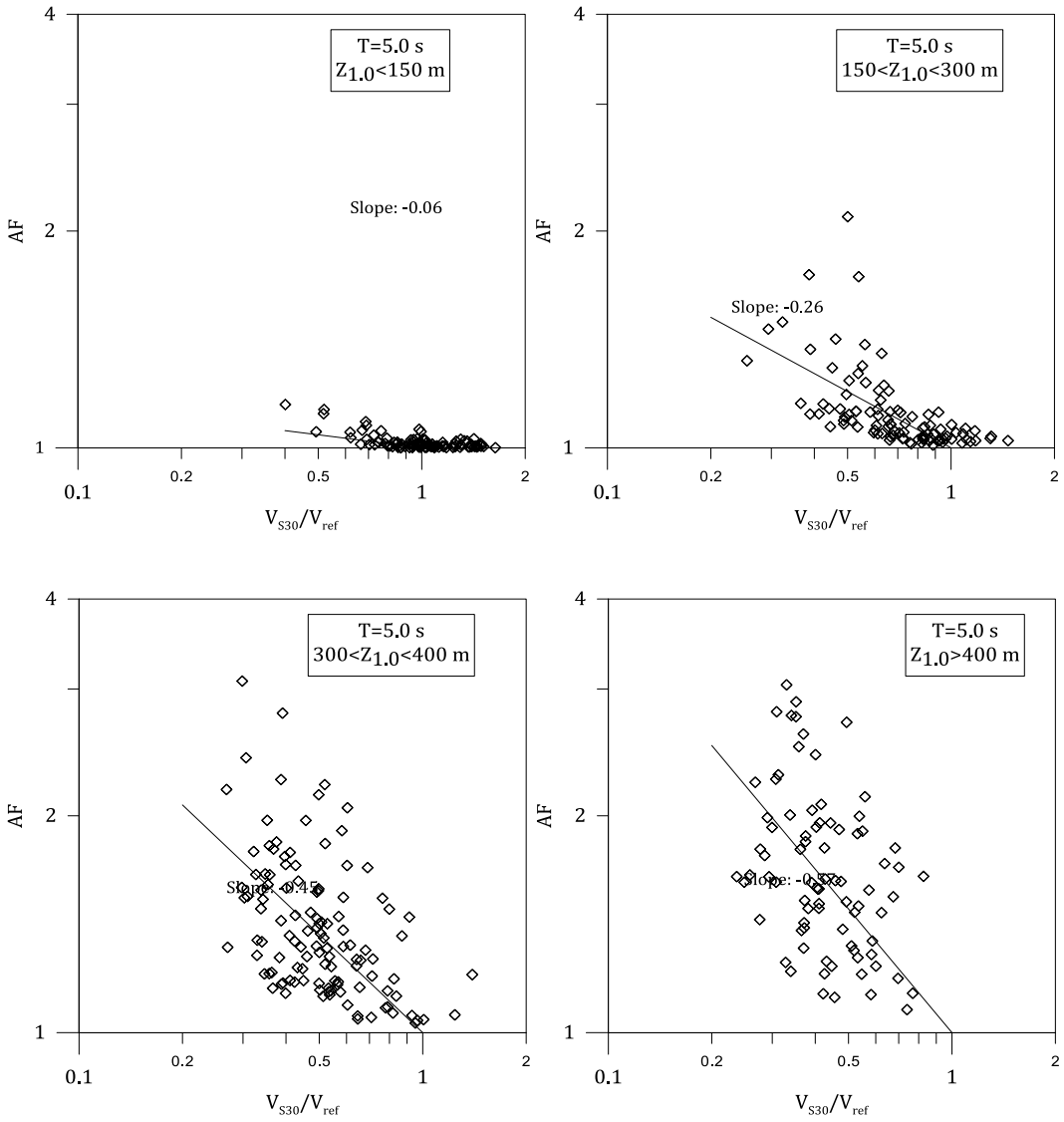

Figure 5.16 AF vesus V_{S30}/V_{ref} for 4 different bins of $Z_{1.0}$ at T=5.0 s.

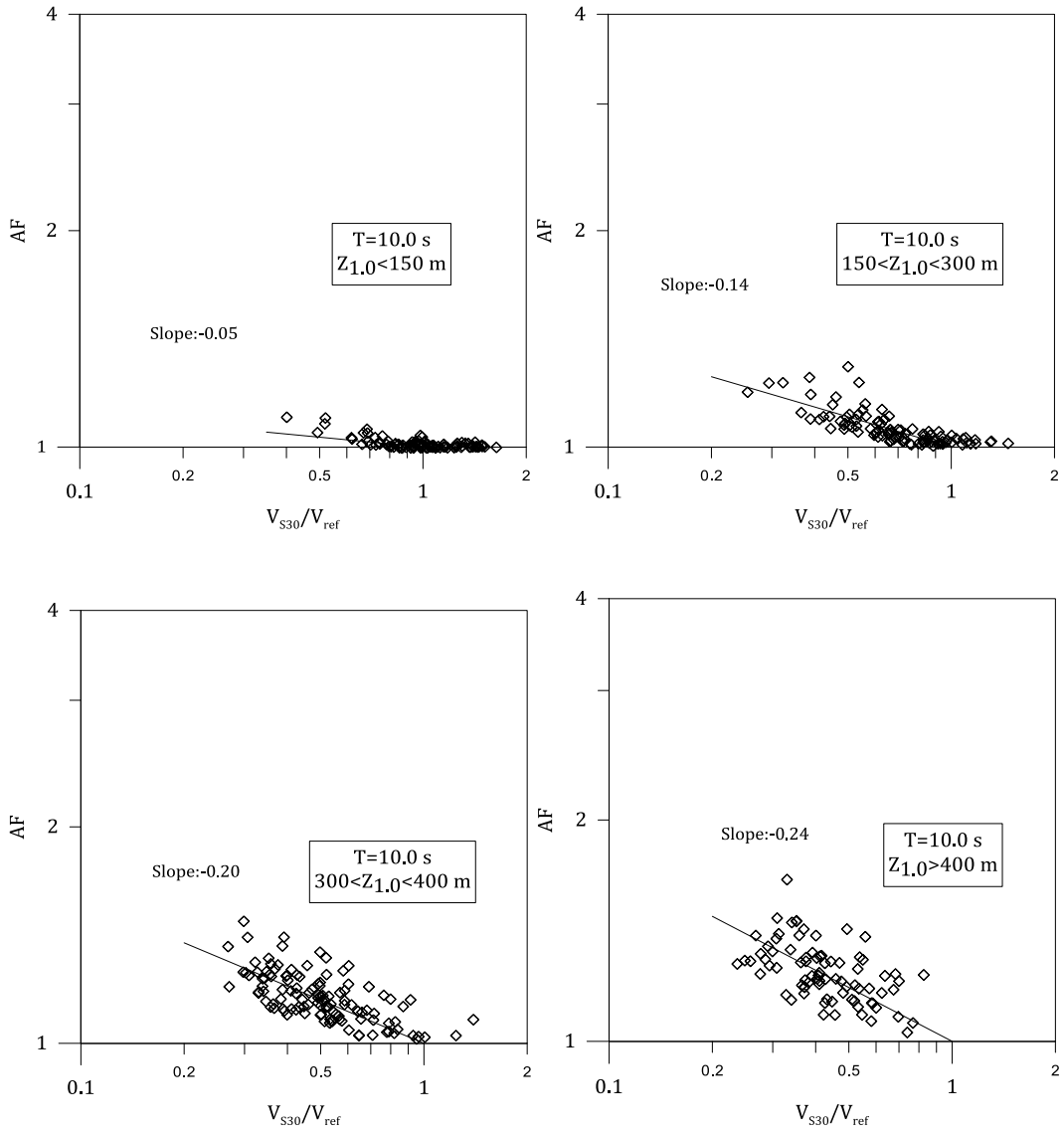

Figure 5.17 AF vesus V_{S30}/V_{ref} for 4 different bins of $Z_{1.0}$ at T=10.0 s.

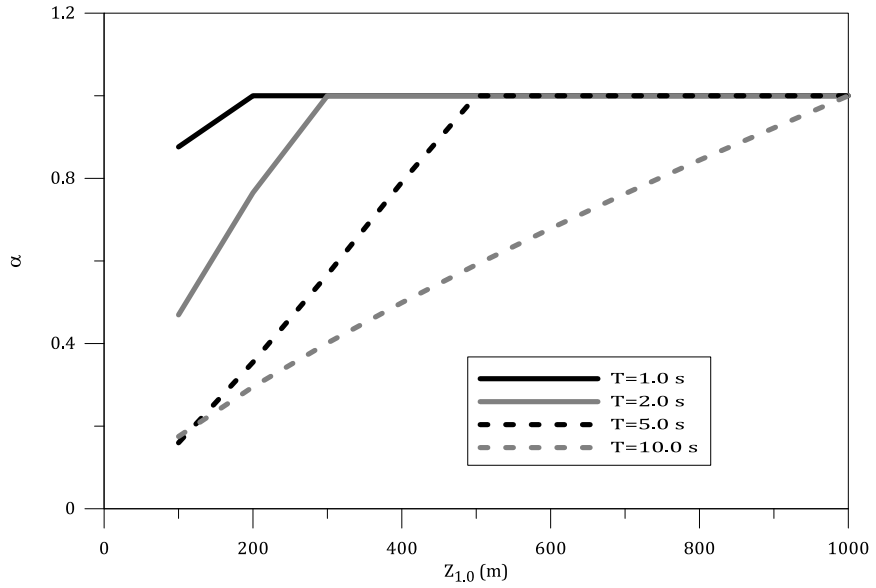

Figure 5.18 Variation of α with $Z_{1.0}$ for different long periods.

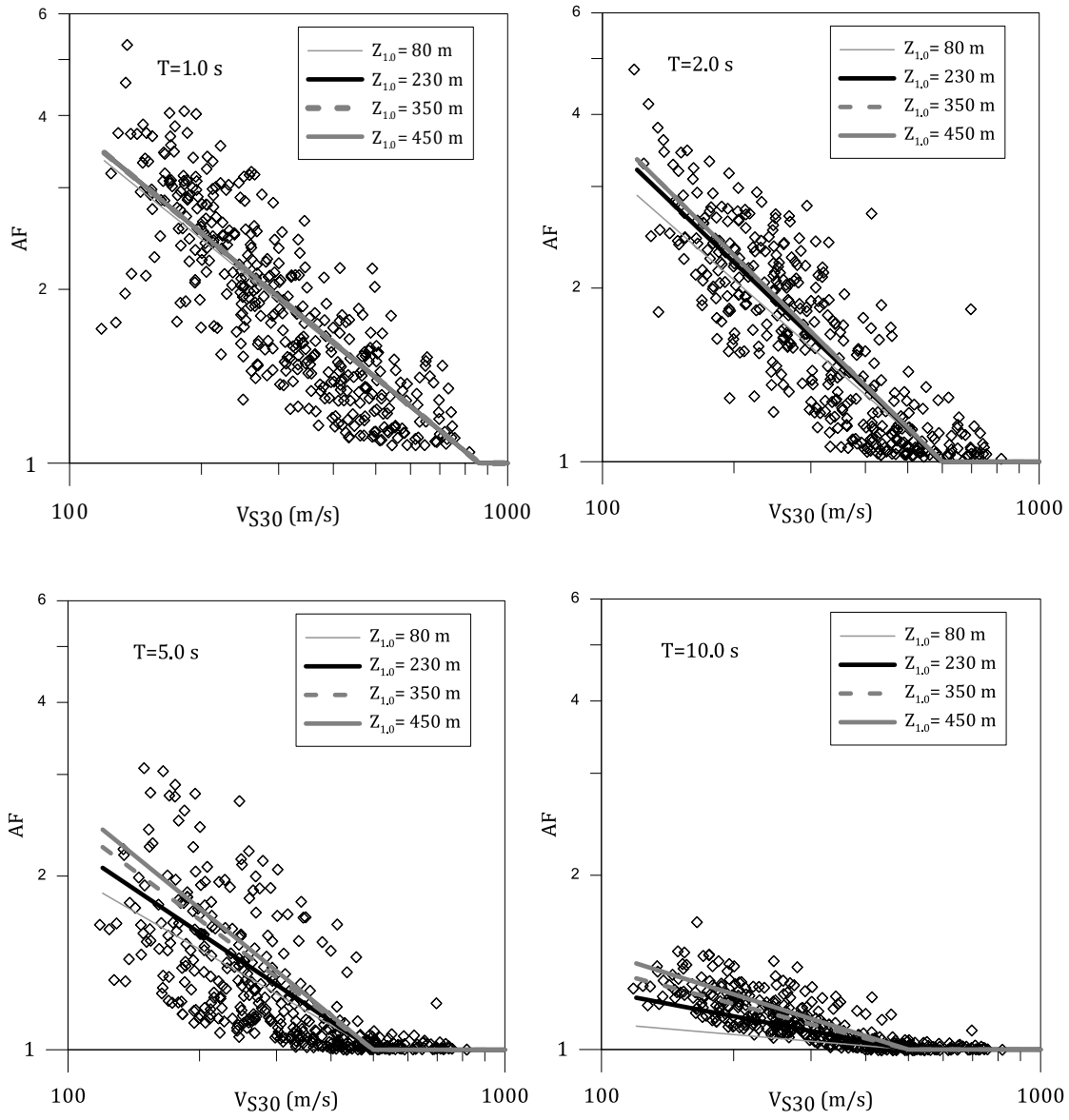

Figure 5.19 Fitted curves to the data for different values of $Z_{1.0}$ at all periods considered.

5.5 Summary

In this chapter, the linear component of the soil amplification models is developed. At short periods, the relationship between AF and normalized V_{S30} (i.e., V_{S30}/V_{ref}) is modified to a polynomial function. It is shown that the polynomial form improves the fattiness of the model to the data. At short periods (T<1.0 s) which Vratio influences the site amplification a term added to the linear component to incorporates the effect of Vratio.

At longer periods (T≥1.0 s), it is shown that the linear relationship between AF and the normalize V_{S30} fits the data the best. It is also identified the slope of this linear relationship is $Z_{1.0}$ dependent and the effect of $Z_{1.0}$ at long periods are considered in the developed linear component of the site amplification model at long periods.

Chapter 6

Models for Nonlinear Site Amplification

6.1 Introduction

As discussed in the previous chapters, the functional form of empirical site amplification models includes two components; a linear elastic component and a nonlinear component. The model for site amplification under linear-elastic conditions is defined in Chapter 5 and the nonlinear component (NL) will be discussed here. A functional form for shorter periods that includes the effects of V_{S30} and Vratio will be presented, and a functional form for longer periods will be presented that includes V_{S30} and $S_{a,rock}$.

6.2 V_{S30} Scaling for Nonlinear Models

The nonlinear component of the soil amplification model includes the effects of soil nonlinearity at high intensity shaking, such that the amplification changes with increasing input shaking intensity. The nonlinear effect can be modeled using a functional form represented by:

$$\ln(AF)_{NL} = b_1 \times \ln(\frac{S_{a,rock}+c}{c}) \quad (6.1)$$

where $S_{a,rock}$ is the spectral acceleration for rock conditions at the spectral period of interest, and b_1 and c are regression coefficients. This functional form was used by Chiou and Youngs(2008) in their NGA model.

It is helpful to consider how parameters b_1 and c control the variation of AF with shaking intensity (i.e., $S_{a,rock}$). Coefficient c essentially represents the $S_{a,rock}$ level in the middle of transition from linear behavior (i.e., where AF does not vary with $S_{a,rock}$) to nonlinear behavior (i.e., where AF does vary with $S_{a,rock}$). Coefficient b_1 represents the degree of nonlinearity in terms of the logarithmic change in AF with a logarithmic increase in the level of shaking .Generally, b_1 is negative such that an increase in $S_{a,rock}$ results in a decrease in AF. A more negative value of b_1 indicates a stronger reduction in AF with $S_{a,rock}$ (i.e. more nonlinearity), and as b_1 approaches zero the site amplification approaches the linear elastic condition. The degree of nonlinearity is a function of the stiffness of the site; with softer sites experiencing more nonlinearity. Therefore, b_1 is a function of V_{S30}.

Figure 6.1 shows AF versus $S_{a,rock}$ as predicted by the Chiou and Youngs (2008) NGA model at periods of PGA, 0.2, and 0.5 s and for 3 different V_{S30} values (150 m/s, 300 m/s and 500 m/s). Also shown are the locations of coefficient c for each period (c is not taken V_{S30} dependent in the Chiou and Youngs (2008) model) and a representative slope (b_1) at larger $S_{a,rock}$. At each of the spectral periods, nonlinearity is stronger at smaller values of $V_{S30.}$ At large values of V_{S30} (e.g., V_{S30}=500m/s in Figure 6.1), the reduction of AF with increasing $S_{a,rock}$ is insignificant which indicates the more linear behavior of stiff sites. The coefficient c, which is the shaking level transitioning from linear to nonlinear behavior, is close to 0.1 g at PGA and 0.5 s, while it is higher (0.25 g) at a spectral period of 0.2 s.

To investigate the dependency of AF on $S_{a,rock}$ and the factors that influence this relationship, the computed AF values for the randomized site profiles subjected to 10 different input intensities are considered. Amplifications of the soil profiles at short and long periods are considered separately in the next sections.

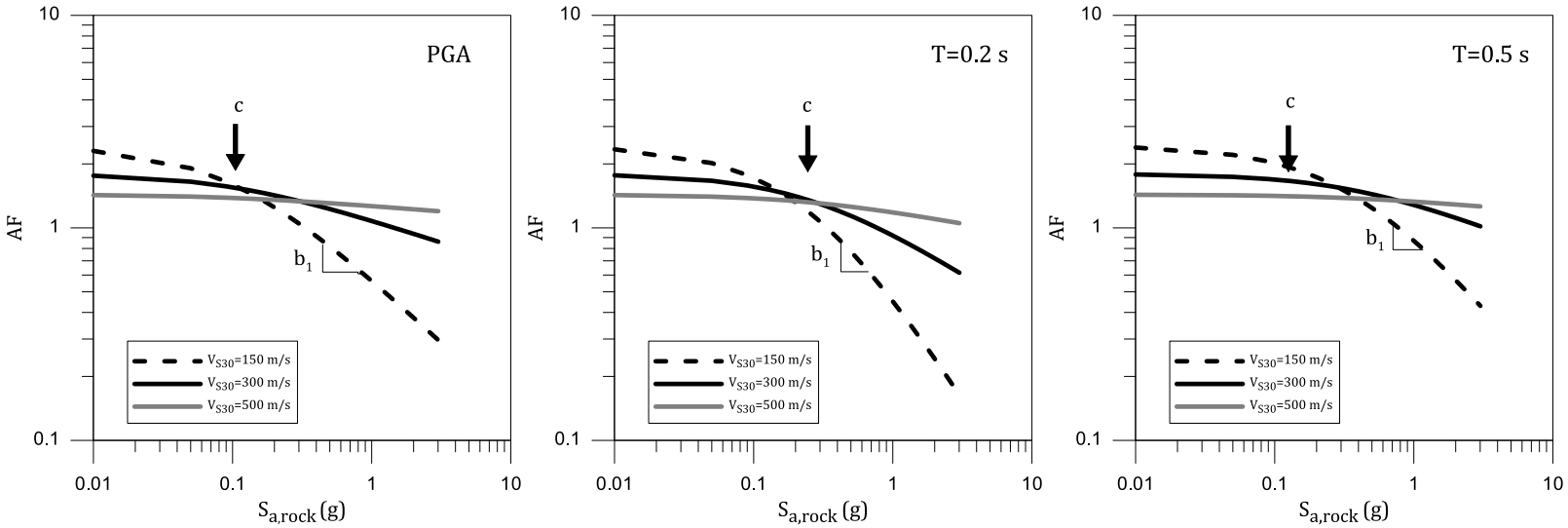

Figure 6.1 Amplification versus $S_{a,rock}$ from the Chiou and Youngs NGA model (2008).

6.3 Nonlinear Site Amplification at Short Periods

Building upon previous work, the nonlinear AF model will be developed from equation (6.1). The dependence of the slope b_1 on V_{S30} is investigated by separating the AF data into the same eight V_{S30} bins used in Chapter 5 (V_{S30}<150 m/s, 150m/s<V_{S30}<200 m/s, 200 m/s <V_{S30}<250m/s, 250 m/s <V_{S30}<300 m/s, 300 m/s <V_{S30}<350 m/s, 350 m/s <V_{S30}<450 m/s, 450 m/s <V_{S30}<550 m/s, and 550 m/s <V_{S30}<750 m/s). Figure 6.2 shows plots of AF versus $S_{a,rock}$ for PGA for the eight bins of V_{S30}. At the smaller V_{S30} values amplification almost immediately starts to decrease as $S_{a,rock}$ increases from 0.01g. At larger V_{S30} (i.e. greater than about 300 m/s) AF remains relatively constant at $S_{a,rock}$ level less than about 0.1g but then decreases as $S_{a,rock}$ increases beyond 0.1g. At the largest V_{S30} values AF does not vary significantly over the $S_{a,rock}$ values analyzed.

To identify the variation of b_1 with V_{S30}, a linear relationship is fit between the logarithm of AF in each V_{S30} bin and the logarithm of $S_{a,rock}$, using only AF data from $S_{a,rock}$ >0.1 g in each bin. Only the data with $S_{a,rock}$ larger than 0.1g is considered because b_1 represents the slope at larger input intensities. The slope of the linear relationship (b_1) is shown in Figure 6.2 and varies across the V_{S30} bins, with larger V_{S30} values displaying smaller slopes. For T=0.2 s and 0.5 s (Figures 6.3 and 6.4, respectively) a similar trend is observed with the slope decreasing with increasing V_{S30}. Figure 6.5 plots the derived values of b_1 versus the median V_{S30} of each bin for periods of PGA, 0.2, and 0.5 s. The data for all 3 periods show b_1 as approximately

constant at smaller V_{S30} and then decreasing towards zero as V_{S30} increases. Above some value of V_{S30}, b1 tends to remains constant.

Using the trends in Figure 6.5, an expression that describes the slope b_1 as a function of V_{S30} is developed. This expression models b_1 as decreasing log-linearly between V_{S30} values of V_1 and V_2, and remaining constant outside of these values.

The V_{S30} below which b_1 stays constant is V_1 and the value above which b_1 stays constant is V_2. b_{o1} and b_{o2} are the values of the slope for V_{S30} less than V_1 and greater than V_2 , respectively. The resulting expression is given by:

$$b_1 = \begin{cases} b_{o1} & \text{if } V_{S30} \leq V_1 \\ b_{o1} + \frac{b_{o2} - b_{o1}}{\ln\left(\frac{V_2}{V_1}\right)} \times \ln\left(\frac{V_{S30}}{V_1}\right) & \text{if } V_1 < V_{S30} \leq V_2 \\ b_{o2} & \text{if } V_{S30} > V_2 \end{cases} \qquad (6.2)$$

V_1, V_2, b_{o1}, and b_{o2} are regression coefficients that are period dependent. This expression will be incorporated into the final form of the nonlinear amplification model.

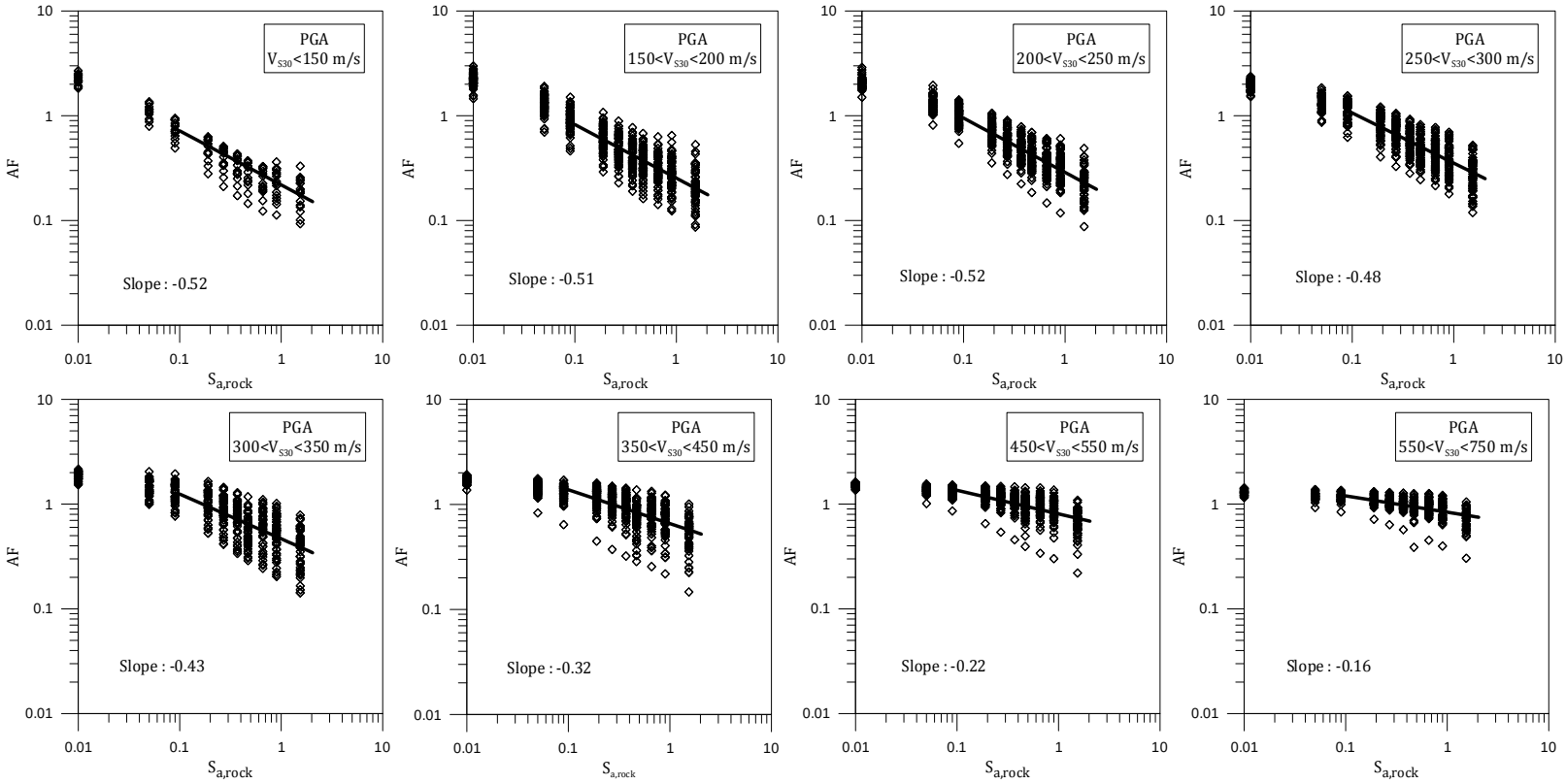

Figure 6.2 Amplification versus $S_{a,rock}$ for different V_{S30} bins at PGA.

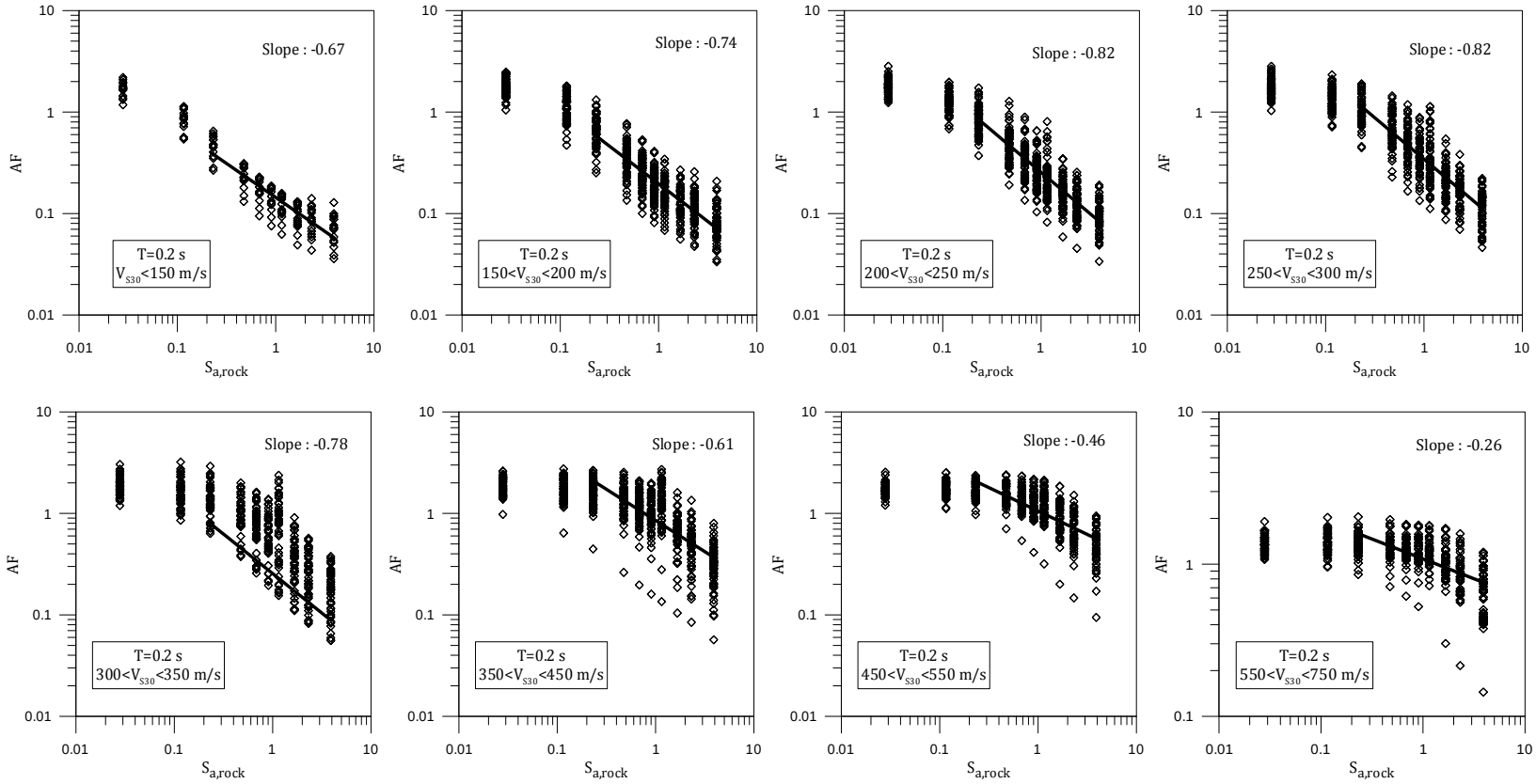

Figure 6.3 Amplification versus $S_{a,rock}$ for different V_{S30} bins at T=0.2 s.

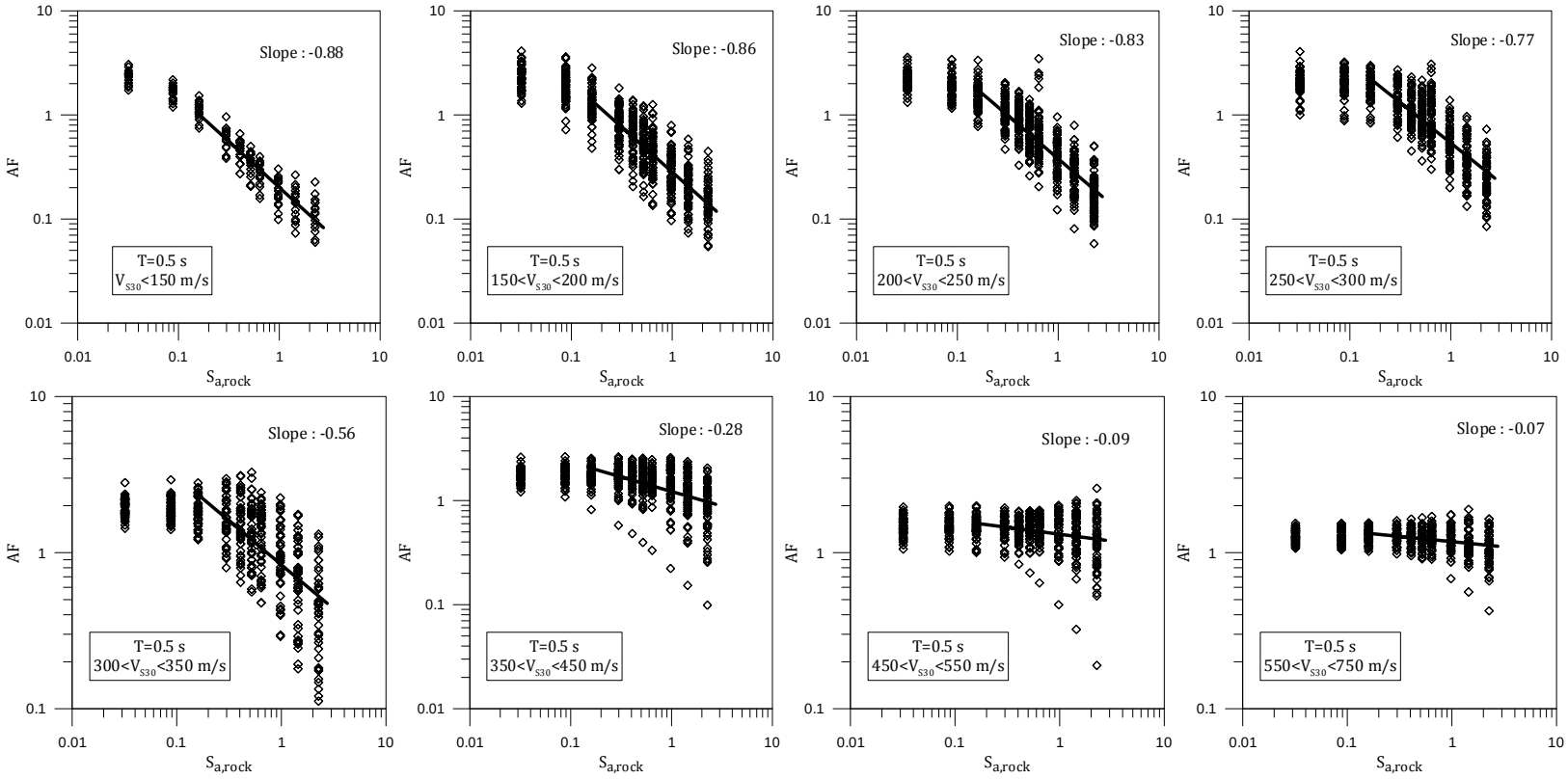

Figure 6.4 Amplification versus $S_{a,rock}$ for different V_{S30} bins at T=0.5 s.

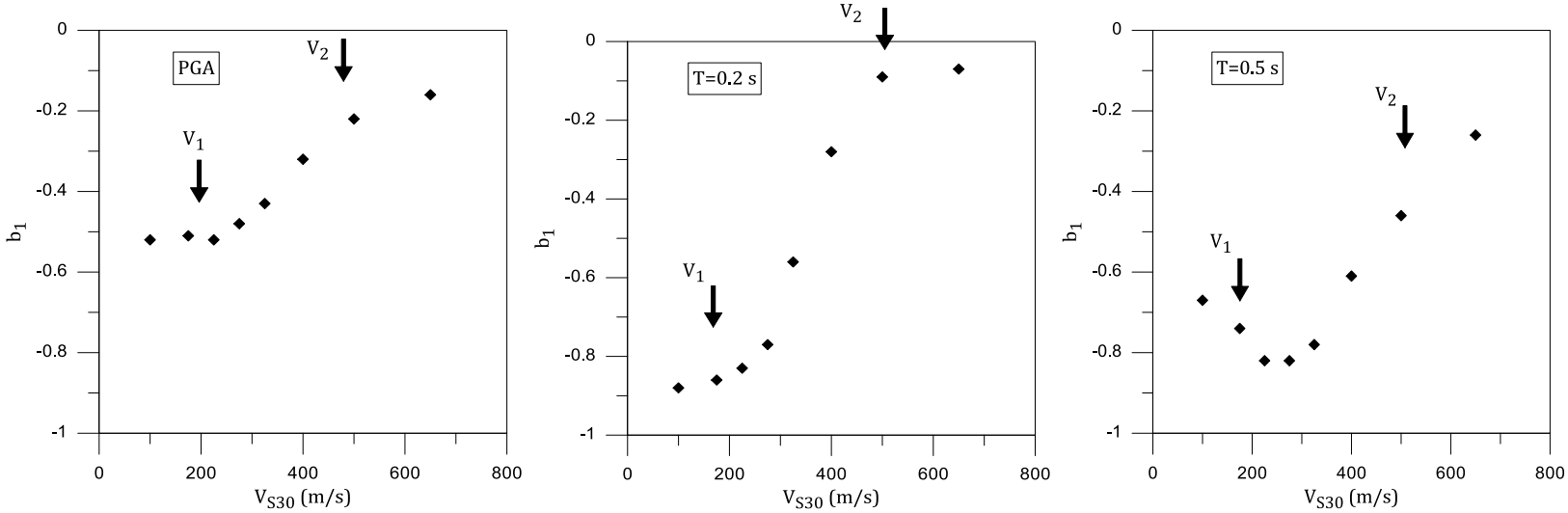

Figure 6.5 b_1 corresponding to eachV_{S30} bin versus median V_{S30} of each bin at PGA, T=0.2 s and 0.5 s.

6.3.1 Influence of Vratio on Nonlinear Site Response

It was shown in Chapter 5 that Vratio influences the linear-elastic amplification of soil sites at shorter periods. Including Vratio into the linear-elastic model reduced the standard deviation by 10 to 30%. The Vratio effect modeled in the linear elastic amplification model will be present at larger intensities, but Vratio may also influence the nonlinear amplification. The AF data in Figures 6.2 through 6.4 clearly show that the scatter in the AF data increases as input intensity increases. Based on the observations at small input intensities, Vratio is likely influencing the computed values of AF at large input intensities.

To investigate the influence of Vratio on the nonlinear component of the site amplification model, AF is plotted versus the normalized Vratio (Vratio/1.4) for each bin of V_{S30} and input intensity. A linear relationship is fit to the ln(AF) versus ln(Vratio/1.4) for each $S_{a,rock}$ to identify if the slope of this relationship (i.e., regression parameter a_3 from Chapter 5) is $S_{a,rock}$ dependent. Figures 6.6 through 6.8 show plots of PGA amplification versus Vratio/1.4 for V_{S30} bins of <150 m/s, 250-350 m/s and 550-750 m/s, respectively. The slope of the log-linear fit for each of the V_{S30} bins generally increases with $S_{a,rock}$. The slope, which indicates how strongly Vratio affects AF for a given V_{S30}, can increase by more than a factor of two as $S_{a,rock}$ increases from 0.01g to 0.9g. For the larger V_{S30} values (Figure 6.8), the slope increases from 0.0 (i.e., no Vratio effect) at $S_{a,rock}$=0.01g to 0.4 at $S_{a,rock}$=0.9g.

The slope of the linear fit between ln(AF) and ln(Vratio/1.4), which represents parameter a_3 in the linear-elastic model of Chapter 5 is plotted versus normalized - $S_{a,rock}$ (i.e., $S_{a,rock}/S_{a,rock\text{-}min}$, where $S_{a,rock\text{-}min}$ is the smallest input rock intensity considered) in Figure 6.9 for all eight V_{S30} bins. Chapter 5 demonstrated that a_3 is V_{S30} dependent; Figure 6.9 allows us to investigate whether the increase in a_3 with $S_{a,rock}$ is also V_{S30} dependent. The data in Figure 6.9 show that a_3 increases linearly with $\ln(S_{a,rock}/S_{a,rock\text{-}min})$ for all V_{S30} bins at PGA.

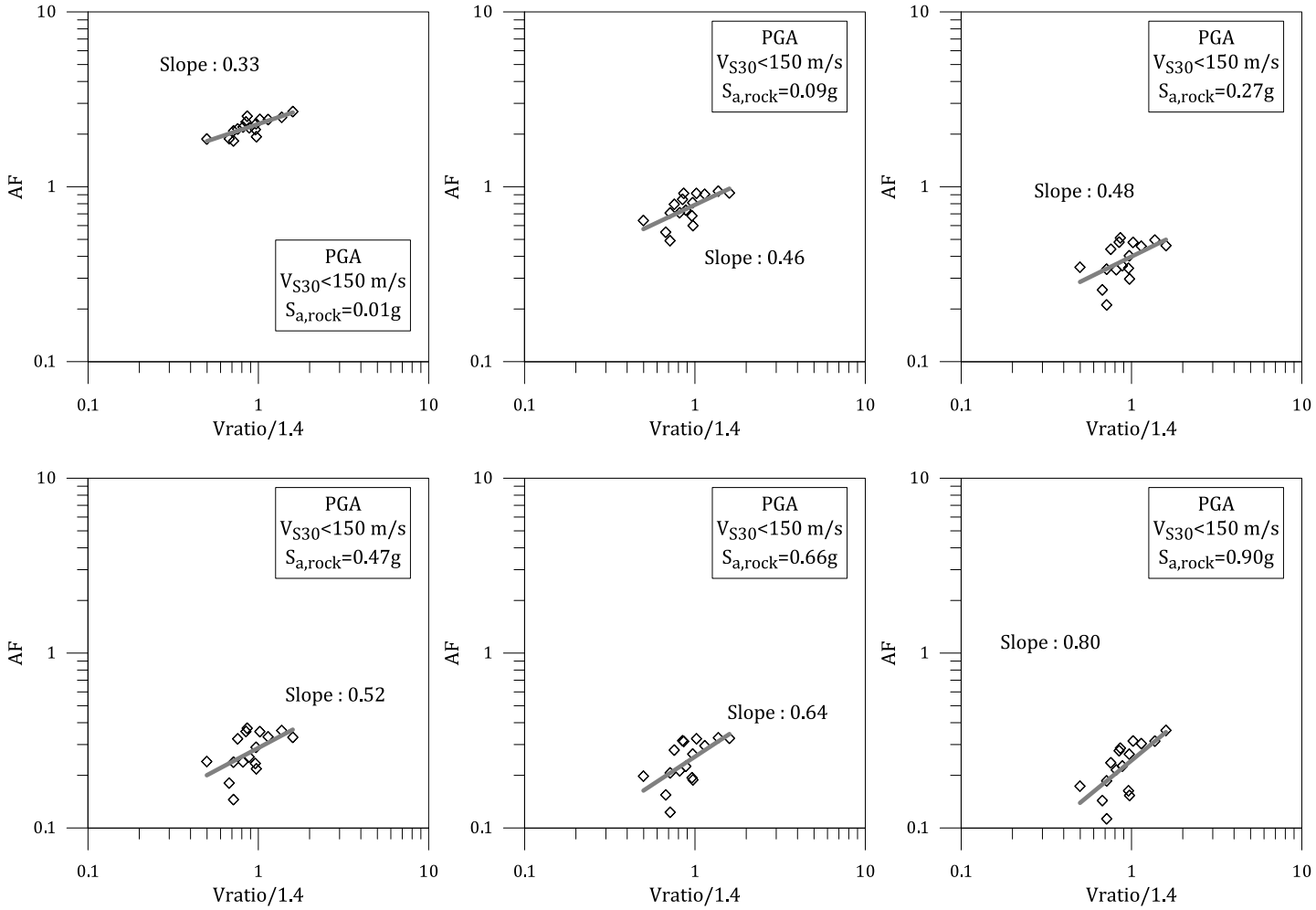

Figure 6.6 Amplification versus normalized Vratio for V_{S30}<150 m/s at PGA.

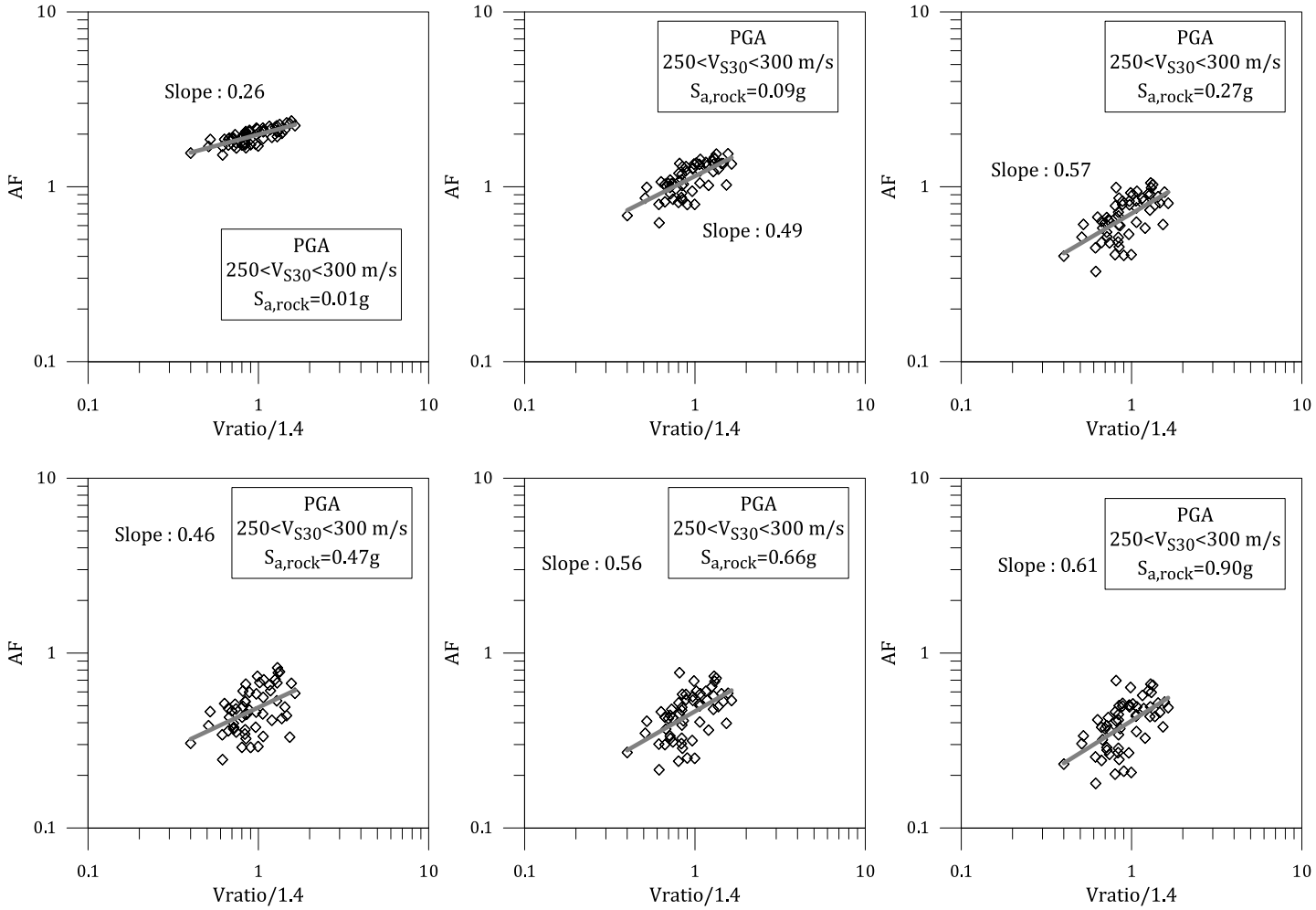

Figure 6.7 Amplification versus normalized Vratio for $250<V_{S30}<300$ m/s at PGA.

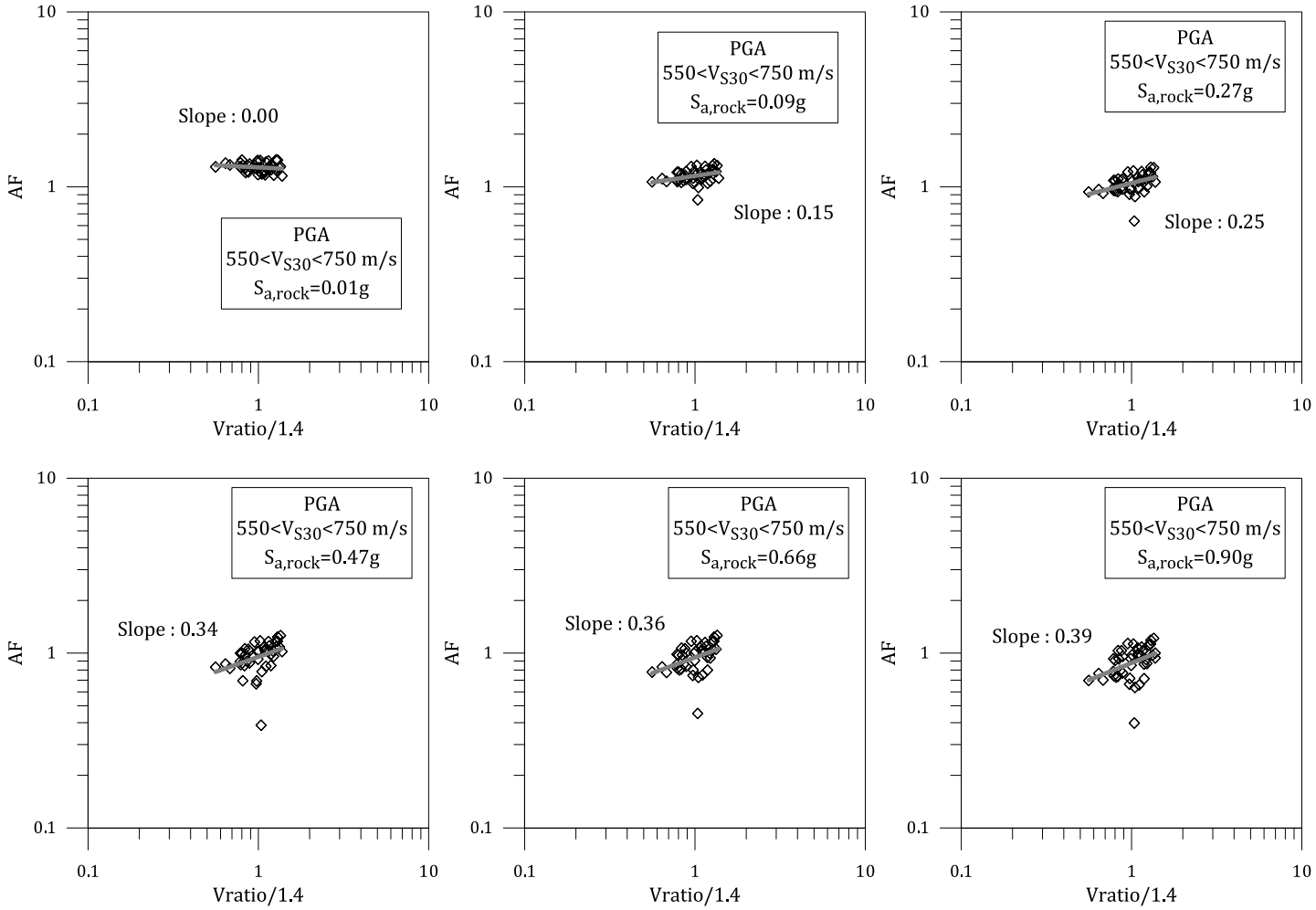

Figure 6.8 Amplification versus normalized Vratio for $550<V_{S30}<750$ m/s at PGA.

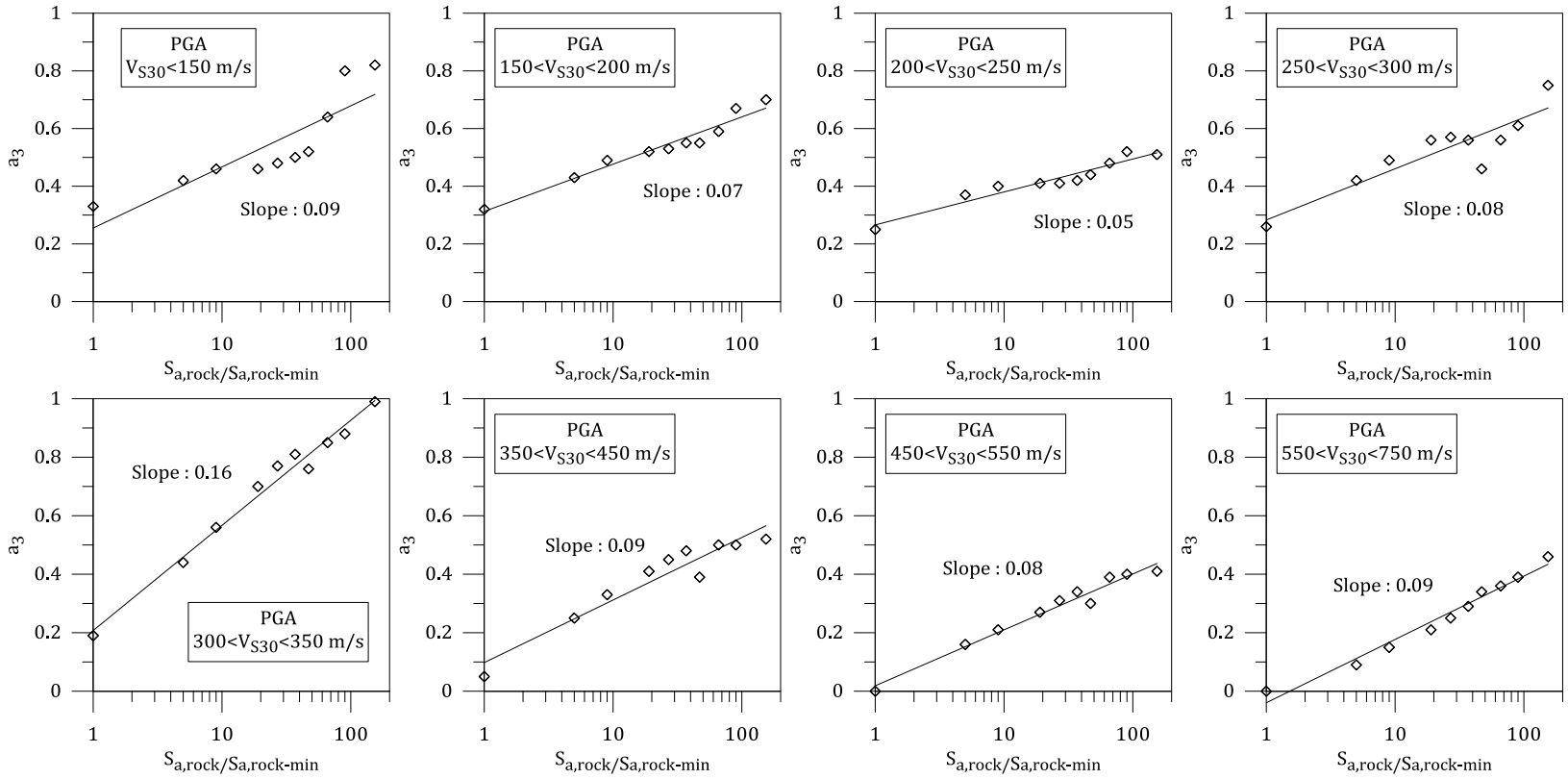

Figure 6.9 The slope of linear fit between ln(AF) and ln(Vratio/1.4) versus $S_{a,rock}$ /$S_{a,rock-min}$ at PGA.

The linear trend between a_3 and ln ($S_{a,rock}/S_{a,rock\text{-}min}$) is quite strong, and the slope of that relationship varies between 0.05 and 0.15, with most of the values between 0.07 and 0.09. The computed slopes are plotted versus V_{S30} in Figure 6.10. The variation of the slope with V_{S30} is not systematic, and therefore, the slope is considered V_{S30} independent.

Generally, the trends shown for PGA are similar for other short periods (i.e., ≤0.5 s), Figure 6.11 plots the slope of the a_3 versus ln ($S_{a,rock}/S_{a,rock\text{-}min}$) relationship versus V_{S30} for these other periods. Again, the slope varies with V_{S30} but not in a systematic manner. Therefore, the slope is modeled as V_{S30}-independent for all of the short periods.

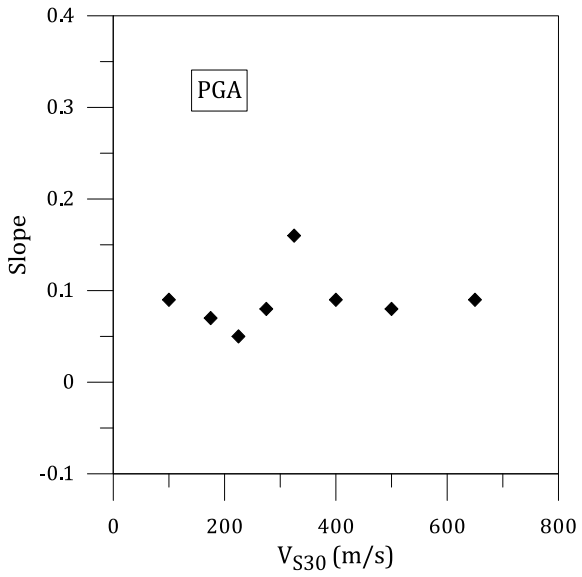

Figure 6.10 The variation of the slope of the linear fit between a_3 and ln($S_{a,rock}$ /$S_{a,rock\text{-}min}$) with V_{S30} at PGA.

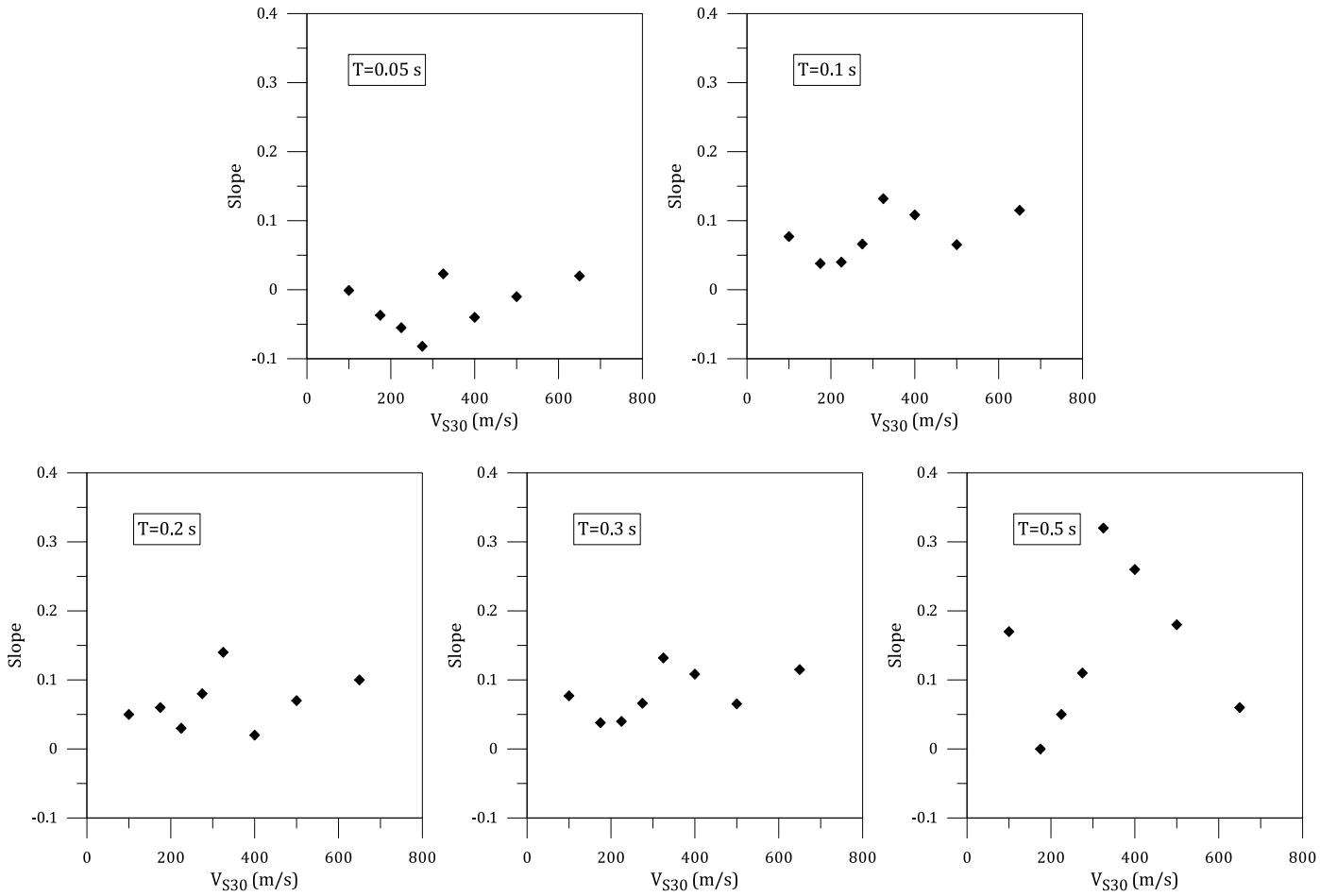

Figure 6.11 The variation of the slope of the linear fit between a_3 and $\ln(S_{a,rock} / S_{a,rock\text{-}min})$ with V_{S30} at T=0.05,0.1, 0.2,0.3 and 0.5 s.

The data presented above indicate that the Vratio effect, previously modeled in the linear elastic case as $a_3 \times \ln(\text{Vratio}/1.4)$ with a_3 being V_{S30} dependent, is intensity dependent. The full Vratio effect can be written as:

$$\ln(\text{AF})_{\text{Vratio}} = \left[a_{3+} b_2 \times \ln\left(\frac{S_{a,\text{rock}}}{S_{a,\text{rock}-\text{min}}}\right)\right] \times \ln\left(\frac{\text{Vratio}}{1.4}\right) \quad (6.3)$$

Where a_3 represents the Vratio effect under linear elastic conditions, as presented in Chapter 5, while $b_2 \times \ln\left(\frac{S_{a,\text{rock}}}{S_{a,\text{rock}-\text{min}}}\right)$ models the effect of input intensity on the Vratio effect. The parameter b_2 represents the slopes shown in Figures 6.9 and this parameter is not V_{S30} dependent based on the data shown in Figures 6.10 and 6.11. To maintain the separation of AF under linear elastic conditions and AF under nonlinear conditions, the second component in equation (6.3) is added to the nonlinear amplification model. Additionally, to ensure that the nonlinear amplification model disappears at small input intensities, the smallest $S_{a,\text{rock}}$ that can be used in equation (6.3) is $S_{a,\text{rock-min}}$.

Based on the above consideration, the nonlinear component of the site amplification model can be written as:

$$\ln(\text{AF})_{\text{NL}} = b_1 \times \ln\left(\frac{S_{a,\text{rock}}+c}{c}\right) + b_2 \times \ln\left(\frac{\max(S_{a,\text{rock}}, S_{a,\text{rock}-\text{min}})}{S_{a,\text{rock}-\text{min}}}\right) \times \ln\left(\frac{\text{Vratio}}{1.4}\right)$$

(6.4)

Where b_1 is V_{S30} dependent, as described by equation (6.2) and the coefficient b_2 is V_{S30}-independent.

6.4 Nonlinear Site Amplification at Long Periods

To investigate the dependency of amplification on input intensity at long periods, AF is plotted versus $S_{a,rock}$ for bins of V_{S30} at the four long periods considered. Figures 6.12 and 6.13 show AF versus $S_{a,rock}$ for two select representative periods: T=1.0s and 5.0 s, respectively. At T= 1.0 s, AF decreases with increasing input intensity ($S_{a,rock)}$ for smaller V_{S30} but the AF remains constant or slightly increases for larger V_{S30} (i.e., greater than about 350 m/s in Figure 6.12). At T=5.0 s (Figure 6.13), amplification generally increases as $S_{a,rock}$ increases for smaller V_{S30}, indicating that the b_1 slope may be positive at long periods. At larger values of V_{S30}, the amplification becomes insensitive to input intensity (slope ~ 0.0) similar to the results for T=1.0 s. A positive value of b_1 is technically justified for T=5.0 s, because most sites have natural periods shorter than 5.0 s and the soil nonlinearity induced by large input intensities will cause period lengthening towards 5.0 s. This lengthening will cause an increase in amplification with increasing input intensity at this period. Sites with larger V_{S30} tend to have natural periods much shorter than 5.0 s and they strain less as $S_{a,rock}$ increases, making the effect of period lengthening minimal.

The slope of the ln(AF)-ln($S_{a,rock}$) relationship at larger values of $S_{a,rock}$ (i.e., b_1) are computed for each V_{S30} bin and are shown in Figures 6.12 and 6.13. Figure 6.14 plots the derived values of b_1 versus the median V_{S30} of each bin for periods of 1.0 s and 5.0 s. Figure 6.14 shows that b_1 is constant at smaller V_{S30}, it varies linearly with

increasing V_{S30}, and then becomes constant again at larger V_{S30}. For T=1.0 s, b_1 is equal to -0.8 at smaller V_{S30} and approaches 0.0 at V_{S30} greater than about 400 m/s. For T=5.0 s, b_1 is about 0.2 for smaller V_{S30} and approaches 0.0 at V_{S30} greater than about 500 m/s. A positive value of b_1 indicates that AF increases with increasing $S_{a,rock}$, and positive values are observed for periods greater than and equal to 2.0 s.

Based on the data presented in Figure 6.14, the same functional form that is used at short periods to describe the variation b_1 with V_{S30} can be used at longer periods (equation 6.2). This relationship defines regions of constant b_1 at smaller and larger V_{S30} values, and a linear relationship with $\ln(V_{S30})$ in between. The regression parameters are the V_{S30} values above and below which b_1 is a constant (V_2 and V_1), and the b_1 values above and below these values (b_{o2} and b_{o1}).

In Chapter 5, it was shown that the site amplification at long periods is not influenced by Vratio, but that it is influenced by $Z_{1.0}$. $Z_{1.0}$ is not affected by soil nonlinearity and therefore is not affected by input intensity (i.e., $S_{a,rock}$). Combining the linear and nonlinear components, the amplification model at long periods can be expressed as:

$$\ln(AF) = \begin{cases} a_1 \times \alpha \times \ln\left(\frac{V_{S30}}{V_{ref}}\right) + b_1 \times \ln\left(\frac{S_{a,rock}+c}{c}\right) & \text{if } V_{S30} < V_{ref} \\ b_1 \times \ln\left(\frac{S_{a,rock}+c}{c}\right) & \text{if } V_{S30} \geq V_{ref} \end{cases} \quad (6.5)$$

where α is a function of $Z_{1.0}$ as defined by Equation (5.8) and b_1 is a function of V_{S30} as defined by equation (6.2).

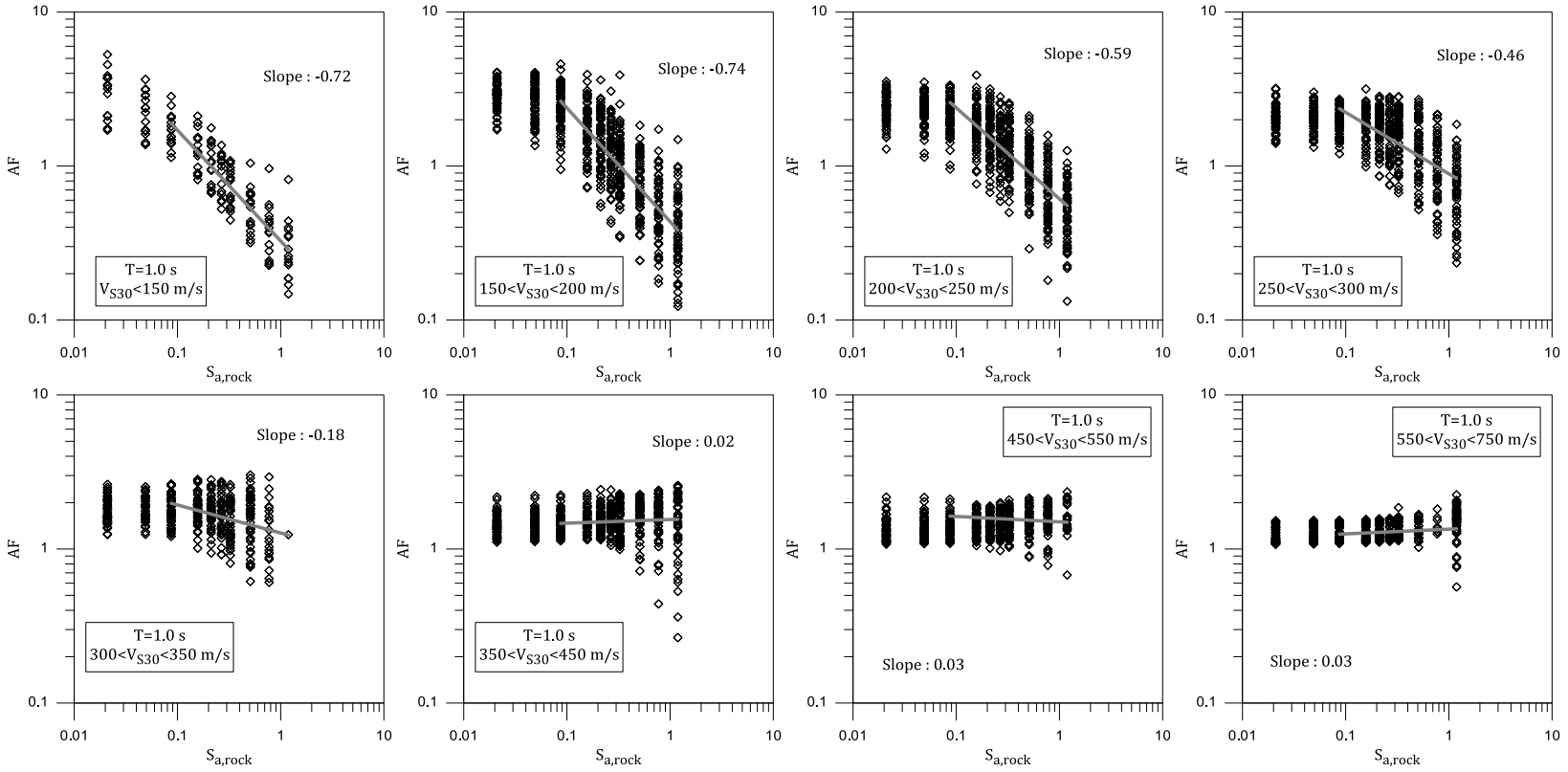

Figure 6.12 Amplification versus $S_{a,rock}$ for different V_{S30} bins at T=1.0 s.

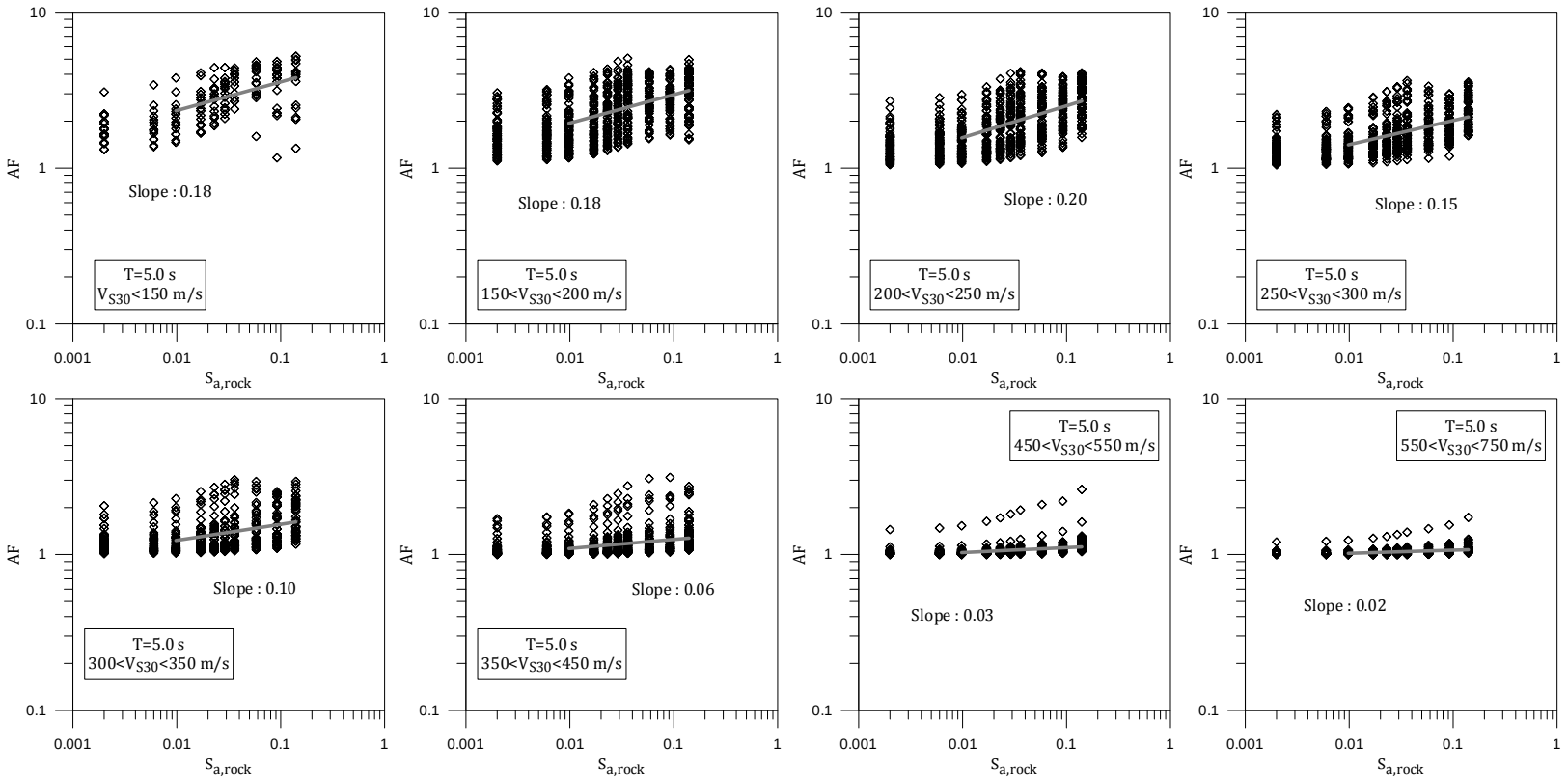

Figure 6.13 Amplification versus $S_{a,rock}$ for different V_{S30} bins at T=5.0 s.

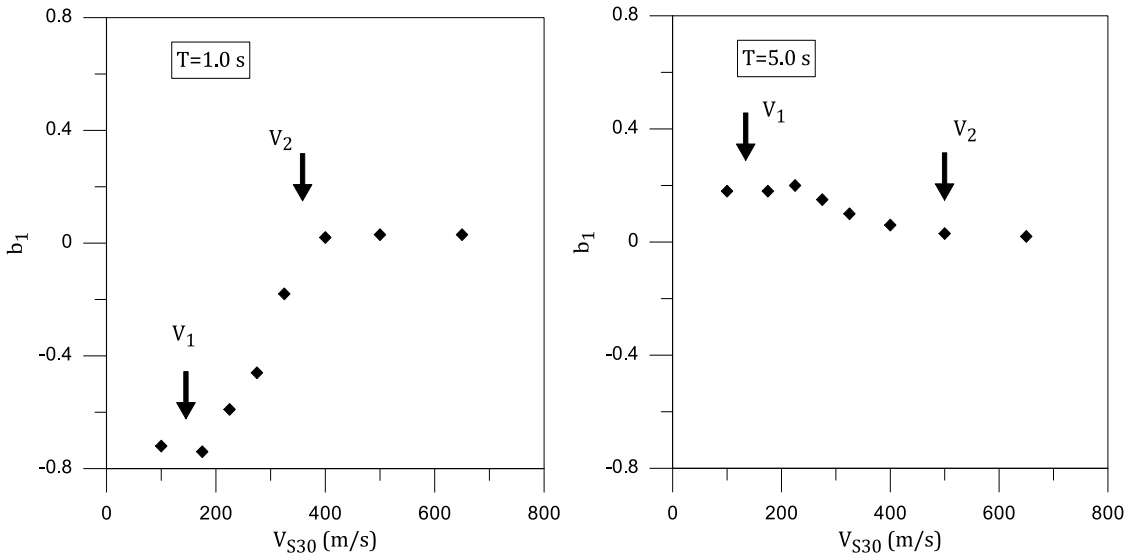

Figure 6.14 b_1 corresponding to eachV_{S30} bin versus median V_{S30} of each bin at T=1.0 s and 5 s.

6.5 Summary

This chapter described the development of the nonlinear amplification model, which describes the variation of site amplification with increases in input shaking intensity (Sa,rock). Separate nonlinear models are developed for short and long periods. It was shown that at short periods , the logarithm of amplification vary with the logarithm of $S_{a,rock}$ and this variation is V_{S30} dependent as softer sites show more nonlinearity (i.e., more reduction in amplification with increase of $S_{a,rock}$). The influence of Vratio is also incorporated at the nonlinear component of the site response model. The influence of Vratio on amplification is $S_{a,rock}$ dependent but V_{S30} independent.

At longer periods, the same functional form for considering the variation of amplification with input intensity at short periods is considered. However, at long periods Vratio does not influence the site amplification.

Chapter 7

Final Site Amplification Model

7.1 Introduction

The linear and nonlinear components of the site amplification model presented in Chapters 5 and 6 are combined in this chapter. Separate functional forms are fit to the amplification data for short and long periods. To demonstrate the fit of the developed model, the amplification data are plotted along with predictions from the developed models. The calculated residuals from the developed functional forms are plotted versus the independent variables in the site amplification model.

7.2 Combined Model for Short Periods

Combining the linear-elastic and nonlinear components of the amplification model for short periods, the following model is proposed for the amplification factor for spectral accelerations at short periods (T≤ 0.5 s):

$$\ln(AF) = a_1 \times \ln\left(\frac{V_{S30}}{V_{ref}}\right) + a_2 \times \left[\ln\left(\frac{V_{S30}}{V_{ref}}\right)\right]^2 + a_3 \times \ln\left(\frac{Vratio}{1.4}\right) + b_1 \times \ln\left(\frac{S_{a,rock}+c}{c}\right) + b_2 \times \ln\left(\frac{\max(S_{a,rock}, S_{a,rock-min})}{S_{a,rock-min}}\right) \times \ln\left(\frac{Vratio}{1.4}\right) \quad \text{if } V_{S30} < V_{ref} \qquad (7.1a)$$

$$\ln(AF) = b_1 \times \ln\left(\frac{S_{a,rock}+c}{c}\right) + b_2 \times \ln\left(\frac{\max(S_{a,rock}, S_{a,rock-min})}{S_{a,rock-min}}\right) \times \ln\left(\frac{Vratio}{1.4}\right) \quad \text{if } V_{S30} \geq V_{ref} \qquad (7.1b)$$

This model is fit independently to each short period. The parameters a_3 and b_1 are V_{S30} dependent, and the V_{S30}-dependencies are described by:

$$a_3 = \begin{cases} a_0 & \text{if } V_{S30} \leq V_a \\ a_0 - \frac{a_0}{(V_b - V_a)} \times (V_{S30} - V_a) & \text{if } V_a < V_{S30} \leq V_b \\ 0 & \text{if } V_{S30} > V_b \end{cases} \qquad (7.2)$$

and

$$b_1 = \begin{cases} b_{o1} & \text{if } V_{S30} \leq V_1 \\ b_{o1} + \frac{b_{o2} - b_{o1}}{\ln\left(\frac{V_2}{V_1}\right)} \times \ln\left(\frac{V_{S30}}{V_1}\right) & \text{if } V_1 < V_{S30} \leq V_2 \\ b_{o2} & \text{if } V_{S30} > V_2 \end{cases} \qquad (7.3)$$

All other parameters are not a function of V_{S30}.

The regression process is executed in three steps. Each step uses the maximum likelihood method for regression. In the first step, the coefficients for the linear-elastic component are estimated (i.e., a_1, a_2, a_0, V_a, V_b) using the AF data from the lowest intensity input motions (i.e., PGA_{rock}=0.01g). These parameters are kept fixed in subsequent steps. In the second step, the parameters for the nonlinear model (b_{o1}, b_{o2}, V_1, V_2, and c) are estimated excluding the effect of Vratio (i.e., b_2) using the AF data for all input intensities. To ensure that the nonlinear component of the model does not influence the computed amplification at small $S_{a,rock}$, a minimum value of c was set to 0.1 g. If c=0.1 g, then the $\ln\left(\frac{S_{a,rock}+c}{c}\right)$ term is equal to 0.095 for $S_{a,rock}$ = 0.01 g. Thus, the nonlinear effect on the computed amplification will be minimal. In the last and final step, all previously parameters are fixed and b_2 (i.e., the Vratio effect in the nonlinear model) is computed. The final estimated values of all coefficients for the 6 short periods studied here are listed in Table 7.1.

Table 7.1 Coefficients of the site amplification model for short periods–Equation (7.1).

	T (sec)	PGA	0.05 s	0.1 s	0.2s	0.3s	0.5s
a_3 model	a_1	-0.69	-0.70	-0.76	-0.9	-0.89	-0.67
	a_2	-0.13	-0.15	-0.21	-0.32	-0.28	-0.10
	a_0	0.34	0.38	0.38	0.44	0.57	0.39
	V_a (m/s)	176	130	110	414	100	100
	V_b (m/s)	481	513	737	726	750	750
b_1 model	b_{o1}	-0.91	-1.26	-0.98	-1.21	-1.93	-2.60
	b_{o2}	-0.24	-0.21	-0.19	-0.16	-0.14	-0.11
	V_1 (m/s)	184	118	192	188	133	103
	V_2 (m/s)	454	581	583	557	530	447
	c	0.1	0.1	0.1	0.21	0.37	0.4
	b_2	0.09	0.08	0.08	0.07	0.08	0.06
	V_{ref} (m/s)	1000	1000	1000	1000	1000	1000
	$S_{a,rock\text{-}min}$ (g)	0.01	0.01	0.02	0.03	0.03	0.03

Figure 7.1 shows the residuals (i.e., ln(data)-ln(predicted) plotted versus V_{S30}, $S_{a,rock}$, and Vratio for the amplification factors for PGA. The residuals indicate overprediction in amplification (negative residuals) for smaller V_{S30} and a slight overprediction over all V_{S30} (overall average residual equal to -0.07). There is no systematic trend between the residuals and the various parameters. However the variability in the residuals increases with the increase of $S_{a,rock}$. For all the other considered short periods, the residual also do not show a systematic trend with any

of independent variables in the model. However, the average residual across these other periods range from about -0.07 to +0.08.

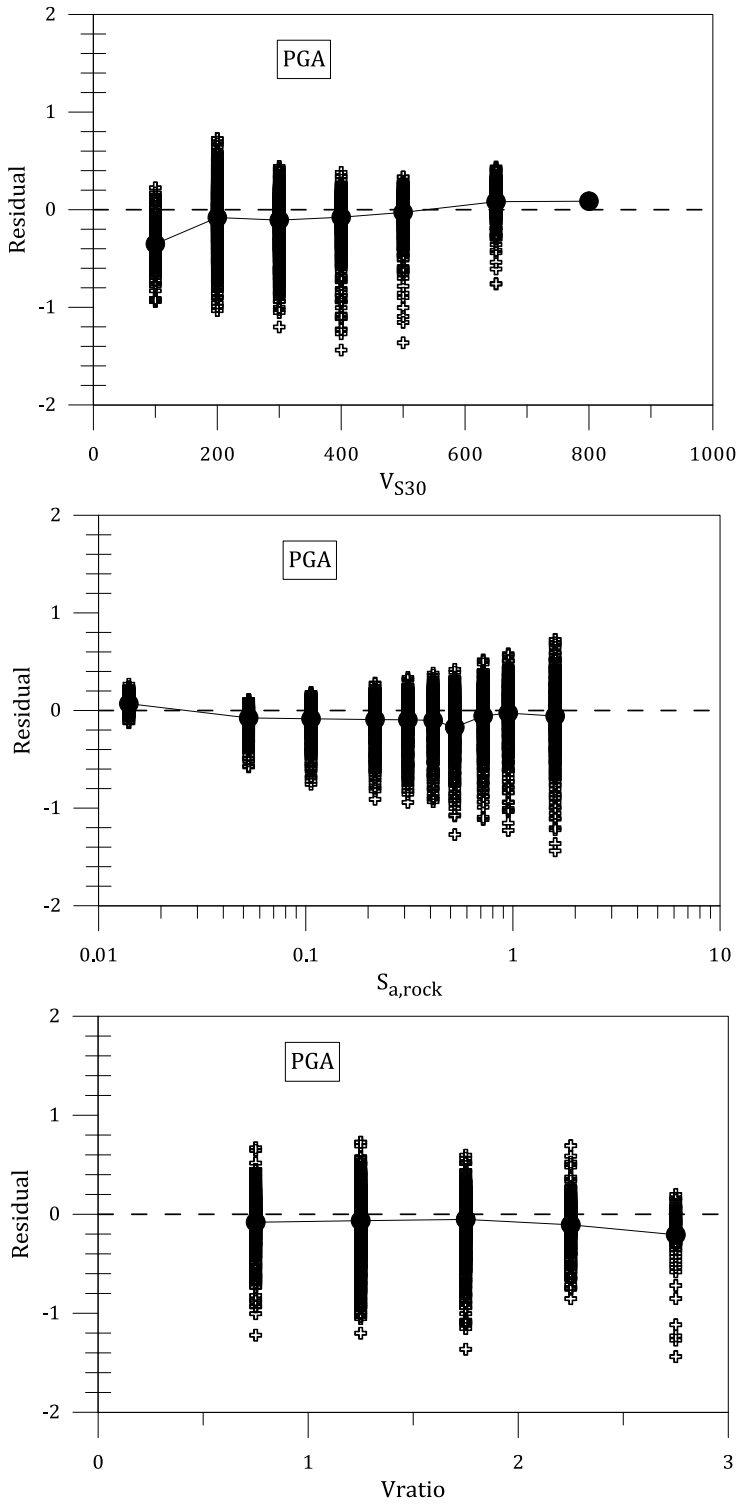

Figure 7.1 The residuals of the fit model versus V_{S30}, $S_{a,rock}$, and Vratio at PGA.

It is difficult to fully evaluate the model looking at the overall residuals, therefore AF predictions are plotted versus $S_{a,rock}$ along with the AF data in the next several figures. To demonstrate the effects of V_{S30} and Vratio on the AF predictions, the predicted AF values are plotted versus $S_{a,rock}$ for select V_{S30} bins and for a range of Vratio values. As discussed previously, the range of Vratio values is slightly different among the V_{S30} bins, but most of the values fall between 0.8 and 2.5. Considering these ranges, AF predictions are shown for Vratio=0.8, 1.4, and 2.5 in Figures 7.2 to 7.7 for the 6 periods considered.

The predictions in Figures 7.2 through 7.7 are in general agreement with the data. Additionally, sites with larger values of Vratio have larger amplification and sites with smaller Vratio have smaller amplification. This effect helps explain some of the scatter shown in the AF data. For each period, the effect of Vratio at low input intensity (i.e., smallest $S_{a,rock}$) is strongest for the smaller values of V_{S30} and essentially non-existent for larger V_{S30} (greater than about 350 m/s). However, the input intensity effect modeled with Vratio results in Vratio becoming important for larger V_{S30} at larger input intensities (note the predictions for V_{S30}=450-550 m/s in Figures 7.2 to 7.7).

While there is general agreement in Figures 7.2 through 7.7, there are some areas of deviation. Note that at the smallest input intensity and the smallest V_{S30} values, the AF predictions tend to be smaller than observed for $T \leq 0.2$ s. This result is due to the parameter c being small ($\sim$ 0.1 g) relative to the smallest $S_{a,rock}$ used in

this study (0.01 g) and the large, negative values of b_1 for small V_{S30} sites. As a result, the nonlinear component of the amplification model contributes to the AF prediction even for $S_{a,rock} \sim 0.01$ g. This issue is not apparent at periods of 0.3 and 0.5 s because the parameter c is larger (Table 7.1). Another challenging area is amplification for the larger V_{S30} values (450 to 550 m/s) at periods of 0.1 and 0.2 s. The model tends to underpredict the amplification at moderate $S_{a,rock}$ and overpredict amplification at larger AF. This issue again appears to be due to c being relatively small and the model for the V_{S30}-dependence for b_1.

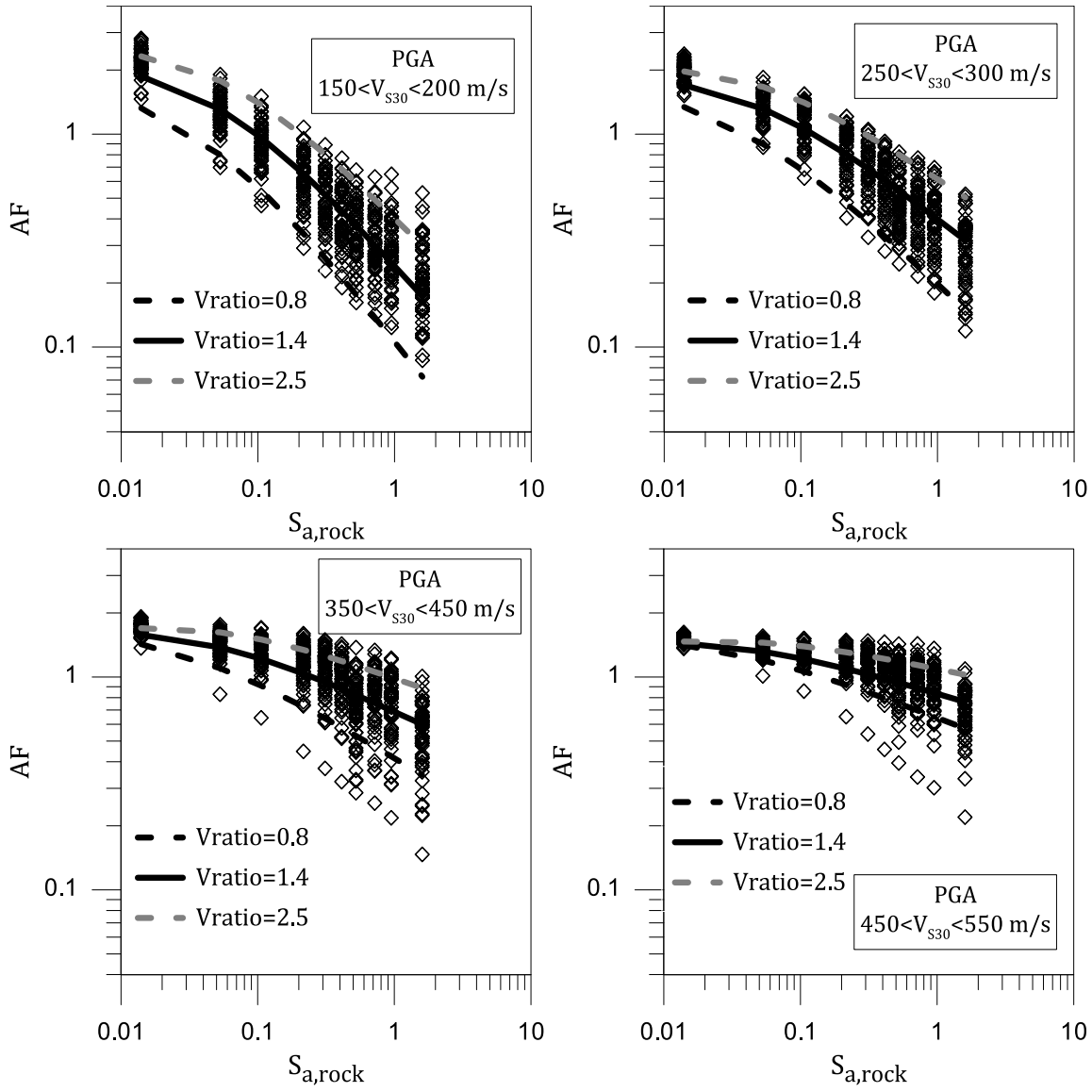

Figure 7.2 AF versus $S_{a,rock}$ and fitted curves to the data for different values of Vratio at PGA.

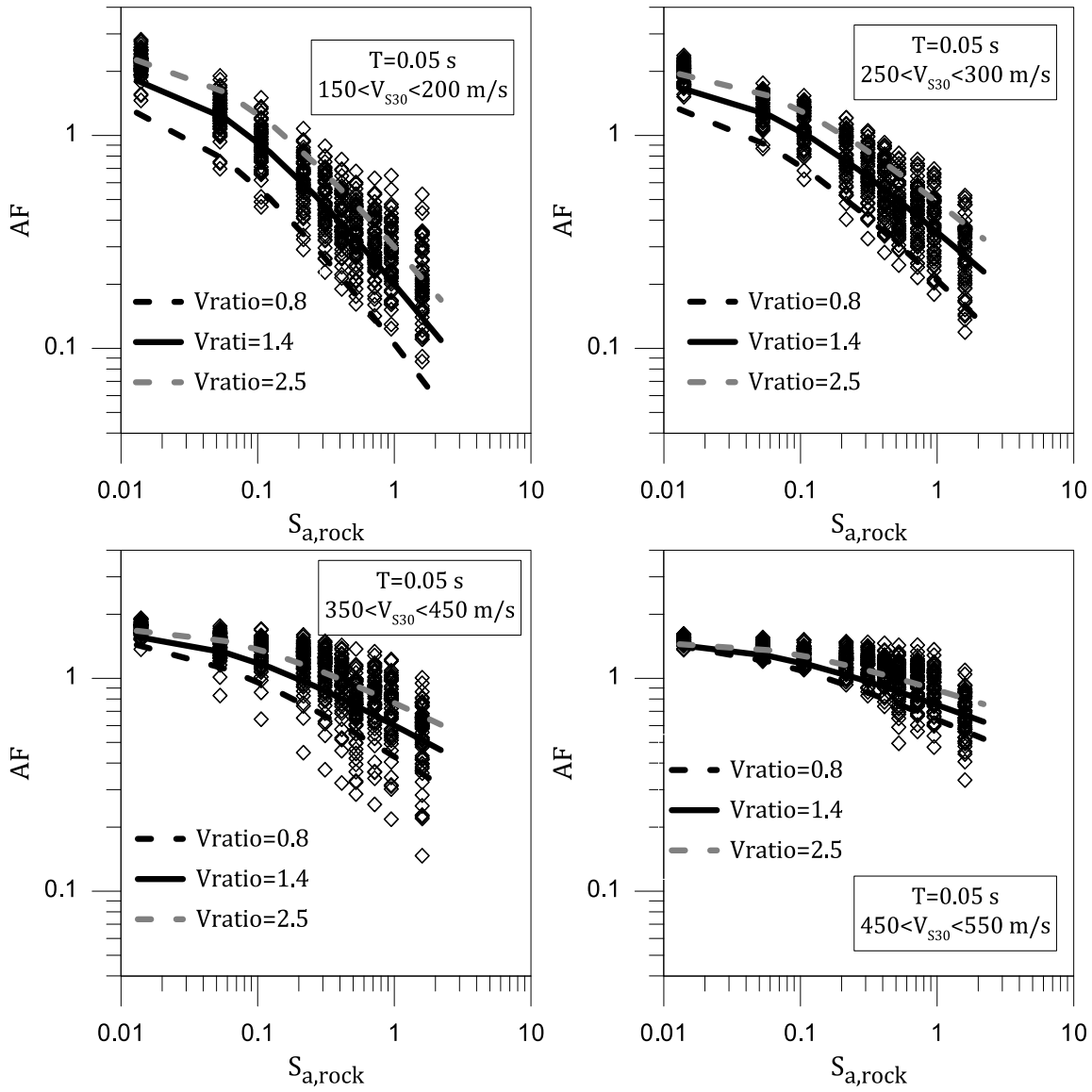

Figure 7.3 AF versus $S_{a,rock}$ and fitted curves to the data for different values of Vratio at T=0.05 s.

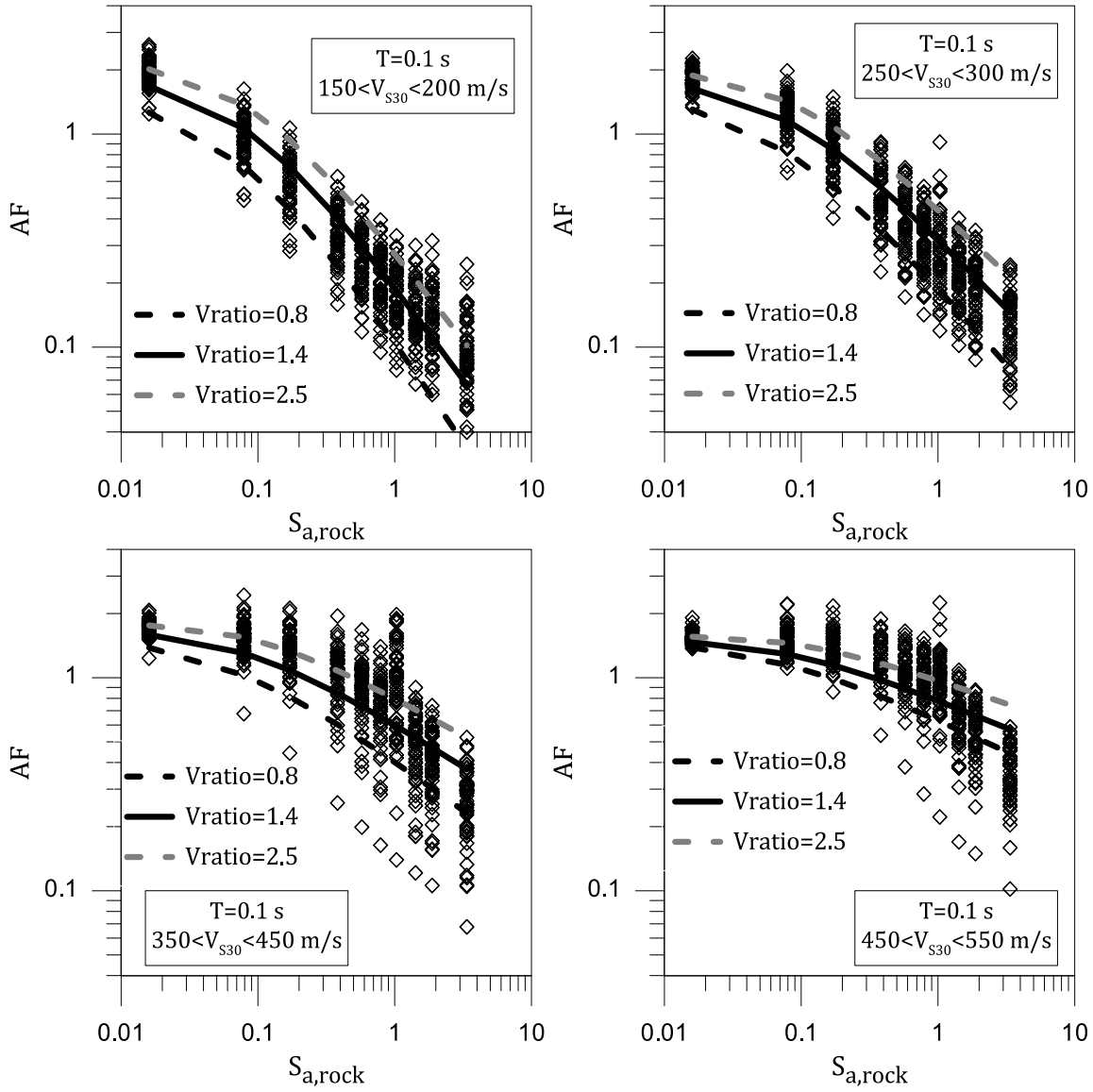

Figure 7.4 AF versus $S_{a,rock}$ and fitted curves to the data for different values of Vratio at T=0.1 s.

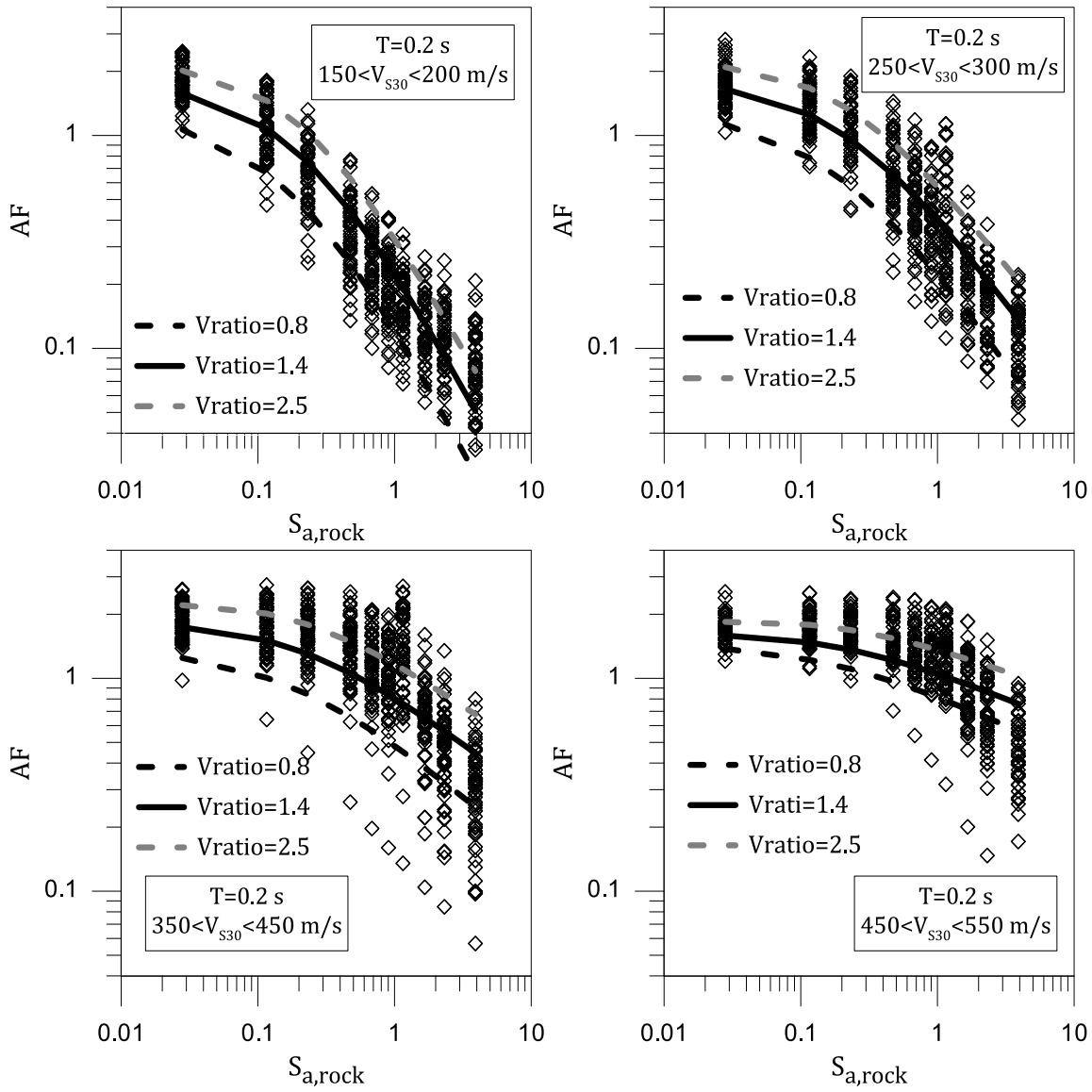

Figure 7.5 AF versus $S_{a,rock}$ and fitted curves to the data for different values of Vratio at T=0.2 s.

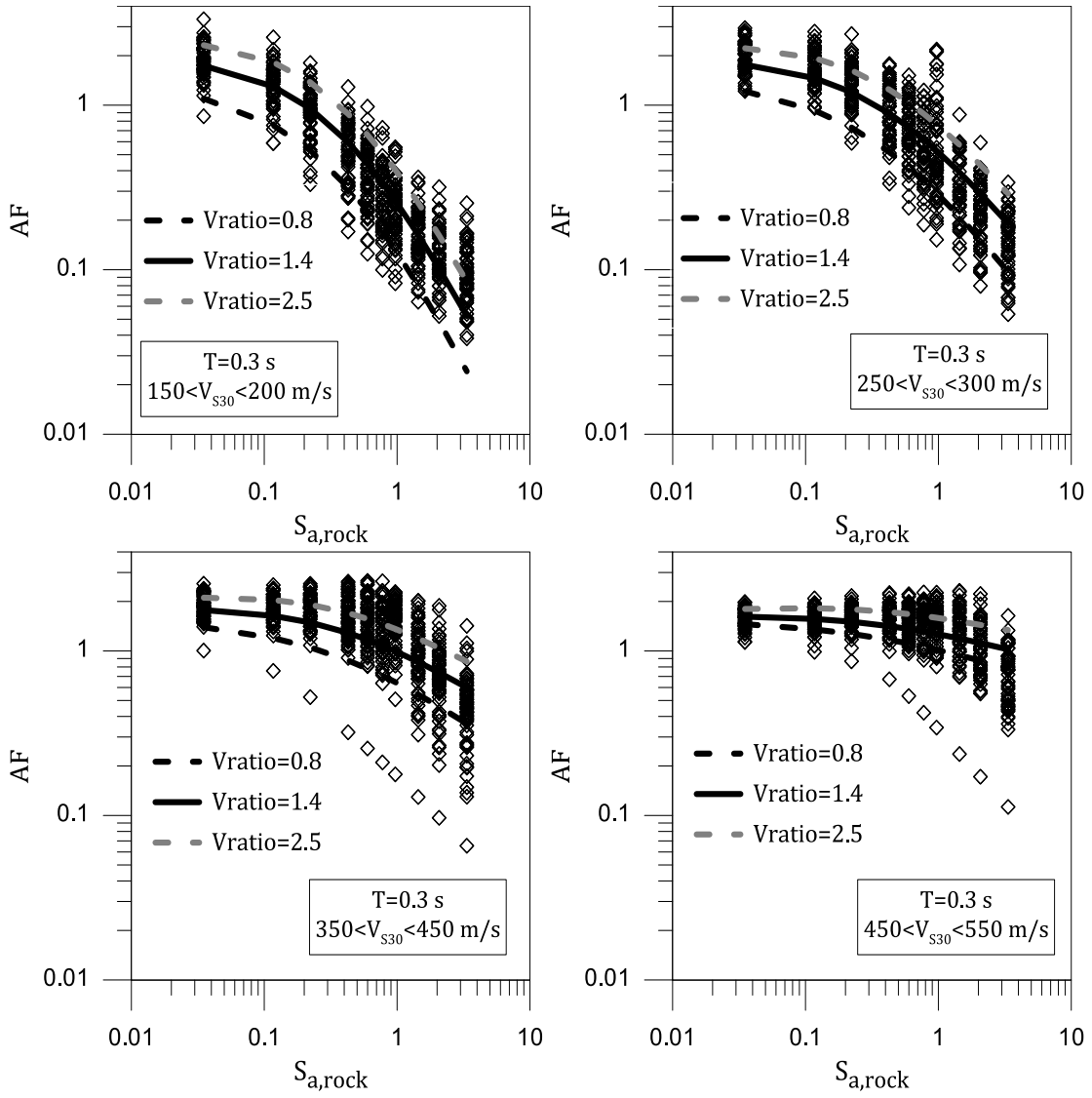

Figure 7.6 AF versus $S_{a,rock}$ and fitted curves to the data for different values of Vratio at T=0.3 s.

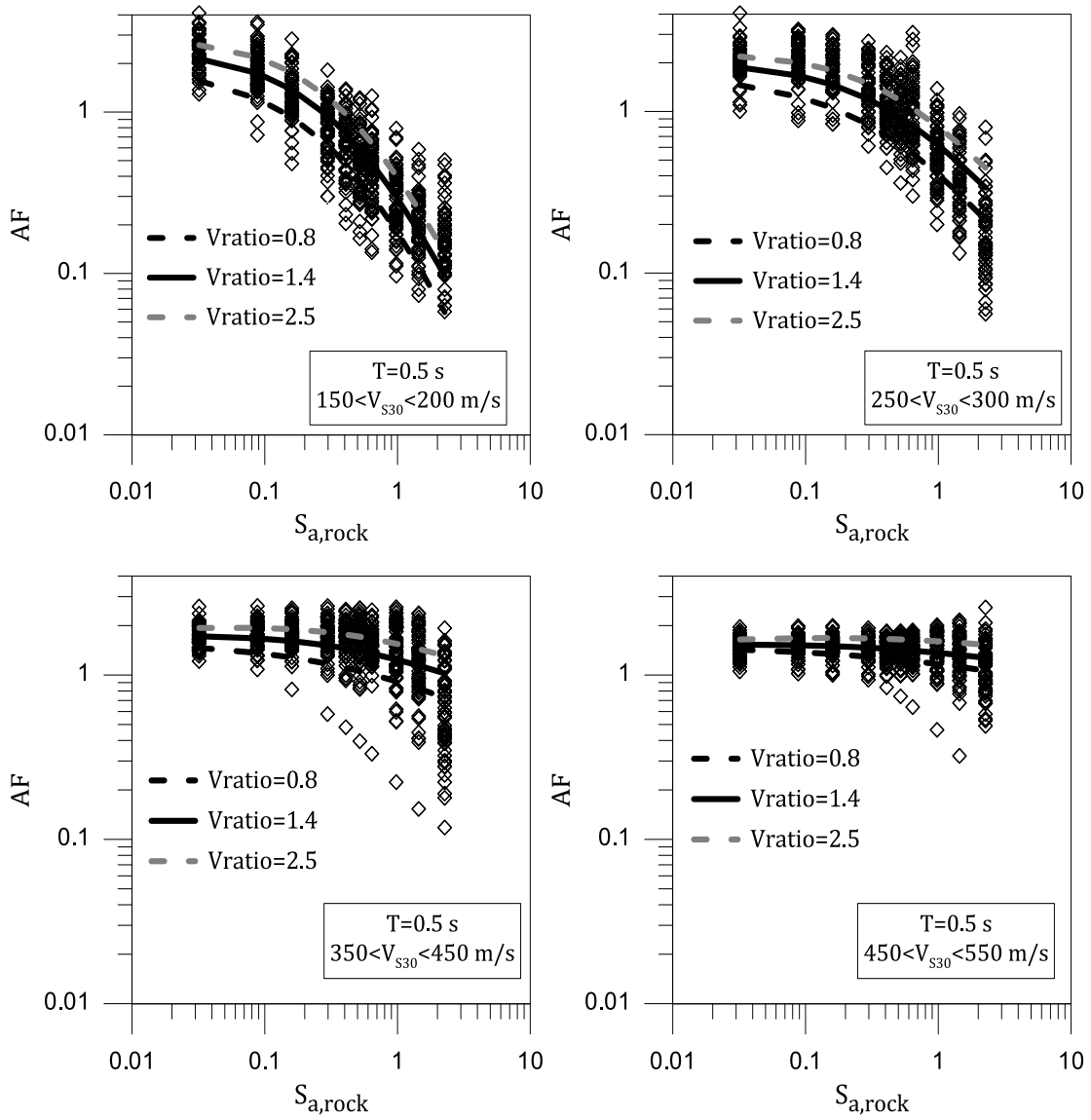

Figure 7.7 AF versus $S_{a,rock}$ and fitted curves to the data for different values of Vratio at T=0.5 s.

To evaluate the effect of adding Vratio to the full amplification model, the standard deviation of the residuals (i.e., ln(data)-ln(predicted)) for models with and without including Vratio is computed. The standard deviations (i.e., σ_{lnAF}) are listed in Table 7.2 for each period. The standard deviation of the full model decreases when including Vratio (in most cases from about 8% to 15%), however the level of reduction is not as significant as it was for the linear model (Chapter 5). The modest reduction in σ_{lnAF} may be influenced by the strength of ln(AF)-ln(Vratio) relationship at larger input intensities. Considering the data shown in Figures 6.6-6.8, the variability about the linear relationship increases with increasing intensity indicating that the strength of the relationship decreases with increasing input intensity. In addition to the standard deviation of the residuals, to compare two models with and without Vartio, R^2_{M1-M2} is calculated at each period. $R^2_{M1-M2}$is defined as :

$$R^2_{M1-M2} = \frac{\sum(Residual_{M1})^2 - \sum(Residual_{M2})^2}{\sum(Residual_{M1})^2} \quad (7.4)$$

where $\sum(\text{Residual}_{M1})^2$ is the sum of the squared residuals from model 1 (i.e. the model that does not include Vratio) and $\sum(\text{Residual}_{M2})^2$ is the sum of the squared residuals from model 2 (i.e. the model that includes Vratio).The calculated R^2_{M1-M2} values for each period is given in Table 7.2. The R^2_{M1-M2} values range from 0.08 to 0.33 indicating that Vratio model explains 8% to 33% of the variation within the non-Vratio model At a spectral period of 0.2 s, the calculated R^2_{M1-M2} reaches its maximum value of 33%.

Table 7.2 Standard deviation and R^2_{M1-M2} of nonlinear amplification models (σ_{lnAF}) with and without considering Vratio.

T(sec)	σ_{lnAF} model without Vratio	σ_{lnAF} model with Vratio	% Reduction	R^2_{M1-M2}
PGA	0.28	0.25	11	0.08
0.05	0.30	0.25	17	0.19
0.1	0.36	0.32	11	0.19
0.2	0.45	0.37	18	0.33
0.3	0.41	0.36	12	0.19
0.5	0.39	0.36	8	0.11

7.3 Combined Model for Long Periods

Combining the linear-elastic and nonlinear components of the amplification model for long periods, the following model is proposed for the amplification factor for spectral accelerations at long periods (T≥ 1.0 s):

$$\ln(AF) = a_1 \times \alpha \times \ln\left(\frac{V_{S30}}{V_{ref}}\right) + b_1 \times \ln\left(\frac{S_{a,rock}+c}{c}\right) \qquad \text{if } V_{S30} < V_{ref} \qquad (7.5.a)$$

$$\ln(AF) = b_1 \times \ln\left(\frac{S_{a,rock}+c}{c}\right) \qquad \text{if } V_{S30} \geq V_{ref} \qquad (7.5.b)$$

where α is defined as:

$$\alpha = \left(\frac{\min(Z^*, Z_{1.0})+1}{Z^*+1}\right)^b \qquad (7.6)$$

and

$$b_1 = \begin{cases} b_{o1} & \text{if } V_{S30} \le V_1 \\ b_{o1} + \frac{b_{o2} - b_{o1}}{\ln\left(\frac{V_2}{V_1}\right)} \times \ln\left(\frac{V_{S30}}{V_1}\right) & \text{if } V_1 < V_{S30} \le V_2 \\ b_{o2} & \text{if } V_{S30} > V_2 \end{cases} \quad (7.7)$$

All other parameters are estimated in the maximum likelihood regression. The regression process is executed in two steps. In the first step, the coefficients of the linear-elastic component of the model (i.e., a_1, Z^*, and b) are estimated. These coefficients are kept fixed in the second step which estimates the parameters in the nonlinear component of the model (b_{o1}, b_{o2}, V_1, V_2, and c). The derived values of all coefficients of Equation (7.5) for the four long periods studied here are listed in Table 7.3. Note that positive values of b_1 (i.e., b_{o1} and b_{o2}) are derived for periods of 5.0 and 10.0 s indicating that amplification increases with increases $S_{a,rock}$ at these periods. At T=1.0 and 2.0 s, b_1 becomes slightly positive at large V_{S30} values (i.e., b_{o2} become positive). The standard deviation for each model (σ_{lnAF}) is also listed in Table 7.3 and ranges from 0.32 to 0.14.

Table 7.3 Coefficients of the site amplification model for long periods –Equation (7.5).

T (sec)	1.0	2.0	5.0	10.0
a_1	-0.62	-0.75	-0.63	-0.44
Z^* (m)	121	292	490	1000
b	0.70	0.71	1.16	0.76
b_{o1}	-1.6	-0.70	0.17	0.36
b_{02}	0.06	0.10	0.02	0.04
V_1 (m/s)	114	120	193	143
V_1 (m/s)	387	380	470	390
c	0.2	0.15	0.005	0.005
V_{ref}(m/s)	850	600	500	500
σ_{lnAF}	0.32	0.27	0.21	0.14

Figure 7.8 shows the residuals (i.e., ln(data)-ln(predicted) plotted versus V_{S30}, $S_{a,rock}$, and $Z_{1.0}$ for spectral period of 1.0 s. The residuals do not show any systematic trend with respect to V_{S30}, $S_{a,rock}$, and $Z_{1.0}$. For all the other considered long periods, the residuals do not show any systematic trend with any of independent variables in the model.

To investigate how the proposed functional form at long periods (T ≥ 1.0 s) fits the data, predictions of AF are plotted versus $S_{a,rock}$ for three different values of $Z_{1.0}$ in Figures 7. 9 to 7.12 for the four long periods considered in this study. The AF data

are also shown in these plots. As discussed before, there is a relationship between V_{S30} of a site and its depth to the bedrock (i.e. $Z_{1.0}$). Stiffer sites reach bedrock at shallower depth. Based on the data shown in Chapter 4 for V_{S30}<300 m/s, $Z_{1.0}$ ranges from about 100 to 600 m. Therefore, the predicted AF values are plotted for $Z_{1.0}$ of 100, 300 and 600 m for V_{S30}>300 m/s. For V_{S30} > 300 m/s, $Z_{1.0}$ ranges from 20 to 400 m. For V_{S30} > 300 m/s, AF predictions are shown for $Z_{1.0}$ of 20, 200, and 400 m. As discussed in the previous chapter, the α parameter incorporates the effect of depth in the model and α is equal to 1.0 for sites with $Z_{1.0}$ greater than Z^*. Therefore, amplification for sites with $Z_{1.0}$ > Z* is not influenced by $Z_{1.0}$.

At a spectral period of 1.0 s (Figure 7.9), Z^* is equal to 121 m such that most of the curves shown do not show any $Z_{1.0}$ effect. The curve with $Z_{1.0}$ equal to 100 m for V_{S30} < 300 m/s shows a very small effect and the curve for $Z_{1.0}$ equal to 20 m for V_{S30} > 300 m/s shows a larger effect. However, few of the data have $Z_{1.0}$ equal to 20 m. Similar trends are observed at T=2.0 s, but with Z* equal to 292 m the $Z_{1.0}$ effect is more apparent. At longer periods (i.e., 5.0 and 10.0 s), Z* is much larger (490 and 1000 m respectively) such that a clear increase in amplification as depth to the bedrock ($Z_{1.0}$) increases is observed for V_{S30}<300 m/s. For larger V_{S30}, the V_{S30} approaches V_{ref} (i.e., V_{ref} = 500 m/s for these periods, and AF= 1.0 for V_{S30} > V_{ref}) such that the $Z_{1.0}$ effect is not significant.

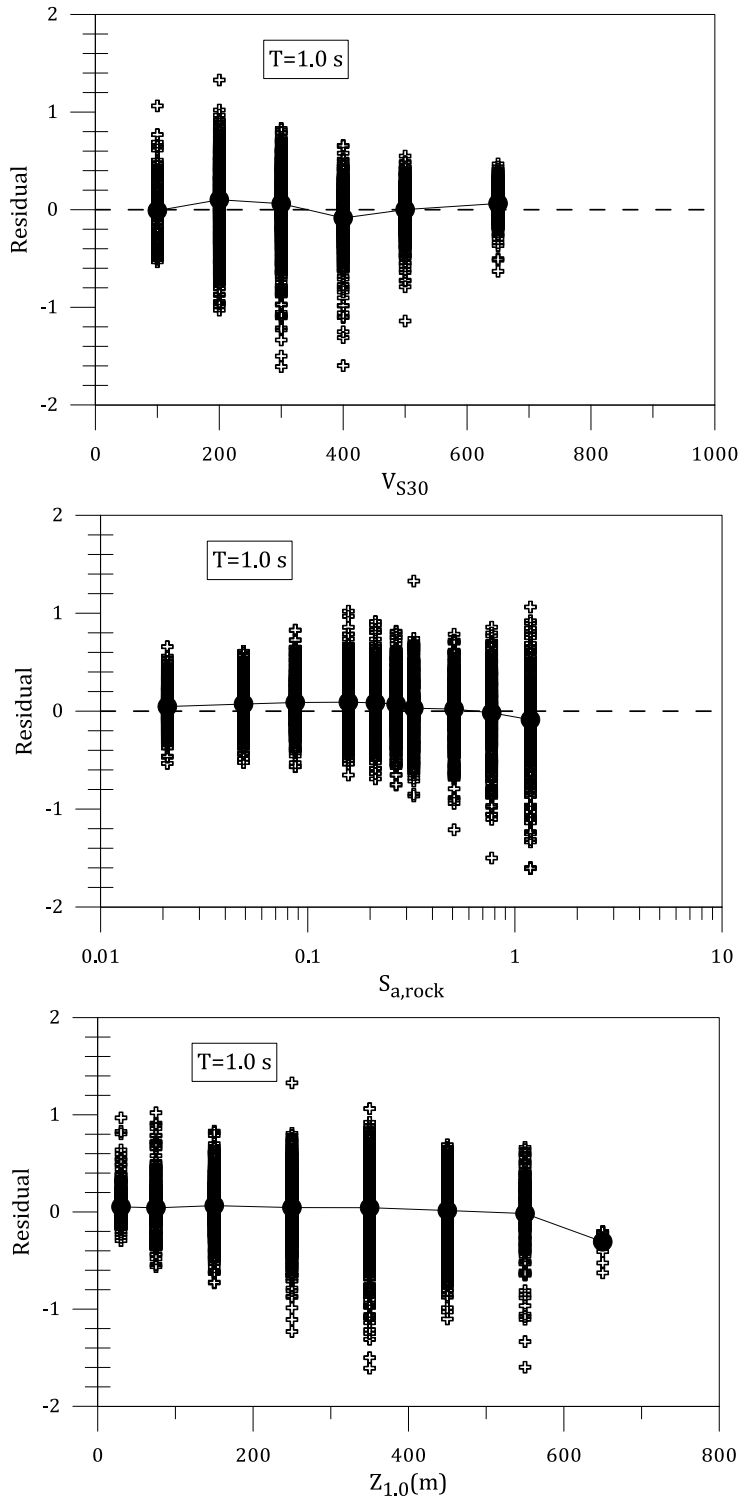

Figure 7.8 The residuals of the fit model versus V_{S30}, $S_{a,rock}$, and $Z_{1.0}$ at T=1.0 s.

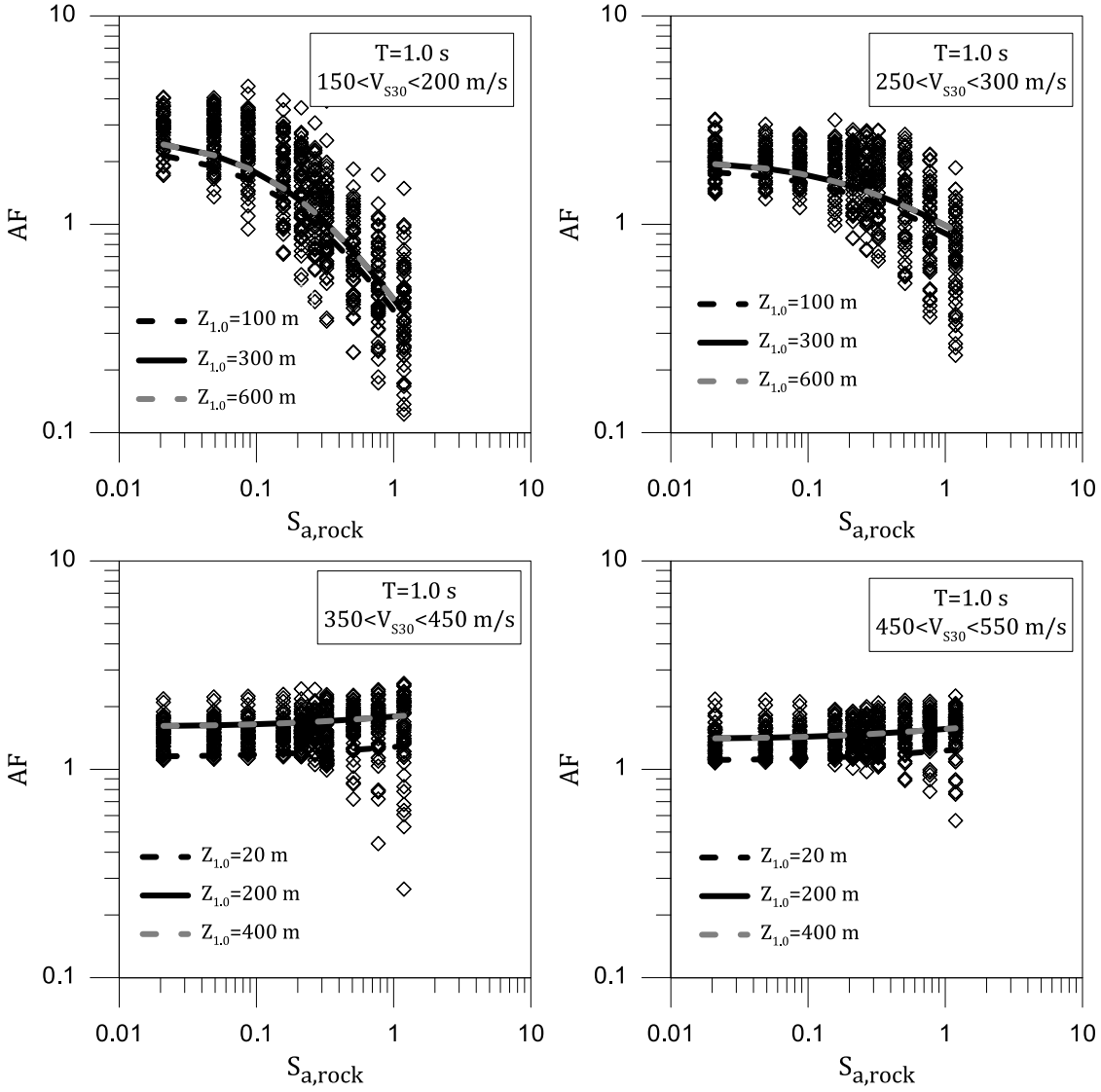

Figure 7.9 Fitted curves to the data for different values of $Z_{1.0}$ for each bin of V_{S30} at T=1.0 s.

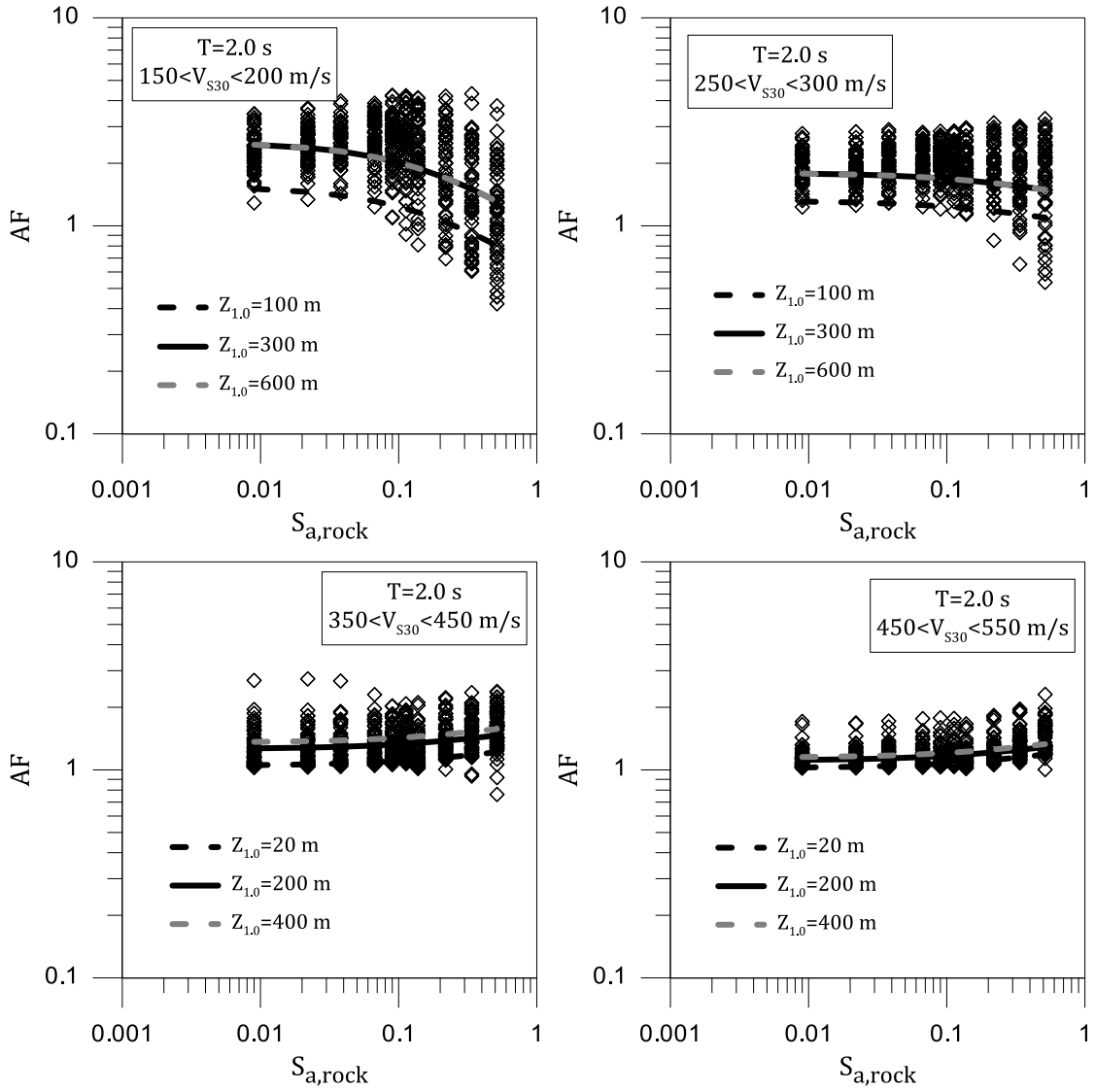

Figure 7.10 Fitted curves to the data for different values of $Z_{1.0}$ for each bin of V_{S30} at T=2.0 s.

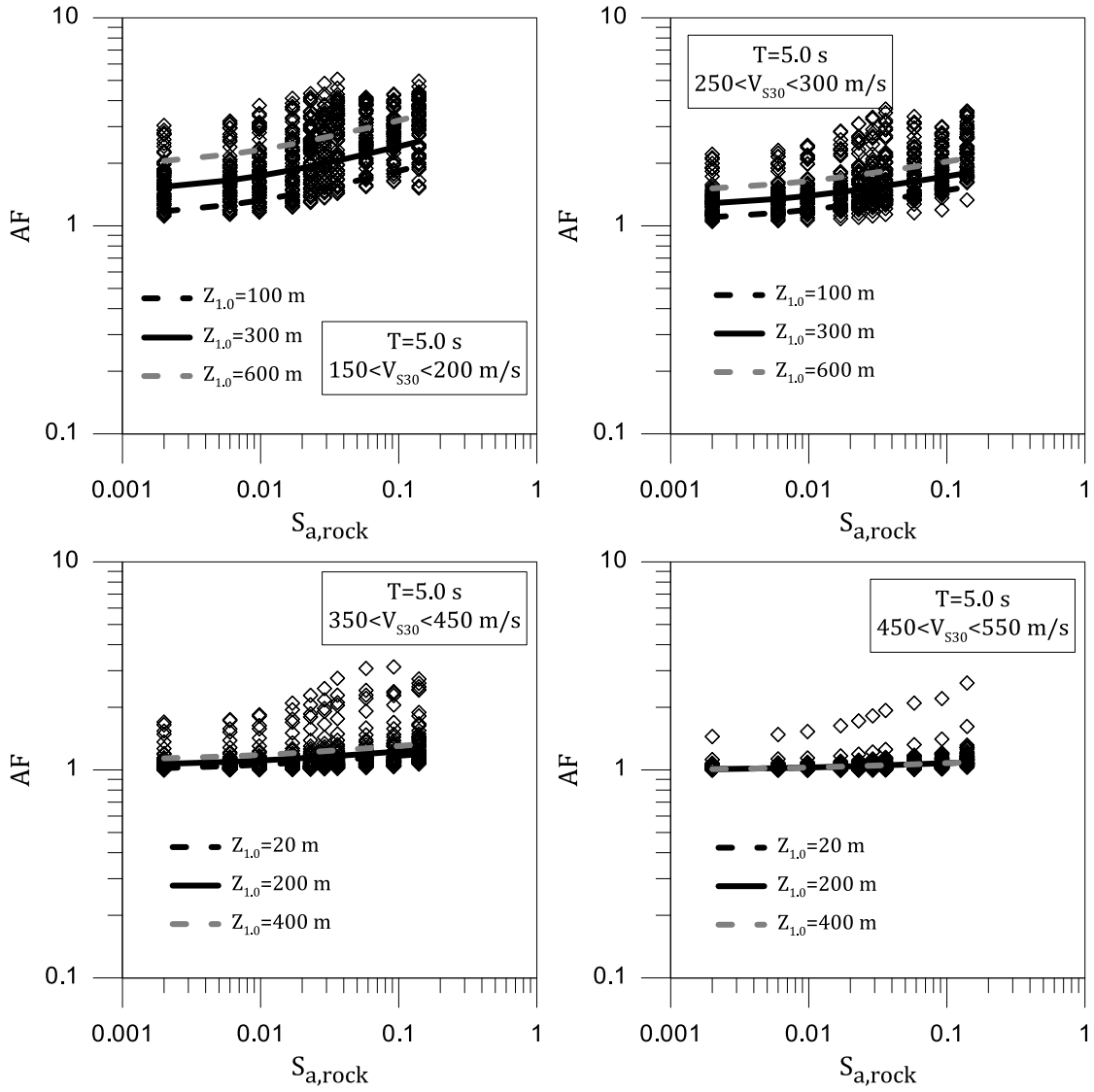

Figure 7.11 Fitted curves to the data for different values of $Z_{1.0}$ for each bin of V_{S30} at T=5.0 s.

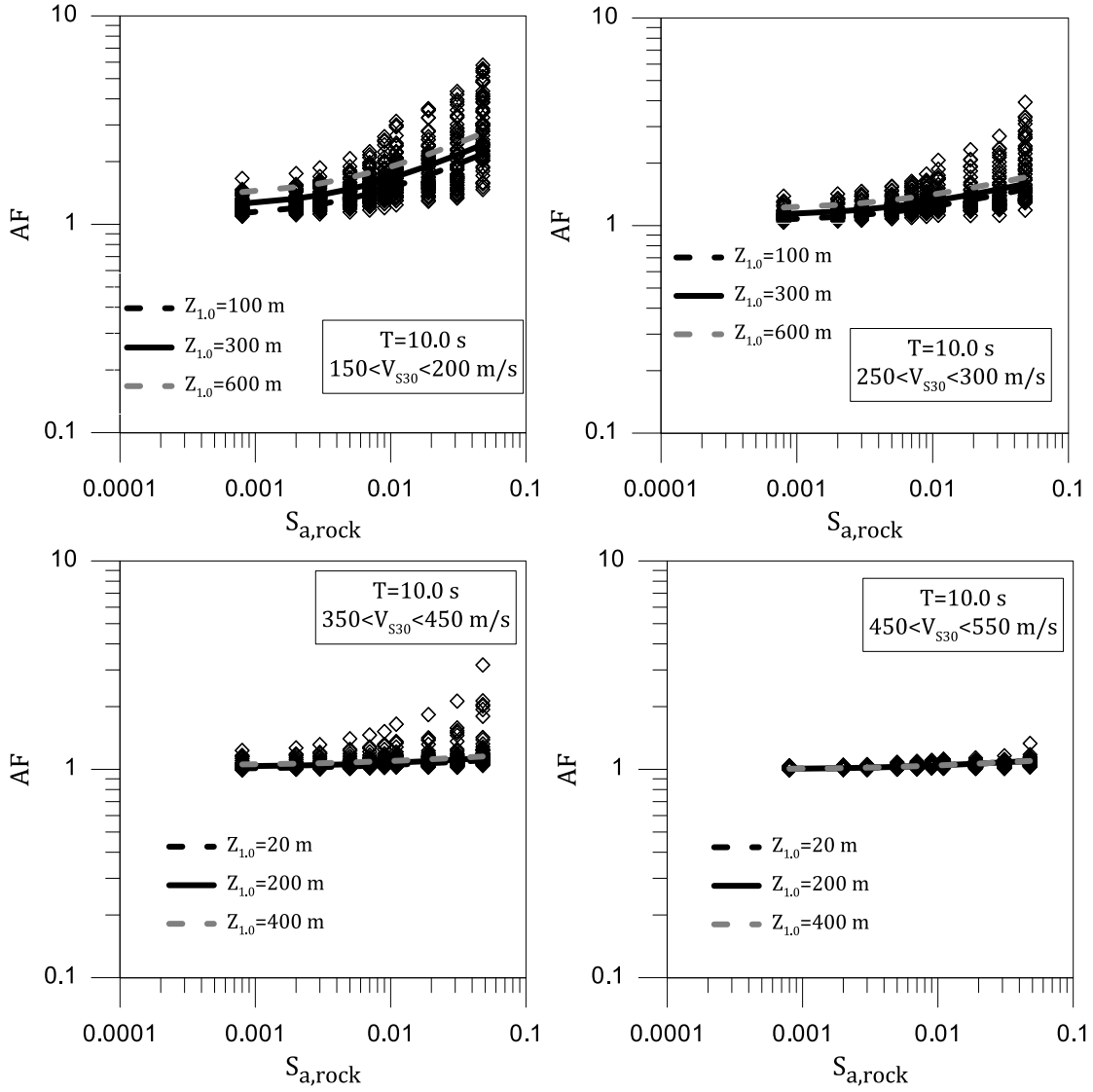

Figure 7.12 Fitted curves to the data for different values of $Z_{1.0}$ for each bin of V_{S30} at T=10.0 s.

7.4 Summary

In this chapter, the linear and nonlinear components of the developed site amplification model are combined. Separate site response models are presented for short and long periods

Chapter 8

Amplification Prediction

8.1 Introduction

To compare the proposed model in this study to the site amplification models already used in ground motion prediction equations, several scenario events (i.e. input motion intensities) and soil profiles are considered. The responses predicted by the model developed in this study are compared to predictions from the NGA models. The influence of Vratio on the predicted amplification is also discussed. The limitation of the developed model and the range of input motion intensities over which the model can be accurately used are addressed.

8.2 Scenario Events

Two sites with different V_{S30} values and three input motion intensities are considered to compare the developed model and the NGA models. To show the influence of Vratio on the prediction of amplification, the amplification for each site is predicted for three values of Vratio (i.e., Vratio=0.85, 1.4, and 2.3) and their

amplifications are compared. Table 8.1 lists the V_{S30} and $Z_{1.0}$ of each considered soil profile. Both V_{S30} values represent medium stiff soil sites.

The response of the soil profiles are predicted for 3 different levels of shaking; low input intensity (i.e., PGA_{rock}=0.06g), medium input intensity (i.e., PGA_{rock}=0.13g), and high input intensity (i.e., PGA_{rock}=0.32g). These input motions are derived using the average of the NGA ground motion prediction equations for Mw = 7.0, V_{S30} = 1,000 m/s, and distances of 5, 20, and 50 km, respectively. The resulting input rock response spectra are shown in Figure 8.1.

Table 8.1 V_{S30} and $Z_{1.0}$ of the considered soil profiles.

Profile No.	V_{S30} (m/s)	$Z_{1.0}$ (m)
1	250	300
2	350	100

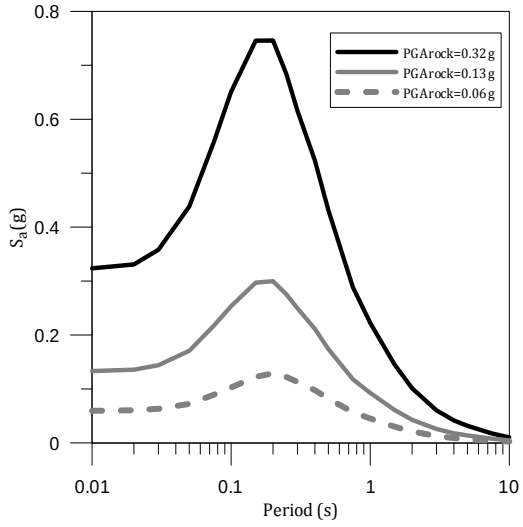

Figure 8.1 Response spectra of the input motions.

8.3 Site Amplification Predicted by NGA Models

Four of the NGA models contain site amplification models that model soil amplification as a continuous function of V_{S30}. The AF predicted by the NGA models varies between the models. Figure 8.2 shows the predicted AF versus period for each model for a site with V_{S30}=250 m/s and the three input motion scenarios (i.e., PGA_{rock}=0.06g, 0.13g, and 0.32g). The average predicted AF across the four models is also shown in Figure 8.2. For the smallest PGA_{rock}, the four models predict similar levels of amplification that range from about 1.5 at short periods to over 3.0 at long periods. The Campbell and Bozorgnia (2008) prediction is noticeably smaller at short periods and the Abrahamson and Silva (2008) prediction is noticeably smaller at long periods. As the input intensity increases, the predicted AF values at short periods decrease while those at long periods remain the same because soil nonlinearity is not modeled strongly at long periods in the NGA models. Across all input intensities, the Campbell and Bozorgnia (2008) prediction is smaller at short periods and the Abrahamson and Silva (2008) prediction is smaller at long periods. Figure 8.3 shows the predicted AF versus period for each NGA model for a site with V_{S30}=350 m/s and the same three input motions scenarios. The trends observed for the site with V_{S30}= 250 m/s in Figure 8.2 are observed for this site as well. Across all input intensities, the Campbell and Bozorgnia (2008) prediction is smaller at short periods and the Abrahamson and Silva (2008) prediction is smaller at long periods.

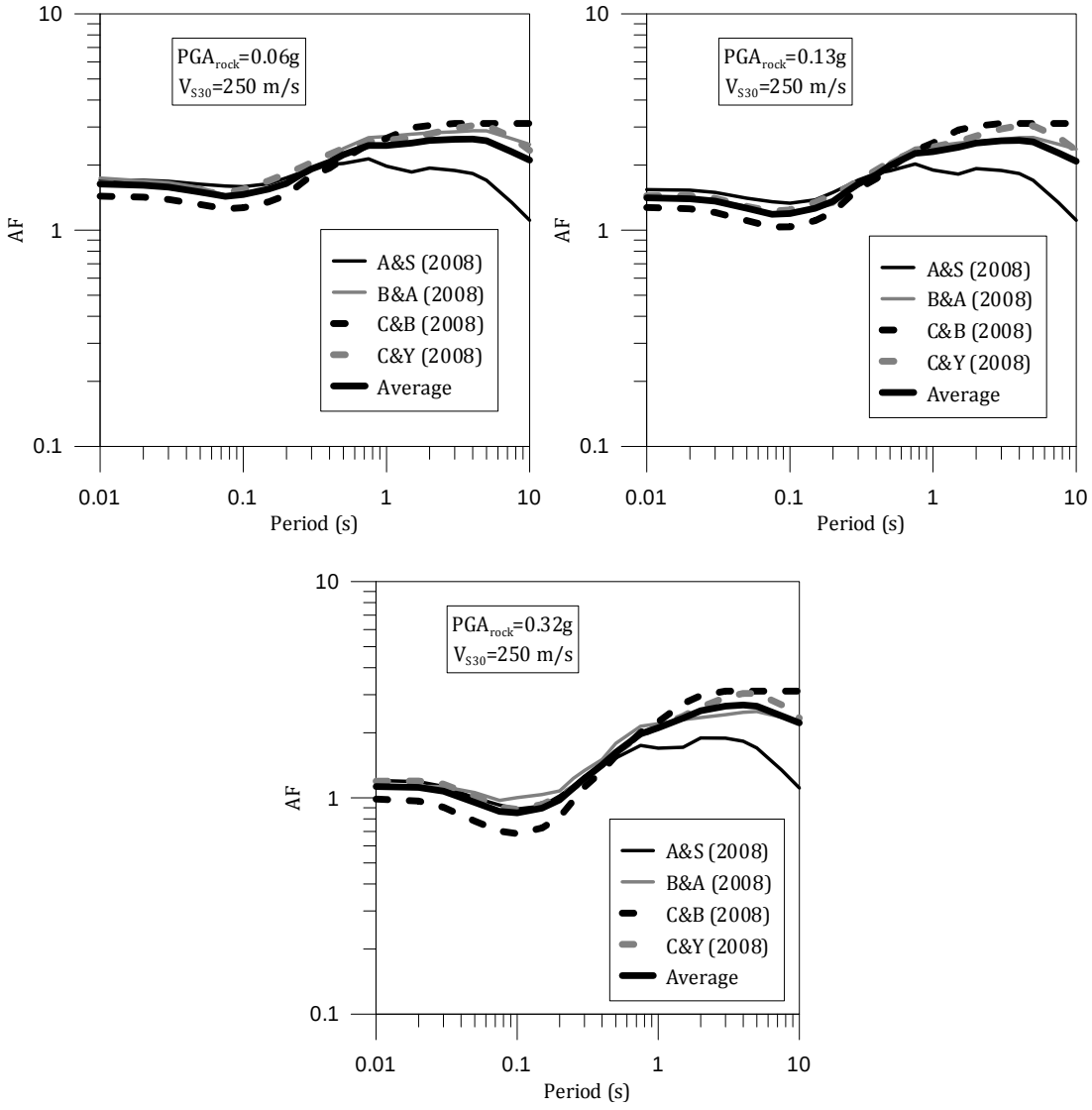

Figure 8.2 Predicted AF by different NGA models for a site with V_{S30}=250 m/s subjected to three input intensities.

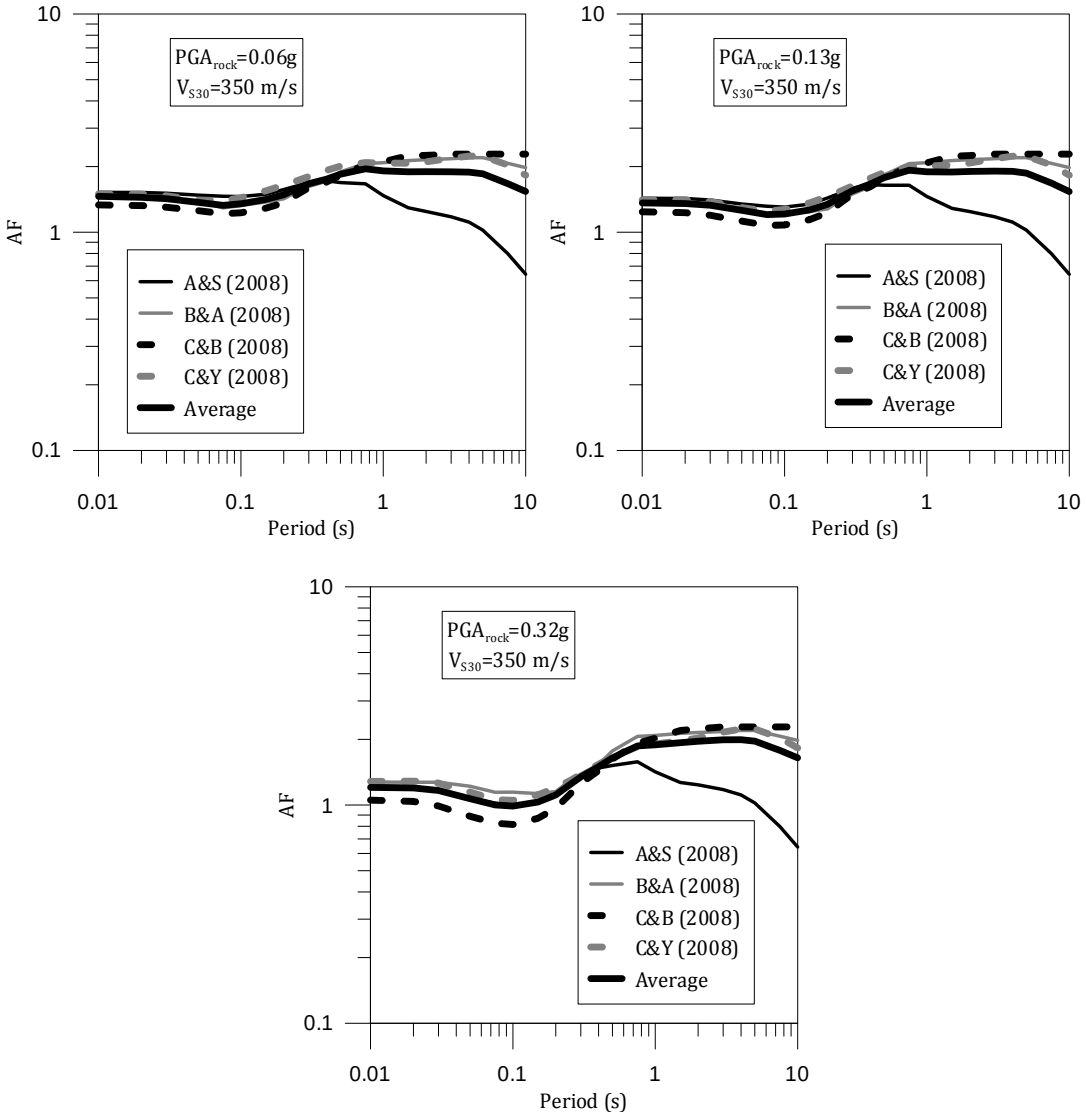

Figure 8.3 Predicted AF by different NGA models for a site with V_{S30}=350 m/s subjected to three input intensities.

8.4 Site Amplification Predicted by the Developed Model

The AF values predicted by the developed site amplification model for the scenarios discussed and Vratio equal to 0.85, 1.4, and 2.3 are shown in Figure 8.4. The different values of Vratio influence amplification at periods less than 1.0 s, and the difference can be significant at high input intensities. Here, an increase in Vratio from 0.85 to 2.3 can increase the amplification by as much as a factor of 2.0. Applying the amplification factors from Figure 8.4 to the rock response spectra from Figure 8.1 result in the soil surface response spectra in Figure 8.5. In all cases, the response of the sites shifts the spectrum to longer periods with the peaks occurring at 0.3 to 0.4 s rather than at 0.2 s. The influence of different values of Vratio is readily apparent, with the PGA and Sa,max significantly larger for larger Vratio.

Figure 8.6 compares the average AF predicted by the NGA models (shown in Figures 8.2 and 8.3) with those predicted by the developed model for the six scenarios. It is clear that the AF values predicted by this study are almost all smaller than those predicted by the NGA models. The difference is most significant for V_{S30} = 250 m/s and PGA_{rock} = 0.32 g.

The differences are most likely due to the different datasets upon which the models were developed. The V_{S30} scaling for the linear elastic component of the NGA models was constrained based on ground motion recordings. Only one-third of

the NGA sites have measured values of V_{S30} and the others sites have inferred values; this uncertainty introduces uncertainty in the V_{S30} scaling of the NGA models. Additionally, the NGA recordings may include effects beyond one-dimensional site amplification and these effects are not modeled in the site response simulations used in this study. The nonlinear V_{S30} scaling in the NGA models is typically constrained by some form of site response simulations (e.g., Walling et al. 2008), yet these simulations mainly focused on V_{S30} values greater than 300 m/s. At long periods, the soil depth scaling of several of the NGA models was constrained using three-dimensional basin simulations (e.g., Day et al 2008), and these simulations will certainly predict larger long period amplification than the one-dimensional simulations used in this study.

One additional issue that may be influencing the amplification factors predicted in the developed models is the level of induced shear strain. At high level of shaking, softer soil profiles may experience significantly large strain. The equivalent linear analysis assumption is often considered invalid at shear strains greater than 1.0%. This issue introduces some limitations when applying the developed model, which is based on the results of equivalent-linear analysis. At stiffer sites, the generated strains often remain smaller than 1.0 % even at high level of shaking, therefore the predicted values by the developed model and the NGA models are more similar for V_{S30}=350m/s than for V_{S30} = 250 m/s.

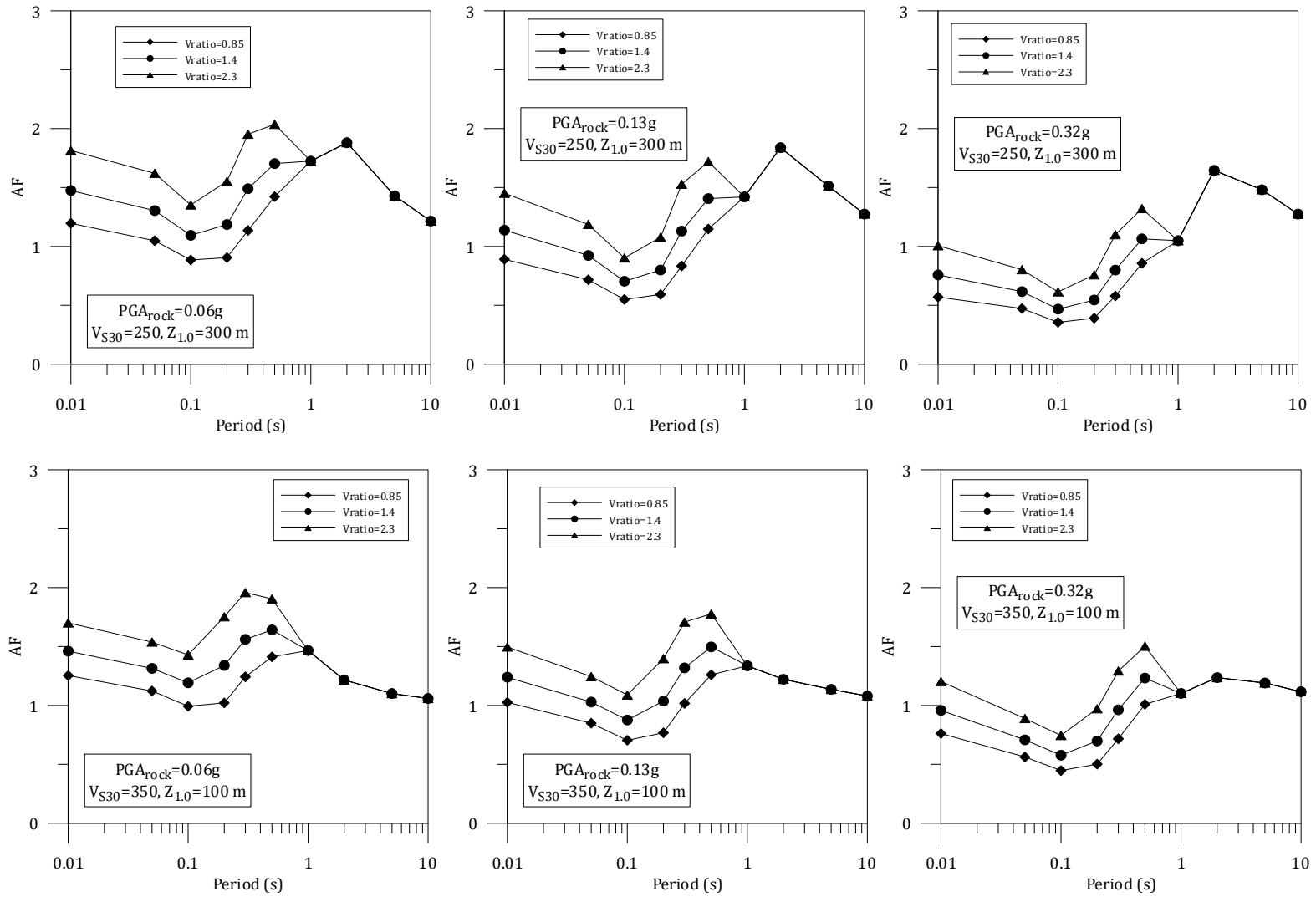

Figure 8.4 The predicted AF by the developed model for different values of Vratio.

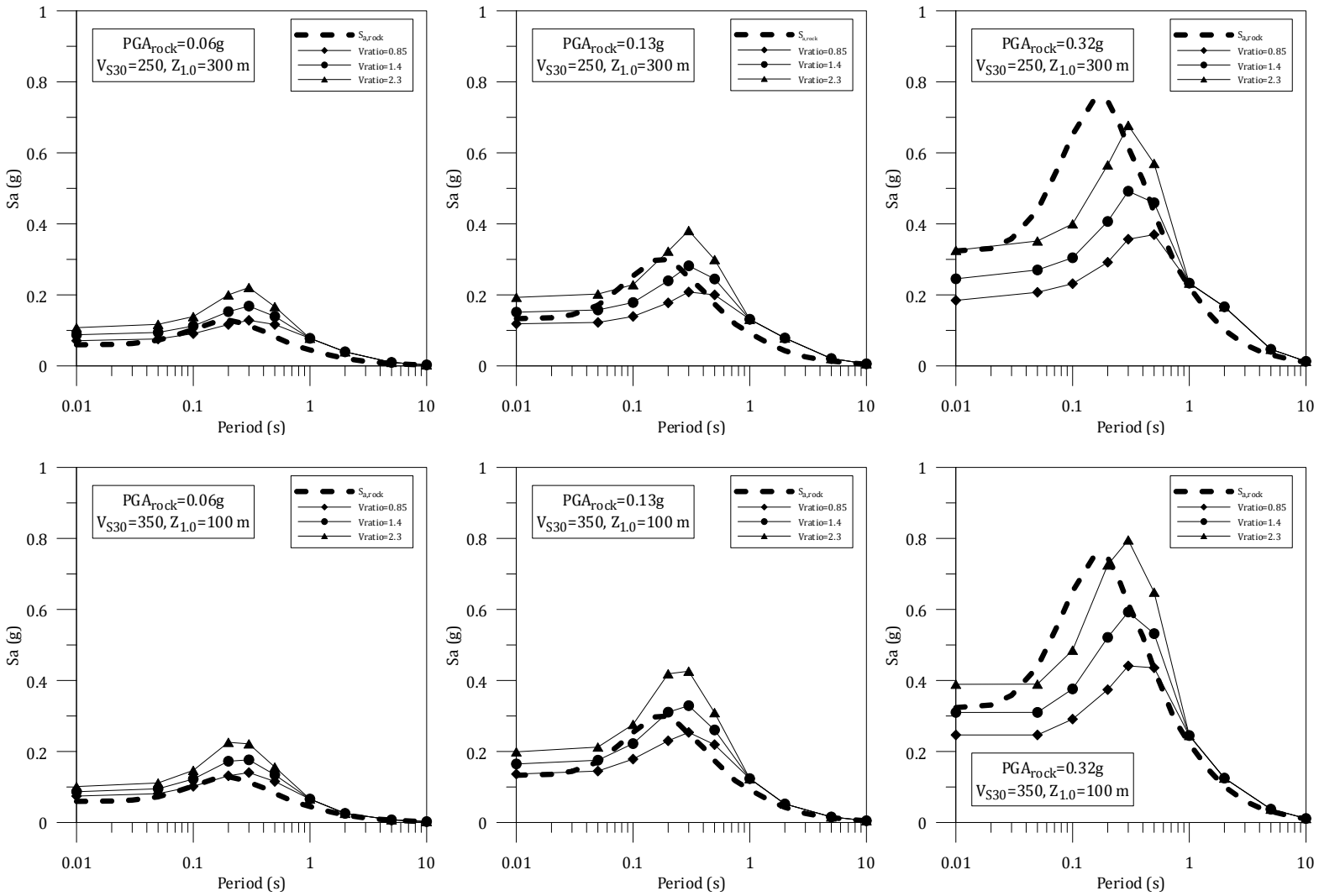

Figure 8.5 The predicted Sa by the developed model for different values of Vratio.

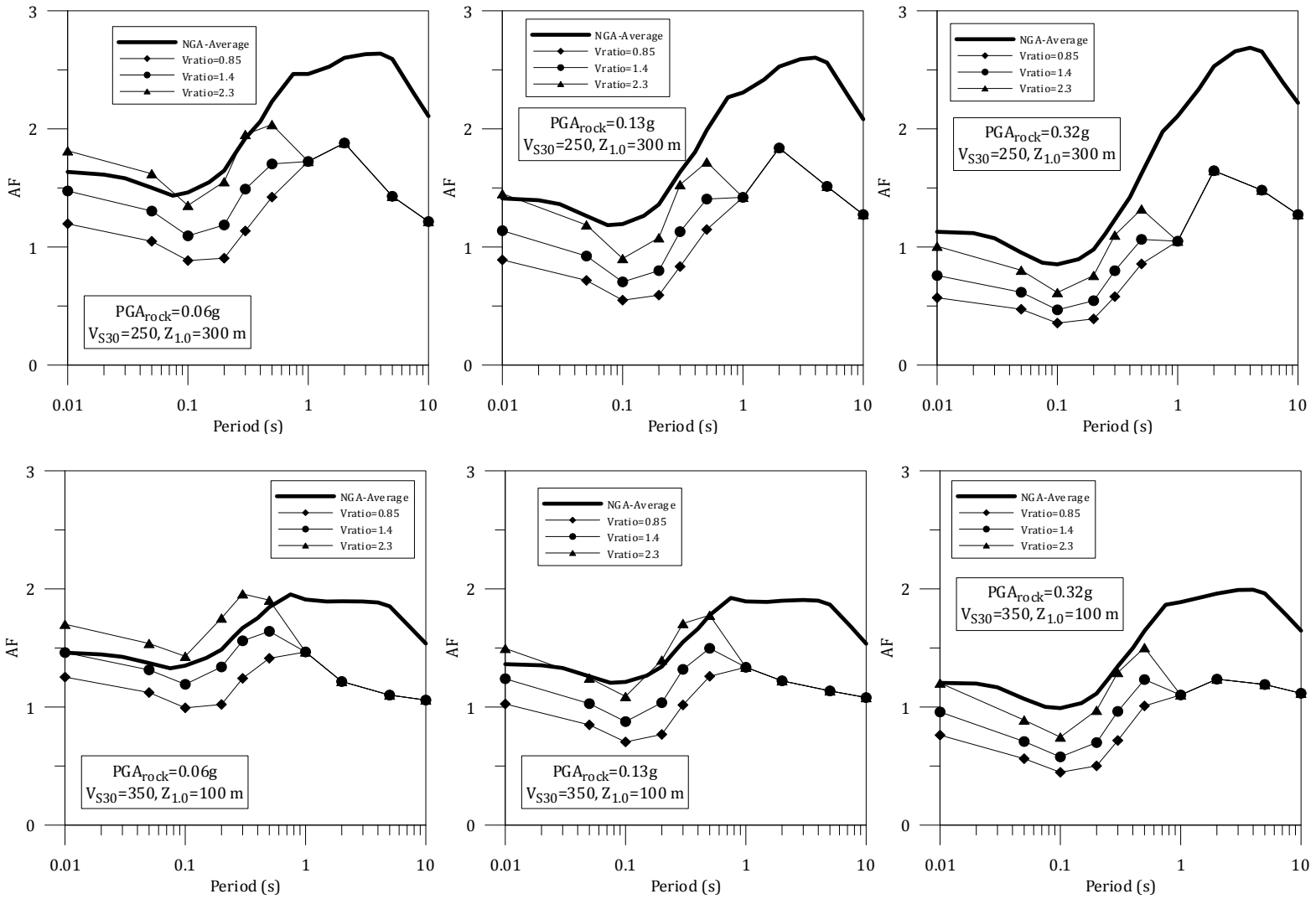

Figure 8.6 Comparison of the predicted AF by the proposed model and NGA models.

8.4 Limitations of the Proposed Model

As previously discussed, soil profiles can experience significantly large shear strains at high level of shaking. Because the equivalent linear assumption breaks down at shear strains greater than about 1% and the AF values developed in this study are all based on equivalent-linear analysis, it is important to identify when excessive shear strains were induced. The level of generated shear strain in a soil profile depends on the stiffness of the site and the level of shaking. Softer soil profiles experience larger strains than stiffer soil profiles subjected to the same level of input intensity. Figure 8.7 plots strain profiles induced in the softest site considered in this study (V_{S30}=118 m/s) for four different input intensities. At PGA_{rock}=0.1 g, the maximum generated strain in the site is about 0.4 %. The maximum induced strain increases as PGA_{rock} increases and exceeds 1% for PGA_{rock}=0.22 g and larger. This result indicates that the AF values from this site are not realistic for PGA_{rock} greater than 0.22 g.

The PGA_{rock} that first induces maximum shear strains greater than 1% is called $PGA_{rock\ -1\%}$. This value is compiled for the profiles analyzed and used to identify the limitations of the developed model. Figure 8.8 plots $PGA_{rock\ -1\%}$ versus V_{S30} for the soil profiles analyzed in this study. For soil profiles with V_{S30} less than 200 m/s, the maximum shear strain exceeds 1% at PGA_{rock} =0.22g. The maximum shear strain exceeds 1% at larger input intensities for stiffer sites (e.g., $PGA_{rock\ -1\%} \sim$ 0.4 g for V_{S30} = 300 m/s, $PGA_{rock\ -1\%} \sim$ 1.0 g for V_{S30} = 400 m/s). For soil profiles with V_{S30} greater

than 500 m/s, the maximum induced shear strain does not exceed 1% for the sites and input motion analyzed in this study. In Figure 8.8, the range of V_{S30} and PGA_{rock} that the developed model can be applied is shown. For stiff sites with V_{S30}> 500 m/s, the developed model can be used all levels of shaking.

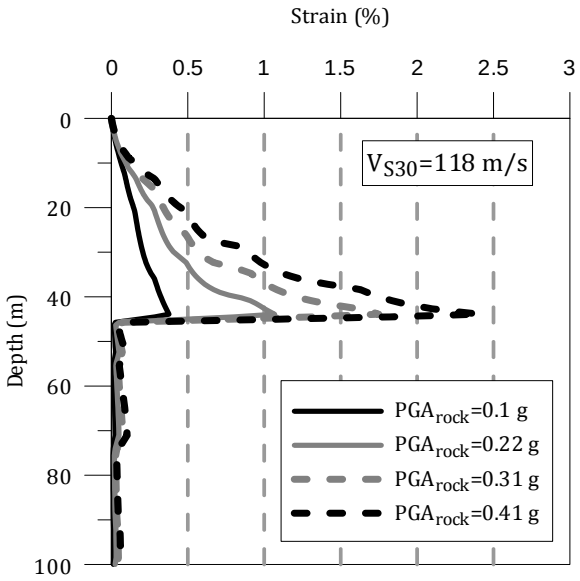

Figure 8.7 Generated strain profile in a site with V_{S30}=118 m/s subjected to different level of shaking.

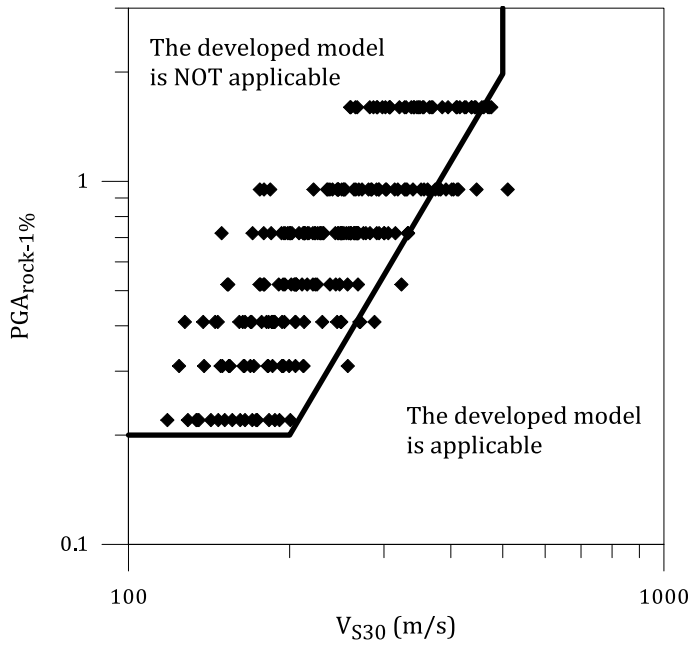

Figure 8.8 The PGA_{rock} and V_{S30} zone that the developed model is applicable.

8.5 Summary

Amplification factors (AF) and acceleration response spectra (Sa) predicted by the developed amplification model and the site amplification models of NGA relationships are compared. The proposed model predicts Sa and AF smaller than the NGA models at high level of shaking and small V_{S30}. The prediction of the proposed model approaches the NGA models prediction as input intensity decreases.

The developed model considers the effect of Vratio in the prediction of amplification. Amplification for sites with larger Vratio is significantly higher than for sites with smaller Vratio, resulting in significantly different surface response spectra. Vratio affects amplification at short periods (T<1.0 s) only.

The developed model is applicable to PGA_{rock} smaller than $PGA_{rock\text{-}1\%}$. $PGA_{rock\text{-}1\%}$ is the level of input intensity above which the maximum strain exceeds 1%. $PGA_{rock\text{-}1\%}$ depends on V_{S30} and increases with the increase of V_{S30}.

Chapter 9

Summary, Conclusions, and Recommendations

9.1 Summary and Conclusions

In this study, an improved site amplification model is developed that considers the effect of multiple site parameters that affect amplification. This model includes parameters previously considered in ground motion predictions equations (e.g., V_{S30} and $Z_{1.0}$), but also identifies an additional parameter that influences site amplification.

To identify the appropriate site parameters to be considered, ninety nine soil profiles were generated manually using five baseline velocity profiles. The top 30 m of each baseline shear wave velocity profile was modified to maintain the same V_{S30} but to simulate a different V_S structure. The seismic responses of the generated profiles were analyzed using the equivalent linear approach as implemented in the site response program, Strata (Kottke and Rathje, 2008). Different site parameters

such as V_{min}, thV_{min}, MAXIR and Vratio are considered to investigate the variation in AF between sites with a common V_{S30}. These analyses identified Vratio as the site parameter that influences site amplification the most and can explain the variation in amplification between sites with the same V_{S30}.

To generalize the findings from the analyses in which only the top 30 m of the velocity profile were varied, a suite of fully randomized velocity profiles are generated and their responses analyzed using Strata. The results of the site response analyses conducted on these four hundred fully randomized velocity profiles confirmed the influence of Vratio on site amplification. The computed amplification factors were used to develop a functional form that incorporates its effect. To consider the effect of soil nonlinearity in the developed model, soil profiles are analyzed under different input rock shaking levels.

The developed amplification model consists of two components; the linear-elastic and nonlinear components. The computed site amplification under low input intensity (PGA_{rock}=0.01g) are used to develop the linear component of the model and the higher input intensities are used to develop the nonlinear component. Vratio affects both the linear and nonlinear behavior of a soil profile; therefore, both linear and nonlinear components include Vratio in their functional forms.

The effect of Vratio on site amplification is only significant at shorter periods (T<1.0 s). Therefore, different models are developed for shorter (T<1.0 s) and longer (T≥1.0 s) periods. At short periods, the linear-elastic component of the model

uses a second-order polynomial functional form for modeling the effect of ln(V_{S30}) on ln(AF) rather than the linear relationship used in other site amplification models. The second-order polynomial better fits the AF data at low intensities, particularly at smaller values of V_{S30}. The linear-elastic model incorporates the effects of Vratio through a linear relationship between ln(Vratio) and ln(AF). The slope of this relationship is V_{S30}-dependent. At longer periods, the model uses a linear relationship between ln(V_{S30}) and ln(AF) rather than a second-order polynomial, and no Vratio effect is modeled. Additionally, at long periods site amplification is affected by the depth to bedrock (i.e., $Z_{1.0}$) in addition to V_{S30}. The effect of $Z_{1.0}$ is considered in the linear component of the proposed model because it is not influenced by soil nonlinearity.

The nonlinear component of the model incorporates the effect of input intensity on the V_{S30} and Vratio scaling. The effect of input intensity is coupled with the V_{S30} scaling by making ln(AF) a function of $S_{a,rock}$ and V_{S30}. The effect of input intensity on the Vratio scaling is incorporated by making the relationship between ln(AF) and ln(Vratio) a function of $S_{a,rock}$.

The resulting amplification model accounts for the influence of V_{S30}, Vratio, $S_{a,rock}$, and $Z_{1.0}$. Generally, larger amplification is predicted for sites with smaller V_{S30}, larger Vratio, and larger $Z_{1.0}$. For sites with the same average shear wave velocity in top 30 m (V_{S30}), a larger value of Vratio indicates a larger change in Vs

over the top 30 m. At larger input intensities, the amplification at short periods will be larger for sites with larger V_{S30}.

The comparison of the developed model with the site amplification models of NGA prediction equations shows that the developed model predicts smaller site amplification at high level of shaking for soft sites. Soil profiles under high level of shaking experience significantly large strain. The equivalent linear assumption is invalid at strain larger than 1%. Therefore, the developed model, which is based on site amplification computed by the equivalent linear method, is invalid in these cases. The shaking level above which the maximum generated shear strain in a profile exceeds 1% is V_{S30} dependent. The application of the proposed model should be limited to the range of shaking level and V_{S30} that the assumption of the equivalent linear method is valid.

9.2 Recommendations for Future Work

The model developed in this study is based on numerical simulations of site amplification and can be expanded in various ways. To provide more valid amplification predictions at small V_{S30} values, nonlinear site response analyses should be performed and the computed amplification factors for these sites should be used in the development of the site amplification model. These data would be most important to include for moderate to large input intensities.

To evaluate the developed model and the relationship between Vratio and ground shaking, recorded strong motion data at sites with measured V_S profiles should be considered. The predicted response spectral values for each recording from a ground motion prediction equation can be computed for the associated magnitude, distance V_{S30}, etc. and the residual computed with respect to the recorded value. The relationship between the residuals and the computed values of Vratio for each site can be investigated to confirm the influence of Vratio on recorded ground motions and to evaluate the functional form of the relationship between ln(AF) and ln(Vratio). Recordings at borehole arrays site, in which recordings are made at the ground surface and at some depth within the bedrock, can also be used to directly compute amplification factors. In this case, the relationship between amplification and Vratio can be investigated directly.

Bibliography

N. Abrahamson and W. Silva. Abrahamson and Silva NGA ground motion relations for the geometric mean horizontal component of peak and spectral ground motion parameters. PEER report200x/xx, University of California, Berkeley, July 2007.

N. Abrahamson and W. Silva. Summary of the Abrahamson and Silva ground motion relationships. Earthquake Spectra, 24(1):67-97, February 2008.

N. Abrahamson, G. Atkinson, D. Boore, Y. Bozorgnia, K. Campbell, B. Chiou, I.M. Idriss, W. Silva, and R. Youngs. Comparison of the NGA ground motion relations. Earthquake Spectra, 24(1):45-66, February 2008.

S. Barani, R. De Ferrari, G. Ferretti, and C. Eva. Assessing the effectiveness of soil parameters for ground response characterization and classification. Earthquake Spectra, 24(3):565-597, August 2008.

P. Bazzuro and C.A. Cornell. Ground motion amplification in nonlinear soil sites with uncertain properties. . Bulletin of Seismological Society of America, 94(6):2090-2109, December 2004.

D.M. Boore and G.M. Atkinson. Ground-motion prediction equations for the average horizontal component of PGA, PGV, and 5%-damped PSA at spectral periods between 0.01s and 10.0 s. Earthquake Spectra, 24(1):99-138, February 2008.

K.W. Campbell and Y.Bozorgnia. NGA Ground motion model for the geometric mean horizontal component of PGA, PGV, PGD, and 5% damped linear elastic response spectra for periods ranging from 0.01 to 10 s. Earthquake Spectra, 24(1):139-171, February 2008.

K.W. Campbell and Y. Bozorgnia. Updated near source ground motions (attenuation) relations for the horizontal and vertical components of peak ground acceleration and acceleration response spectra. Bulletin of Seismological Society of America, 93(1):314-331, February 2003.

K.W. Campbell. Emperical near-source attenuation relationships for horizontal and vertical components of peak ground acceleration, peak ground velocity, and pseudo-

absolute acceleration response spectra. Seismological Research letters, 68(1):154-179, January/ February 1997.

B.S.J. Chiou and R.R.Youngs. An NGA model for the average horizontal component of peak ground motion and response spectra. Earthquake Spectra, 24(1):173-215, February 2008.

B. Chiou, R. Darragh, N. Abrahamson, and W. Silva. NGA project strong motion database. Earthquake Spectra, 24(1):23-44, February 2008.

Y. Choi and J.P. Stewart. Nonlinear site amplification as function of 30 m shear wave velocity. Earthquake Spectra, 21(1):1-30, February 2005.

C.J. Costantino, E. Heymsfield, and Y.T. Gu. Site specific estimates of surface ground motions for the K-reactor site, Savannah River Plant. Upton, New York: Structural Analysis Division, Nuclear Energy Department, Brookhaven National Laboratory, 1991.

M.B. Darendeli. Development of s new family of normalized modulus reduction and material damping curves. Austin, Texas: The University of Texas,2001.

J.L. Devore. Probability and statistics for engineering and science. Third Edition. Brooks/Cole Publishing Company, Pacific Grove, Clifornia, 1990.

I.M. Idriss. An NGA empirical model for estimating the horizontal spectral values generated by shallow crustal earthquakes. Earthquake Spectra, 24(1):217-242, February 2008.

A.R. Kottke and E.M. Rathje. Technical manual for strata. PEER 2008/10 publication, University of Texas, Austin, February 2009.

A.R. Kottke, Site amplification model considering V_{S30} and depth, unpublished report, October 2011.

S.L. Kramer. Geotechnical earthquake engineering. Prentice Hall, Saddle River, New Jersey, 1996.

R.K. McGuire, G.R. Toro, T.P. O'Hara, J.P. Jacobson, and W.J. Silva. Probabilistic seismic hazard evaluation at nuclear plant sites in the Central and Eastern United States: Resolution of the Charleston Earthquake Issue. Palo Alto, California: Electric Power Research Institute, 1989.

R. Ramanathan. Introductory econometrics with applications. Fourth Edition. The Dryden Press, Harcourt Brace College Publishers, 1998.

A. Rodriguez-Markez, J.D. Bray, and N.A. Abrahamson. An empirical geotechnical seismic site response procedure. Earthquake Spectra, 17(1): 65-87, February 2001.

W.J. Silva. Site response simulations for the NGA project. University of California, Berkeley, 2008.

J.P. Stewart, A.H. Liu, and Y. Choi. Amplification factors for spectral acceleration in tectonically active regions. Bulletin of the Seismological Society of America, 93(1), 332-352, February 2003.

G.R. Toro. Probabilistic models of site velocity profiles for generic and site-specific ground-motion amplification studies. Upton New York: Brookhaven National Laboratory, 1995.

G.R. Toro, W.J. Silva, R.K. McGuire, and R.B. Hermann. Probabilistic seiemic hazard mapping of the Mississippi embayment. Seismological Research Letters, 63(3),449-475,1992

M. Walling, W. Silva, and N. Abrahamson. Nonlinear site amplification factors for constraining the NGA models. Earthquake Spectra, 24(1):243-255, February 2008.